SEISMIC ANALYSIS OF BUILDINGS TO RECORDED MOTIONS

By

Rakesh K. Goel
Department of Civil & Environmental Engineering
California Polytechnic State University, San Luis Obispo

Data Utilization Report
California Strong Motion Instrumentation Program

Jointly Funded By
CALIFORNIA STRONG MOTION INSTRUMENTATION PROGRAM
CALIFORNIA GEOLOGICAL SURVEY
CALIFORNIA DEPARTMENT OF CONSERVATION

Report No. CP/SEAM-09/01

December 2009

ABSTRACT

This investigation focused on developing an improved understanding of challenges associated with computation of nonlinear response of three-dimensional building to recorded ground motions, and if the base shear estimated from recorded motions, denoted as "estimated base shear" in this report, is an accurate indicator of the true base shear. For this purpose, three-dimensional models of two buildings – one reinforced-concrete building and one steel building – are developed in *OpenSees* and *Perform3D*. The analysis of these models included pushover analysis for lateral force distribution proportional to the first mode in each of the two principle directions, and nonlinear response history analysis (RHA) to compute response for 30 ground motions recorded during past earthquakes. It was found that modeling assumptions as well as different software may lead to significantly different pushover curves: concentrated plasticity model leads to lower strength, early initiation of yielding, and post yielding strength loss in pushover curves compared to spread plasticity model, strength loss model for beams/columns leads to significant post yielding strength loss in the pushover curve, and differences in solution schemes and convergence criteria available in different software programs also affect the pushover curves. It was also found that there prediction of median peak response from different software can differ from 10% to 40%. Finally, the median estimated base shear exceeds the true base shear by 10% to 20% with the value exceeding by as much as 50% for individual earthquake. Therefore, estimated base shear should be used with caution as an estimate of the true base shear.

ACKNOWLEDGMENT

This investigation is supported by the California Department of Conservation, California Geological Survey, Strong Motion Instrumentation Program, Contract No. 1007-907. This support is gratefully acknowledged. However, these contents do not necessarily represent the policy of that agency, nor endorsement by the State Government.

The authors are grateful to Drs. Anthony Shakal and Moh Huang of SMIP for providing the recorded motions and structural plans of the selected buildings. The author would also like to acknowledge the support provided by Prof. Graham Powell on implementation of *Perform3*, by Dr. Charles Chadwell on use of *Xtract*, and Karen Nishimoto on section moment-curvature and P-M interaction analysis for all beam and column sections of buildings considered in this investigation.

TABLE OF CONTENTS

CHAPTER 1. INTRODUCTION

Buildings are typically instrumented with accelerometers at selected number of floors: low-rise buildings (1 to 3 stories) at every floor; and mid- and high-rise buildings at base, roof, and a few intermediate floors. The raw (or uncorrected) acceleration recorded during earthquakes from these accelerometers are processed using well-established procedures to obtain base-line corrected (or processed) accelerations, velocity, and displacements. The processed floor accelerations and displacements may be used to estimate additional engineering demand parameters such as inter-story drift ratio defined as the differential displacement between two adjacent floors divided by the story height, and base shear defined as the summation of floor inertial forces above the base; the floor inertial forces are computed as the product of floor acceleration and floor mass. The engineering demand parameters thus estimated from recorded motions of buildings may be compared to those computed from various analytical procedures, such as nonlinear static pushover and nonlinear response history analysis, to evaluate the accuracy of these analytical procedures. These parameters may also be compared with limiting values to check if the building suffered damage during an earthquake and may need detailed inspection/evaluation.

For buildings with limited number of instrumented floors, estimation of various engineering demand parameters requires that the motions at non-instrumented floors be interpolated from those available at the instrumented floors. Typically, a piece-wise cubic polynomial interpolation procedure is used for conventional buildings (Naeim, 1997; De la Llera and Chopra, 1998; Goel, 2005, 2007; Limongelli, 2003) and a combination of cubic-linear interpolation is recommended for base-isolated buildings (Naeim, et al., 2004). It is generally believed that such interpolation procedures provide reasonable estimates of motions at non-instrumented floors (Naeim, 1997; Naeim et al., 2004; De la Llera and Chopra, 1998).

A recent study by Goel (2008) re-examined the adequacy of the traditionally used cubic polynomial interpolation procedure. It was found that results from the cubic polynomial interpolation procedure are sensitive to location of instrumented floors. While the cubic polynomial interpolation procedure may provide good estimate of floor displacements with proper selection of instrumented floors, this procedure may not accurately predict inter-story drifts and floor accelerations. This finding was also confirmed by Bernal (2007).

Another investigation by Goel and Chadwell (2007) compared the base shear estimated from motions interpolated using the traditional cubic polynomial interpolation procedure with the base shear capacity estimated from nonlinear pushover analysis of buildings. It was found that the base shear estimated from interpolated motions significantly exceeded the base shear capacity for several buildings. However, post earthquake inspection of these buildings did not reveal significant damage. This indicates that such base shear estimates may be questionable and possibly unreliable.

The preceding discussion clearly indicates that there is a need to comprehensively re-evaluate existing interpolation procedures. In particular, it is desirable to establish the level of accuracy that can be achieved in estimates of floor displacements and floor accelerations. Furthermore, it is necessary to examine if the base shear estimated from inertial floor forces, denoted as “estimated base shear” in rest of this report, is an accurate estimate of the “true” base shear which is defined as summation of shear forces in all columns at the base.

The aforementioned evaluation of interpolation procedures requires that “true” motions of buildings be available at each floor level. Since buildings are rarely instrumented at all floors and thus complete set of recorded responses that is needed for evaluating interpolation procedures is not readily available, response of buildings due to recorded ground motions

computed from response history analysis (RHA) offers a viable alternative to recorded motions. However, there are several modeling and software challenges in implementing the RHA for buildings that are expected to be deformed beyond the linear elastic limit during strong ground shaking.

The primary objective of this investigation is to develop an improved understanding of challenges associated with computation of nonlinear response of three-dimensional building to recorded ground motions. Another objective is to evaluate the accuracy of the estimated base shear as an indicator of the true base shear using the results from the RHA. For this purpose, nonlinear response – floor displacements, floor accelerations, and base shear – of two buildings – 20-Story Reinforced Concrete Hotel in North Hollywood, and 19-Story Steel Office Building in Los Angeles – were computed from RHA for 30 ground motions recorded during past earthquakes using two different computer program – *OpenSees* and *Perform3D*. Also computed were the pushover curves of these buildings included pushover analysis for lateral force distribution proportional to the first mode in each of the two principal directions. First, challenges associated in computation of nonlinear response from the two computer programs are documented. Next differences in peak responses from the two programs are examined for effects of modeling and software. Finally, peak values of estimated and true base shears are compared to understand if the estimated base shear can provide accurate estimate of true base shear.

CHAPTER 2. SELECTED BUILDINGS AND STRONG-MOTION DATA

Two buildings – 20-Story Hotel in North Hollywood (Figure 2.1) and 19 Story Office Building in Los Angeles (Figure 2.2) – are selected in this investigation (Table 2.1). This buildings are selected as representative of instrumented mid- to high-rise reinforced-concrete and steel buildings in California.

Table 2.1. Five concrete buildings selected.

Buildings name	CSMIP Station	Number of Stories	Structural System
Los Angeles – 19-Story Office Building	24643	19/4	Steel Concentric Brace Frame (Transverse) and Moment Frames (Longitudinal)
North Hollywood – 20-Story Hotel	24464	20/1	Concrete Moment Frames

Figure 2.1. 20-Story Hotel in North Hollywood.

Figure 2.2. 19-Story Office Building in Los Angeles.

20-Story Hotel in North Hollywood

This building has 20 stories above and one floor below the ground (Figure 2.3). Designed in 1966, its vertical load carrying system consists of 11.4 cm (4.5 inch) to 15 cm (6 inch) thick RC slabs supported by concrete beams and columns. The lateral load system consists of ductile moment resisting concrete frames in both directions. The foundation system consists of spread footing below columns.

19-Story Office Building in Los Angeles

This building has 19 stories above the ground level and 4 stories of parking below the ground level (Figure 2.4). The building was designed in 1966-67 and constructed in 1967. The vertical load carrying system consists of 11.4 cm (4.5 in.) thick reinforced concrete slabs supported on steel frames. The lateral load resisting system consists of four moment resisting steel frames in the longitudinal direction, and five X-braced steel frames in the transverse

direction. The foundation system consists of 22 m (72 ft- 4 in) long driven-steel I-beam piles (Hart, 1973; Naeim, 1998). The piles are capped in groups of three to ten with pile caps varying in thickness from 1.12m (3 ft-8 in) to 1.73 m (5 ft – 8 in). All pile caps are connected with 0.61m by 0.61 m (2 ft by 2 ft) reinforced concrete tie beams. The subsurface soil conditions are generally fine sand throughout the depth of the piles (Hart, 1973).

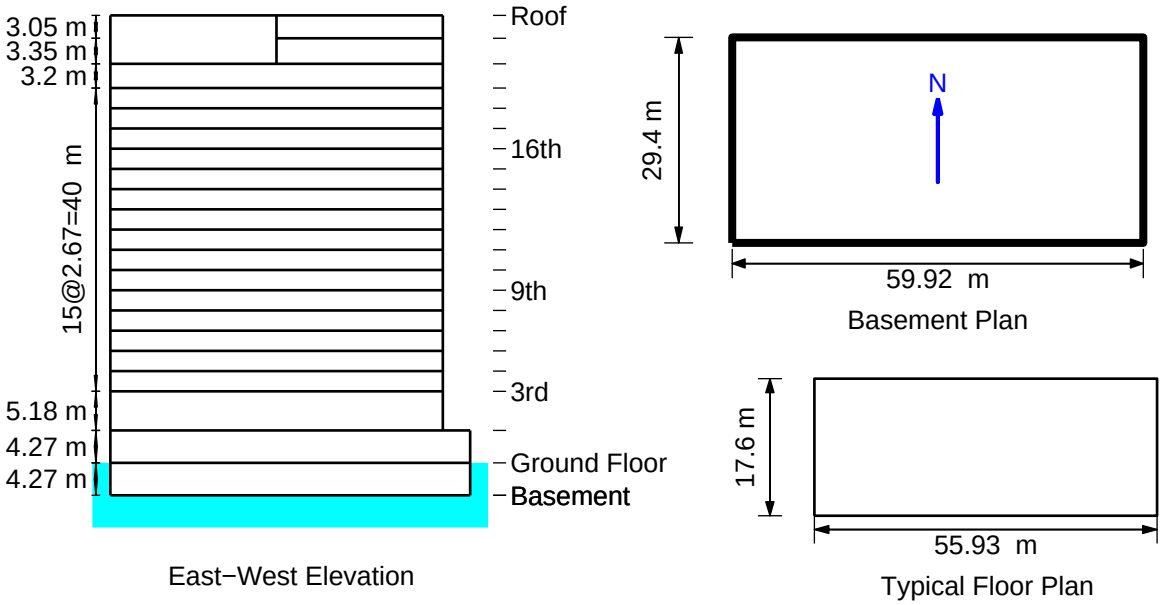

Figure 2.3. Elevation and plan of 20-Story Hotel in North Hollywood.

Selected Ground Motions

A suite of 30 ground motions have been selected in this investigation (Table 2.2); acceleration histories and linear elastic response spectra for the selected ground motion are available in Appendix I. Each ground motion consists of a pair of two horizontal components of ground motion recorded during indicated earthquake. These earthquakes are selected for a wide range of parameters: proximity to the fault, magnitude, peak ground accelerations and velocities. These ground motions were not selected to match any design spectrum but to ensure that they will induce different levels of inelastic behavior in the selected buildings: selected buildings are expected to remain within the linear elastic range for a few earthquakes where as these buildings

are expected to be deformed well into the nonlinear range, and possibly collapse, during other earthquakes. Because some of the ground motions were very long and would require excessive computational time for analysis of selected buildings, truncated histories were selected for several ground motions; these time histories of selected time segments are also included in Appendix I.

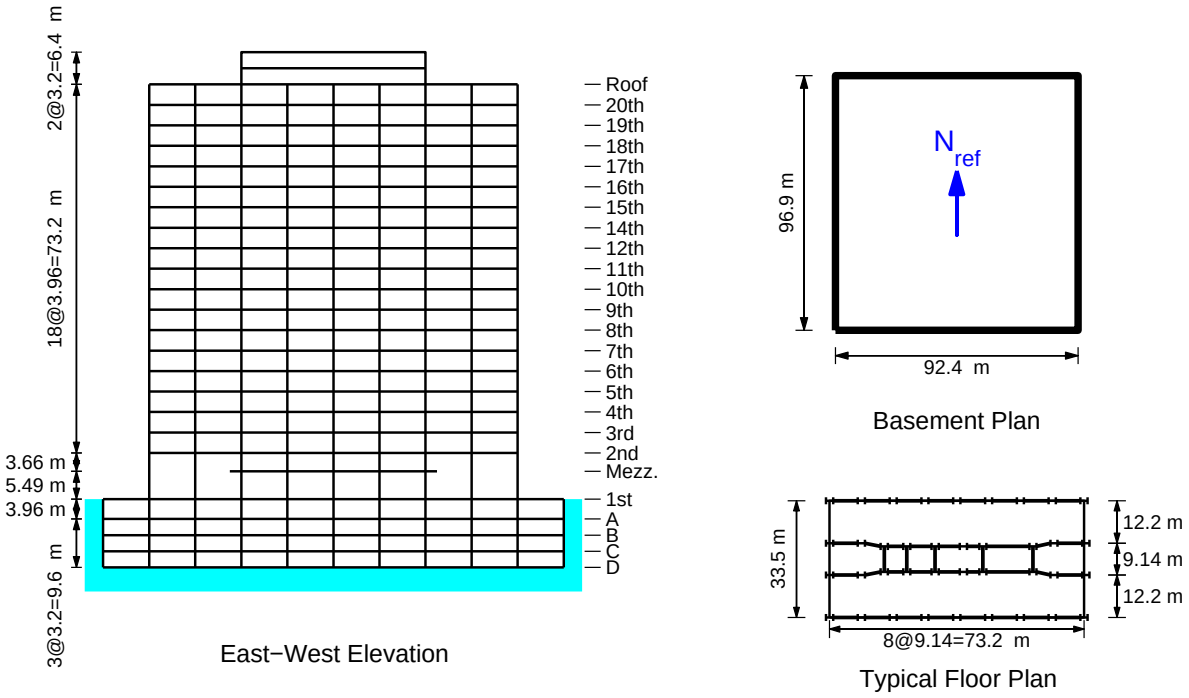

Figure 2.4. Elevation and plan of 19-Story Office Building in Los Angeles.

Table 2.2. Selected ground motions.

Serial No.	Station Name	Earthquake	Mag.	Epic. Dist. (km)	PGA (H1, H2, V) - g	PGV (H1, H2, V) - cm/s
1	Parkfield-Fault Zone 1	Parkfield, September 28, 2004	6.0	9	0.59, 0.82, 0.26	63, 81, 10
2	Parkfield-Fault Zone 14	Parkfield, September 28, 2004	6.0	12	1.31, 0.54, 0.56	83, 42, 23
3	Templeton-1-story Hospital GF	San Simeon, December 22, 2003	6.5	38	0.42, 0.46, 0.26	33, 27, 16
4	Amboy	Hector Mine, October 16, 1999	7.1	48	0.15, 0.18, 0.13	20, 27, 12
5	Taiwan-CHY028	Chi-Chi, September 21, 1999	7.6	7 to fault	0.82, 0.65, 0.34	67, 72, 36
6	Taiwan-TCU129	Chi-Chi, September 21, 1999	7.6	1 to fault	0.63, 1.01, 0.34	36, 60, 35
7	Taiwan-TCU068	Chi-Chi, September 21, 1999	7.6	1 to fault	0.46, 0.56, 0.49	176, 263, 187
8	Taiwan-CHY028	Chi-Chi, September 21, 1999	7.6	10 to fault	0.42, 1.16, 0.34	46, 115, 25
9	Sylmar-County Hospital Lot	Northridge, January 17, 1994	6.7	16	0.59, 0.83, 0.53	77, 129, 19
10	Newhall-LA County Fire Station	Northridge, January 17, 1994	6.7	20	0.57, 0.58, 0.54	75, 95, 31
11	Los Angeles-Rinaldi Rec. Station FF	Northridge, January 17, 1994	6.7	9	0.47, 0.83, 0.83	166, 73, 51
12	Santa Monica-City Hall Grounds	Northridge, January 17, 1994	6.7	23	0.88, 0.37, 0.23	42, 25, 14
13	Lucerne Valley	Landers, June 28, 1992	7.4	1 to fault	0.72, 0.78, 0.82	98, 32, 46
14	Yermo-Fire Station	Landers, June 28, 1992	7.4	84	0.15, 0.24, 0.13	29, 51, 13
15	Big Bear Lake-Civic Center Grounds	Big Bear, June 28, 1992	6.5	11	0.48, 0.55, 0.19	28, 34, 11
16	Petrolia-Fire Station	Cape Mendocino, April 26, 1992	6.6	35	0.59, 0.43, 0.15	61, 30, 13
17	Petrolia-Fire Station	Petrolia, April 25, 1992	7.1	8	0.65, 0.58, 0.16	90, 48, 21
18	Cape Medocino	Petrolia, April 25, 1992	7.1	11	1.04, 1.50, 0.75	41, 126, 60
19	Rio Dell-Hwy101/Painter Street	Petrolia, April 25, 1992	7.1	18	0.39, 0.55, 0.20	45, 43, 10

	Overpass FF					
20	Corralitos-Eureka Canyon Road	Loma Prieta, October 17, 1989	7.0	7	0.48, 0.63, 0.44	48, 55, 19
21	Los Gatos-Linahan Dam Left Abutment	Loma Prieta, October 17, 1989	7.0	19	0.40, 0.44, 0.13	95, 84, 26
22	Saratoga-Aloha Ave.	Loma Prieta, October 17, 1989	7.0	4	0.32, 0.49, 0.35	44, 41, 26
23	El Centro-Imperial County Center Grounds	Superstition Hills, November 24, 1987	6.6	36	0.26, 0.34, 0.12	41, 47, 8
24	Los Angeles-Obregon Park	Whittier, October 1, 1987	6.1	10	0.43, 0.41, 0.13	22, 13, 5
25	Chalfant-Zack Ranch	Chafant Valley, July 21, 1986	6.4	14	0.40, 0.44, 0.30	43, 36, 12
26	El Centro-Array #6	Imperial Valley, October 15, 1979	6.6	1 to fault	0.43, 0.37, 0.17	109, 63, 56
27	El Centro-Array #7	Imperial Valley, October 15, 1979	6.6	1 to fault	0.45, 0.33, 0.50	108, 45, 26
28	El Centro-Imperial County Center Grounds	Imperial Valley, October 15, 1979	6.6	28	0.24, 0.21, 0.24	64, 36, 17
29	El Centro-Hwy8/Meloland Overpass FF	Imperial Valley, October 15, 1979	6.6	19	0.31, 0.29, 0.23	72, 91, 29
30	El Centro-Irrigation District	El Centro, May 18, 1940	6.9	17	0.34, 0.21, 0.21	33, 37, 11

CHAPTER 3. ANALTYICAL MODELS

The three-dimensional analytical models of the selected buildings were developed using the structural analysis software Open System for Earthquakes Engineering Simulation (*OpenSees*) (McKenna and Fenves, 2001) and *Perform3D* (CSI, 2006). This chapter presents the modeling procedures and assumptions.

20-Story Hotel in North Hollywood

OpenSees Model

The beams and columns for the North Hollywood Hotel were modeled with *beamWithHinges* element in *OpenSees*. This element used fiber section containing confined concrete, unconfined concrete, and steel reinforcing bars. The stress-strain behavior of concrete, both confined and confined, was modeled with several different available concrete materials in *OpenSees*. The first concrete material model used in this investigation is *Concrete01* (Figure 3.1a) which has residual strength after crushing strain. The second model is a modified version of the *Concrete01* model (Figure 3.1b) which has no residual strength after reaching crushing strain. Further details of these two material models are available in Mander et al. (1988) and Karson and Jirsa (1969). The third concrete model is *Concrete04* which is similar to the modified *Concrete01* model but uses slightly different parameters (see Popovics, 1973 for details). The crushing strain of the unconfined concrete was selected to be equal to 0.004 and that for confined concrete was selected to be that corresponding to the rupture of confining steel using the well established Mander model (Mander et al., 1988). The stress-strain behavior of steel was modeled with *ReinforcingSteel* material in *OpenSees* (Figure 3.1c). The strength of concrete and steel was selected based on the values specified in the structural drawings. The P-Delta effects were included in the pushover analysis and the RHA by applying the gravity loads prior to pushover analysis or RHA.

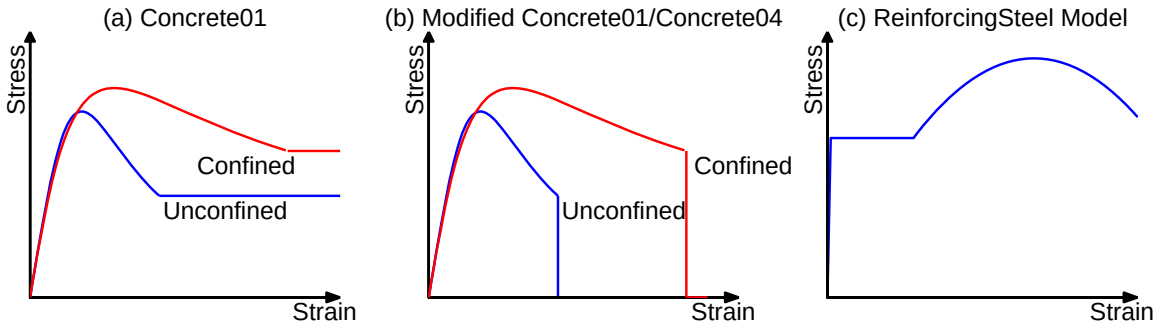

Figure 3.1. OpenSees material models: (a) Concrete01 model; (b) Modified *Concrete01* and *Concrete04* models; and (c) *ReinforcingSteel* model.

Perfrom3D Model

In the *Perform3D* model, beams were modeled with FEMA Concrete Beam with strength loss and unsymmetrical section strength, columns were modeled with FEMA Concrete Column with strength loss and symmetrical section strength, and basement shear walls were modeled with linear elastic column elements. The FEMA Beam element requires moment-plastic-rotation relationship of Figure 3.2a. The yield moment of the beam section needed to define the FEMA force-deformation behavior is computed from section moment-curvature analysis using computer program *XTRACT* (TRC, 2008).

The plastic rotation values and the residual strength needed for the FEMA Concrete Beam model in *Perform3D* are selected as per FEMA-356 (ASCE, 2000) recommendations: plastic rotations are selected as 0.02 for point U and 0.03 for point X, and the residual strength for points R and X are selected as 20% of the yield moment (Figure 3.2a). The plastic rotation value for point R is selected as 0.022 to model gradual strength loss between points U and R.

The FEMA Concrete Column with strength loss element requires moment-plastic-rotation behavior (Figure 3.2a), P-M interaction diagram for bending about axis-2 and axis-3 (Figure 3.2b), and M-M interaction diagram between moments about axis-2 and axis-3 (Figure 3.2c). The yield moment needed to define the force-deformation behavior (Figure 3.2a) was

obtained from *XTRACT* moment-curvature analyses of column sections about axis-2 and axis-3. Similarly, the parameters needed to define P-M interaction diagrams about axis-2 and axis-3 (Figure 3.2b) were estimated from *XTRACT* P-M interaction analyses of columns sections. The shapes of the P-M interaction diagrams (Figure 3.2b) and M-M interaction diagram (Figure 3.2c) were defined using default values of various exponents in *Perform3D*. The material models used for columns in *XTRACT* analysis were the same as for beams.

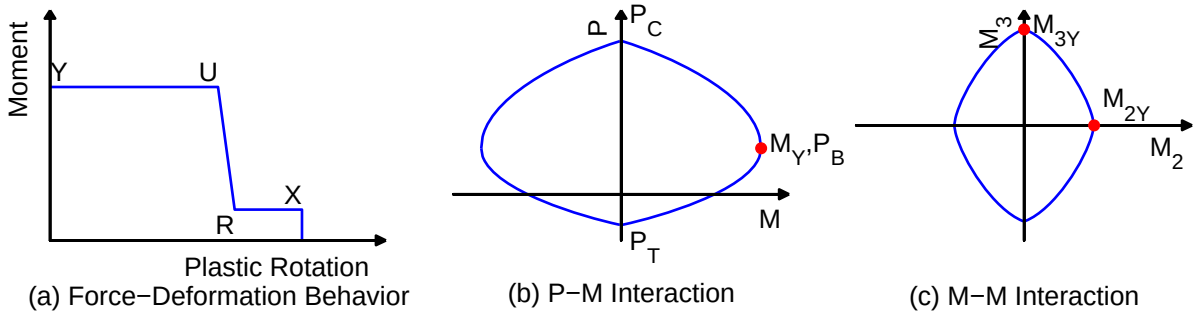

Figure 3.2. FEMA concrete beam/column element in *Perform3D*: (a) Force-deformation behavior of beam or column, (b) P-M interaction diagram for column; and (c) M-M interaction diagram for column.

Similar to the beams, the plastic rotation values and the residual strength needed for the FEMA Concrete Column model in *Perform3D* are selected as per FEMA-356 recommendations: plastic rotations are selected as 0.02 for point U and 0.03 for point X, and the residual strength for points R and X are selected as 20% of the yield moment (Figure 3.2a). The plastic rotation value for point R is selected as 0.022 to model gradual strength loss between points U and R.

19-Story Office Building in Los Angeles

OpenSees Model

In *OpenSees* model of the Los Angeles building, the beams and columns were modeled with *nonlinearBeamColumn* elements, and braces were modeled with nonlinear *truss* elements between 1st floor and roof; and beams, columns, and shear walls were modeled with linear *elasticBeamColumn* elements and braces were modeled with linear *truss* elements in the

basement. The *nonlinearBeamColumn* element used fiber steel sections with stress-strain behavior of steel fibers modeled with *ReinforcingSteel* material in *OpenSees* (Figure 3.1c). The nonlinear *truss* elements were modeled with *Hysteretic* material in *OpenSees* (Figure 3.3). This material model assumed that the stress linearly reduces to zero from the bucking stress at strain value equal to twice the buckling strain; the buckling stress was computed from Euler's Buckling stress formulation. It is useful to note that *OpenSees* does not have an explicit buckling model for steel braces; the buckling options in the *ReinforcingSteel* material are designed only for reinforcing bars in reinforced-concrete beams and columns and can not be conveniently used for steel braces.

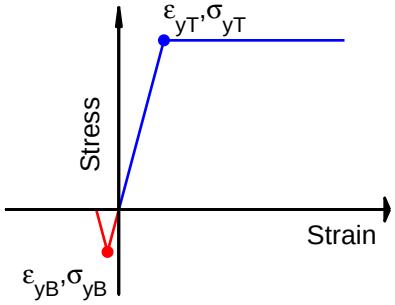

Figure 3.3. *OpenSees* material model for nonlinear *truss* element.

Perfrom3D Model

In the *Perform3D* model of the Los Angeles building, beams were modeled with FEMA Steel Beam with strength loss and symmetrical section strength, columns were modeled with FEMA Steel Column with strength loss and symmetrical section strength, shear walls were modeled with linear elastic column elements, and braces were modeled with Simple Bar element. The material properties for braces were specified by Inelastic Steel Buckling material in *Perform3D*. The FEMA Steel Beam element requires moment-plastic-rotation relationship of Figure 3.4a. The yield moment of the steel beam section was computed automatically by *Perform3D* using section properties and steel strength. The plastic rotation values and the

residual strength needed for the FEMA Steel Beam model in *Perform3D* are selected as per FEMA-356 recommendations: plastic rotations are selected as $9\theta_y$ for point U and $11\theta_y$ for point X in which θ_y is the yield rotation, and the residual strength for points R and X are selected as 60% of the yield moment (Figure 3.4a). The plastic rotation value for point R is selected as $9.5\theta_y$ to model gradual strength loss between points U and R.

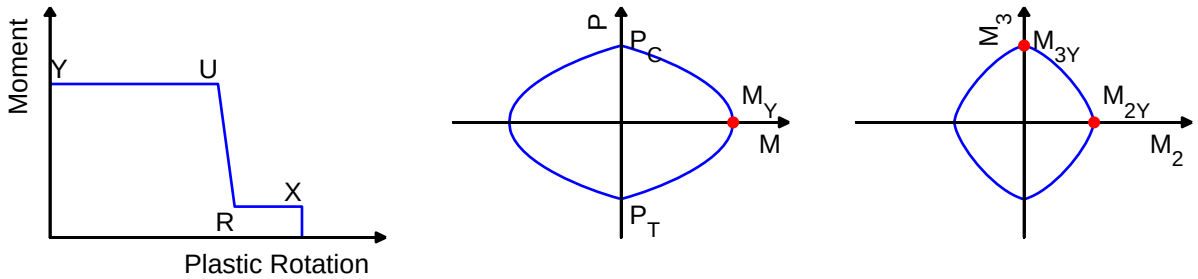

(a) Force−Deformation Behavior (b) P−M Interaction (c) M−M Interaction

Figure 3.4. FEMA steel beam/column element in Perform3D: (a) Force-deformation behavior of beam or column, (b) P-M interaction diagram for column; and (c) M-M interaction diagram for column.

The FEMA Steel Column with strength loss element requires moment-plastic-rotation behavior of Figure 3.4a, P-M interaction diagram for bending about axis-2 and axis-3 (Figure 3.4b), and M-M interaction diagram between moments about axis-2 and axis-3 (Figure 3.4c). The yield moment needed to define the force-deformation behavior (Figure 3.4a) was automatically computed by *Perform3D* based on section properties and material strength. Similar to the beams, the plastic rotation values and the residual strength needed for the FEMA Steel Column model in *Perform3D* are selected as per FEMA-356 recommendations: plastic rotations are selected as $9\theta_y$ for point U and $11\theta_y$ for point X in which θ_y is the yield rotation, and the residual strength for points R and X are selected as 60% of the yield moment (Figure 3.4a). The shapes of the P-M interaction diagrams (Figure 3.4b) and M-M interaction diagram (Figure 3.4c) were also automatically generated in *Perform3D* based on the specified section properties and

material strength.

CHAPTER 4. PUSHOVER CURVES

Pushover curves for the selected buildings were developed for transverse and longitudinal direction using height-wise distribution of lateral loads proportional to the first mode in each direction. These curves are presented in this chapter.

20-Story Hotel in North Hollywood

Figure 4.1 compares the pushover curves for the North Hollywood Hotel computed from *OpenSees* and *Perform3D*. This comparison indicates that the two programs lead to pushover curves that may differ significantly. The two programs provide essentially identical pushover curves for first transverse and longitudinal modes in the initial elastic region (Figures 4.1a and 4.1b). Thereafter, the pushover curves from the two programs differ significantly. The pushover curves from *Perfom3D* exhibit early initiation of nonlinear action, much lower yield strength, and significant post yielding strength loss compared to the pushover curves from *OpenSees* (Figures 4.1a and 4.1b). This is the case because *Perform3D* used FEMA-356 models for force-deformation behavior of beams and columns with strength loss (see Figure 3.2a) whereas *OpenSees* used fiber section models for beams and columns with concrete and steel material properties defined by Figure 3.1a and 3.1c, respectively. As elements begin to yield and loose strength during pushover analysis, pushover curves from *Perform3D* would begin to yield earlier, would have lower strength, and would show strength loss as more and more elements are deformed beyond point *U* on the force-deformation relationship (see Figure 3.2a). On the other hand, the elements in the *OpenSees* model continue to support the load because of gradual spread of plasticity over the member fiber section.

One major concern with the original *OpenSees* model is that the concrete model (*Concrete01*) did not adequately represent concrete crushing, i.e., the concrete fibers continue to support stresses even after crushing strain (see Figure 3.1a). Therefore, two other material

models were considered that adequately address this issue: a modified version of *Concrete01* and *Concrete04* material model with no residual strength after crushing strain (see Figure 3.1b). The pushover curves were generated from OpenSees with these two additional material models and are compared in Figure 4.2 with those from the original model. These results indicate that the concrete material model has minimal effect on the pushover curves as the pushover curves for all material models are essentially identical.

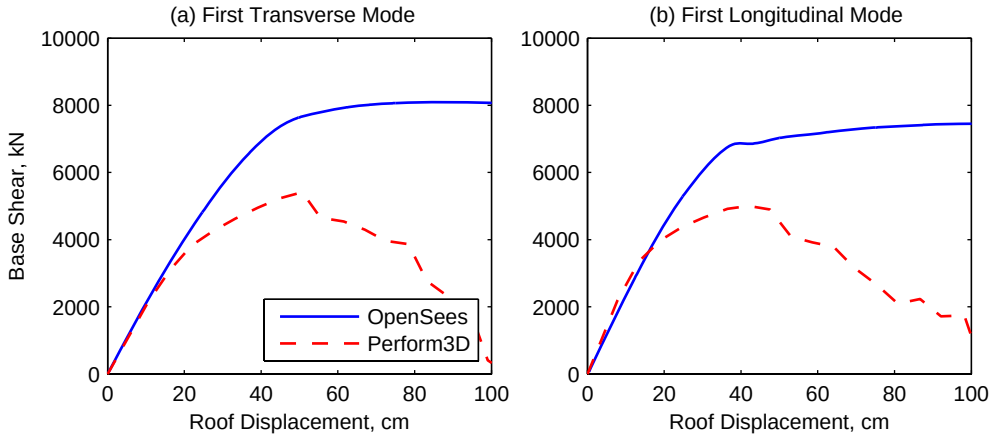

Figure 4.1. Comparison of pushover curves from *OpenSees* and *Perform3D* for 20-Story Hotel in North Hollywood.

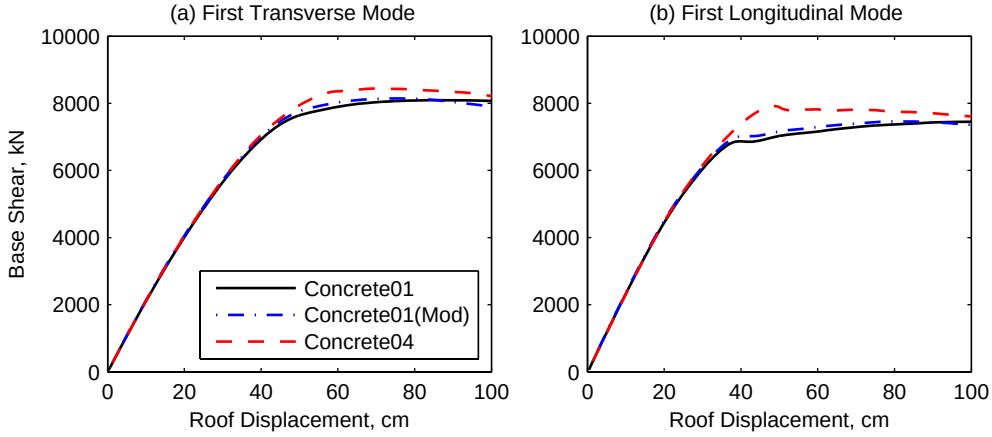

Figure 4.2. Comparison of "modal" pushover curves from *OpenSees* for three different concrete material models – *Concrete01*, modified *Concrete01*, and *Concrete04* – for 20-Story Hotel in North Hollywood.

Since the original *Perform3D* model modeled beams and columns with strength loss,

which is quite different from the *OpenSees* modeling, a second *Perform3D* model was developed in which no strength loss was considered, i.e., the moment in the force-deformation behavior of beams and columns retained the yield moment value even after point *U* (Figure 3.2a). The pushover curves from the revised *Perform3D* model are compared in Figure 4.3 with those from the *OpenSees* model. These results indicate that pushover curves from *Perform3D* exhibit lower strength in several modes but no strength loss when compared to pushover curves from *OpenSees* (Figures 4.3a and 4.3b).

The results of Figure 4.3 also lead to another important observation: the models based on concentrated plasticity may lead to lower estimate of building strength than models based on spread plasticity. It is useful to recall that *Perform3D* model is based on concentrated plasticity as it uses a concentrated hinge at the beam-column ends and elastic behavior in-between. The *OpenSees* model on the other hand is a spread plasticity model as the nonlinear action spreads gradually across the beam-column section as material fibers undergo increasing stresses and strains.

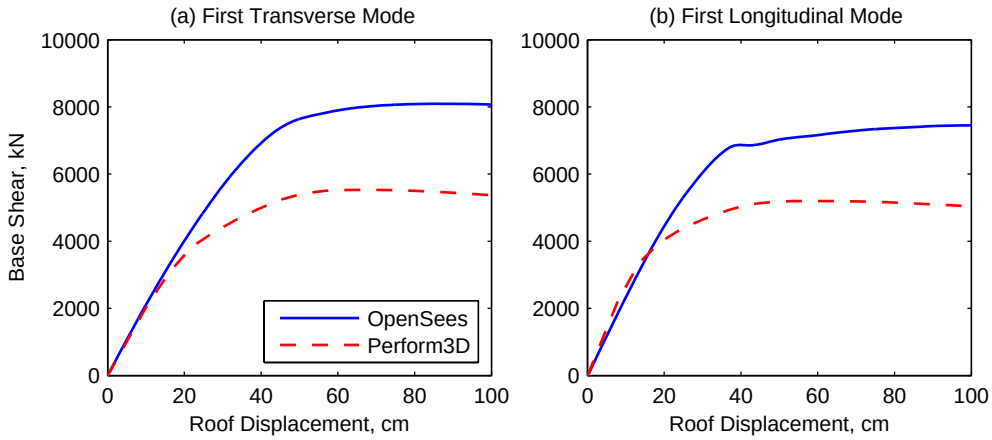

Figure 4.3. Comparison of pushover curves from *OpenSees* and *Perform3D* for 20-Story Hotel in North Hollywood; *Perform3D* results are using no strength loss model for beams and columns.

19-Story Office Building in Los Angeles

Figure 4.4 compares the pushover curves for the Los Angeles Office Building computed

from *OpenSees* and *Perform3D*. It is useful to recall that the lateral load resisting system in this building consists of steel moment resisting frames in the longitudinal direction and concentric braced frames in the transverse direction. This comparison also indicates that the two programs lead to pushover curves that differ significantly. In the transverse direction, the direction in which lateral load resisting system consists of concentric braced frames, *Perform3D* provides pushover curves that has slightly lower strength and much earlier initiation of nonlinear action compared to the curves from *OpenSees* (Figures 4.4a). The pushover curve from *Perform3D* also exhibits post yield strength loss whereas that from *OpenSees* does not show strength loss (Figure 4.4a).

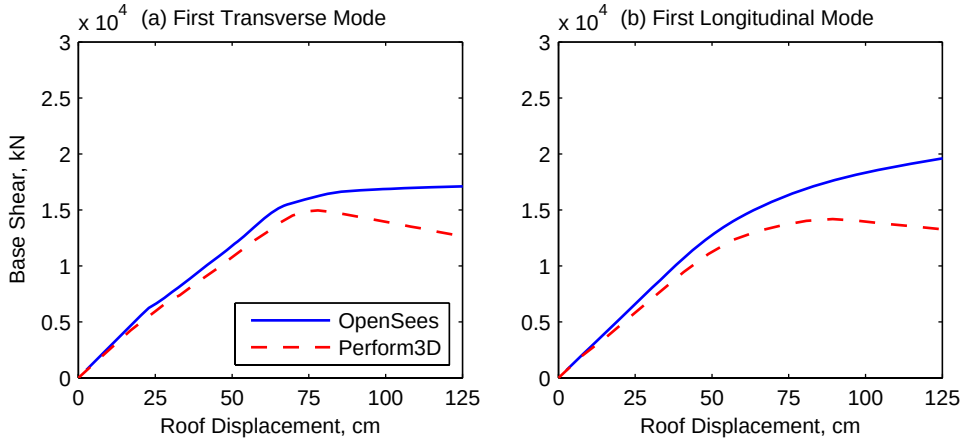

Figure 4.4. Comparison of "modal" pushover curves from *OpenSees* and *Perform3D* for 19-Story Office Building in Los Angeles.

In the longitudinal direction, the direction in which lateral load resisting system consists of moment resisting frames, *Perform3D* led to pushover curves with lower strength and earlier initiation of nonlinear action compared to *OpenSees* (Figures 4.4b). The pushover curve from *Perform3D* also exhibits post yielding strength loss (Figure 4.4b). As noted previously for the North Hollywood building, these differences in the longitudinal pushover curves are due to different modeling assumptions in the two programs: *Perform3D* used FEMA-356 models for force-deformation behavior of beams and columns with strength loss (see Figures 3.3a) whereas

OpenSees used fiber section models for beams and columns with concrete and steel material properties defined by Figure 3.1c, respectively.

Effects of Modeling Assumptions and Software on Pushover Curves

The results presented so far indicate that modeling assumptions may significantly affect the pushover curves: (1) The concentrated plasticity model leads to lower strength, early initiation of yielding, and post yielding strength loss in pushover curves compared to spread plasticity model; and (2) Consideration of strength loss in beam/column model leads to significant strength loss in the pushover curve. The concrete material model, on the other hand, appears to have minimal effect on the pushover curves of reinforced concrete buildings.

The pushover curves may also depend on the software that is used for analysis. While most of the differences may be attributed to differences in modeling options available in different programs (e.g., *OpenSees* does not have an option for modeling FEMA-356 force-deformation behavior with strength loss whereas *Perform3D* does), some differences may also occur due to differences in solution schemes and convergence criteria.

CHAPTER 5. COMPARISON OF RESPONSES FROM RHA

Responses – floor displacements, floor accelerations, and base shear – of the two selected buildings were computed for the suite of 30 selected ground motions using *OpenSees* and *Perform3D*; results are included in Appendix II. A convergence summary of the these analyses is presented in Table 5.1 for the North Hollywood Hotel and Table 5.2 for the Los Angeles Building. This summary indicates that the selected buildings undergo excessive deformation due to several of the selected ground motions. For such ground motions, these buildings are likely to collapse. This summary also indicates that *OpenSees* has much more convergence problem compared to *Perform3D*. While *Perform3D* failed to converge only for a few cases where the building is likely to collapse, *OpenSees* failed to converge even for some cases where the building is not likely to collapse. For these cases, *OpenSees* failed to converge even when different solution strategies were used. *Perform3D*, on the other hand, converged even for some of the cases where building is likely collapse. It is useful to note that *OpenSees* models of the two selected buildings are much more complex compared to *Perform3D* models; *OpenSees* models used fiber section modeling whereas *Peform3D* used concentrated plasticity modeling for beams and columns.

Table 5.1. Convergence summary of RHA results for 20-Story North Hollywood Hotel.

Eq.	Station Name	Earthquake	OpenSees	Perform3D	Comment
1	Parkfield-Fault Zone 1	Parkfield, 9/28/04	Convergence	Convergence	
2	Parkfield-Fault Zone 14	Parkfield, 9/28/04	Convergence	Convergence	
3	Templeton-1-story Hospital GF	San Simeon, 12/22/03	Convergence	Convergence	
4	Amboy	Hector Mine, 10/16/99	Convergence	Convergence	
5	Taiwan-CHY028	Chi-Chi, 9/21/99	Analysis stops	Convergence	
6	Taiwan-TCU129	Chi-Chi, 9/21/99	Convergence	Convergence	
7	Taiwan-TCU068	Chi-Chi, 9/21/99	Analysis stops	Analysis stops	Building collapse
8	Taiwan-CHY028	Chi-Chi, 9/21/99	Analysis stops	Convergence	Excessive def. in trans. direction
9	Sylmar-County Hospital Lot	Northridge, 1/17/94	Analysis stops	Convergence	Excessive def. in trans. direction
10	Newhall-LA County Fire Station	Northridge, 1/17/94	Analysis stops	Analysis stops	Excessive def. in trans. direction
11	Los Angeles-Rinaldi Rec. Station FF	Northridge, 1/17/94	Analysis stops	Convergence	Excessive def. in both direction
12	Santa Monica-City Hall Grounds	Northridge, 1/17/94	Convergence	Convergence	
13	Lucerne Valley	Landers, 6/28/92	Analysis stops	Analysis stops	Building collapse
14	Yermo-Fire Station	Landers, 6/28/92	Convergence	Convergence	
15	Big Bear Lake-Civic Center Grounds	Big Bear, 6/28/92	Convergence	Convergence	
16	Petrolia-Fire Station	Cape Mendocino, 4/26/92	Analysis stops	Convergence	
17	Petrolia-Fire Station	Petrolia, 4/25/92	Analysis stops	Convergence	Excessive def. in long. direction

18	Cape Medocino	Petrolia, 4/25/92	Analysis stops	Convergence	Excessive def. in trans. direction
19	Rio Dell-Hwy101/Painter Street Overpass FF	Petrolia4/25/92	Analysis stops	Convergence	
20	Corralitos-Eureka Canyon Road	Loma Prieta, 10/17/89	Convergence	Convergence	
21	Los Gatos-Linahan Dam Left Abutment	Loma Prieta, 10/17/89	Analysis stops	Convergence	Excessive def. in long. direction
22	Saratoga-Aloha Ave.	Loma Prieta, 10/17/89	Convergence	Convergence	
23	El Centro-Imperial County Center Grounds	Superstition Hills, 11/24/87	Convergence	Convergence	
24	Los Angeles-Obregon Park	Whittier, 10/1/87	Convergence	Convergence	
25	Chalfant-Zack Ranch	Chafant Valley, 7/21/86	Convergence	Convergence	
26	El Centro-Array #6	Imperial Valley, 10/15/79	Analysis stops	Analysis stops	Building collapse
27	El Centro-Array #7	Imperial Valley, 10/15/79	Analysis stops	Convergence	Excessive def. in trans. direction
28	El Centro-Imperial County Center Grounds	Imperial Valley, 10/15/79	Analysis stops	Convergence	Excessive def. in trans. direction
29	El Centro-Hwy8/Meloland Overpass FF	Imperial Valley, 10/15/79	Analysis stops	Analysis stops	Building collapse
30	El Centro-Irrigation District	El Centro, 5/18/40	Convergence	Convergence	

Table 5.2. Summary of RHA results for 19-Story Office Building in Los Angeles.

Eq.	Station Name	Earthquake	OpenSees	Perform3D	Comment
1	Parkfield-Fault Zone 1	Parkfield, 9/28/04	Convergence	Convergence	
2	Parkfield-Fault Zone 14	Parkfield, 9/28/04	Convergence	Convergence	
3	Templeton-1-story Hospital GF	San Simeon, 12/22/03	Convergence	Convergence	
4	Amboy	Hector Mine, 10/16/99	Convergence	Convergence	
5	Taiwan-CHY028	Chi-Chi, 9/21/99	Analysis stops	Convergence	
6	Taiwan-TCU129	Chi-Chi, 9/21/99	Analysis stops	Convergence	
7	Taiwan-TCU068	Chi-Chi, 9/21/99	Analysis stops	Analysis stops	Building collapse
8	Taiwan-CHY028	Chi-Chi, 9/21/99	Analysis stops	Convergence	Excessive def. in trans. direction
9	Sylmar-County Hospital Lot	Northridge, 1/17/94	Convergence	Convergence	Excessive def. in trans. direction
10	Newhall-LA County Fire Station	Northridge, 1/17/94	Convergence	Convergence	Excessive def. in trans. direction
11	Los Angeles-Rinaldi Rec. Station FF	Northridge, 1/17/94	Convergence	Convergence	Excessive def. in trans. direction
12	Santa Monica-City Hall Grounds	Northridge, 1/17/94	Convergence	Convergence	
13	Lucerne Valley	Landers, 6/28/92	Convergence	Convergence	Excessive def. in long. direction
14	Yermo-Fire Station	Landers, 6/28/92	Convergence	Convergence	
15	Big Bear Lake-Civic Center Grounds	Big Bear, 6/28/92	Convergence	Convergence	
16	Petrolia-Fire Station	Cape Mendocino, 4/26/92	Convergence	Convergence	
17	Petrolia-Fire Station	Petrolia, 4/25/92	Convergence	Convergence	Excessive def. in trans. direction

18	Cape Medocino	Petrolia, 4/25/92	Convergence	Convergence	Excessive def. in trans. direction
19	Rio Dell-Hwy101/Painter Street Overpass FF	Petrolia4/25/92	Convergence	Convergence	
20	Corralitos-Eureka Canyon Road	Loma Prieta, 10/17/89	Convergence	Convergence	
21	Los Gatos-Linahan Dam Left Abutment	Loma Prieta, 10/17/89	Convergence	Convergence	
22	Saratoga-Aloha Ave.	Loma Prieta, 10/17/89	Convergence	Convergence	
23	El Centro-Imperial County Center Grounds	Superstition Hills, 11/24/87	Convergence	Convergence	
24	Los Angeles-Obregon Park	Whittier, 10/1/87	Convergence	Convergence	
25	Chalfant-Zack Ranch	Chafant Valley, 7/21/86	Convergence	Convergence	
26	El Centro-Array #6	Imperial Valley, 10/15/79	Analysis stops	Convergence	Excessive def. in both directions
27	El Centro-Array #7	Imperial Valley, 10/15/79	Analysis stops	Convergence	Excessive def. in trans. direction
28	El Centro-Imperial County Center Grounds	Imperial Valley, 10/15/79	Convergence	Convergence	Excessive def. in trans. direction
29	El Centro-Hwy8/Meloland Overpass FF	Imperial Valley, 10/15/79	Convergence	Convergence	Excessive def. in both directions
30	El Centro-Irrigation District	El Centro, 5/18/40	Convergence	Convergence	

The differences in the peak floor displacements, accelerations, and base shear from the two programs are investigated next by examining height-wise variation of the ratio of peak floor displacements, u_{OS}/u_{P3D}, peak floor accelerations, a_{OS}/a_{P3D}, and peak base shear, V_{OS}/V_{P3D},

from *OpenSees* and *Perform3D*. The results are presented in Figures 5.1 to 5.6 for earthquakes for which the building did not to collapse. The results for the North Hollywood Hotel are for the *OpenSees* model which used *Concrete01* material model with residual strength and *Perform3D* model with beams and columns modeled with FEMA-356 force-deformation behavior with strength loss. The other two concrete models – *Concrete01* without residual strength and *Concrete04* model – led to responses similar to the *Concrete01* material model with residual strength when the solution converged. However, *OpenSees* model with these two concrete materials experienced much more convergence problem compared to the model with *Concrete01* material with residual strength. The results for the Los Angeles Building are for the *OpenSees* Model with *Hysteretic* steel material for braces to capture post-buckling strength loss and for the *Perform3D* model with beams and columns modeled with FEMA-356 force-deformation behavior with strength loss.

The presented results include variation of the ratios for individual earthquakes along with the median values and median plus/minus one standard deviation. Median is an indicator of *OpenSees* over or under predicting response compared to *Perform3D* whereas the band formed by median plus/minus one standard deviation is an indicator of the dispersion in the response prediction.

20-Story Hotel in North Hollywood

The median of displacement ratios in Figure 5.1 for the North Hollywood Hotel indicates that *OpenSees* tends to provide larger estimate of displacements in lower and upper floors and about the same estimates of displacements in middle floors compared to the *Perform3D*. The difference in median value of the displacement ratio in upper and lower floors varies from 1.1 to 1.4 indicating that the response from the two programs can differ by 10% to 40%. The width of

the median+σ or median-σ band is about 0.15 implying that there is about 15% dispersion in the response prediction from the two programs.

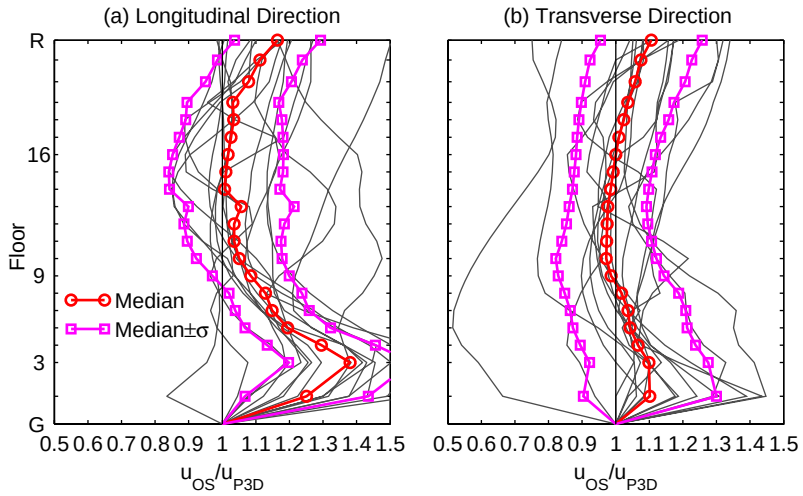

Figure 5.1. Height wise variation of ratio of peak floor displacements from *OpenSees* and *Perform3D* for North Hollywood Hotel.

The median of acceleration ratios in Figure 5.2 show that the *OpenSees* generally provides comparable estimates of floor accelerations throughout the building height as those from *Perform3D*: the median of the floor accelerations ratio is very close to one. The exception may occur at a few floors where the ratio may differ from one by 0.05 to 0.15, e.g., 2nd floor and roof in the longitudinal direction (Figure 5.2a). The width of the median+σ or median-σ band for floor accelerations varies from 0.05 (Figure 5.2b) to 0.1 (Figure 5.2a) implying that there is 5% to 10% dispersion in the response prediction from the two programs.

The median of ratio in Figure 5.3 shows that the *OpenSees* generally provides comparable estimates of base shear to that from *Perform3D*: the median of the base shear ratio is very close to one. The width of the median+σ or median-σ band is about 0.1 implying that there is 10% dispersion in the response prediction from the two programs.

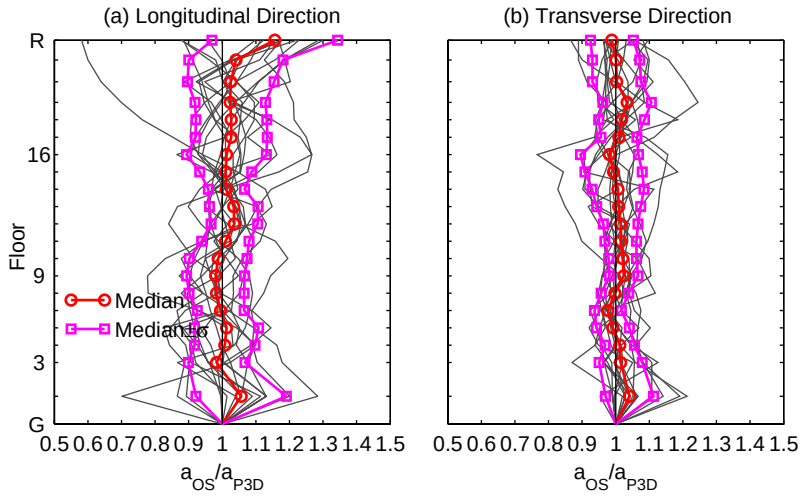

Figure 5.2. Height wise variation of ratio of peak floor accelerations from *OpenSees* and *Perform3D* for North Hollywood Hotel.

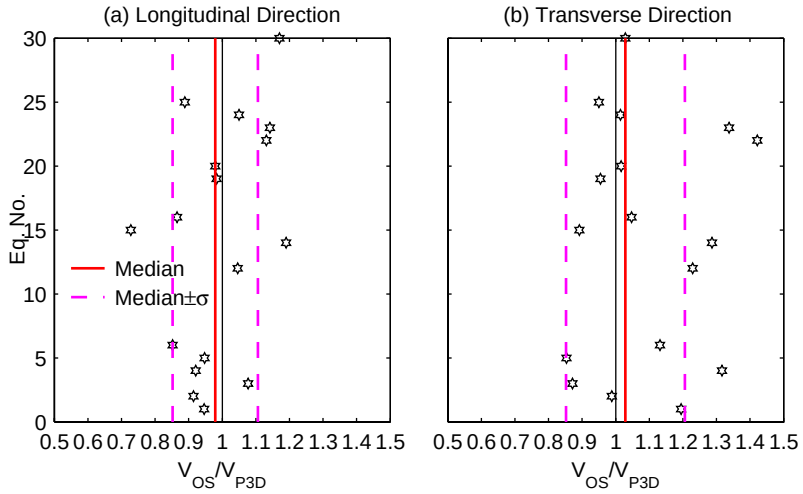

Figure 5.3. Ratio of base shear from *OpenSees* and *Perform3D* for North Hollywood Hotel.

19-Story Office Building in Los Angeles

The median of displacement ratios in Figure 5.4 for the Los Angeles Building indicates that *OpenSees* tends to provide larger estimate of displacements throughout the building height in the longitudinal direction (Figure 5.4a) and in upper floors in the transverse direction (Figure 5.4b) compared to the *Perform3D*. The difference in median value of the displacement ratio in upper and lower floors varies from 1.05 to 1.1 indicating that the response from the two programs can differ by 5% to 10%. The width of the median+σ or median-σ band is about 0.1

implying that there is 10% dispersion in the response prediction from the two programs.

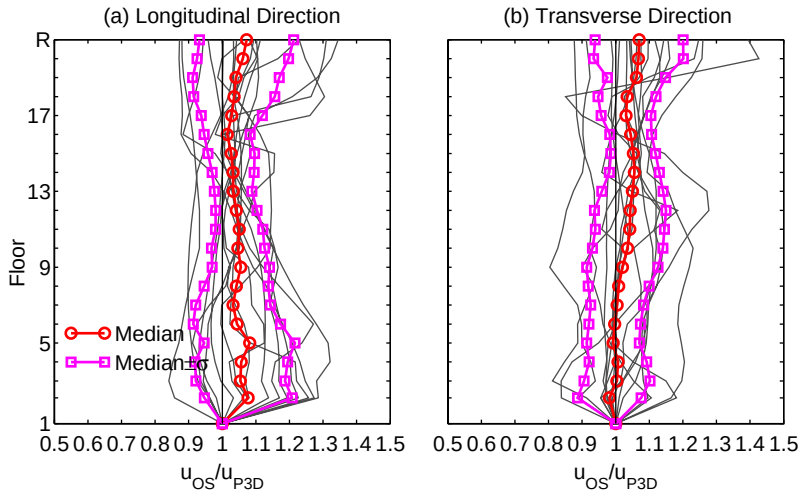

Figure 5.4. Height wise variation of ratio of peak floor displacements from *OpenSees* and *Perform3D* for Los Angeles Building.

The median of acceleration ratios in Figure 5.5 show that the *OpenSees* generally provides comparable estimates of upper floor accelerations as those from *Perform3D*: the median of the floor accelerations ratio is very close to one. For lower floors, where a soft story condition occurs in the Los Angeles building due to taller story height, the ratio may differ from one by 0.1 to 0.25, e.g., 2nd floor (Figures 5.5a and 5.5b). The width of the median+σ or median-σ band for floor accelerations varies from 0.05 (Figure 5.5a) to 0.1 (Figure 5.5b) implying that there is 5% to 10% dispersion in the response prediction from the two programs.

The median of ratio in Figure 5.6 show that the *OpenSees* provides lower base shear in the longitudinal direction and comparable base shear in transverse direction than that from *Perform3D*. The width of the median+σ or median-σ band varies from 0.05 to 0.1 implying that there is 5% to 10% dispersion in the response prediction from the two programs.

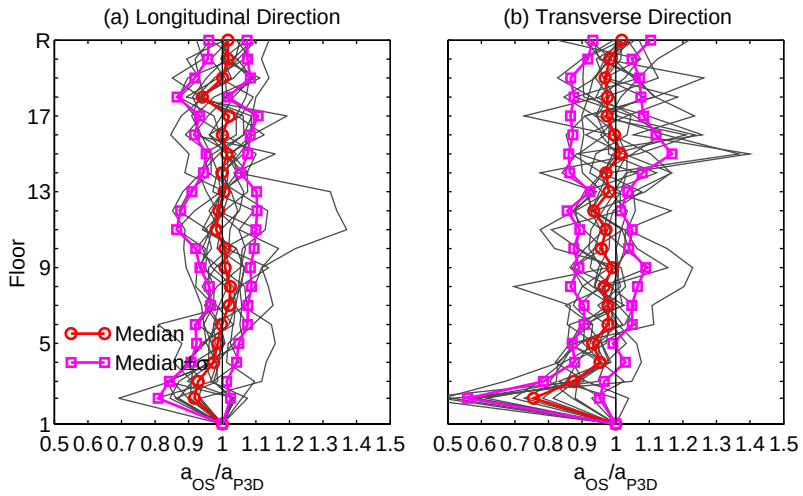

Figure 5.4. Height wise variation of ratio of peak floor accelerations from *OpenSees* and *Perform3D* for Los Angeles Building.

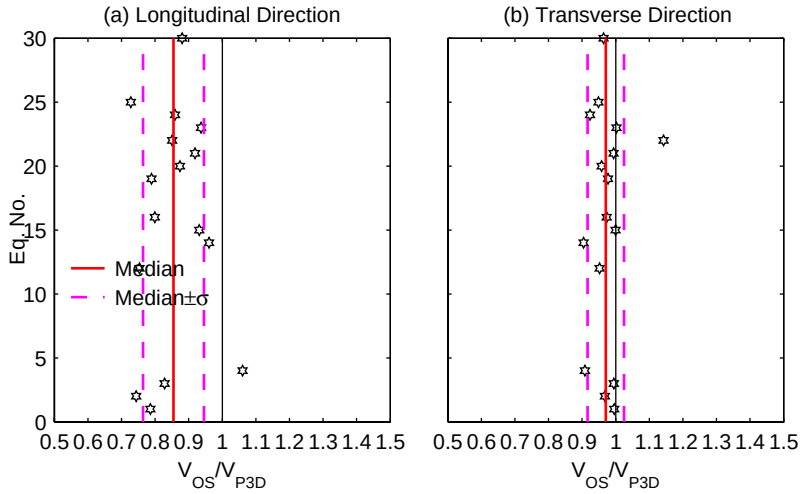

Figure 5.6. Ratio of peak base shear from *OpenSees* and *Perform3D* for Los Angeles Building.

Effects of Software on Peak Response from RHA

The results presented so far indicate that there can be 10% to 40% difference in prediction of median peak response from different software. The difference is much higher for reinforced concrete building compared to the steel building, and in median prediction of floor displacements compared to prediction of floor accelerations and base shear. It is useful to recall that *OpenSees* used a fiber section model which captured spread of inelastic action over the member section whereas *Perform3D* used a FEMA-356 type concentrated plastic hinge with

strength loss. Therefore, larger variability in the response prediction for the reinforced concrete building appears to be due to significant behavior differences in reinforced-concrete beam/columns models available in the two selected computer programs. On the other hand, smaller variability in the response of the steel building appear to be due to less significant differences in the steel beam-column models available in the two programs. Furthermore, there is 10% to 15% dispersion as apparent from median$\pm\sigma$ band. It is useful to emphasize that above observations are for median response ratios only. Response ratio for individual ground motions from the two programs may vary by as much as 50%.

CHAPTER 6. COMPARISON OF ESTIMATED AND TRUE BASE SHEARS

As mentioned previously, base shear in buildings with recorded motions is typically estimated from summation of floor inertial forces above the building's base (Figure 6.1a). For this purpose, the floor inertial forces are computed by multiplying the floor masses with the total floor accelerations. The base shear thus calculated is designated as the "estimated base shear" in this investigation. This base shear is generally accepted to provide a good estimate of the "true base shear" which is equal to sum of shears in all columns at the building's base (Figure 6.1b).

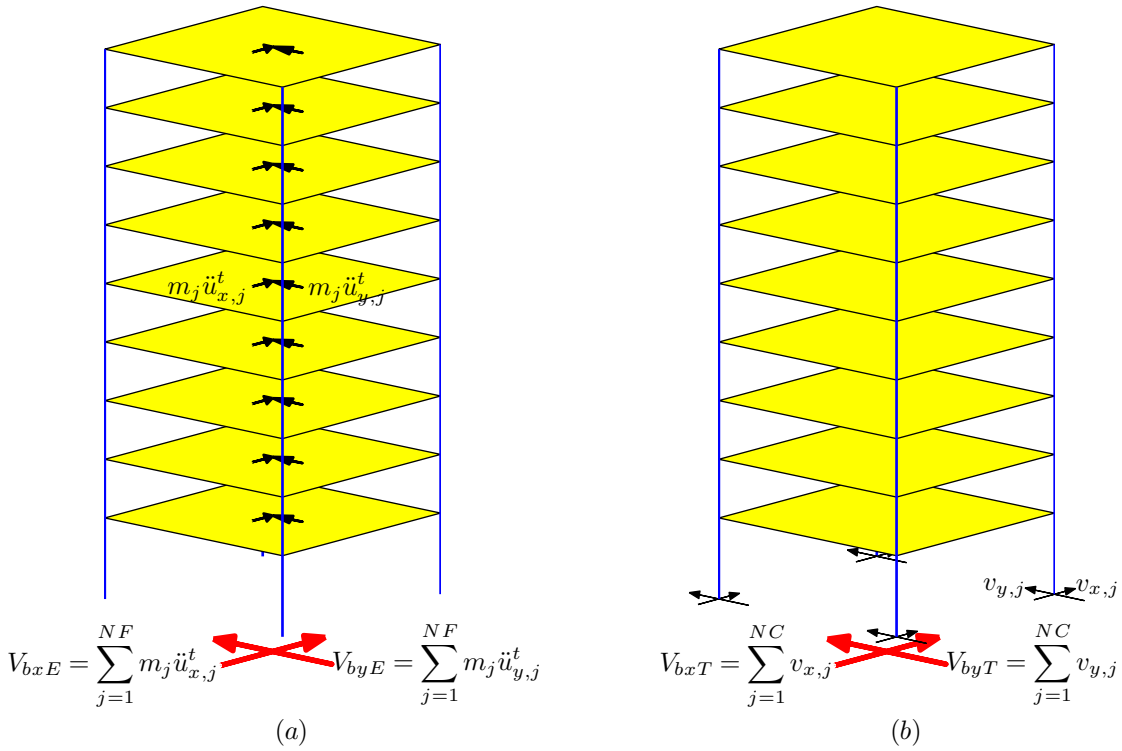

Figure 6.1. Computation of base shear: (a) Base shear computed from summation of inertial floor forces; and (b) Base shear computed from summation of column base shears.

This chapter re-examines if the estimated base shear, V_{bE}, provides a good estimate of the true base shear, V_{bT}. For this purpose, ratios of the estimated and true base shears for the two buildings were computed from *OpenSees* and *Perform3D*. The accelerations used in computing the estimated base shear were those computed from RHA.

Response Histories

Examined first is the time-variation of estimated and true base shears. This examination showed that the estimated base shear matched the true base shear quite well for some earthquakes but the difference was very large for others. Selected results are presented for each of the two buildings in Figures 6.2 to 6.5 to demonstrate cases where the two base shears matched quite well and where they differed significantly; results for all cases are included in Appendix III.

The results for the North Hollywood Hotel indicate that the estimated base shear tracks the true base shear quite well for earthquake no. 14. Furthermore, the peak value of estimated base shear is essential equal to the true base shear in the longitudinal direction (Figure 6.2a) and exceeds the true base shear by no more than 4% in the transverse direction (Figure 6.2b). For earthquake no. 9, however, the peak value may differ by more than 10% in the longitudinal direction (Figure 6.3a) and by more than 20% in the transverse direction (Figure 6.3b).

The results presented for the Los Angeles Building indicates a very good match between estimated and true base shears for earthquake no. 4 (Figure 6.4). For earthquake no. 15, however, the estimated base shear differs significantly from the true base shear (Figure 6.5). The peak value of the estimated base shear exceeds the true base shear by about 70% in the longitudinal direction (Figure 6.5a) and by about 35% in the transverse direction (Figure 6.5b). The results of Figure 6.5 also show that the estimated base shear has significantly larger high-frequency content compared to the true base shear. Therefore, it appears that the estimated base shear may significantly exceed the true base shear for ground motions with very large high-frequency content.

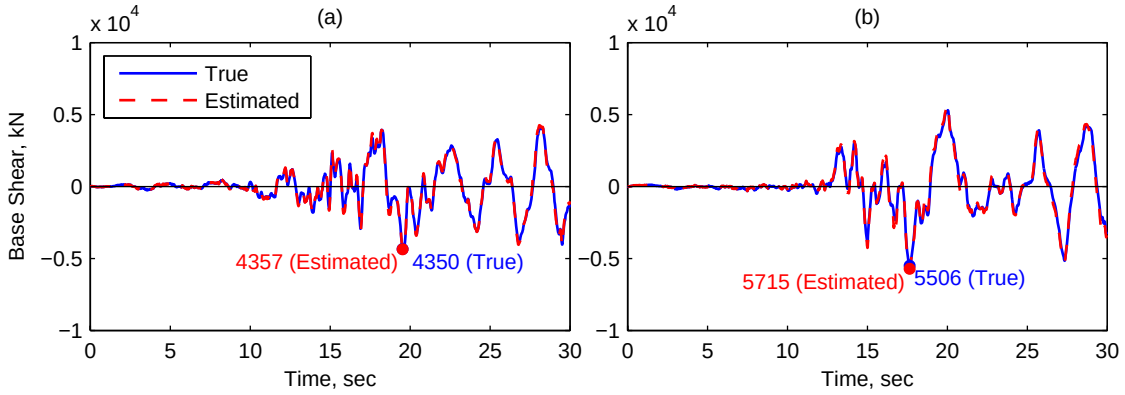

Figure 6.2. Comparison of estimated and true base shears for North Hollywood Hotel for Earthquake No. 14: (a) Longitudinal direction, and (b) Transverse direction.

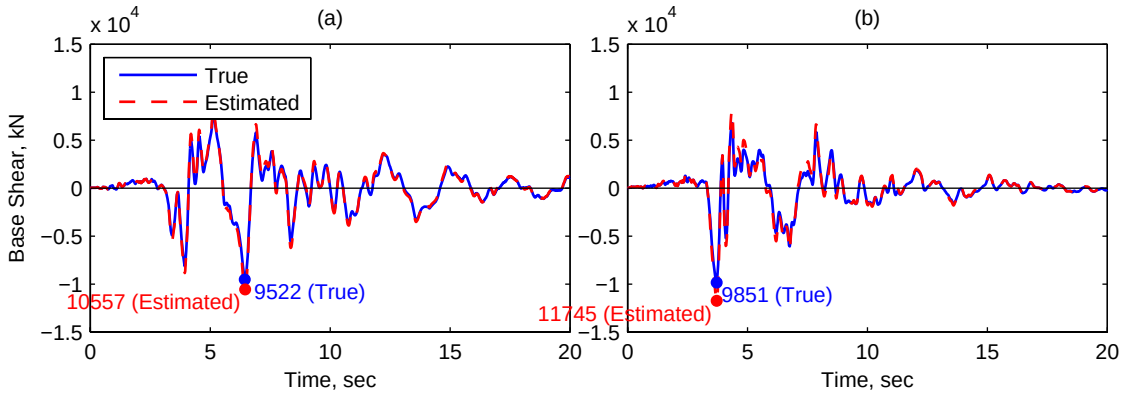

Figure 6.3. Comparison of estimated and true base shears for North Hollywood Hotel for Earthquake No. 9: (a) Longitudinal direction, and (b) Transverse direction.

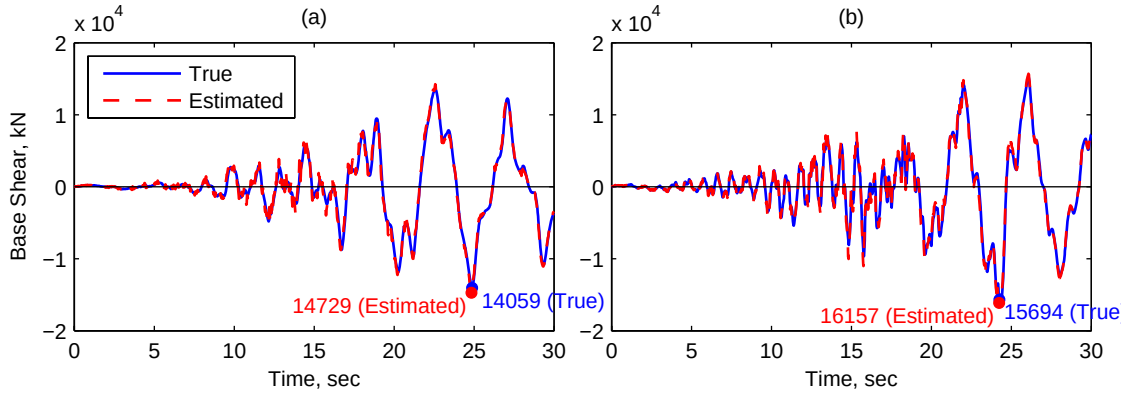

Figure 6.4. Comparison of estimated and true base shears for Los Angeles Building for Earthquake No. 4: (a) Longitudinal direction, and (b) Transverse direction.

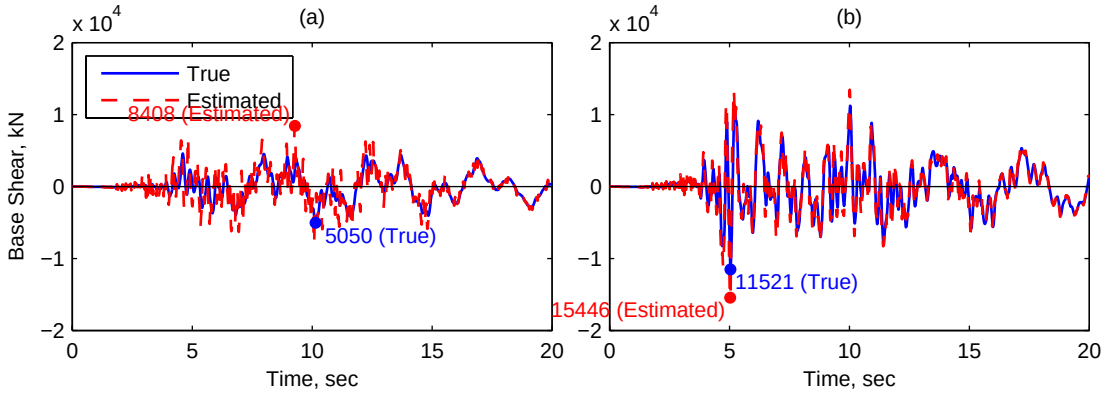

Figure 6.5. Comparison of estimated and true base shears for Los Angeles Building for Earthquake No. 15: (a) Longitudinal direction, and (b) Transverse direction.

Peak Values

Examined next are the ratios, V_{bE}/V_{bT} , of the estimated and true base shears for the two buildings. The results are presented in Figures 6.6 and 6.9 for earthquakes for which the building did not to collapse. The presented results include ratio, V_{bE}/V_{bT} , for individual earthquakes along with the median values and median±σ values.

20-Story Hotel in North Hollywood

The results presented in Figure 6.6 for the North Hollywood Hotel show that the ratio V_{bE}/V_{bT} from *OpenSees* for some earthquakes can be as high as 1.25. This indicates that estimated base shear may over predict the true base shear by up to 25%. The median value of the ratio is, however, much smaller: the median ratio is from 1.08 (Figure 6.6a) to 1.12 (Figure 6.6b). Therefore, it may be expected that the inertial force will over predict the true base shear in the median by about 10%. The width of the median+σ or median-σ band varies from 0.05 to 0.08 implying that there is 5% to 8% dispersion in the response prediction. The results presented in Figure 6.7 for *Perform3D* results show trends similar to those for *OpenSees* results in Figure 6.6 with the variations being slightly smaller for the former program.

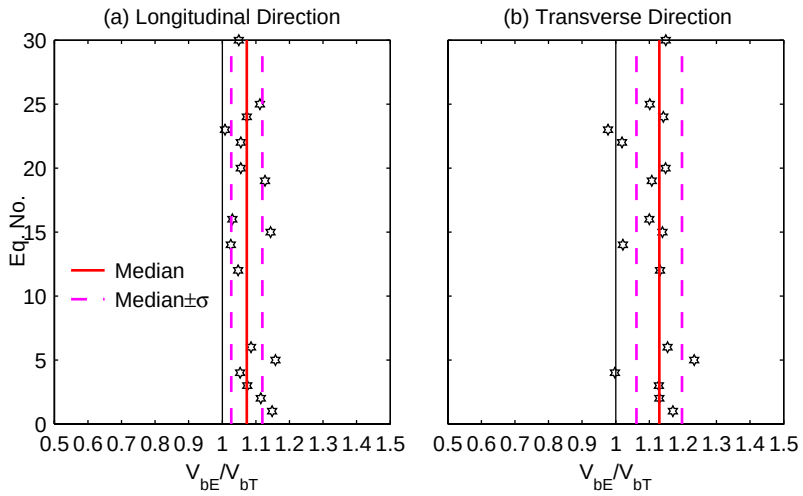

Figure 6.6. Ratio of peak estimated and true base shears from *OpenSees* for North Hollywood Hotel.

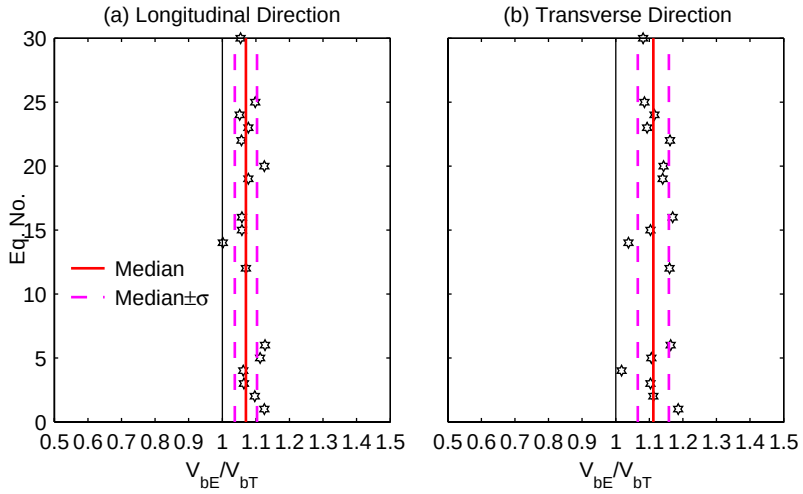

Figure 6.7. Ratio of peak estimated and true base shears from *Perform3D* for North Hollywood Hotel.

19-Story Office Building in Los Angeles

The results presented in Figure 6.8 for the Los Angeles building show very little variation in V_{bE}/V_{bT} from *OpenSees*: the median is very close to one (Figures 6.8a and 6.8b). The width of the median+σ or median-σ band is about 0.2 in the longitudinal direction (Figure 6.8a) and very small in the transverse direction (Figure 6.8b). The results from *Perform3D* show median value of the ratio to range from 1.05 (Figure 6.9a) to 1.2 (Figure 6.9b) with the width of the median+σ

or median-σ band to range from 0.1 (Figure 6.9b) to 0.2 (Figure 6.9a). For individual earthquake, however, the estimated base shear may exceed the true base shear by as much as 75% (see Figures 6.8a and 6.9a).

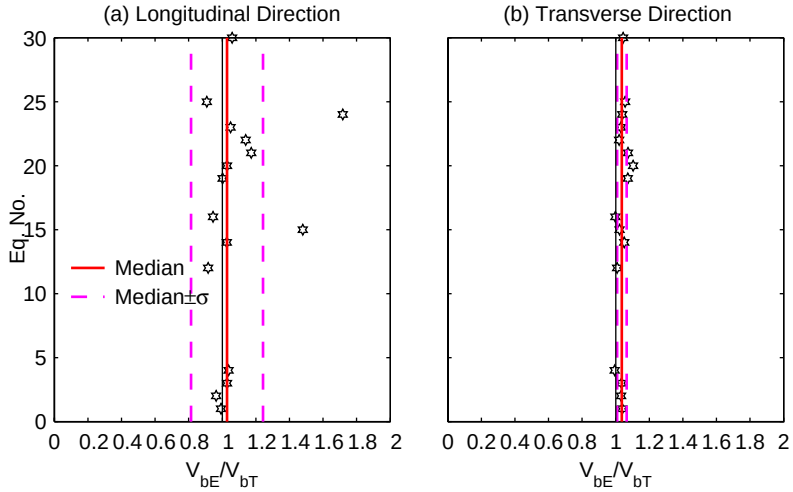

Figure 6.8. Ratio of peak estimated and true base shears from *OpenSees* for Los Angeles Building.

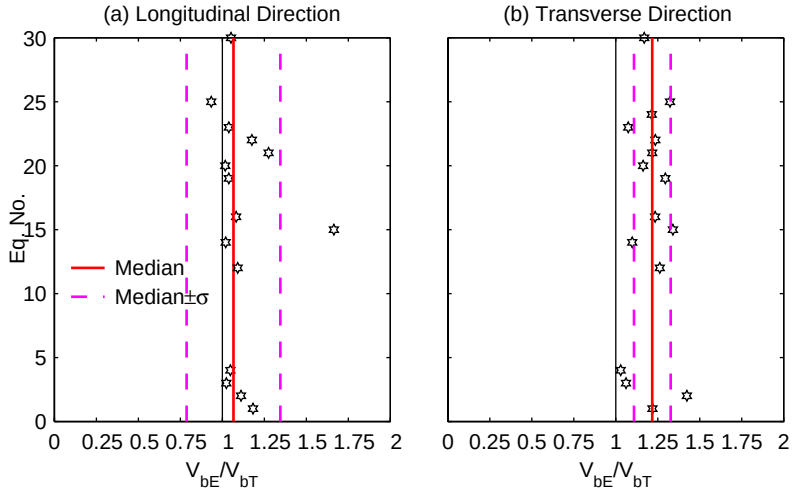

Figure 6.9. Ratio of peak estimated and true base shears from *Perform3D* for Los Angeles Building.

The presented so far indicate that the median estimated base shear exceeds the true base shear by 10 to 20%. For individual earthquakes, however, the estimated base shear may overestimate the true base shear by as much as 75%. Therefore, estimated base shear should be

used with caution as an estimate of the true base shear.

CONCLUSIONS

The investigation first examined the effects of modeling assumptions and two different computer programs on nonlinear response of three-dimensional buildings. It was found that modeling assumptions may significantly affect the pushover curves: concentrated plasticity model leads to lower strength, early initiation of yielding, and post yielding strength loss in pushover curves compared to spread plasticity model; and strength loss model for beams/columns leads to significant post yielding strength loss in the pushover curve. The concrete material model, on the other hand, appears to have minimal effect on the pushover curves of reinforced concrete buildings. While most of the differences may be attributed to differences in modeling options available in different programs (e.g., *OpenSees* does not have an option for modeling FEMA-356 force-deformation behavior with strength loss whereas *Perform3D* does), some differences may also occur due to differences in solution schemes and convergence criteria available in different software programs.

It was also found that the prediction of median peak response from different software can differ from 10% to 40%. The difference tends to be much higher for reinforced concrete building compared to the steel building, and for floor displacements compared to floor accelerations and base shear. Furthermore, there is dispersion of about 10% to 15% in the median prediction as apparent from median±σ band. For individual ground motions, the peak responses from different computer programs may vary by as much as 50%.

This investigation also examined if the “estimated base shear”, defined as summation of floor inertial forces above the building’s base with the floor inertial forces computed by multiplying the floor masses with the total floor accelerations, can provide an accurate estimate of the “true base shear” which is equal to sum of shears in all columns at the building’s base.

This investigation indicated that the median estimated base shear exceeds the true base shear by 10 to 20%. For individual earthquakes, however, the estimated base shear may overestimate the true base shear by as much as 50%. Therefore, estimated base shear should be used with caution as an estimate of the true base shear.

REFERENCES

ASCE (2000). Prestandard and Commentary for the Seismic Rehabilitation of Buildings. *Report No. FEMA-356*, Building Seismic Safety Council, Federal Emergency Management Agency, Washington, D.C.

Bernal, D. (2007). Predictive Capability of Nonlinear Static Analysis Procedures for Seismic Evaluation of Buildings, *CSMIP Data Interpretation Report*, Strong Motion Instrumentation Program, CDMG, Sacramento, CA.

Chadwell, C. (2007). Capacity Analysis and Pushover Program (Capp): Version 1.04. Imbsen & Associates, Inc., <www.imbsen.com)>.

CSI (2006). Perform3D: Nonlinear Analysis and Performance Assessment for 3d Structures: Version 4. Computers and Structures, Inc., Berkeley. <www.csiberkeley.com)>.

De la Llera, J. C. and Chopra, A. K. (1998). "Evaluation of Seismic Code Provisions Using Strong-Motion Building Records from the 1994 Northridge Earthquake," Report No. UCB/EERC-97/16, Earthquake Engineering Research Center, University of California, Berkeley, CA.

Goel, R.K. (2005). "Evaluation of Modal and FEMA Pushover Procedures Using Strong-Motion Records of Buildings," Earthquake Spectra, 21(3): 653-684, 2005.

Goel, R.K. (2007). "Evaluation of Current Nonlinear Static Procedures Using Strong Motion Records," *Proceedings of the 2007 Structures Congress, Long Beach, CA*, American Society of Civil Engineers, Reston, VA.

Goel, R.K. (2008). "Mode-Based Procedure to Interpolate Strong Motion Records of Instrumented Building." *ISET Journal of Earthquake Technology*, 45(3-4), December.

Goel, R.K. and Chadwell, C. (2007). Evaluation of Current Nonlinear Static Procedures for Concrete Buildings Using Recorded Strong-Motion Data, *CSMIP Data Interpretation Report*, Strong Motion Instrumentation Program, CDMG, Sacramento, CA.

Hart, G. (1973). 1901 Avenue of the Stars Building, *San Fernando, California, Earthquake of February 9, 1971*, N. A. Benfer and J. L. Coffman (Eds.), U.S. Department of Commerce and National Oceanic and Atmospheric Administration, **I of III:** 597-607.

Karsan, I. D., and Jirsa, J. O. (1969). "Behavior of concrete under compressive loading." *Journal of Structural Division ASCE*, 95(ST12).

Limongelli, M. P. (2003). “Optimal Location of Sensors for Reconstruction of Seismic Response through Spline Function Interpolation,” Earthquake Engineering and Structural Dynamics, 32(7):1055-1074.

Mander, J. B., Priestley, M. J. N., and Park, R. (1988). "Theoretical stress-strain model for confined concrete." *Journal of Structural Engineering ASCE*, 114(8), 1804-1825.

McKenna, F. and Fenves, G. (2001). The Opensees Command Language Manual: 1.2. Pacific Earthquake Engineering Center, University of California, Berkeley,(http://opensees.berkeley.edu).

Naeim, F., Lee, H., Bhatia, H., Hagie, S., and Skliros, K. (2004). “CSMIP Instrumented Building Response Analysis and 3-D Visualization System (CSMIP-3DV),” Proceedings, SMIP04 Seminar on Utilization of Strong-Motion Data, Strong Motion Instrumentation Program, CDMG, Sacramento, CA.

Naeim, F. (1998). Performance of 20 Extensively-Instrumented Buildings During the 1994 Northridge Earthquake, *The Structural Design of Tall Buildings*, **7**(3): 179-194.

Naeim, F. (1997). Performance of Extensively Instrumented Buildings During the January 17, 1994 Northridge Earthquake: An Interactive Information System, Report No. 97-7530.68, John A. Martin & Associates, Los Angeles, CA, 1997.

Popovics, S. (1973). "A numerical approach to the complete stress strain curve for concrete." *Cement and concrete research*, 3(5), 583-599.

TRC (2008), Cross Sectional Analysis of Structural Components, v3.0.8, TRC/Imbsen Software Systems, Rancho Cordova, CA. <http://www.imbsen.com/>

APPENDIX I. SELECTED GROUND MOTIONS

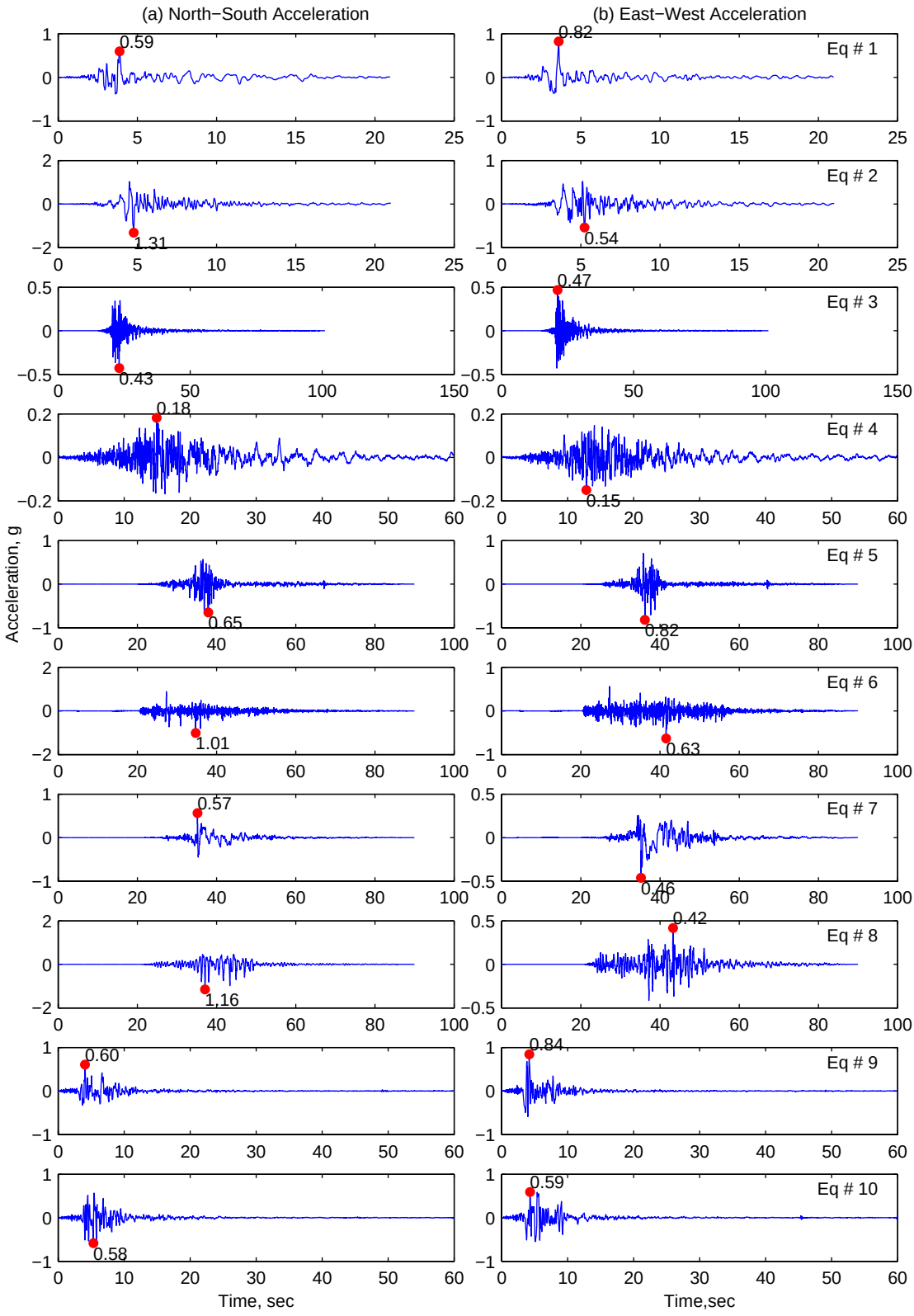

Figure I.1. Acceleration histories of ground motions 1 to 10.

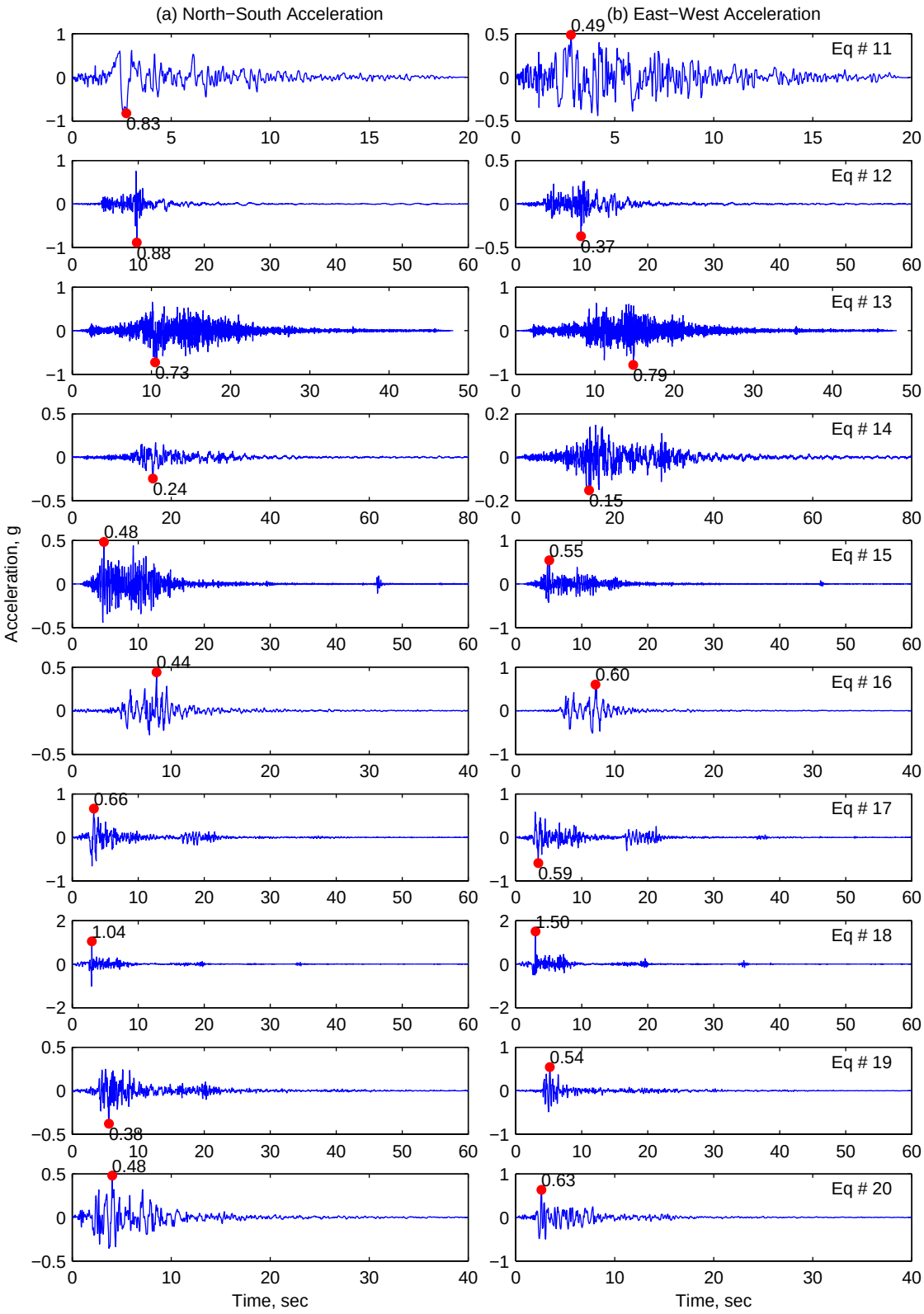

Figure I.2. Acceleration histories of ground motions 11 to 20.

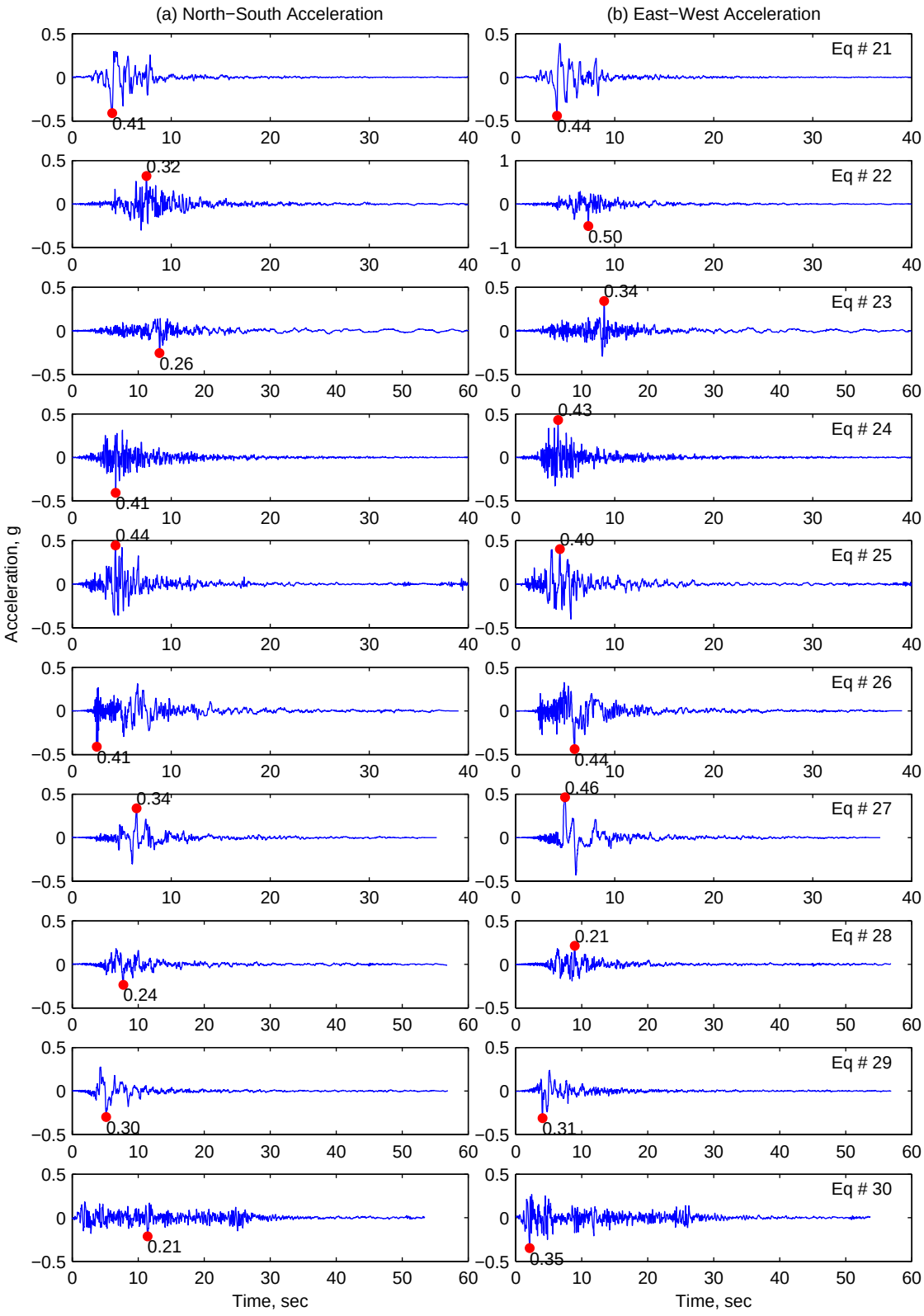

Figure I.3. Acceleration histories of ground motions 21 to 30.

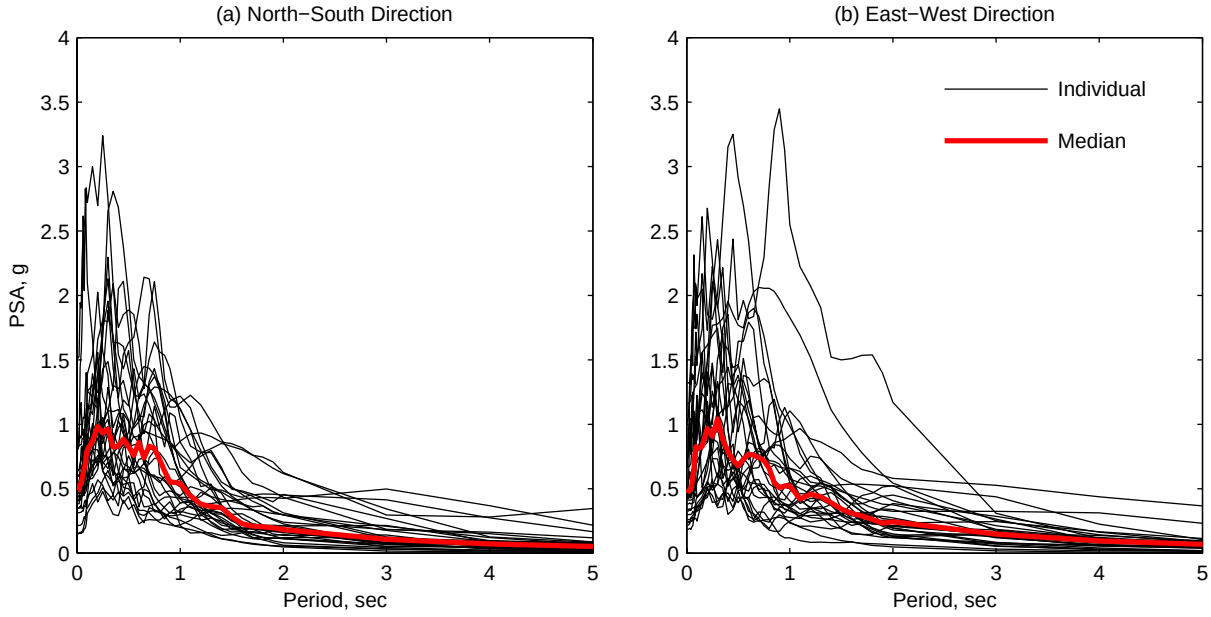

Figure I.4. Linear elastic response spectra fro selected ground motions.

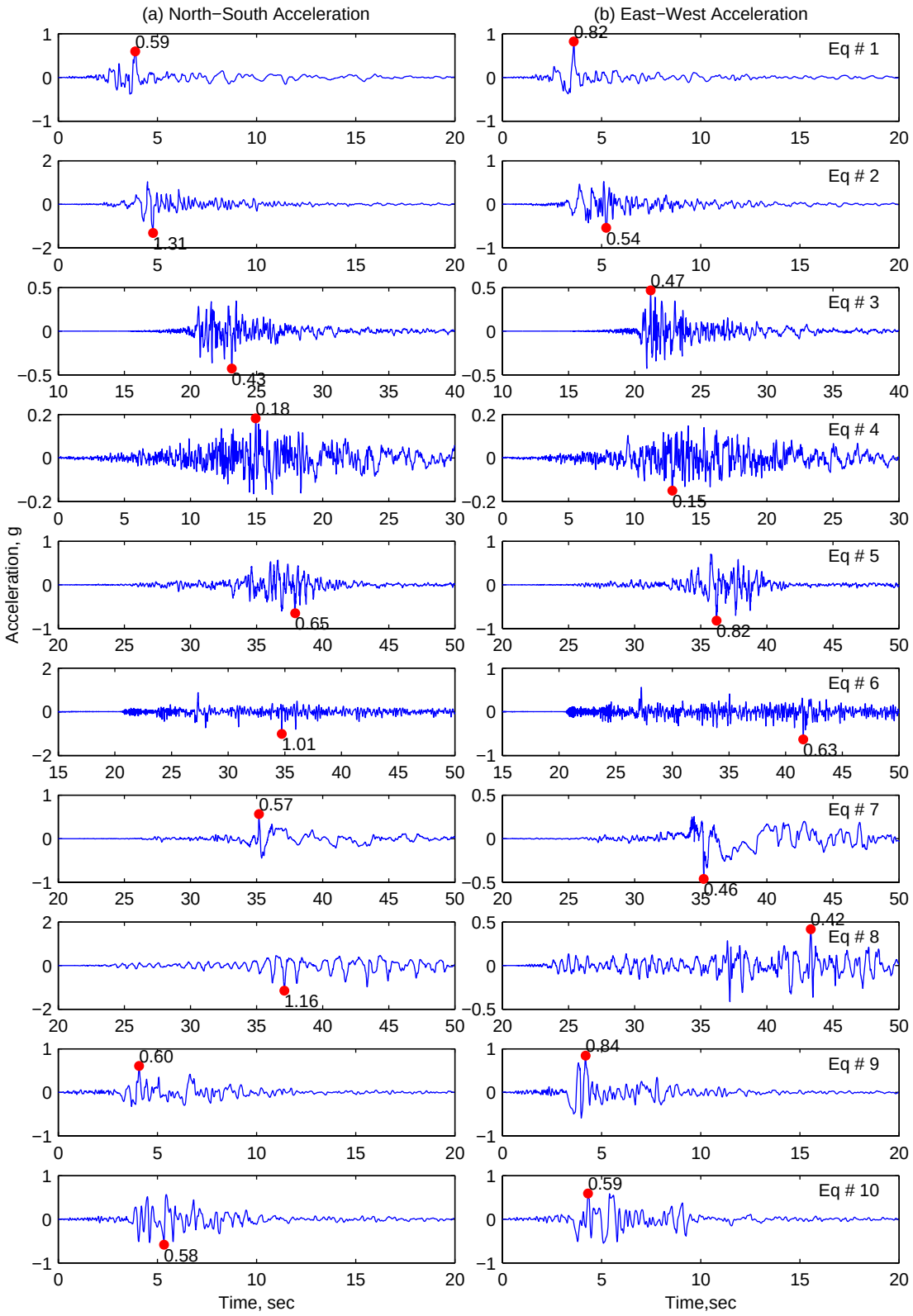

Figure I.5. Segments of acceleration histories selected for analysis: motions 1 to 10.

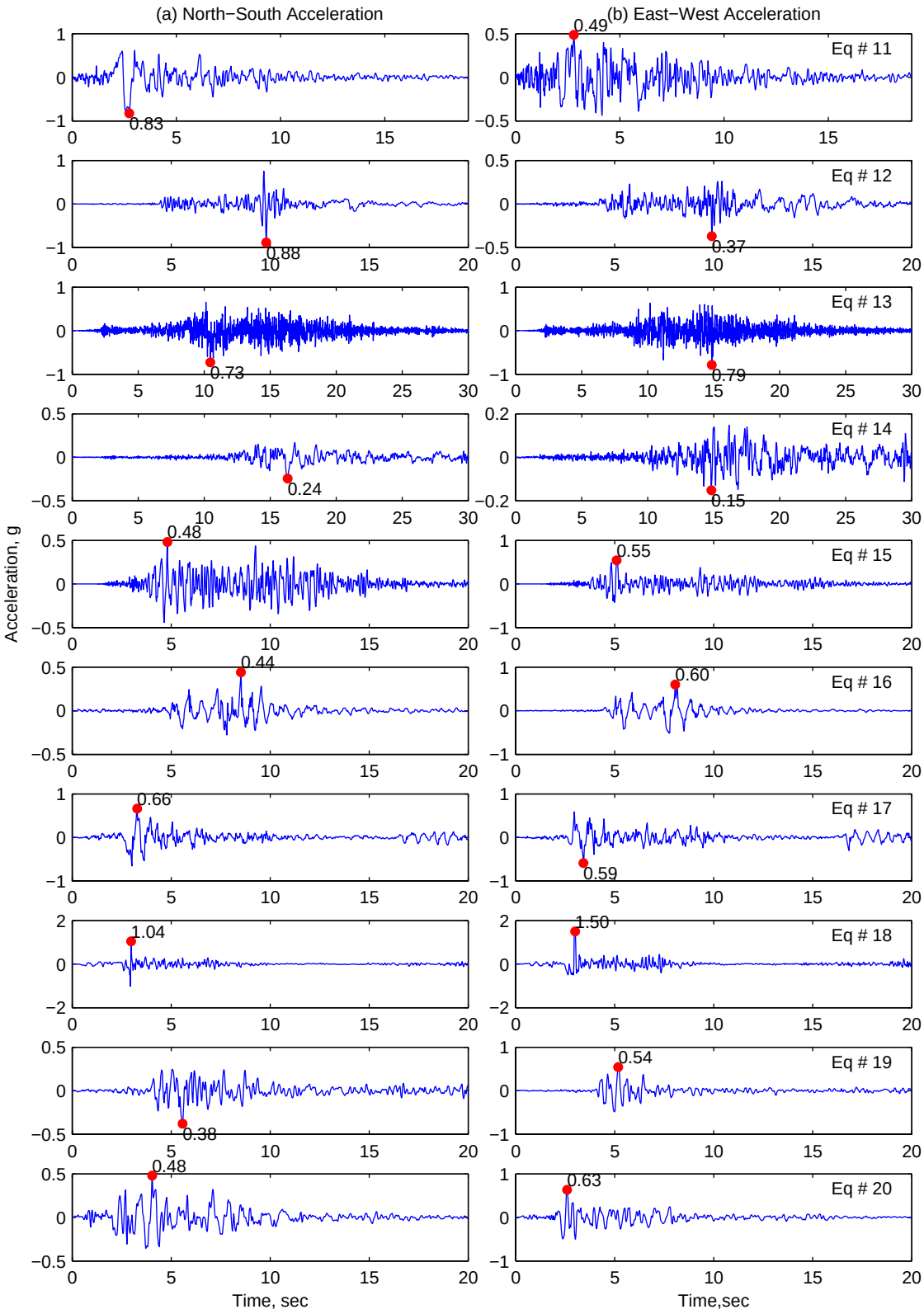

Figure I.6. Segments of acceleration histories selected for analysis: motions 11 to 20.

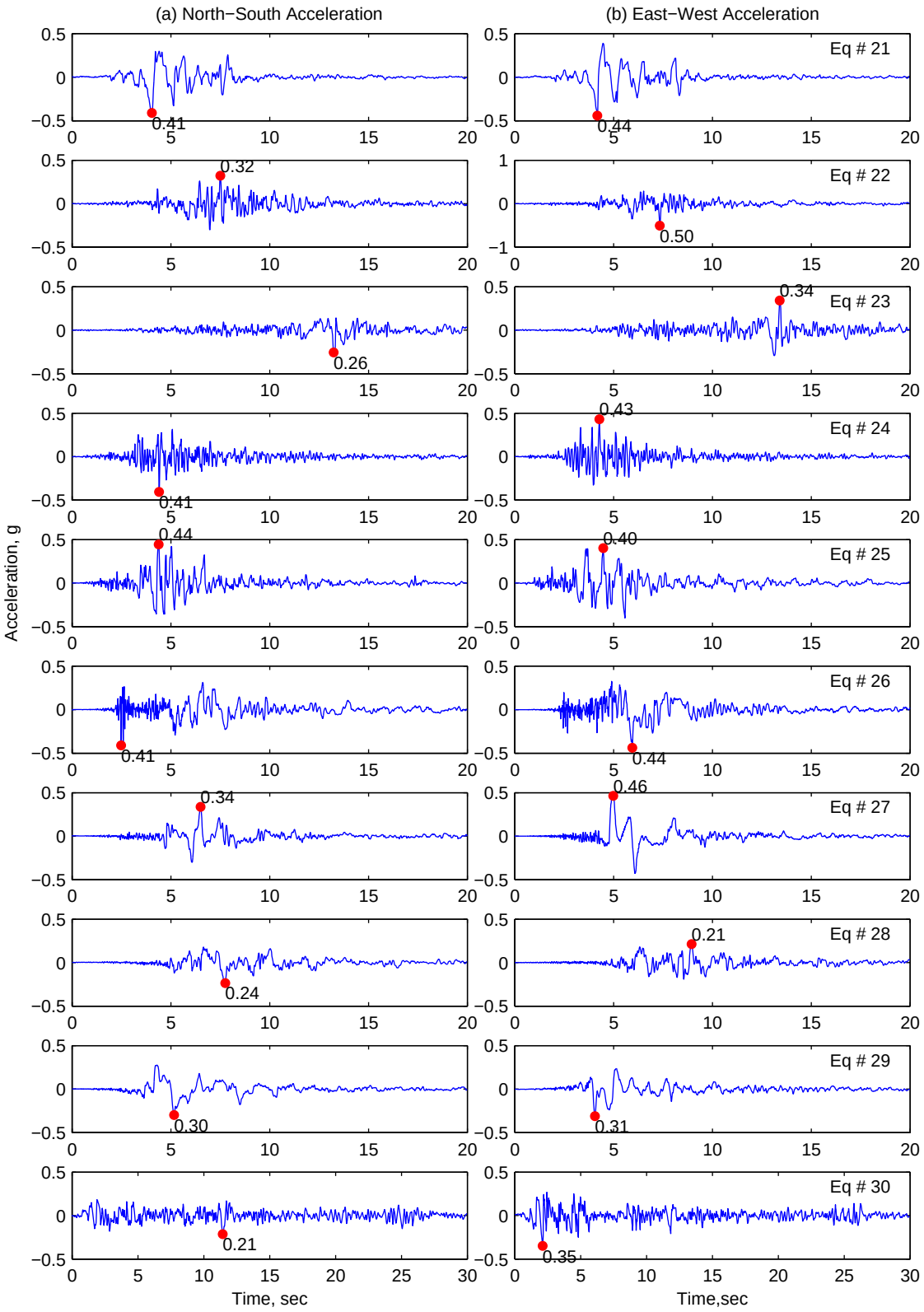

Figure I.7. Segments of acceleration histories selected for analysis: motions 21 to 30.

APPENDIX II. RESPONSE HISTORY RESULTS

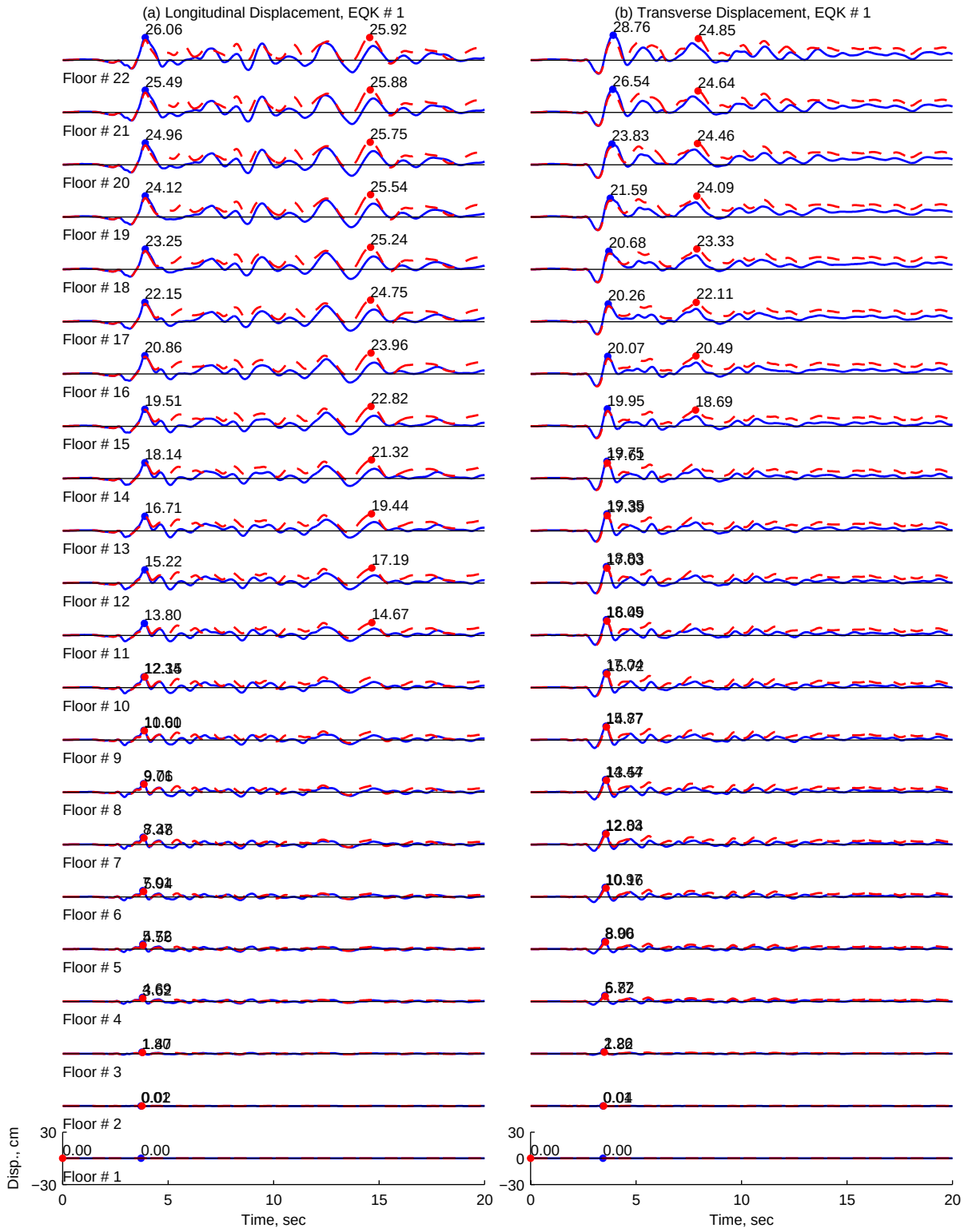

Figure II.1. Floor displacements of 20-Story North Hollywood Hotel from *OpenSees* (solid line) and *Perform3D* (dashed lines) for ground motion 1.

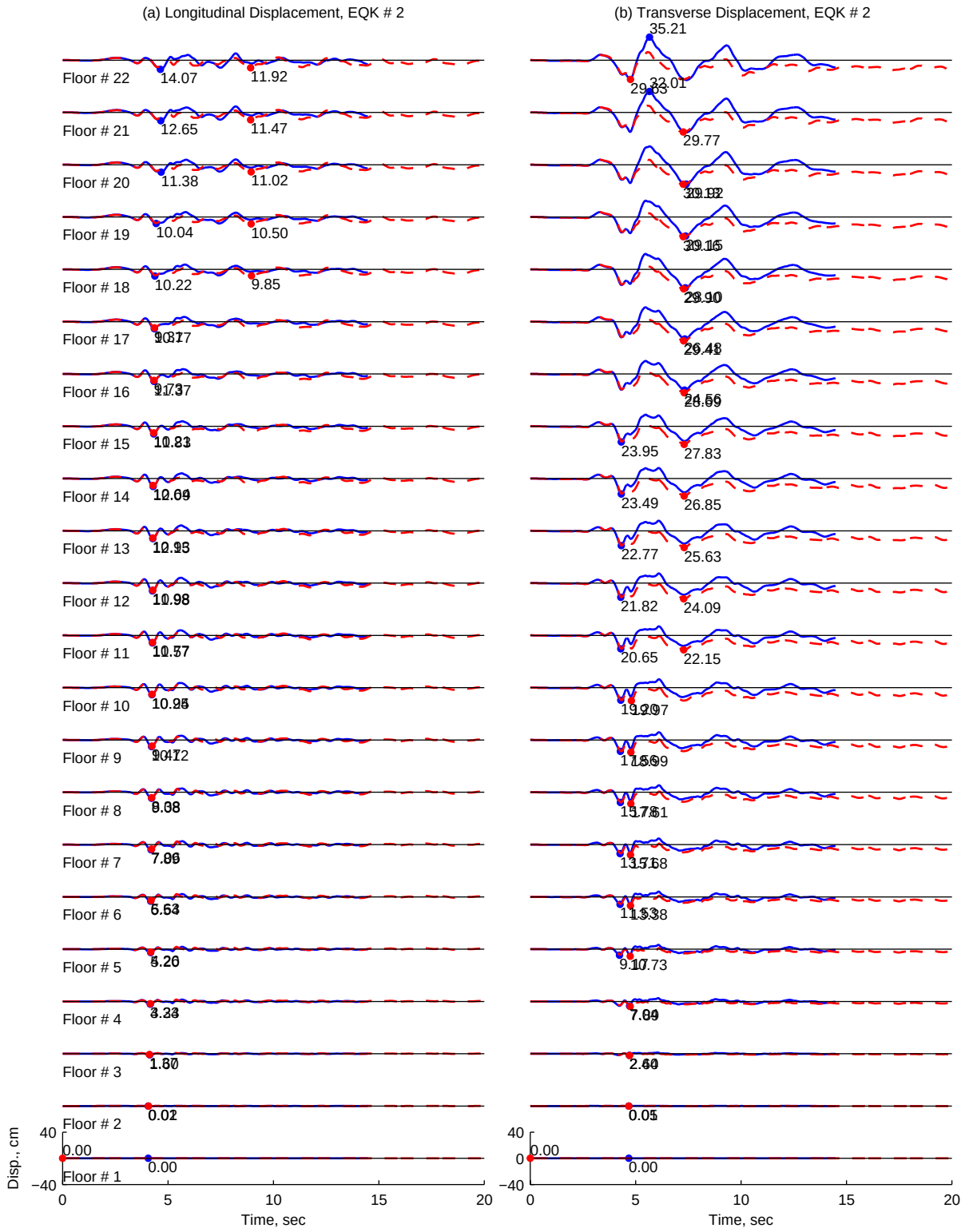

Figure II.2. Floor displacements of 20-Story North Hollywood Hotel from *OpenSees* (solid line) and *Perform3D* (dashed lines) for ground motion 2.

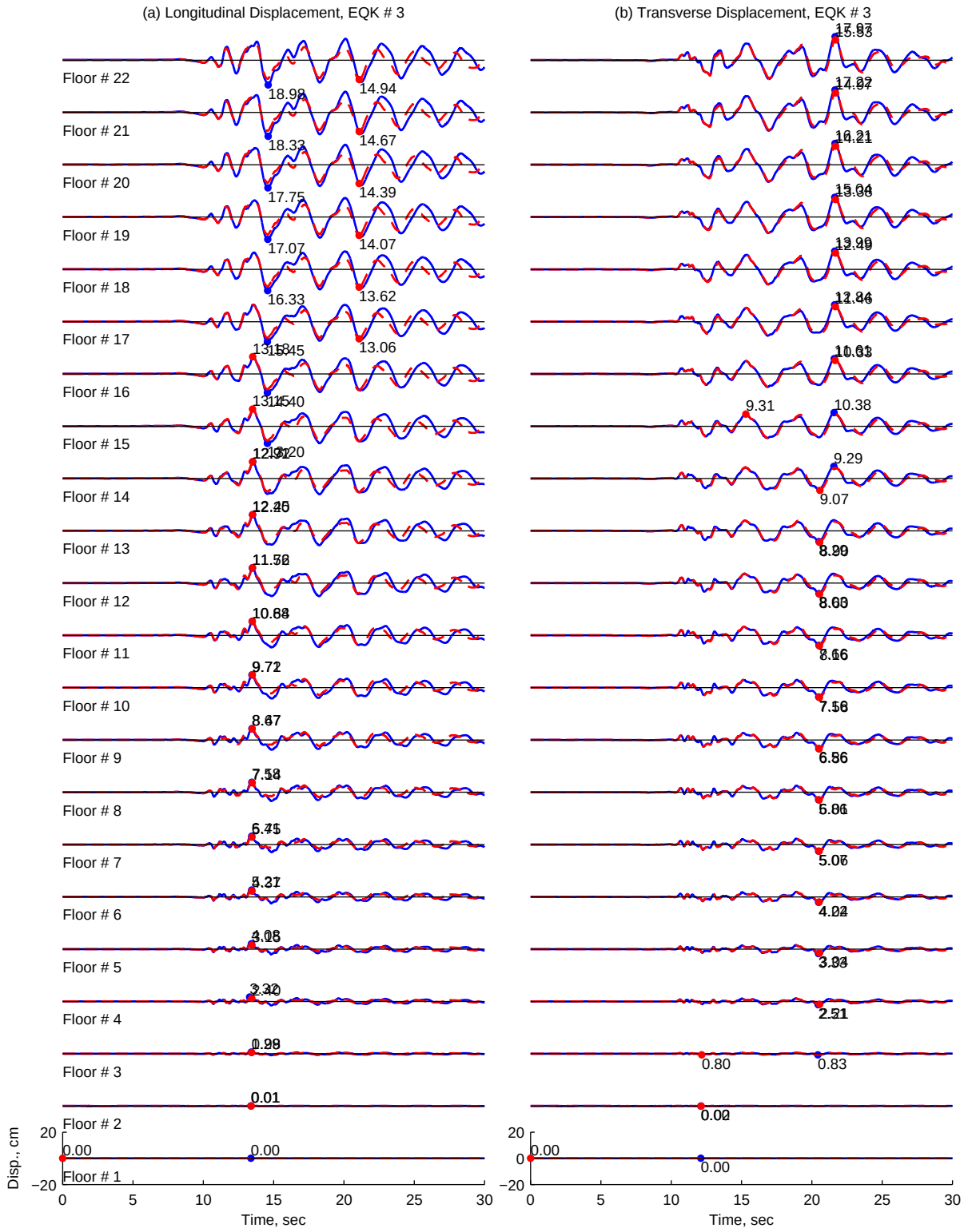

Figure II.3. Floor displacements of 20-Story North Hollywood Hotel from *OpenSees* (solid line) and *Perform3D* (dashed lines) for ground motion 3.

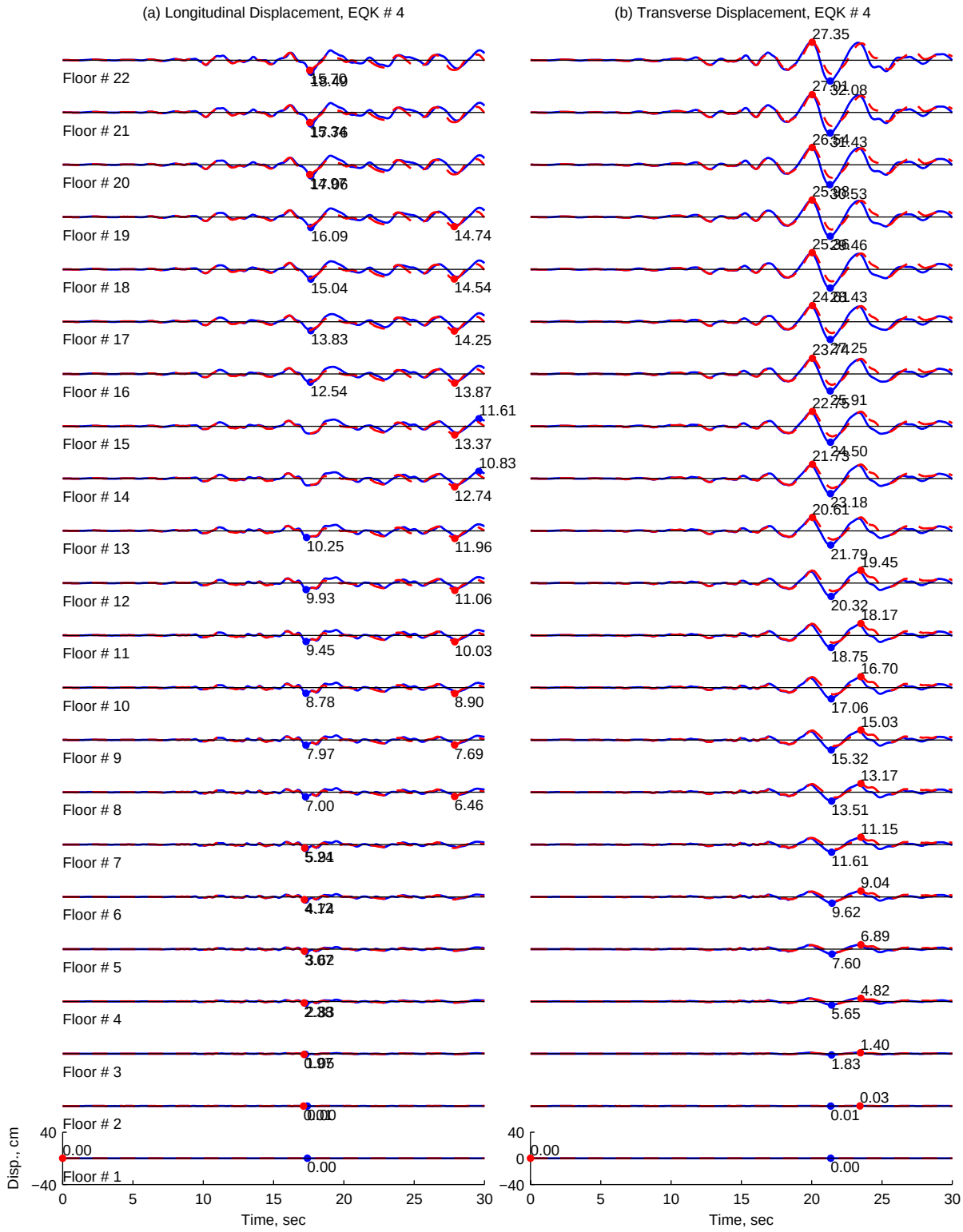

Figure II.4. Floor displacements of 20-Story North Hollywood Hotel from *OpenSees* (solid line) and *Perform3D* (dashed lines) for ground motion 4.

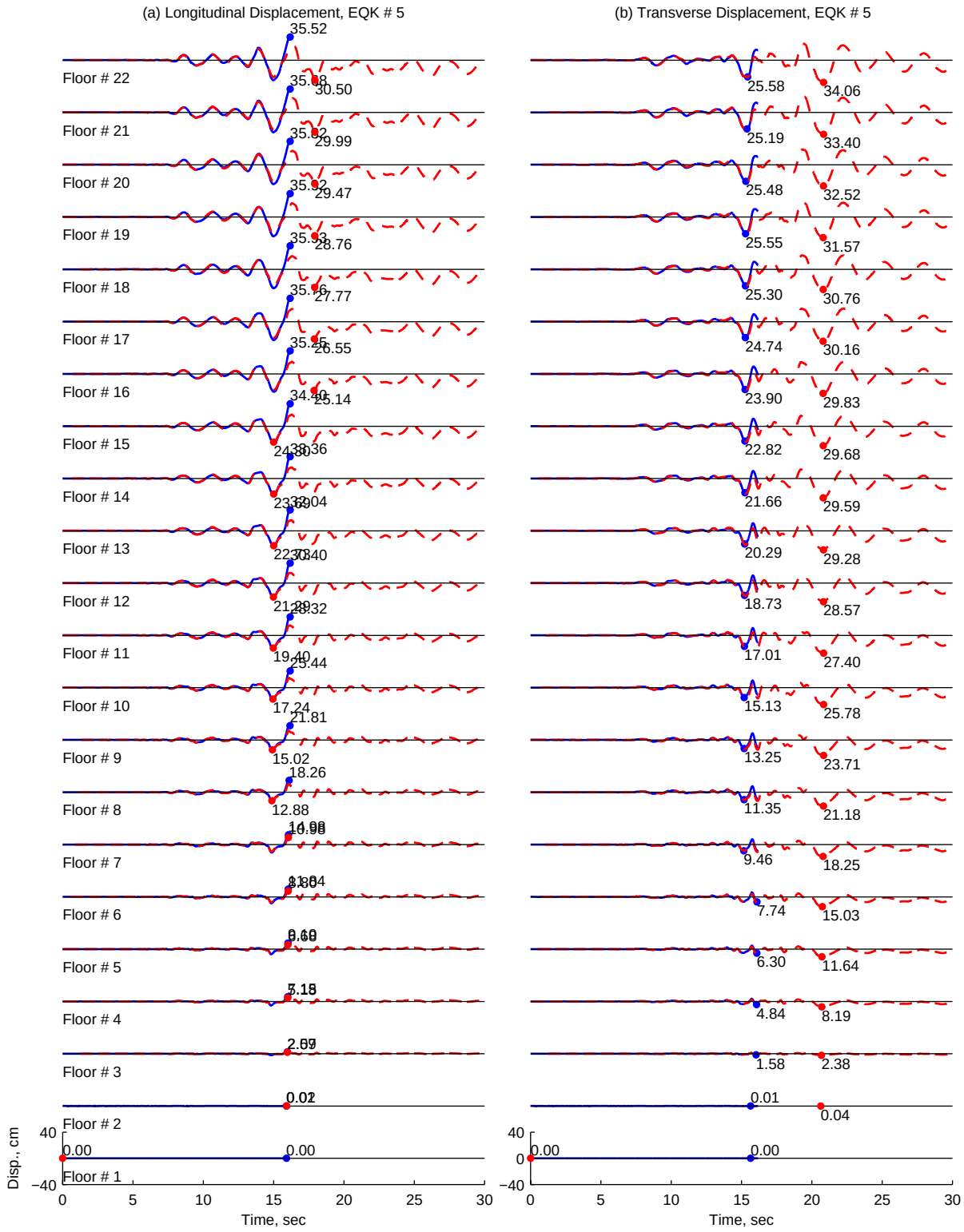

Figure II.5. Floor displacements of 20-Story North Hollywood Hotel from *OpenSees* (solid line) and *Perform3D* (dashed lines) for ground motion 5.

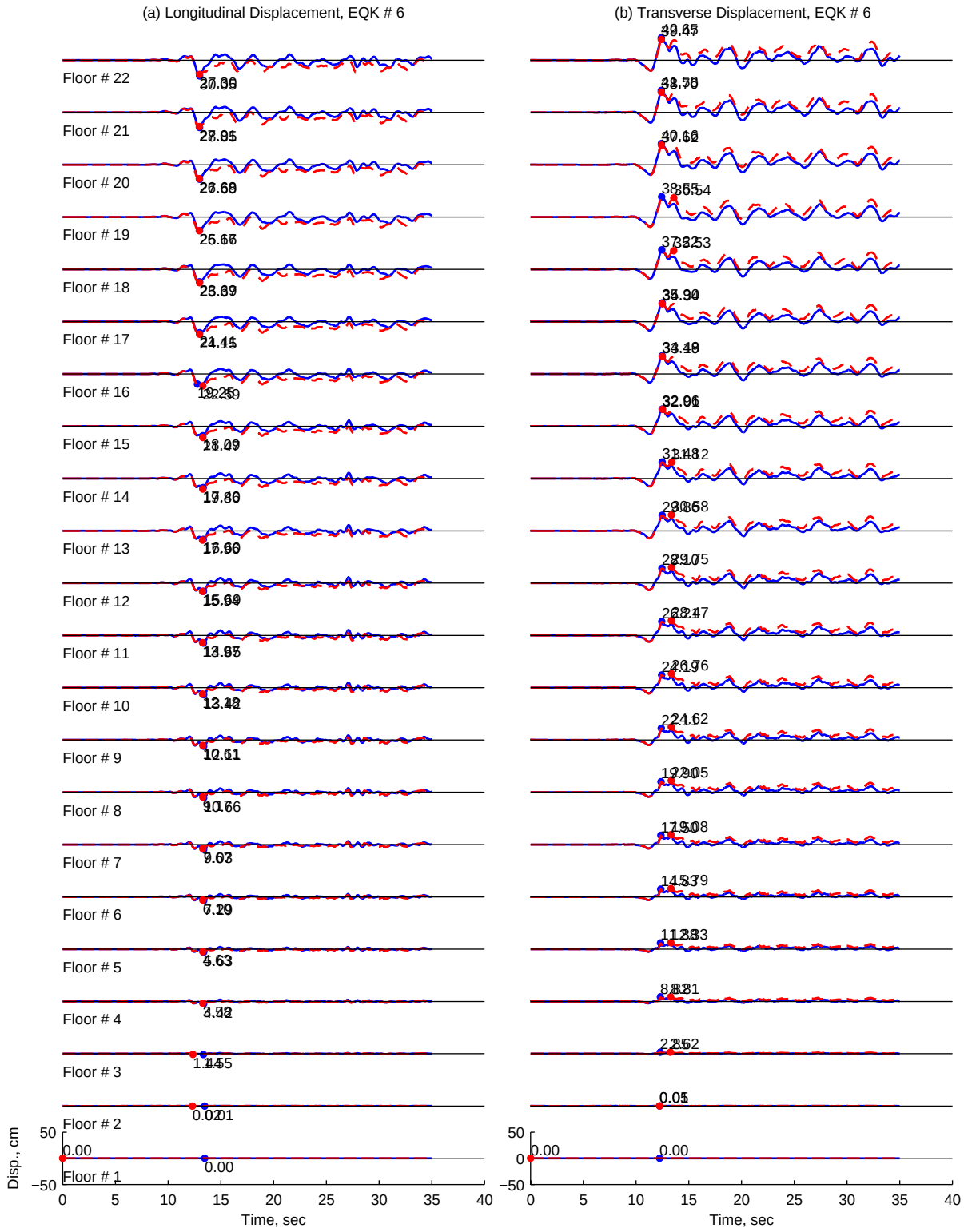

Figure II.6. Floor displacements of 20-Story North Hollywood Hotel from *OpenSees* (solid line) and *Perform3D* (dashed lines) for ground motion 6.

Figure II.7. Floor displacements of 20-Story North Hollywood Hotel from *OpenSees* (solid line) and *Perform3D* (dashed lines) for ground motion 7.

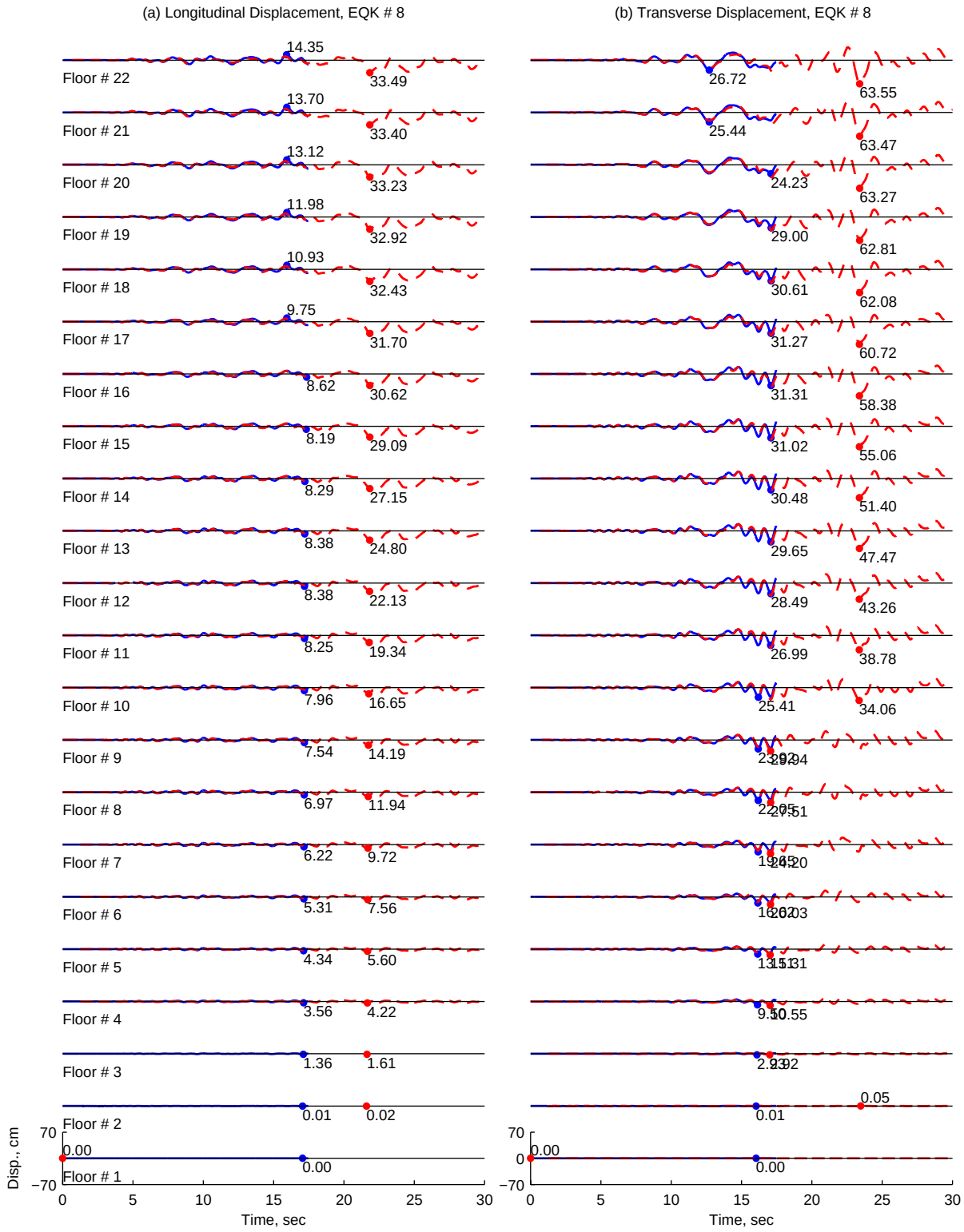

Figure II.8. Floor displacements of 20-Story North Hollywood Hotel from *OpenSees* (solid line) and *Perform3D* (dashed lines) for ground motion 8.

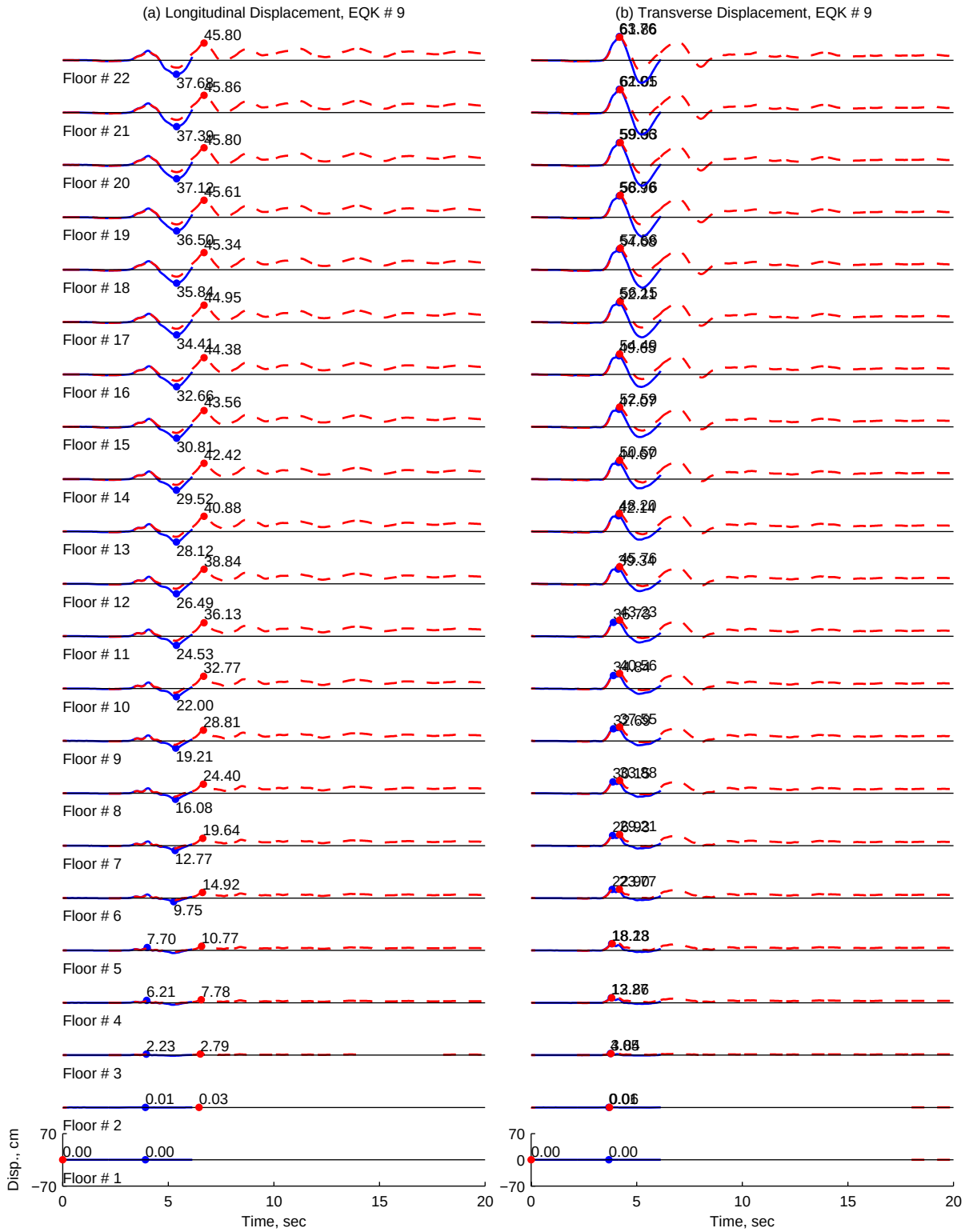

Figure II.9. Floor displacements of 20-Story North Hollywood Hotel from *OpenSees* (solid line) and *Perform3D* (dashed lines) for ground motion 9.

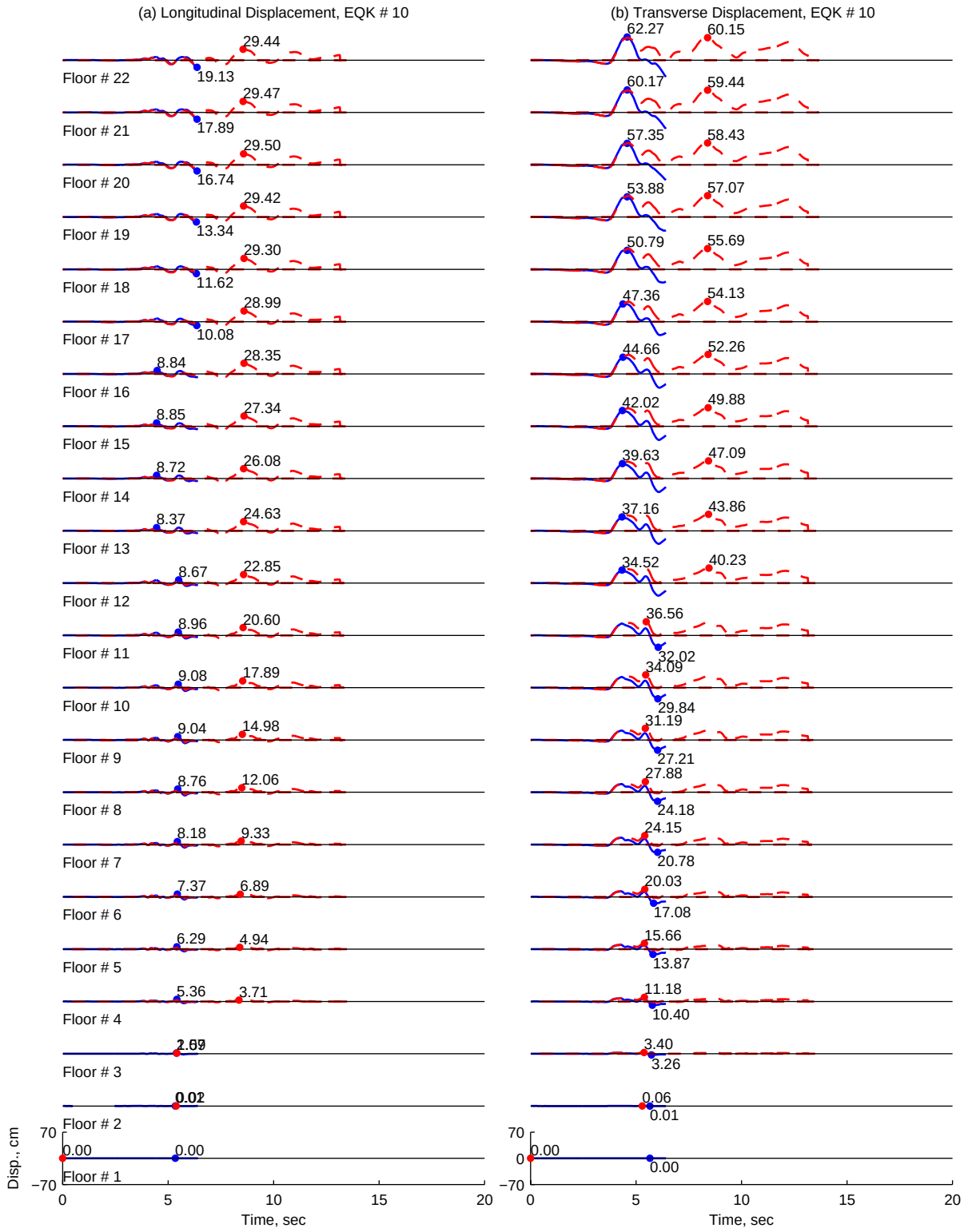

Figure II.10. Floor displacements of 20-Story North Hollywood Hotel from *OpenSees* (solid line) and *Perform3D* (dashed lines) for ground motion 10.

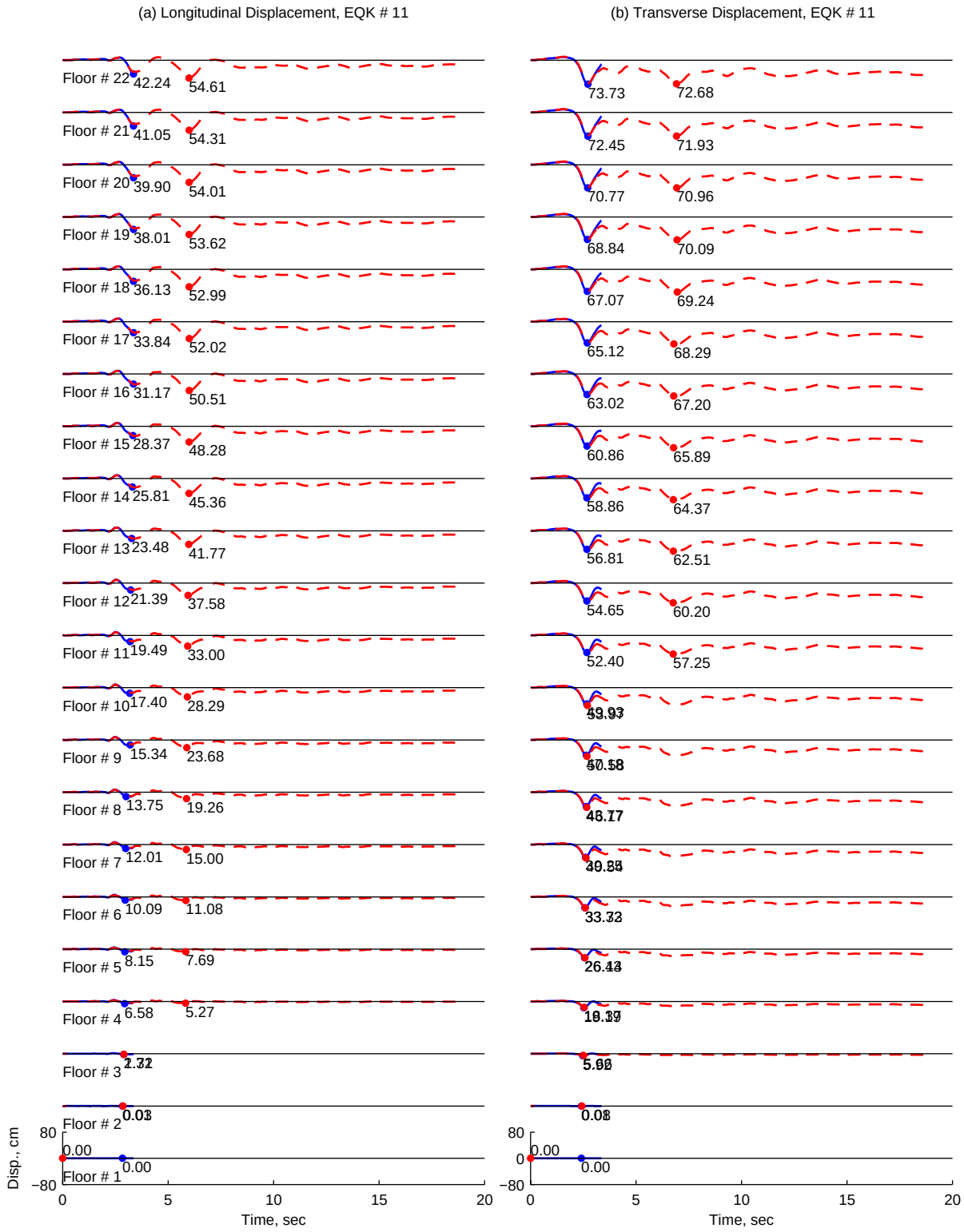

Figure II.11. Floor displacements of 20-Story North Hollywood Hotel from *OpenSees* (solid line) and *Perform3D* (dashed lines) for ground motion 11.

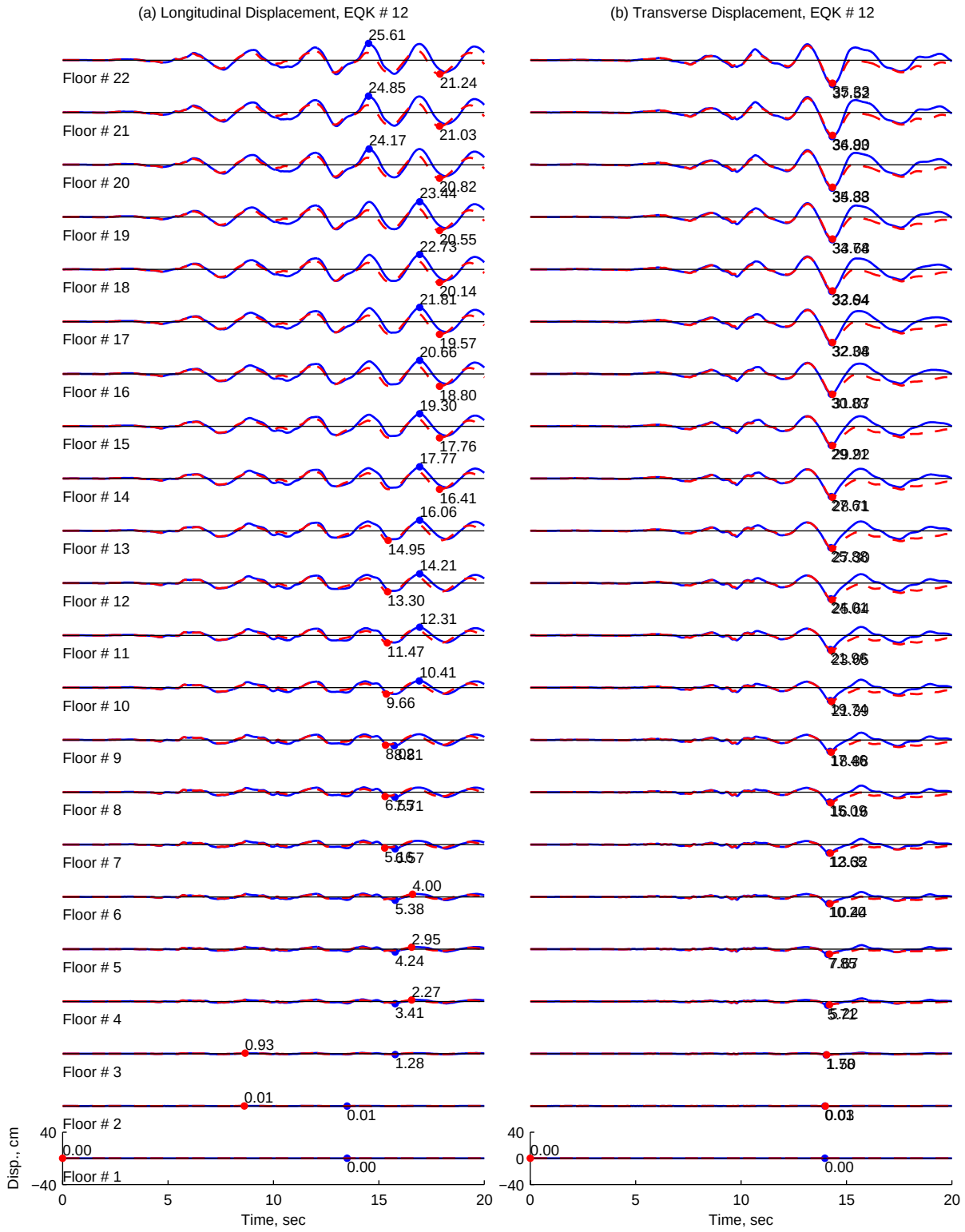

Figure II.12. Floor displacements of 20-Story North Hollywood Hotel from *OpenSees* (solid line) and *Perform3D* (dashed lines) for ground motion 12.

Figure II.13. Floor displacements of 20-Story North Hollywood Hotel from *OpenSees* (solid line) and *Perform3D* (dashed lines) for ground motion 13.

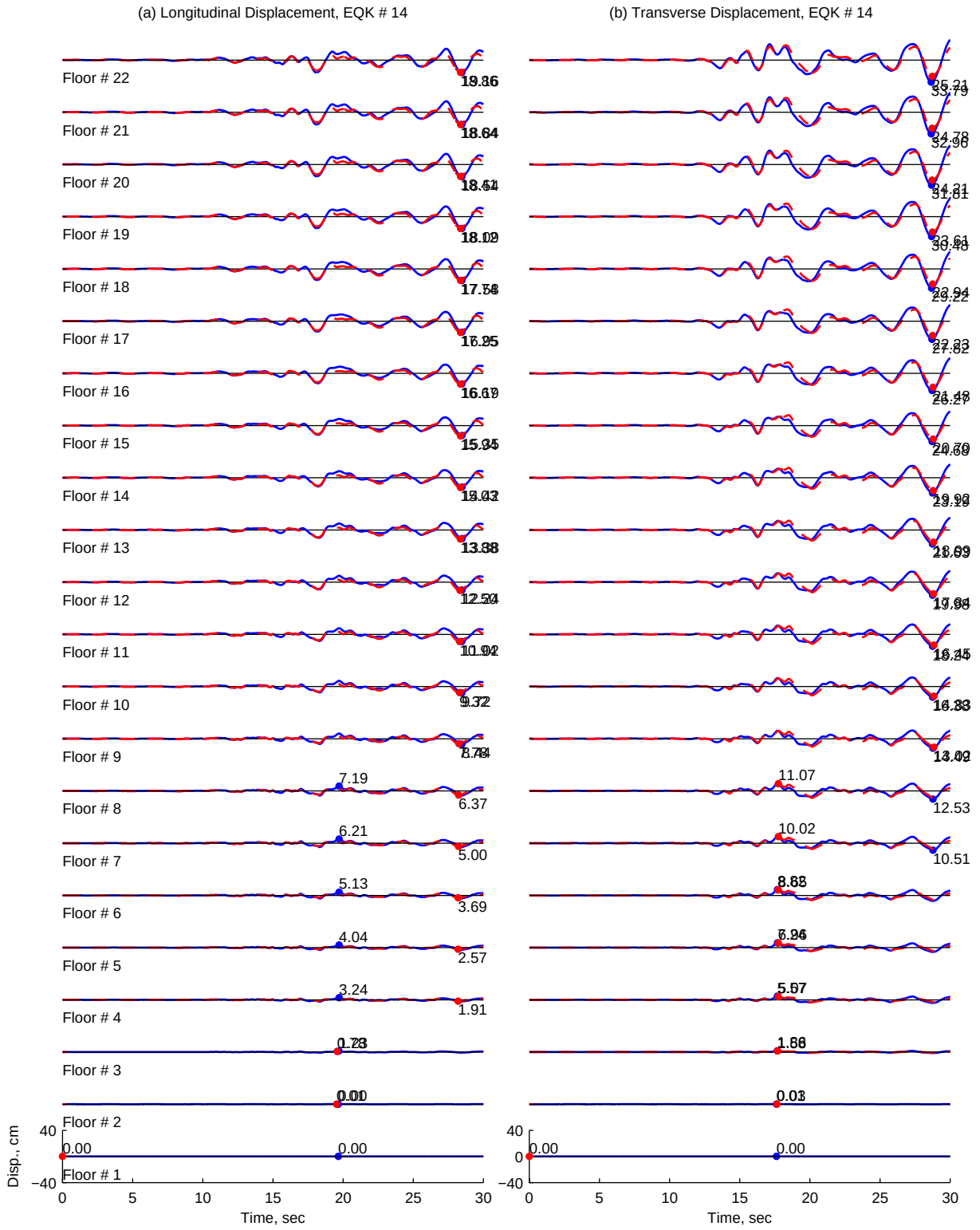

Figure II.14. Floor displacements of 20-Story North Hollywood Hotel from *OpenSees* (solid line) and *Perform3D* (dashed lines) for ground motion 14.

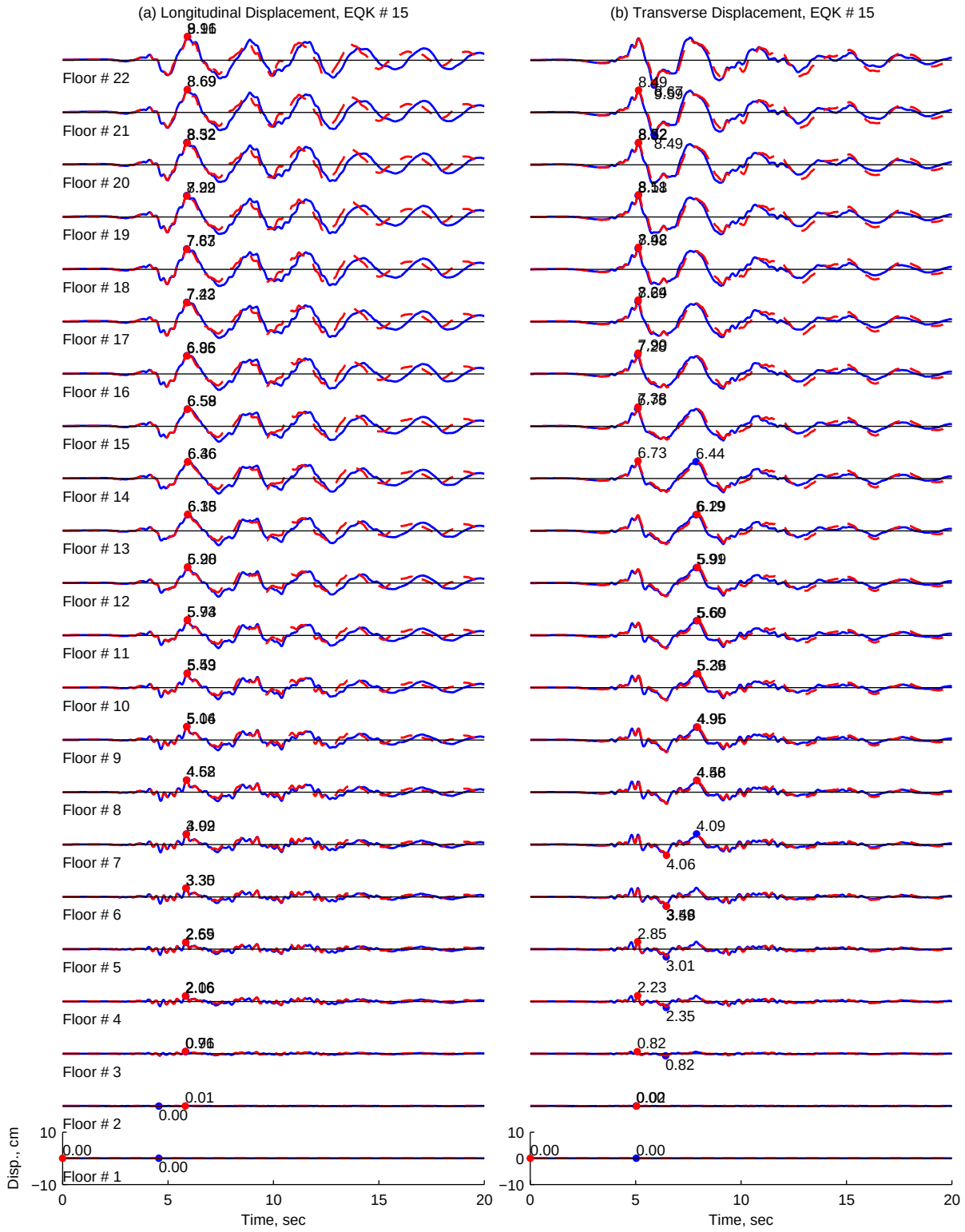

Figure II.15. Floor displacements of 20-Story North Hollywood Hotel from *OpenSees* (solid line) and *Perform3D* (dashed lines) for ground motion 15.

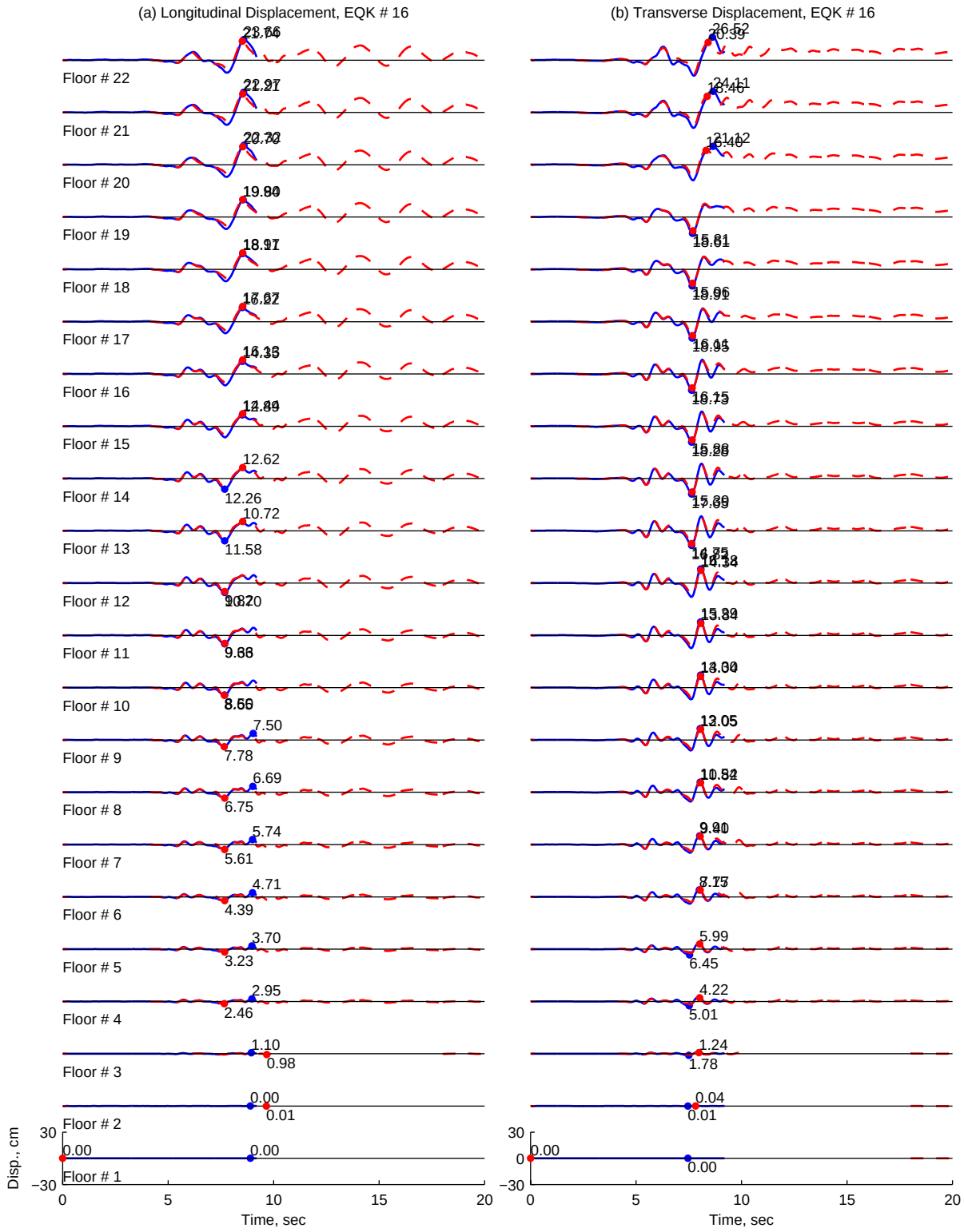

Figure II.16. Floor displacements of 20-Story North Hollywood Hotel from *OpenSees* (solid line) and *Perform3D* (dashed lines) for ground motion 16.

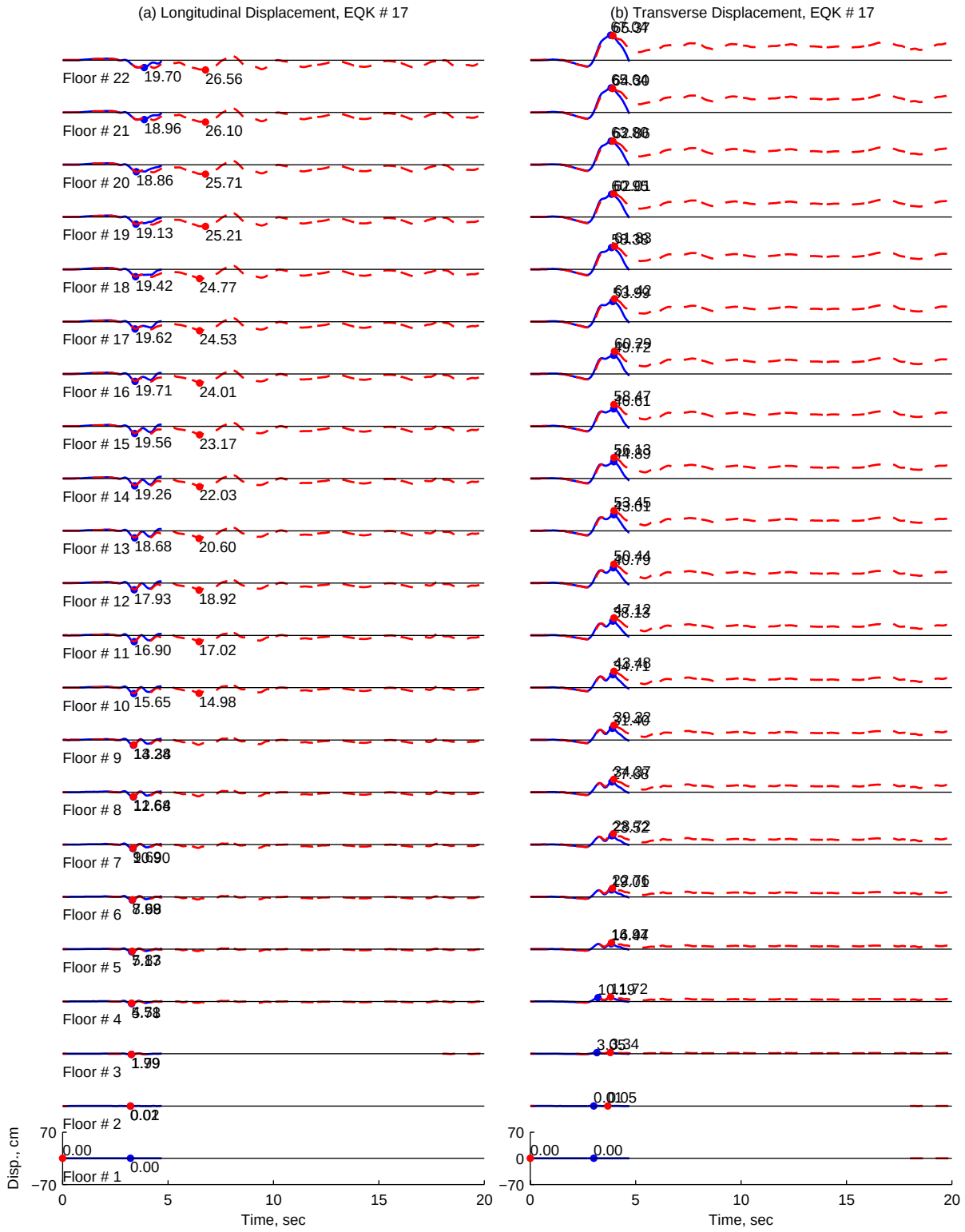

Figure II.17. Floor displacements of 20-Story North Hollywood Hotel from *OpenSees* (solid line) and *Perform3D* (dashed lines) for ground motion 17.

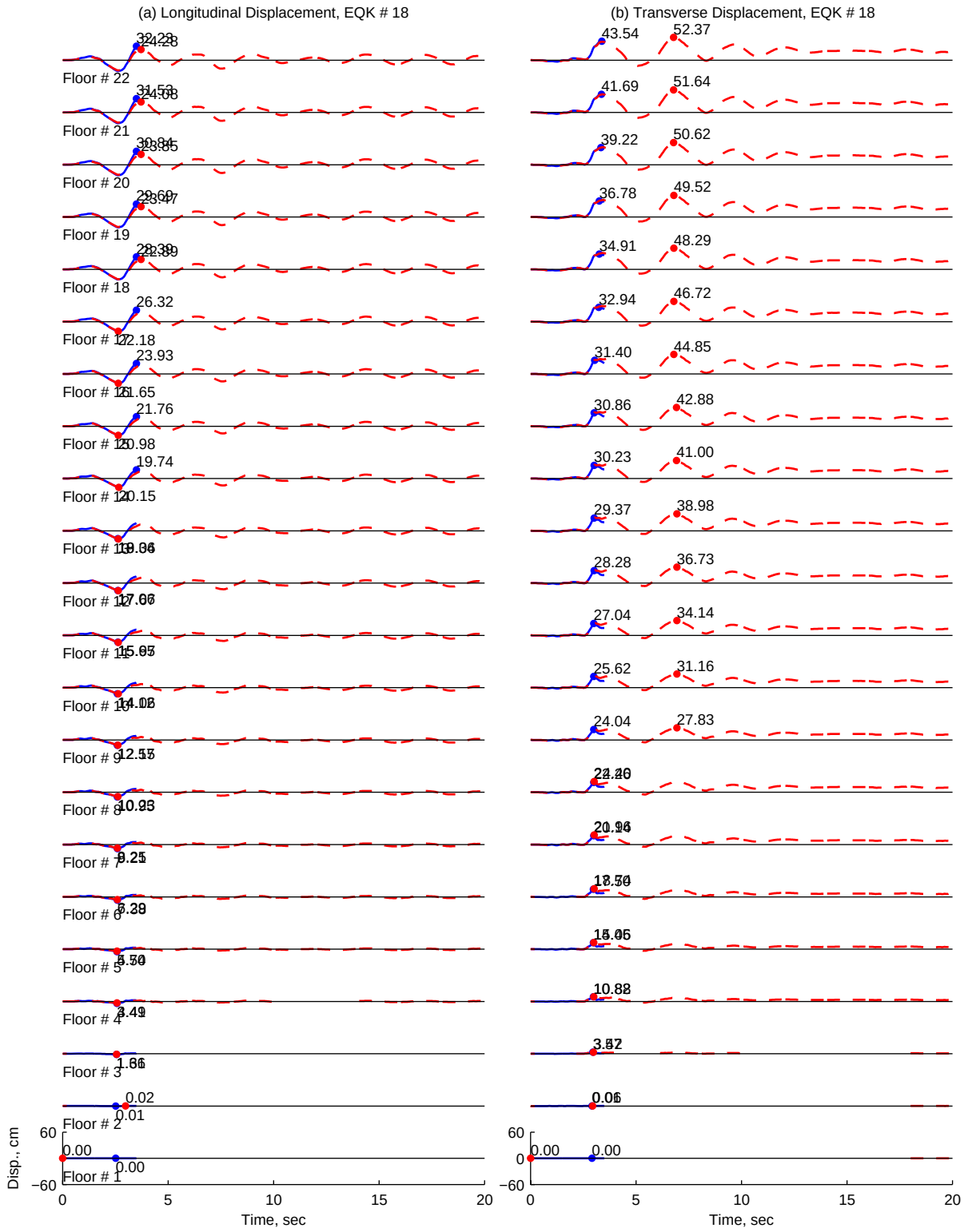

Figure II.18. Floor displacements of 20-Story North Hollywood Hotel from *OpenSees* (solid line) and *Perform3D* (dashed lines) for ground motion 18.

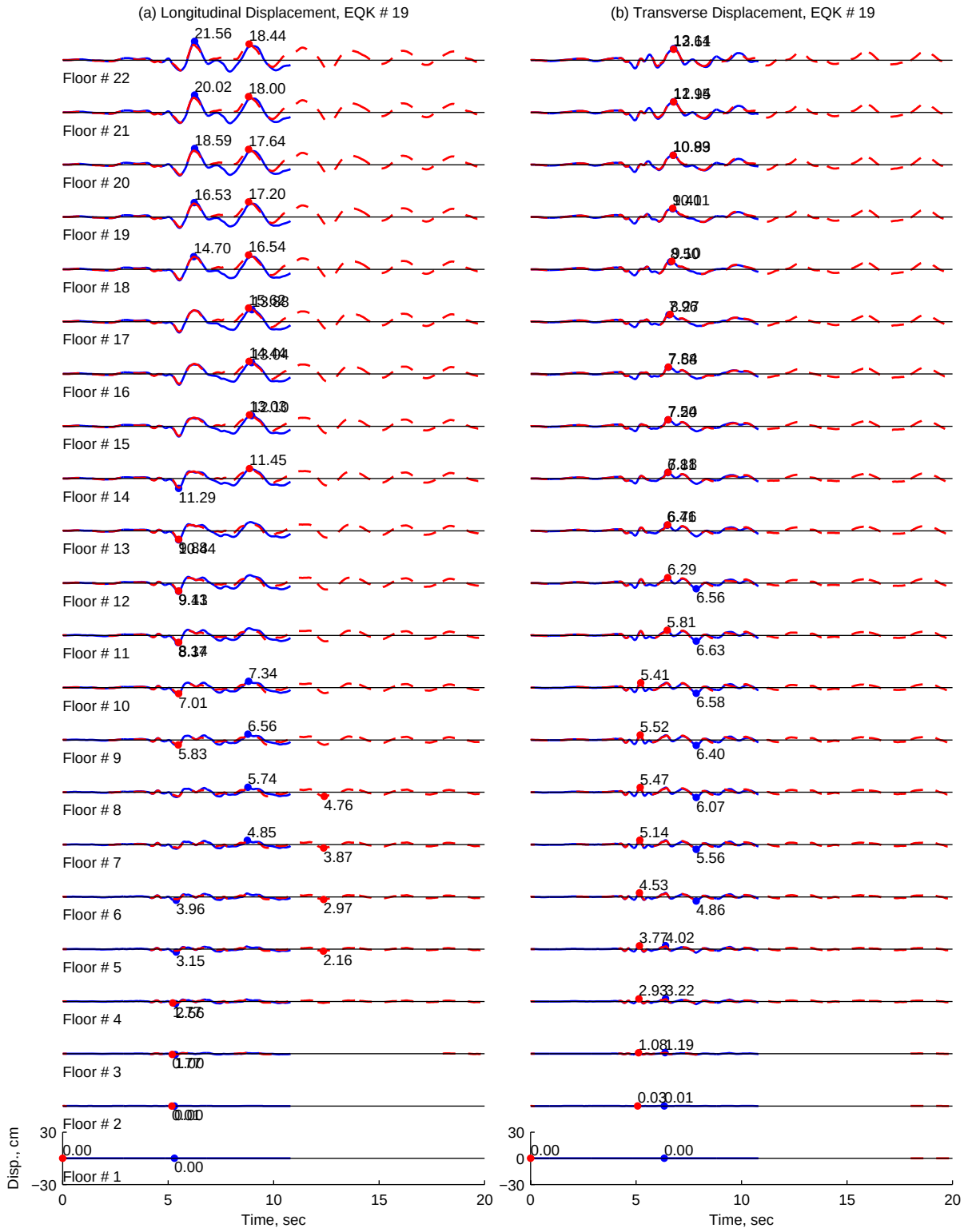

Figure II.19. Floor displacements of 20-Story North Hollywood Hotel from *OpenSees* (solid line) and *Perform3D* (dashed lines) for ground motion 19.

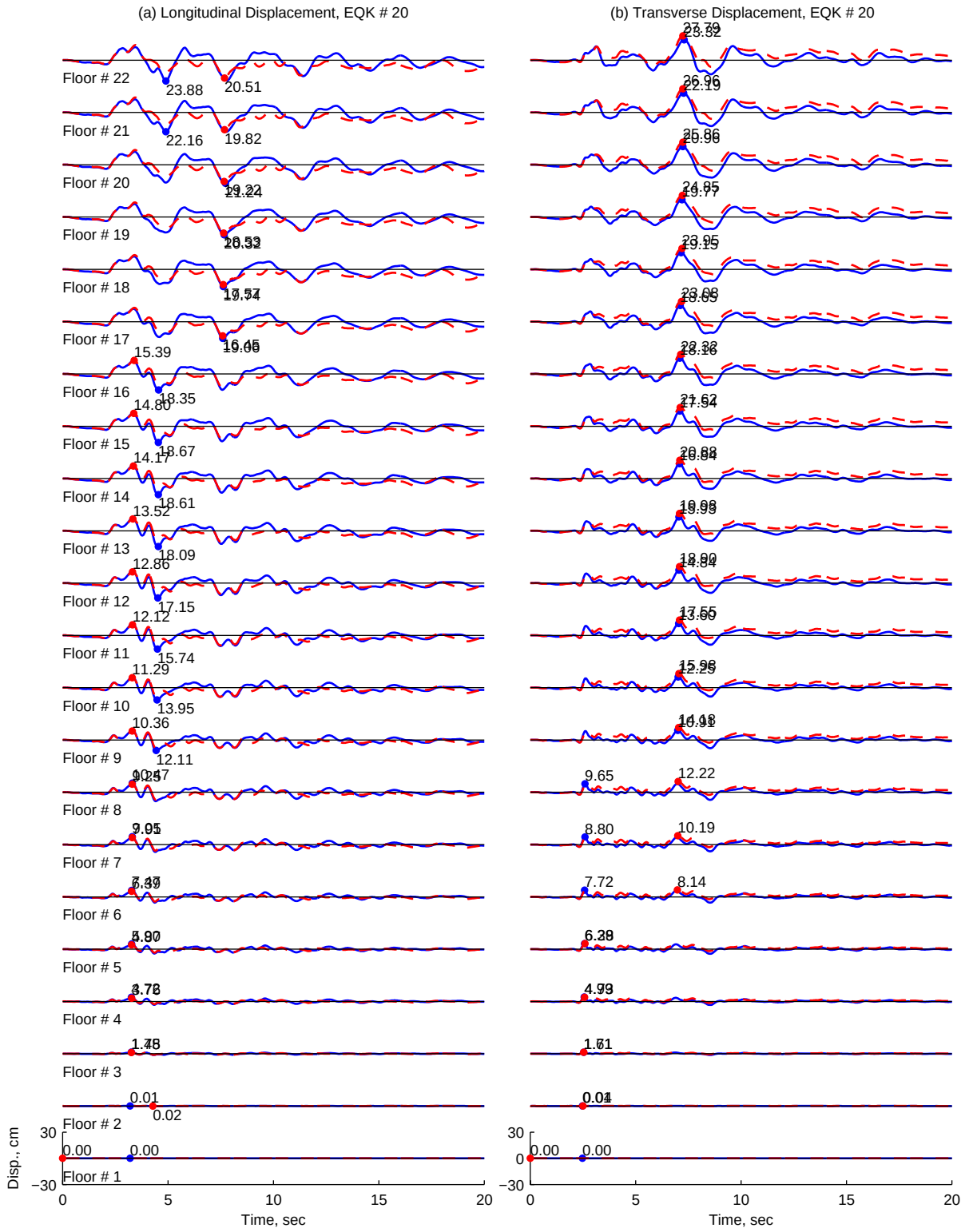

Figure II.20. Floor displacements of 20-Story North Hollywood Hotel from *OpenSees* (solid line) and *Perform3D* (dashed lines) for ground motion 20.

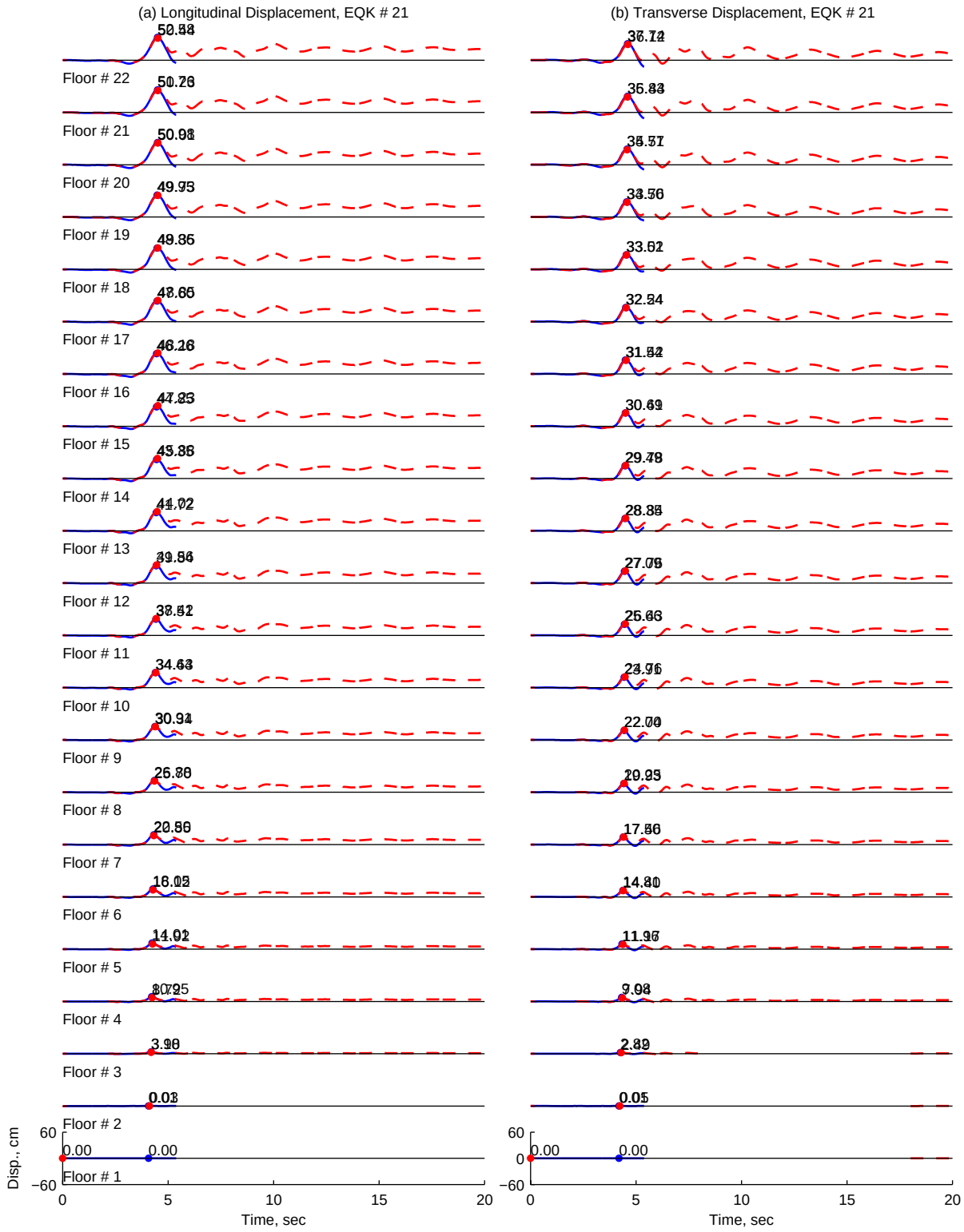

Figure II.21. Floor displacements of 20-Story North Hollywood Hotel from *OpenSees* (solid line) and *Perform3D* (dashed lines) for ground motion 21.

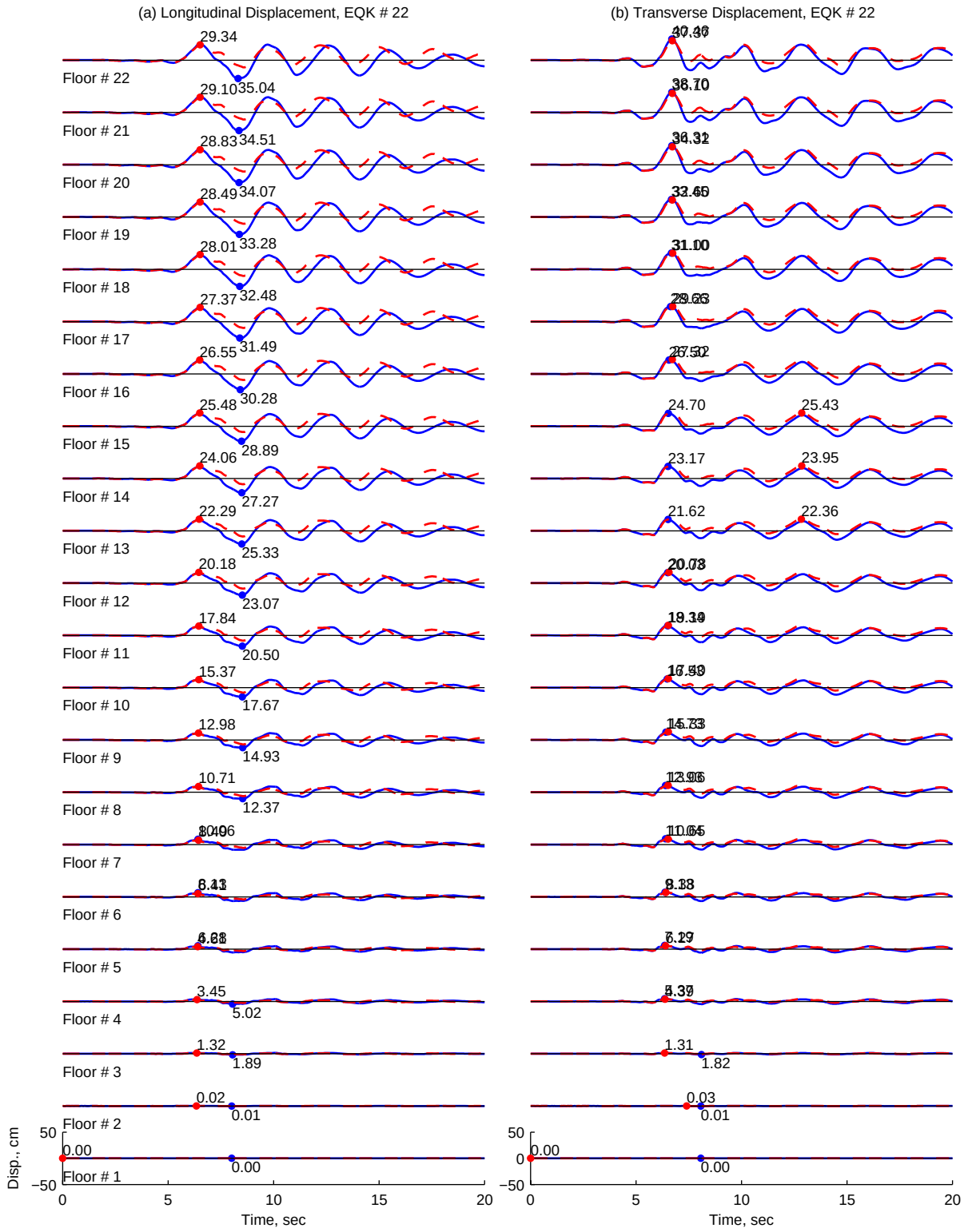

Figure II.22. Floor displacements of 20-Story North Hollywood Hotel from *OpenSees* (solid line) and *Perform3D* (dashed lines) for ground motion 22.

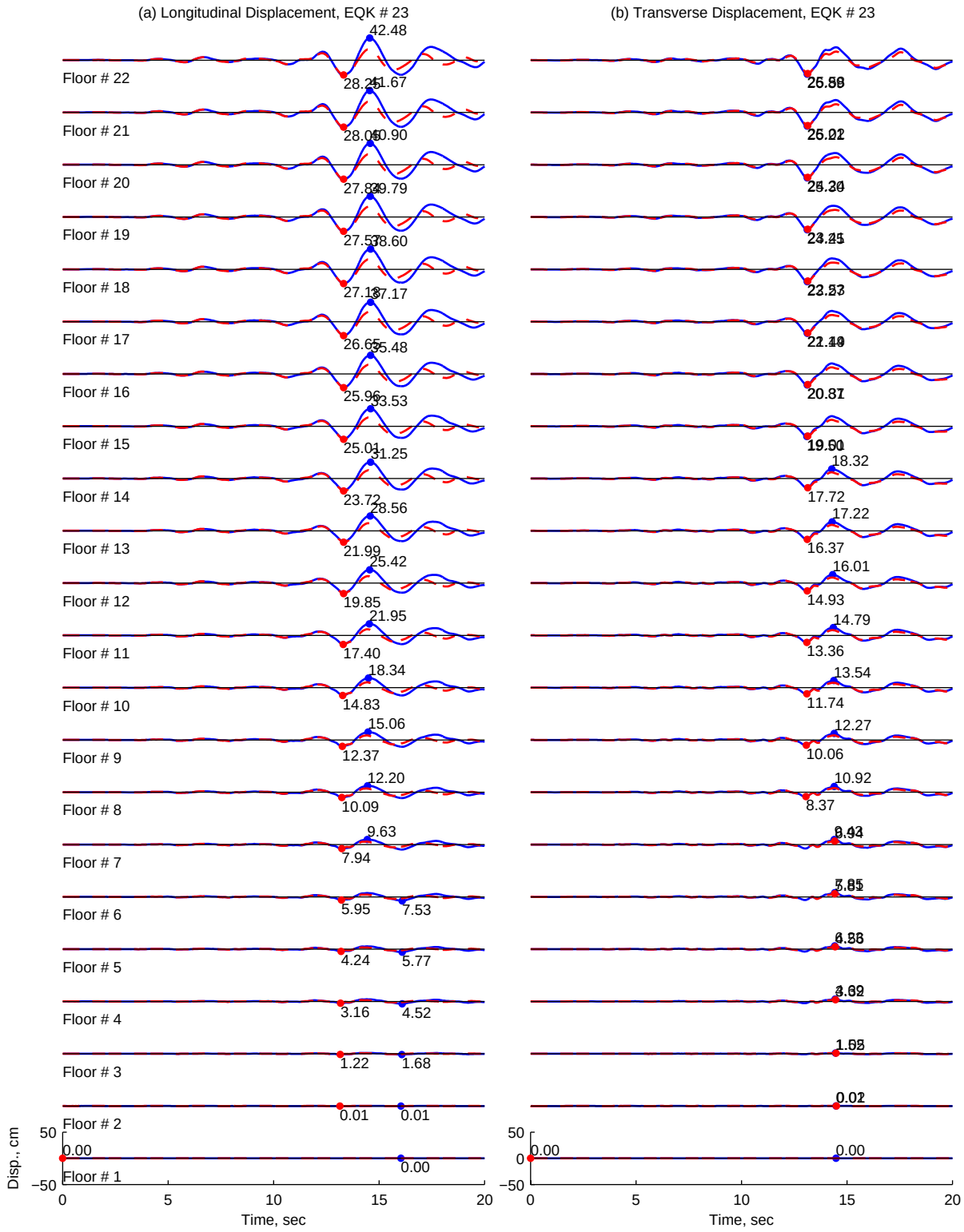

Figure II.23. Floor displacements of 20-Story North Hollywood Hotel from *OpenSees* (solid line) and *Perform3D* (dashed lines) for ground motion 23.

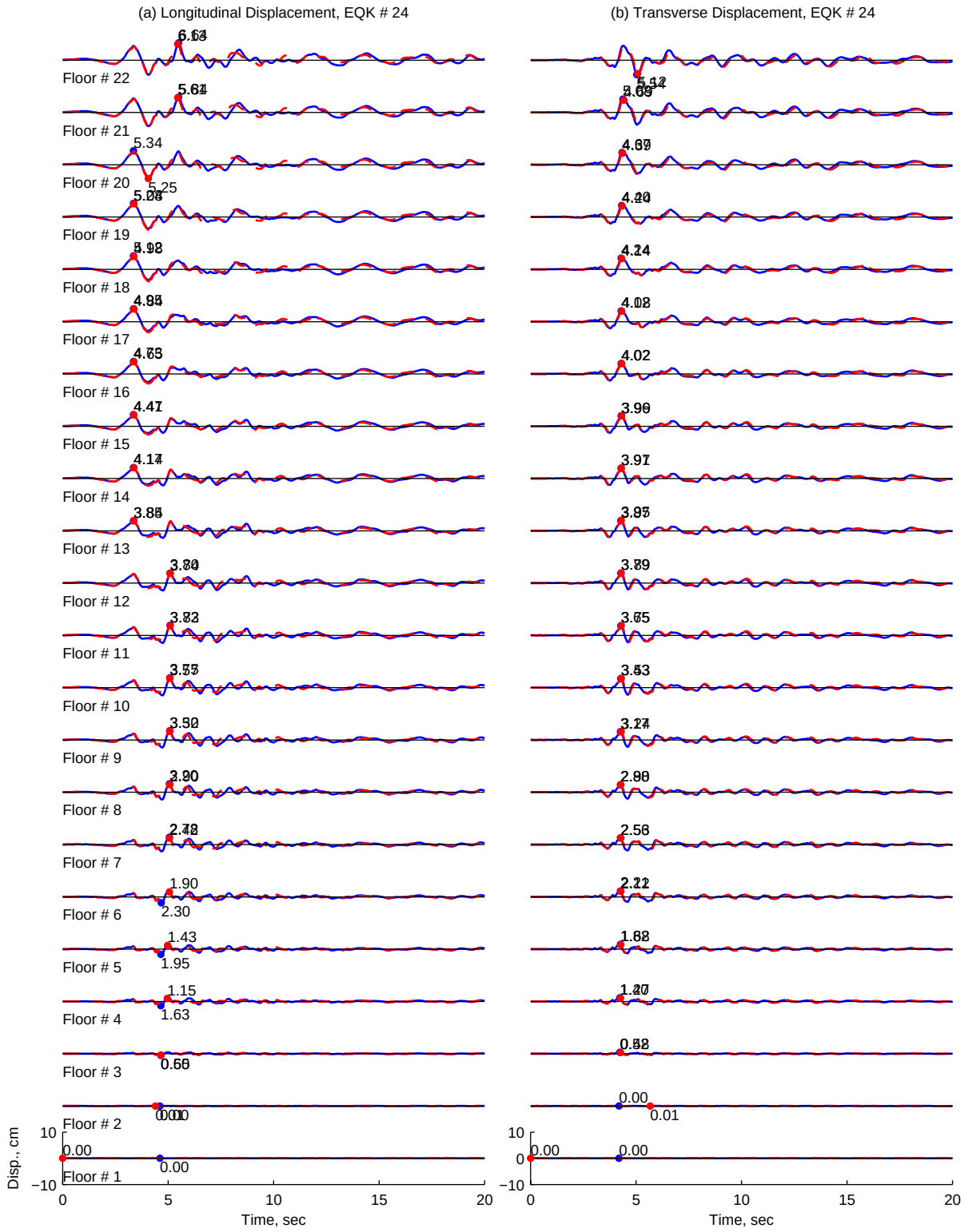

Figure II.24. Floor displacements of 20-Story North Hollywood Hotel from *OpenSees* (solid line) and *Perform3D* (dashed lines) for ground motion 24.

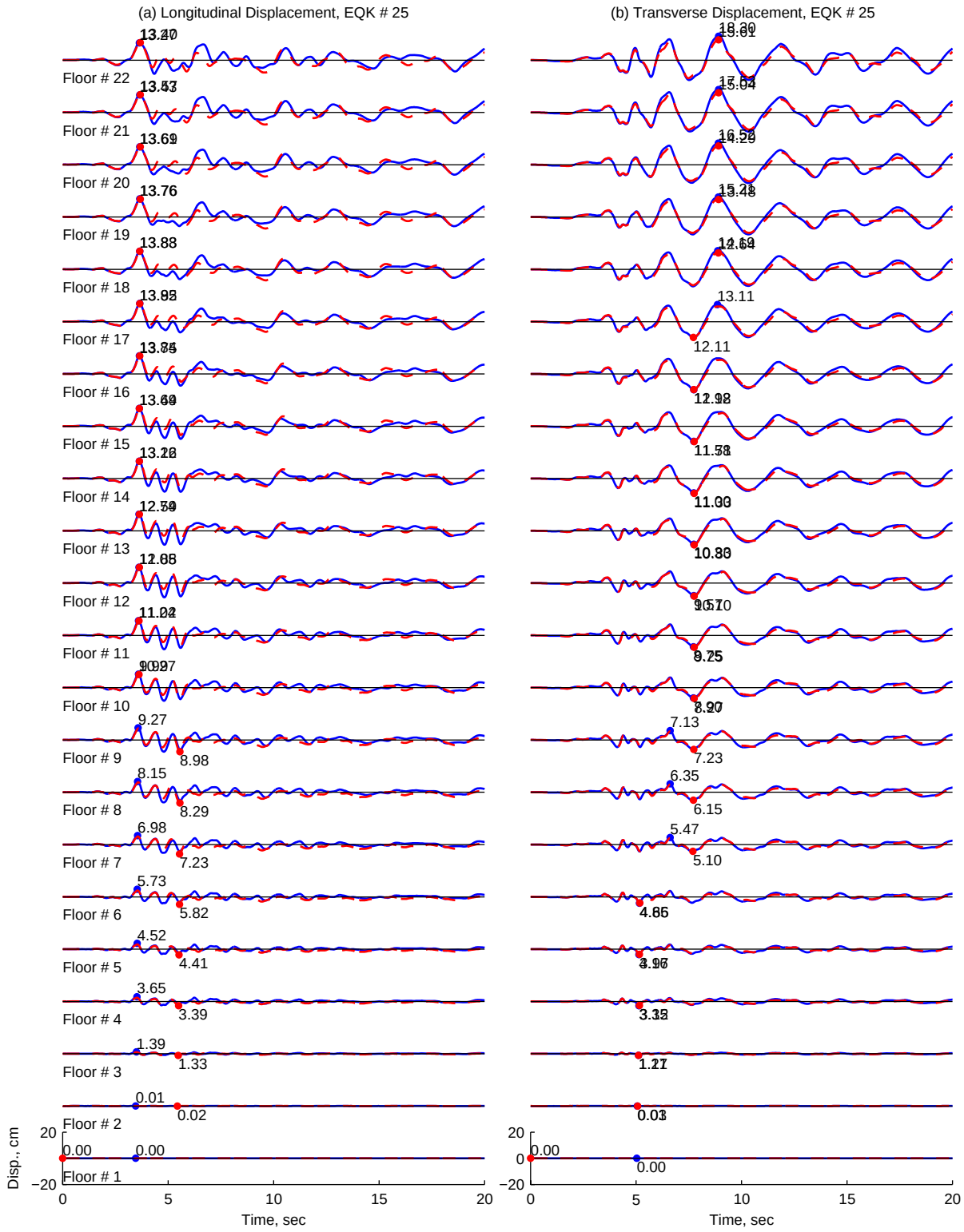

Figure II.25. Floor displacements of 20-Story North Hollywood Hotel from *OpenSees* (solid line) and *Perform3D* (dashed lines) for ground motion 25.

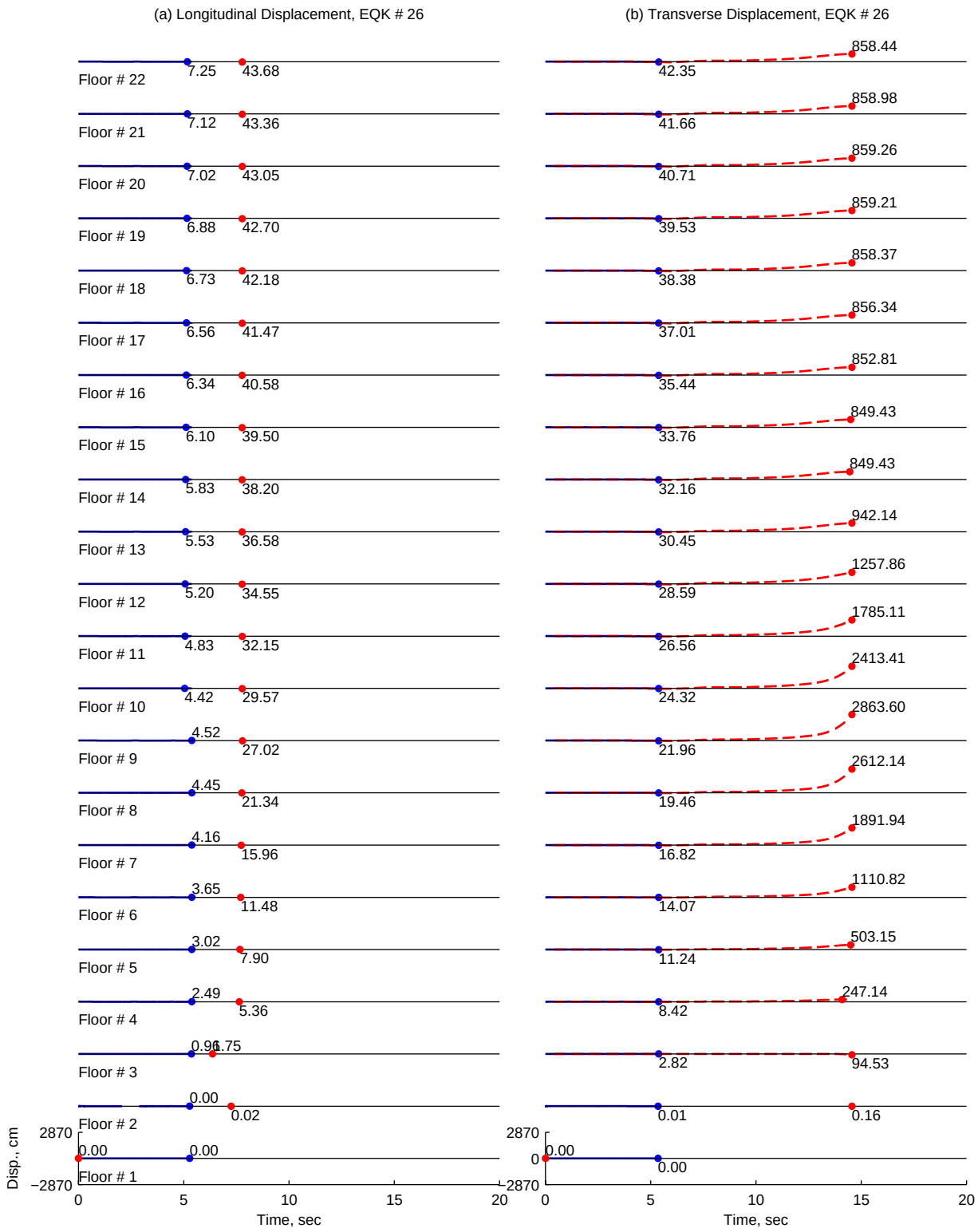

Figure II.26. Floor displacements of 20-Story North Hollywood Hotel from *OpenSees* (solid line) and *Perform3D* (dashed lines) for ground motion 26.

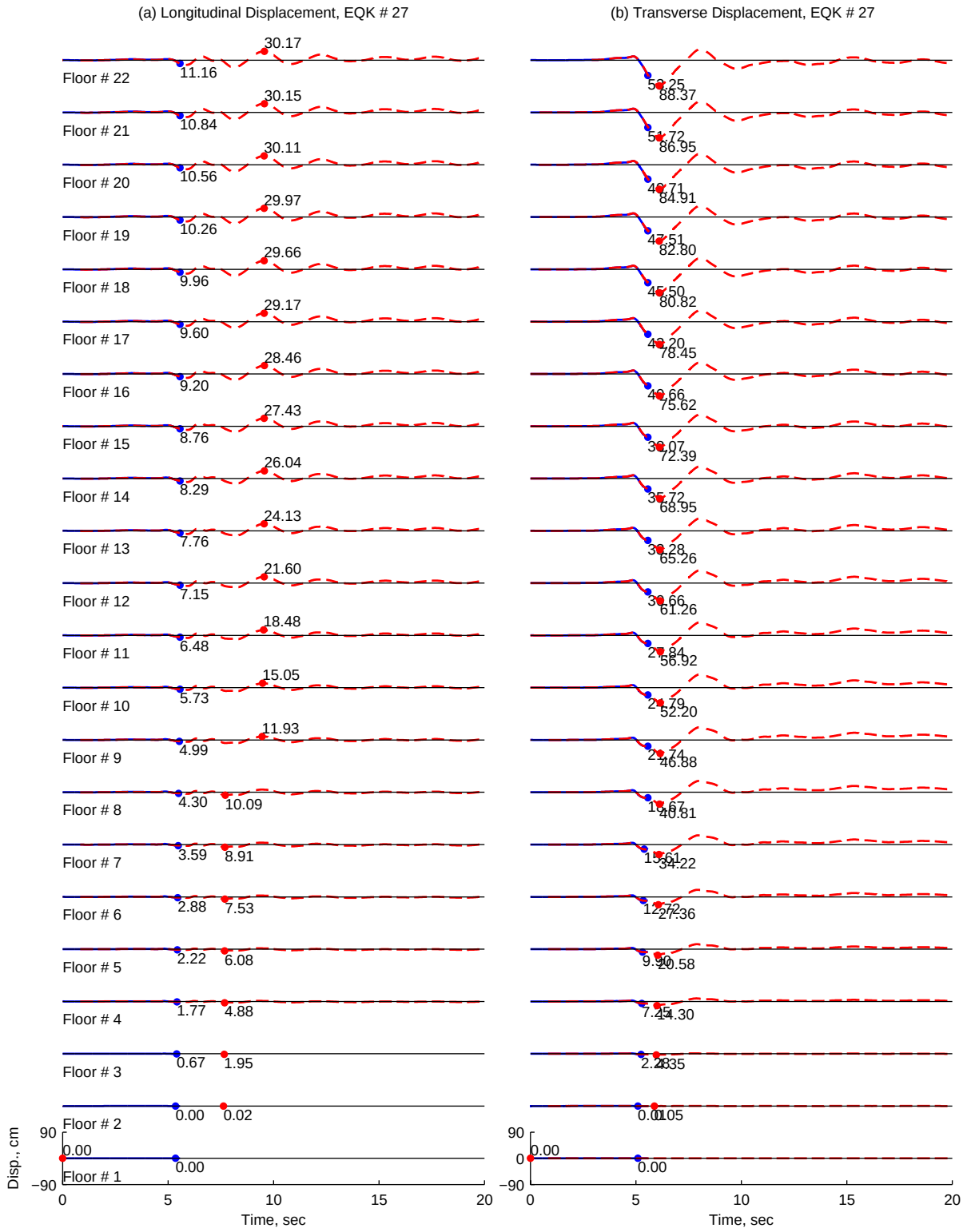

Figure II.27. Floor displacements of 20-Story North Hollywood Hotel from *OpenSees* (solid line) and *Perform3D* (dashed lines) for ground motion 27.

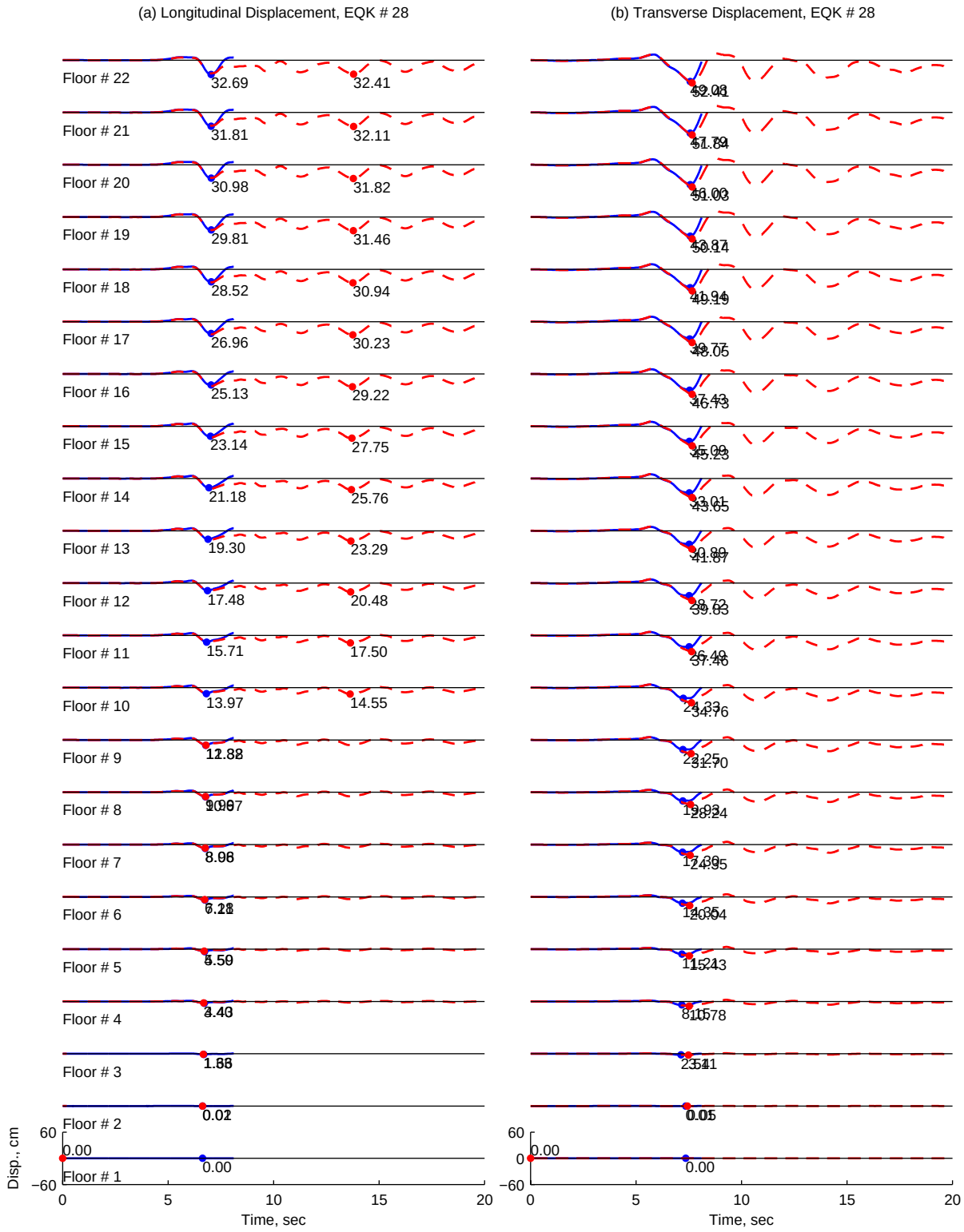

Figure II.28. Floor displacements of 20-Story North Hollywood Hotel from *OpenSees* (solid line) and *Perform3D* (dashed lines) for ground motion 28.

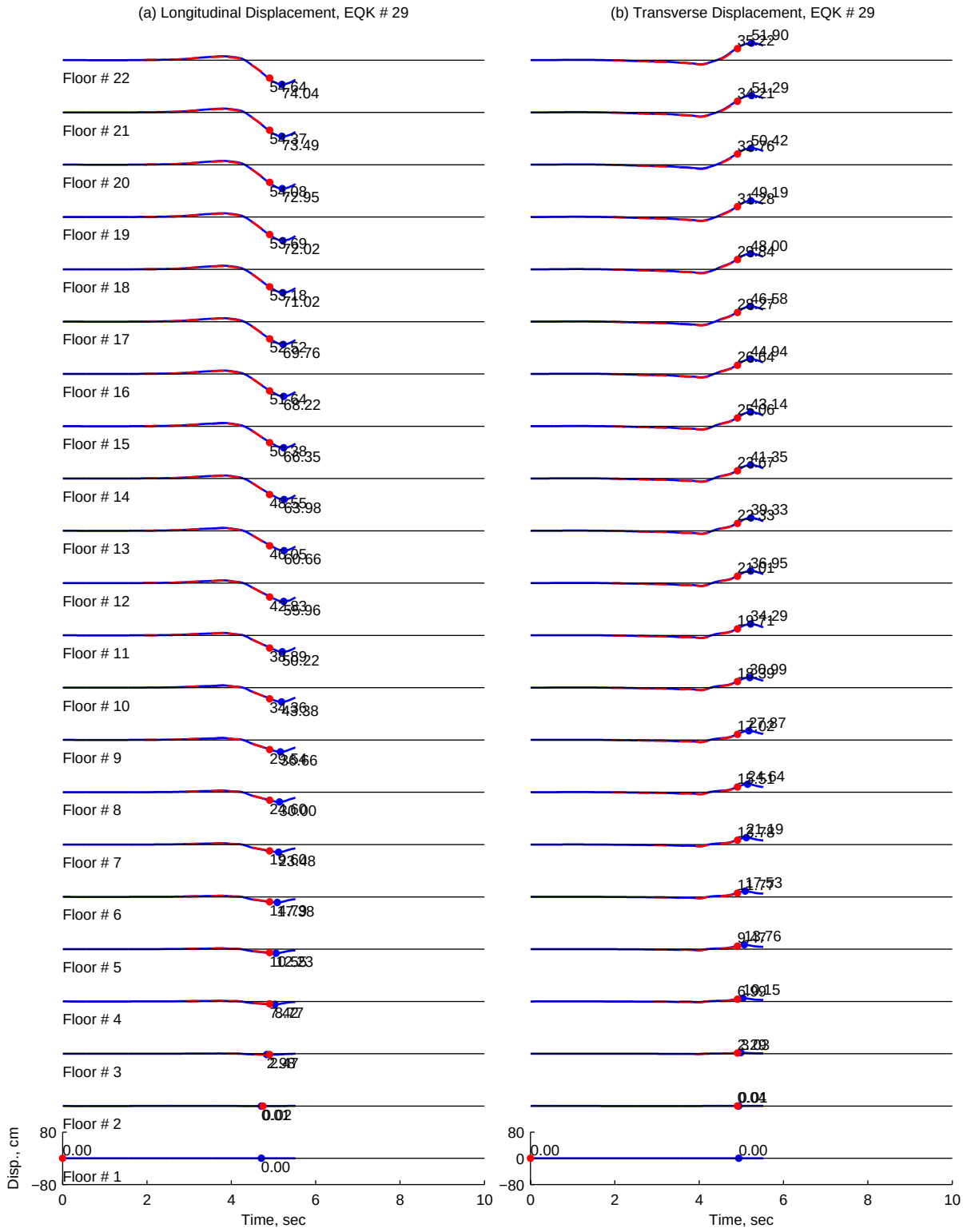

Figure II.29. Floor displacements of 20-Story North Hollywood Hotel from *OpenSees* (solid line) and *Perform3D* (dashed lines) for ground motion 29.

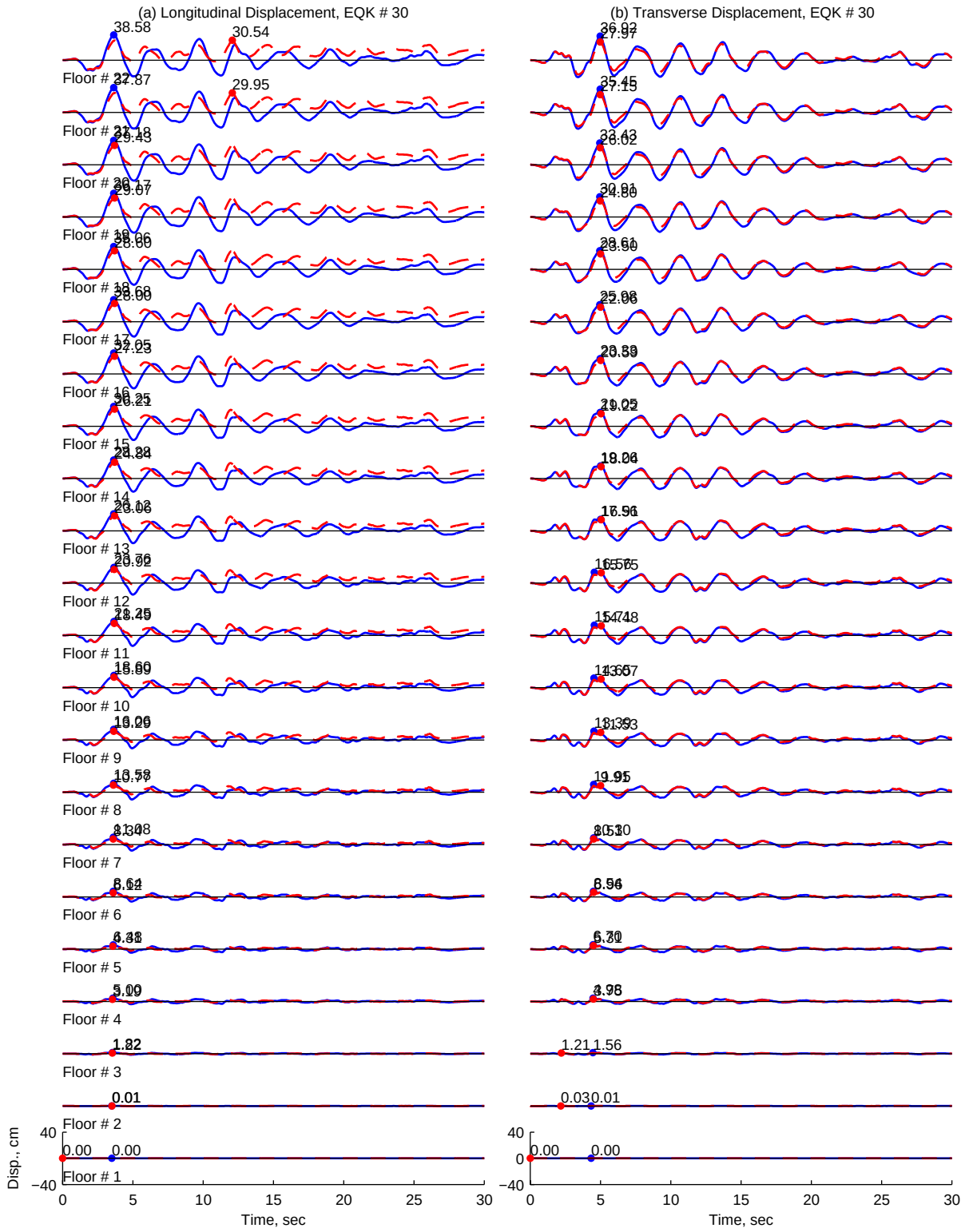

Figure II.30. Floor displacements of 20-Story North Hollywood Hotel from *OpenSees* (solid line) and *Perform3D* (dashed lines) for ground motion 30.

Figure II.31. Floor accelerations of 20-Story North Hollywood Hotel from *OpenSees* (solid line) and *Perform3D* (dashed lines) for ground motion 1.

Figure II.32. Floor accelerations of 20-Story North Hollywood Hotel from *OpenSees* (solid line) and *Perform3D* (dashed lines) for ground motion 2.

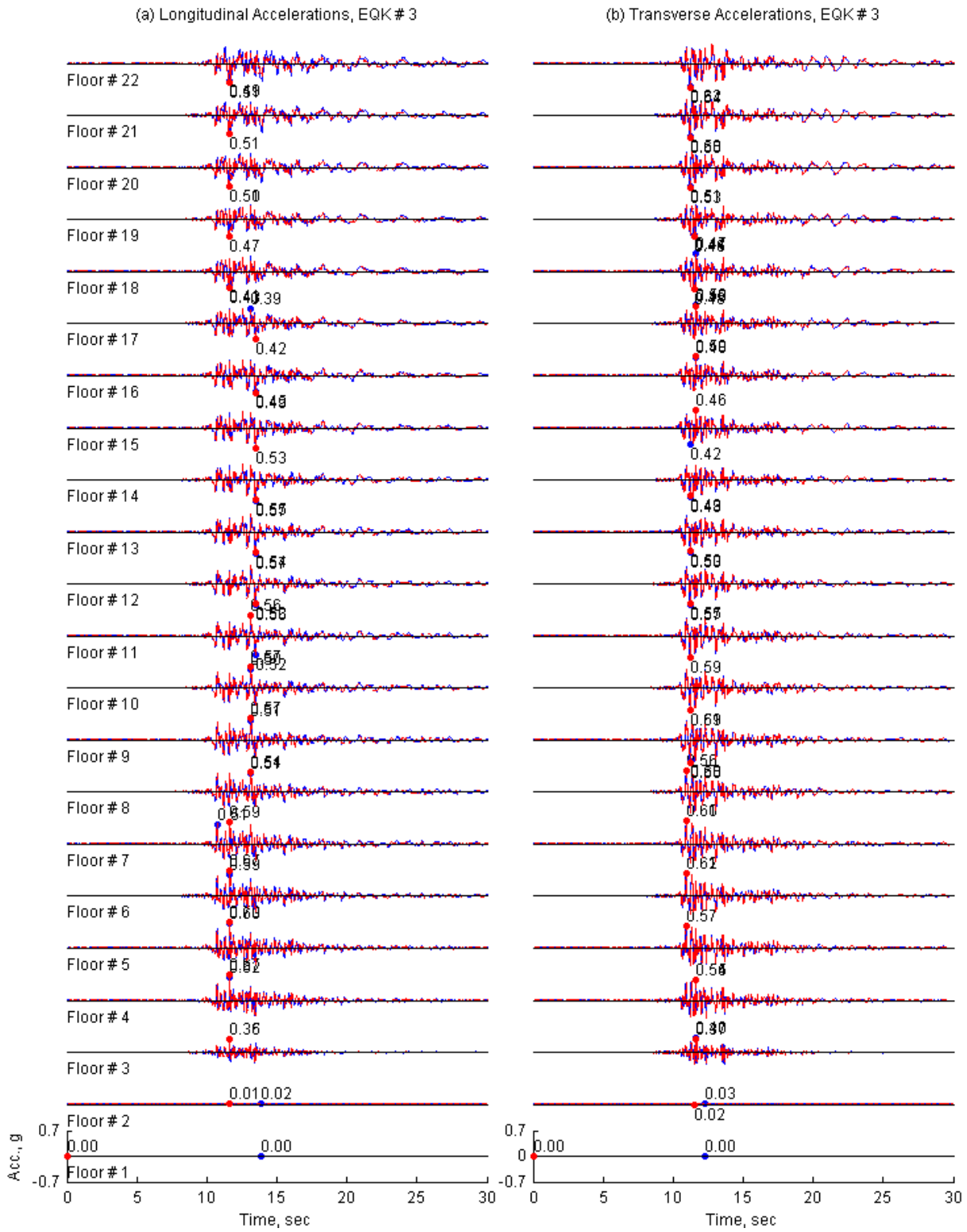

Figure II.33. Floor accelerations of 20-Story North Hollywood Hotel from *OpenSees* (solid line) and *Perform3D* (dashed lines) for ground motion 3.

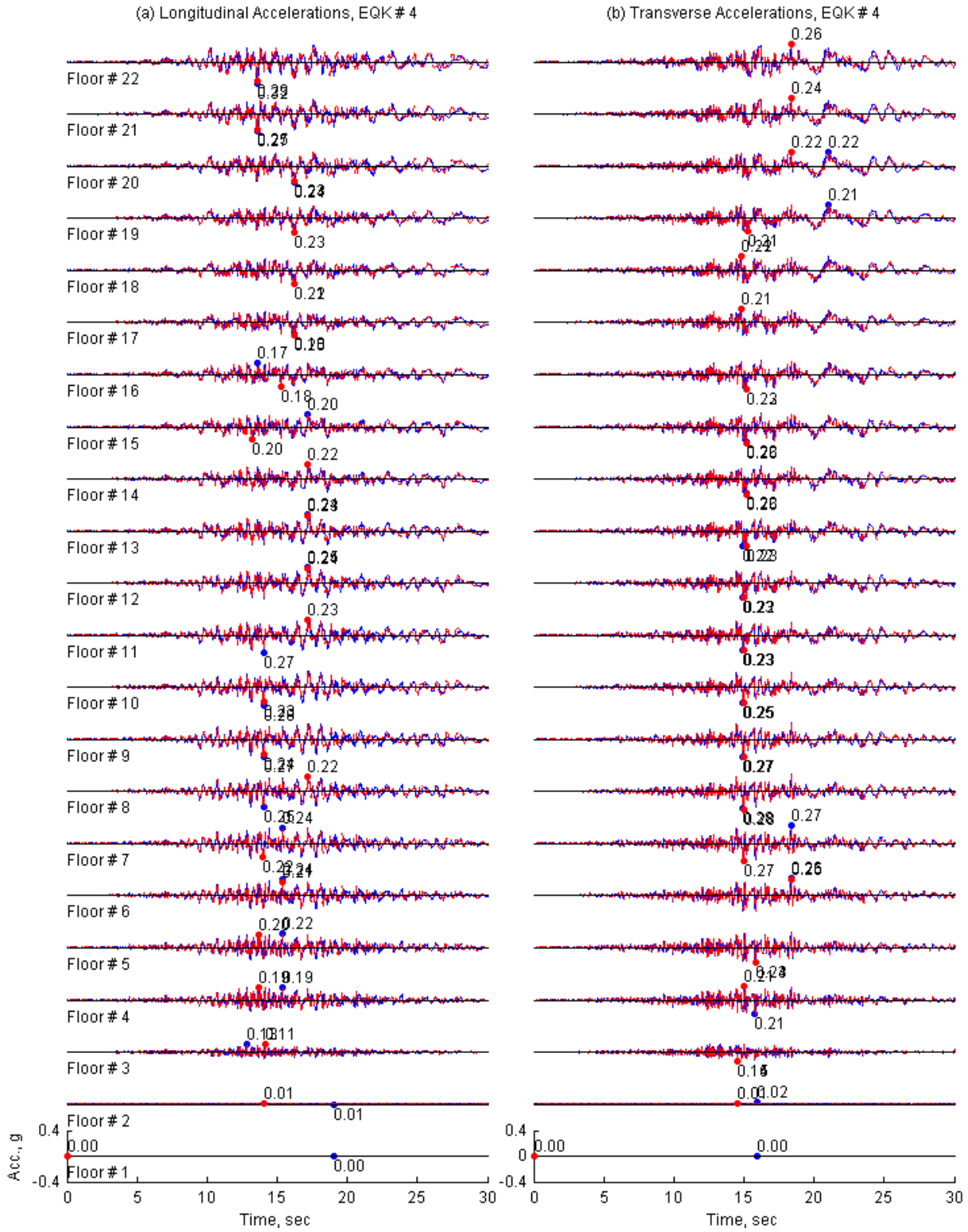

Figure II.34. Floor accelerations of 20-Story North Hollywood Hotel from *OpenSees* (solid line) and *Perform3D* (dashed lines) for ground motion 4.

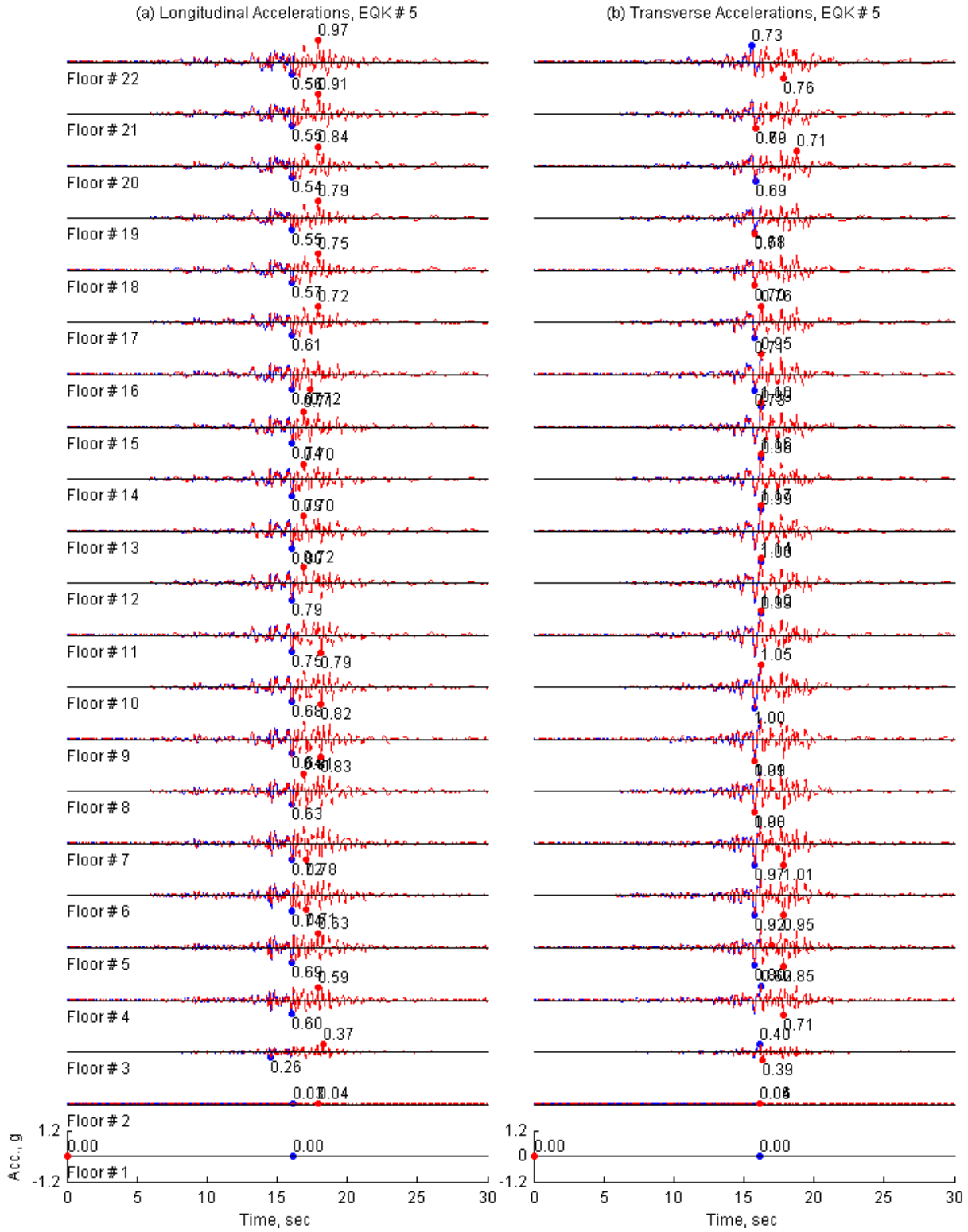

Figure II.35. Floor accelerations of 20-Story North Hollywood Hotel from *OpenSees* (solid line) and *Perform3D* (dashed lines) for ground motion 5.

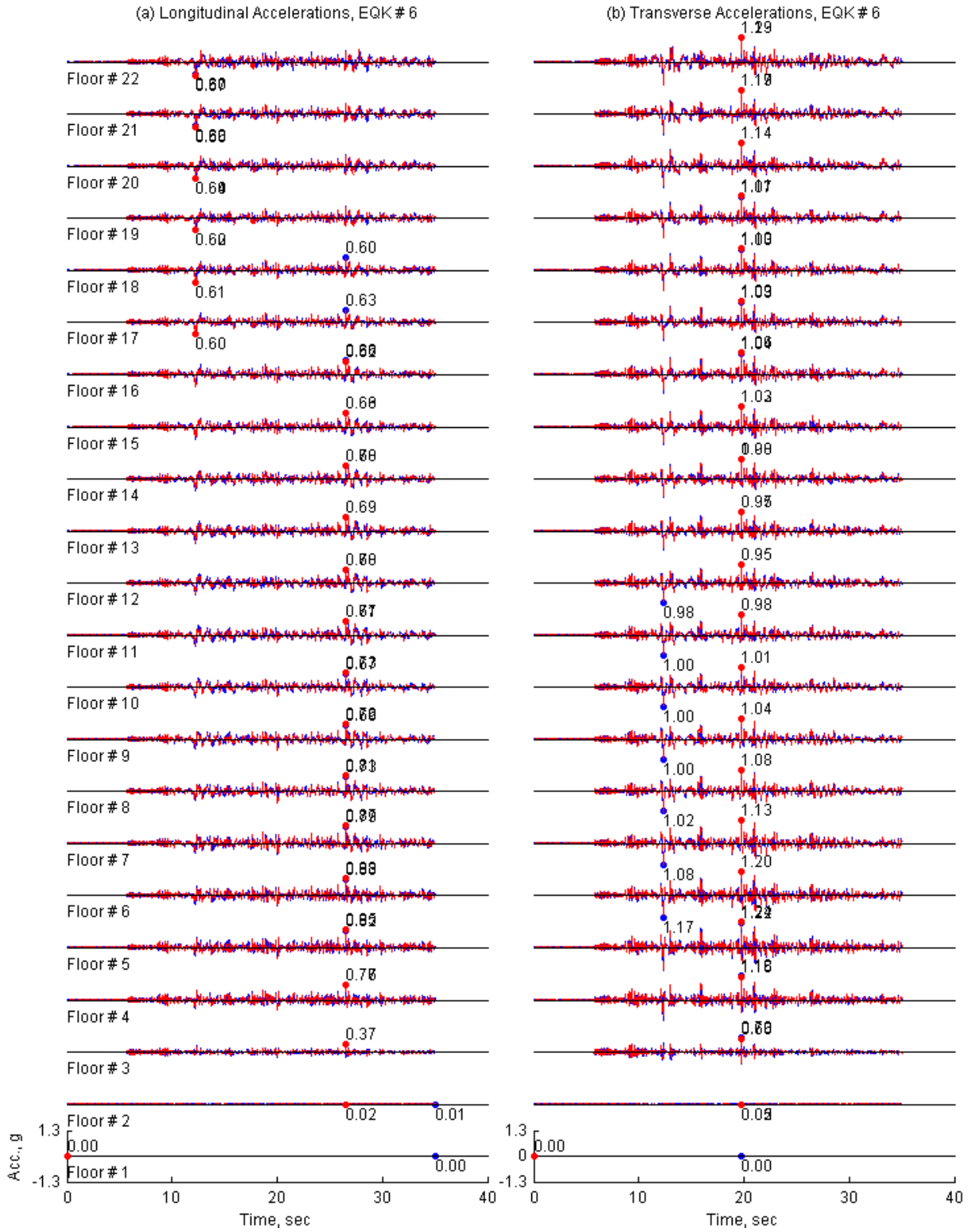

Figure II.36. Floor accelerations of 20-Story North Hollywood Hotel from *OpenSees* (solid line) and *Perform3D* (dashed lines) for ground motion 6.

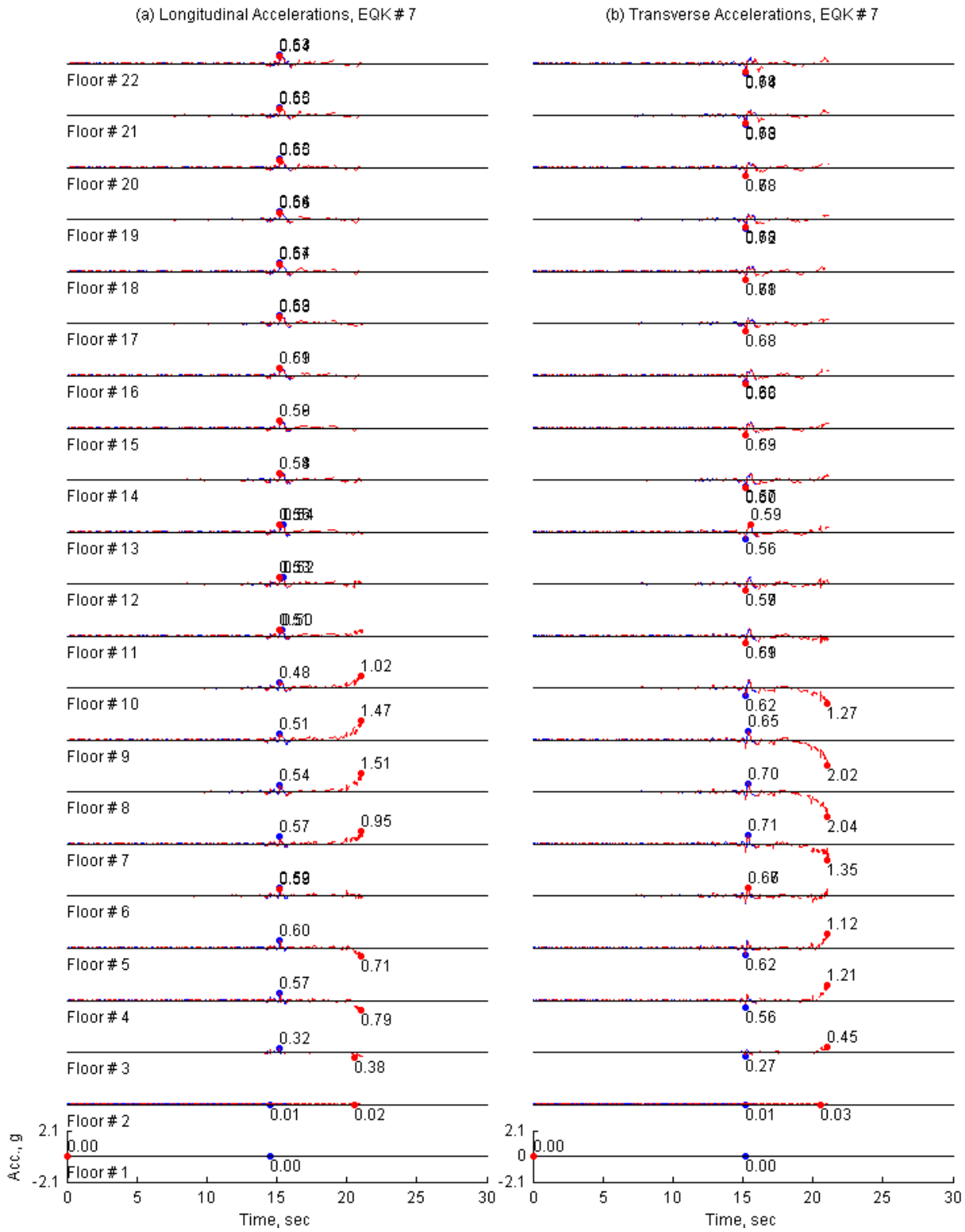

Figure II.37. Floor accelerations of 20-Story North Hollywood Hotel from *OpenSees* (solid line) and *Perform3D* (dashed lines) for ground motion 7.

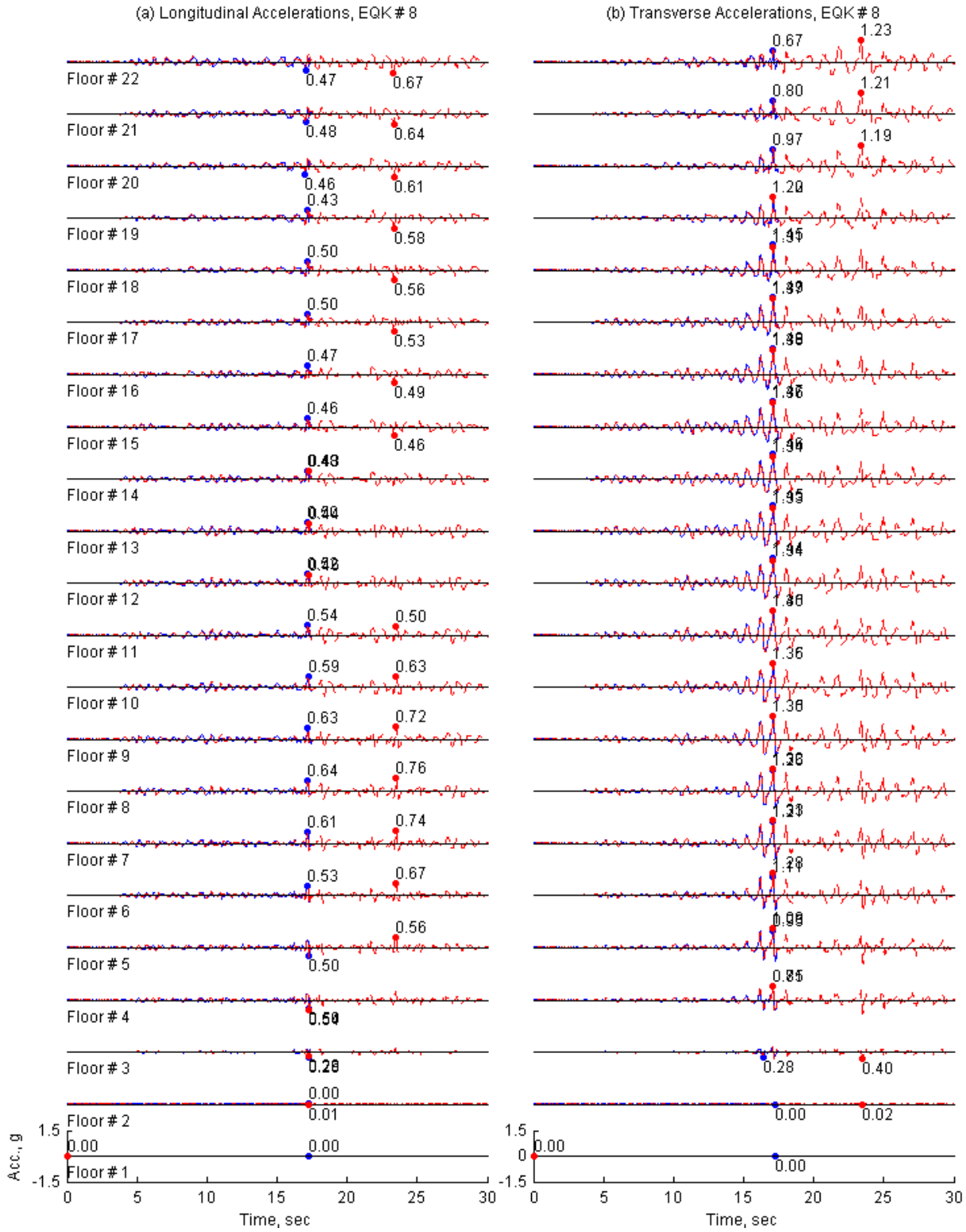

Figure II.38. Floor accelerations of 20-Story North Hollywood Hotel from *OpenSees* (solid line) and *Perform3D* (dashed lines) for ground motion 8.

Figure II.39. Floor accelerations of 20-Story North Hollywood Hotel from *OpenSees* (solid line) and *Perform3D* (dashed lines) for ground motion 9.

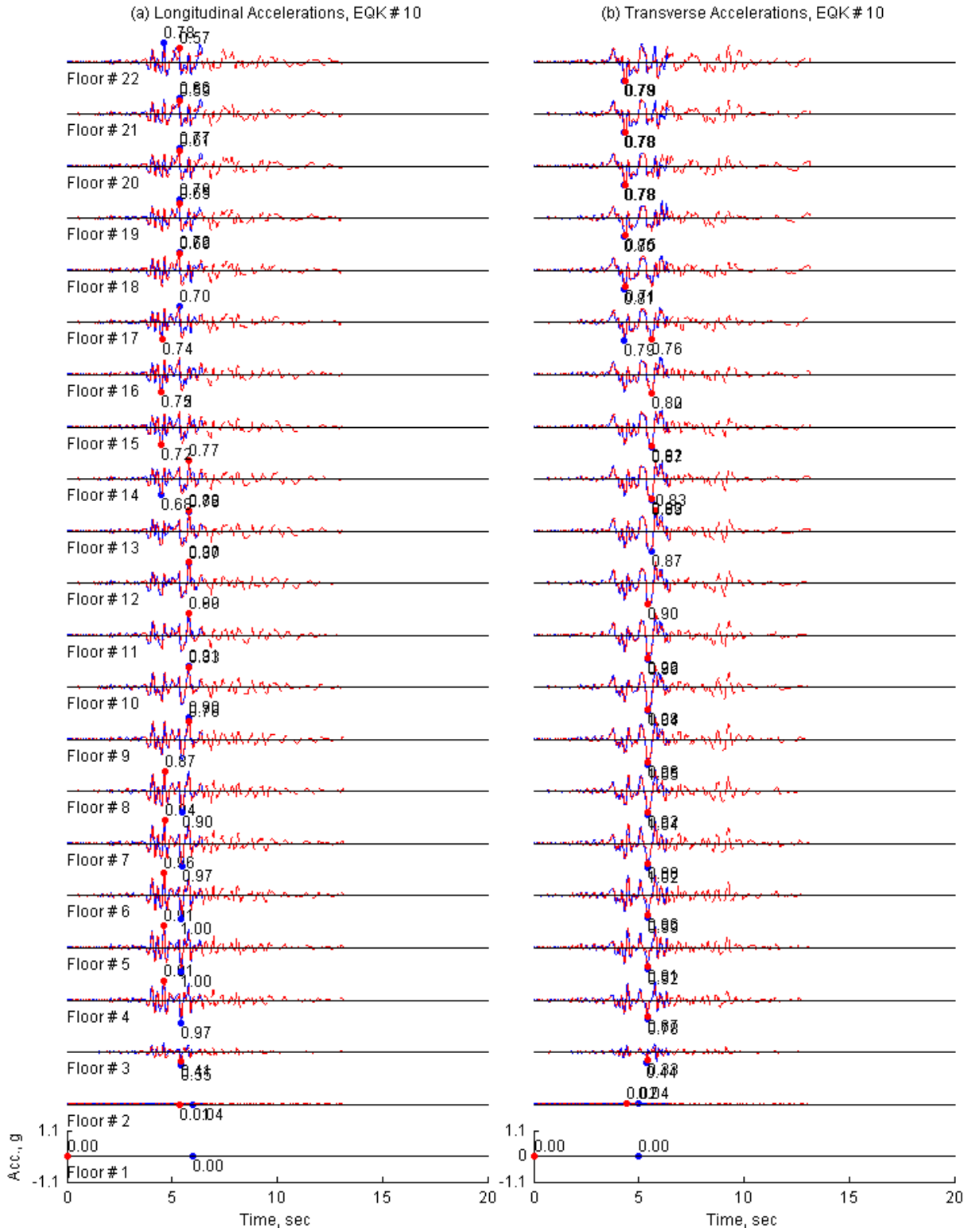

Figure II.40. Floor accelerations of 20-Story North Hollywood Hotel from *OpenSees* (solid line) and *Perform3D* (dashed lines) for ground motion 10.

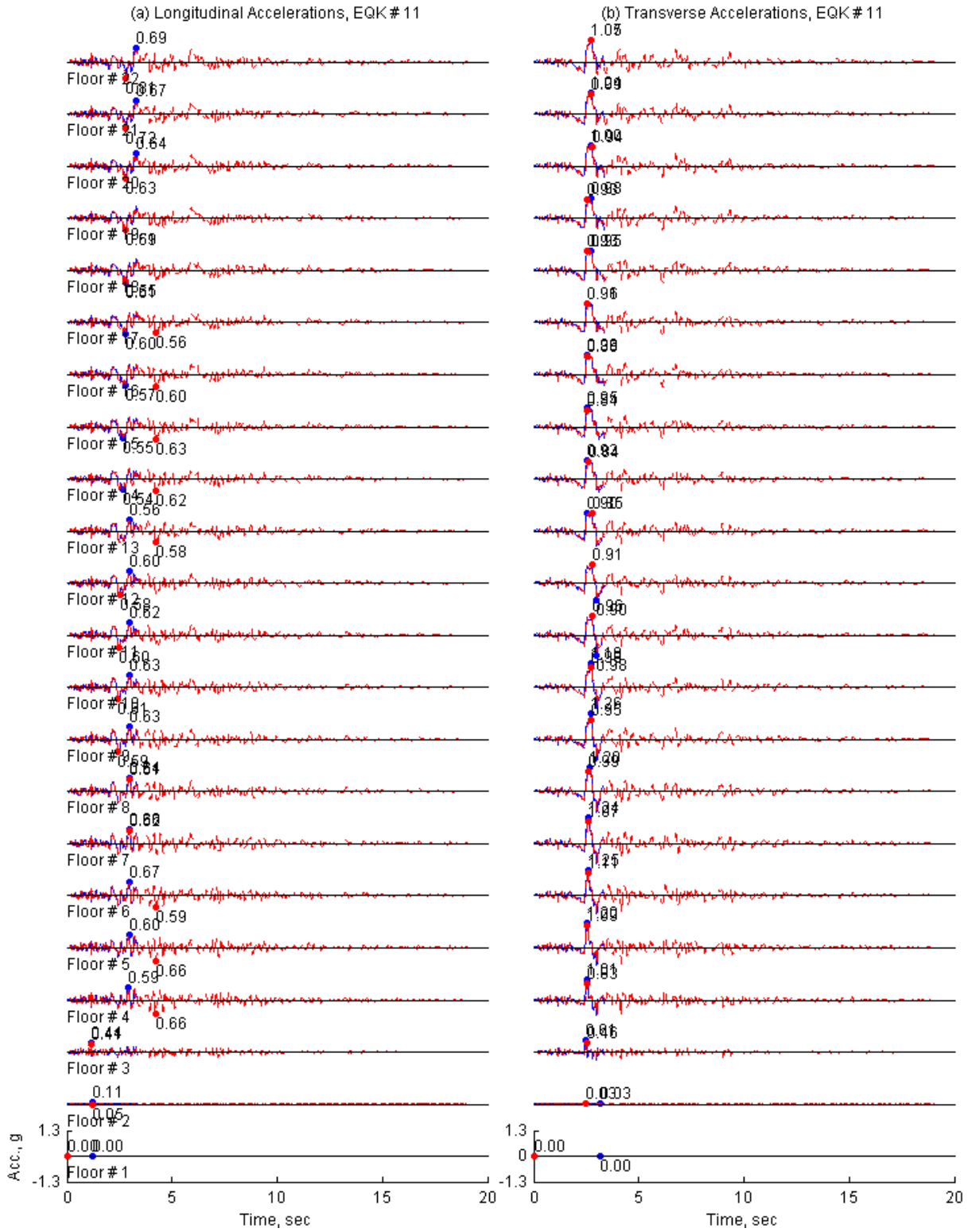

Figure II.41. Floor accelerations of 20-Story North Hollywood Hotel from *OpenSees* (solid line) and *Perform3D* (dashed lines) for ground motion 11.

Figure II.42. Floor accelerations of 20-Story North Hollywood Hotel from *OpenSees* (solid line) and *Perform3D* (dashed lines) for ground motion 12.

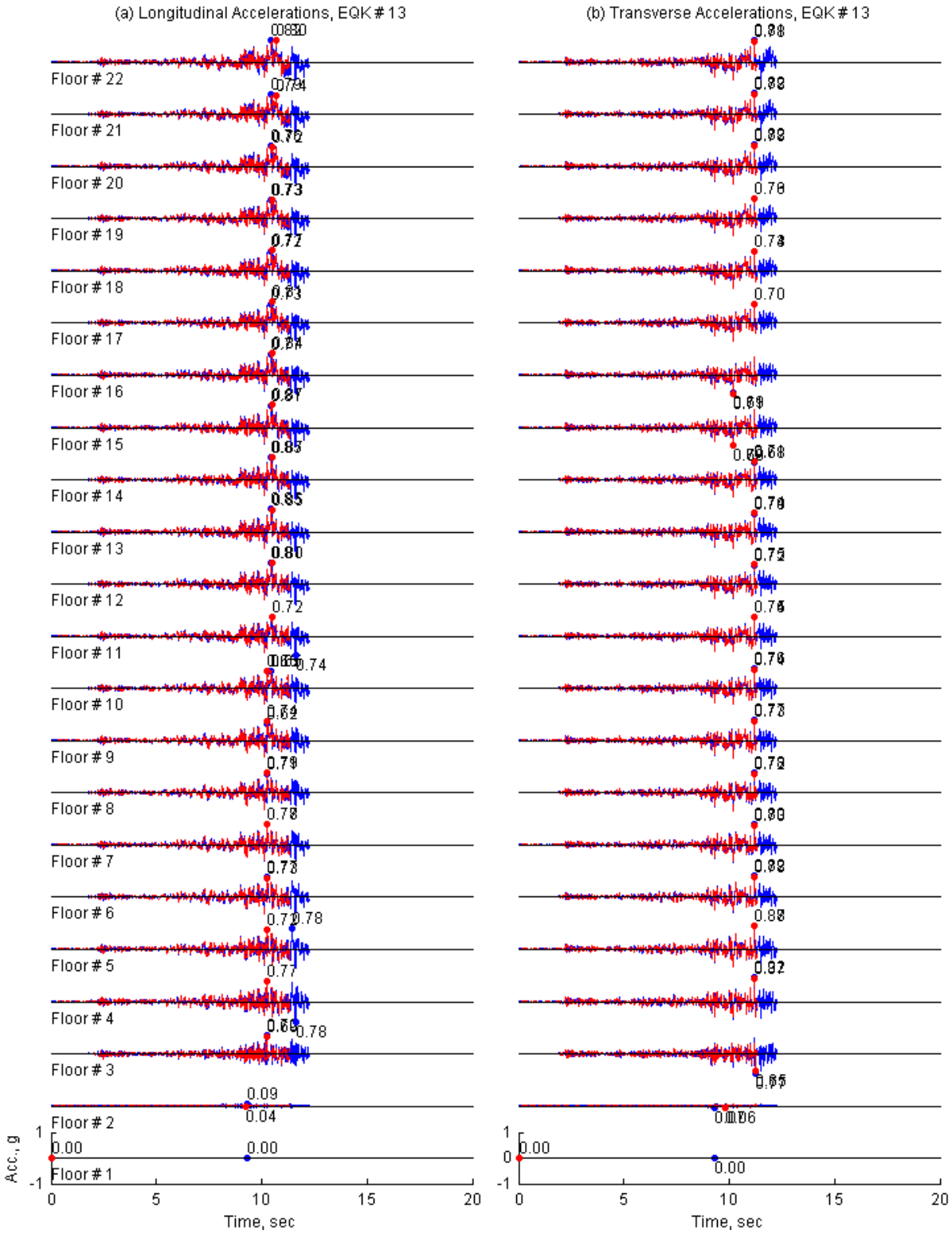

Figure II.43. Floor accelerations of 20-Story North Hollywood Hotel from *OpenSees* (solid line) and *Perform3D* (dashed lines) for ground motion 13.

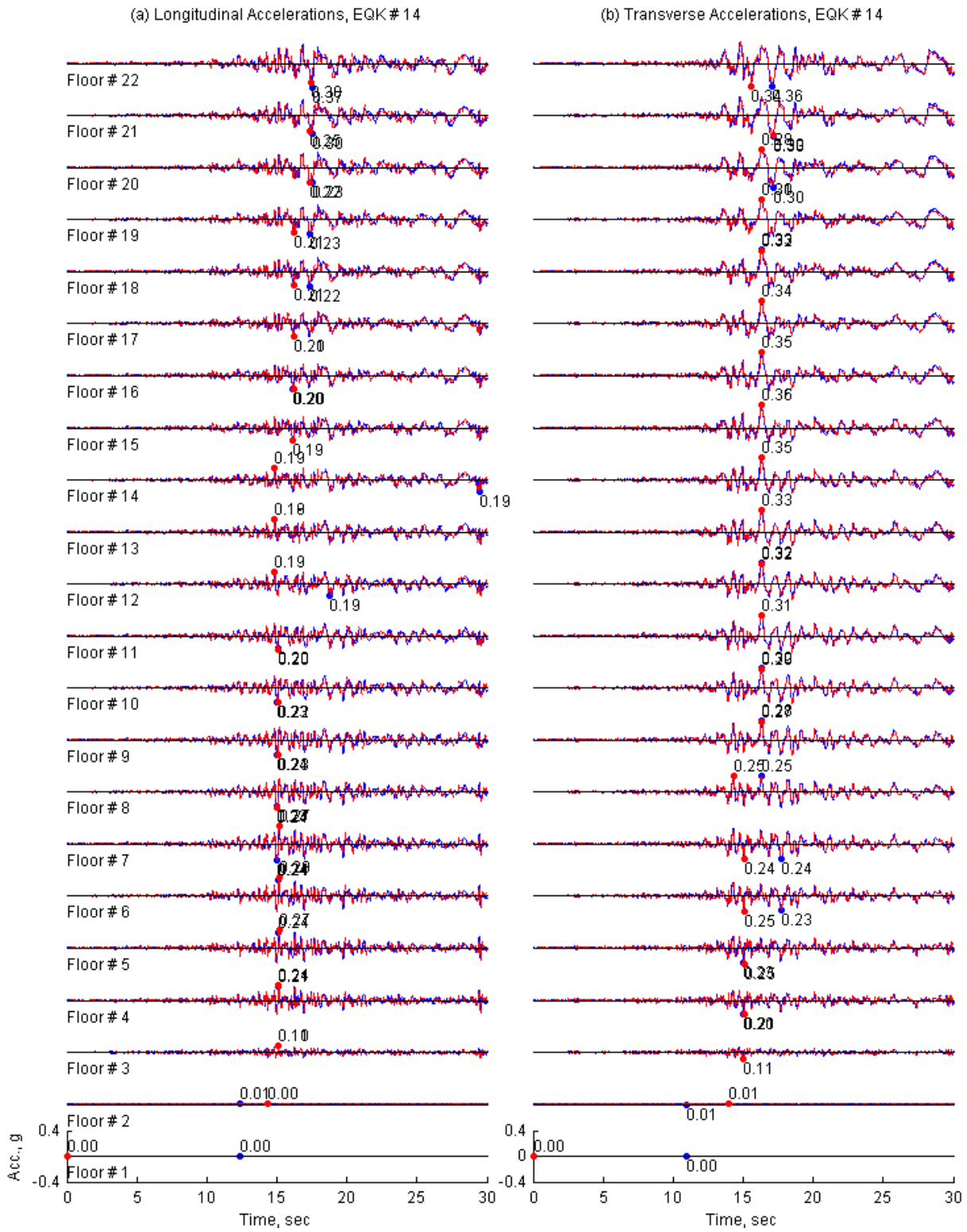

Figure II.44. Floor accelerations of 20-Story North Hollywood Hotel from *OpenSees* (solid line) and *Perform3D* (dashed lines) for ground motion 14.

Figure II.45. Floor accelerations of 20-Story North Hollywood Hotel from *OpenSees* (solid line) and *Perform3D* (dashed lines) for ground motion 15.

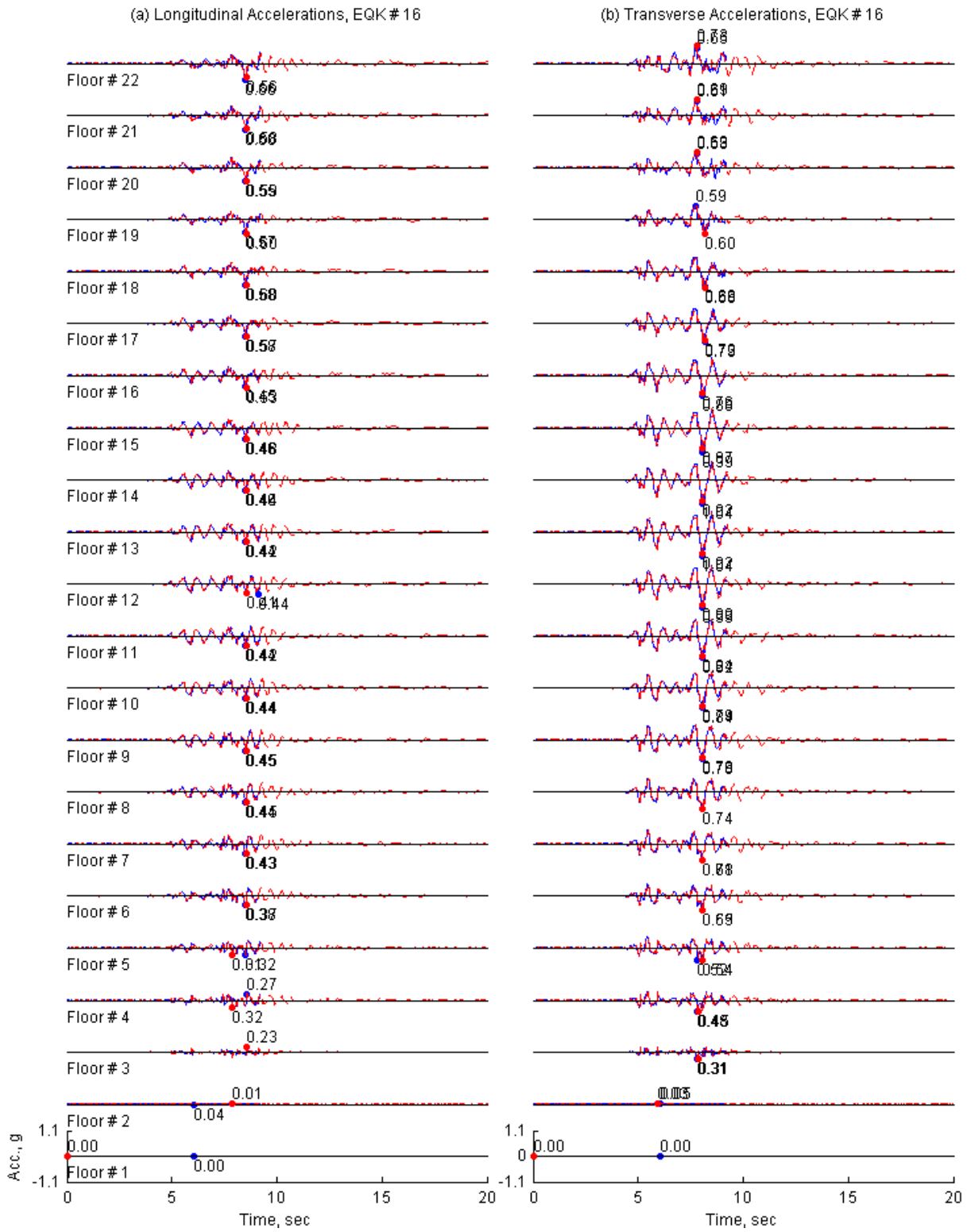

Figure II.46. Floor accelerations of 20-Story North Hollywood Hotel from *OpenSees* (solid line) and *Perform3D* (dashed lines) for ground motion 16.

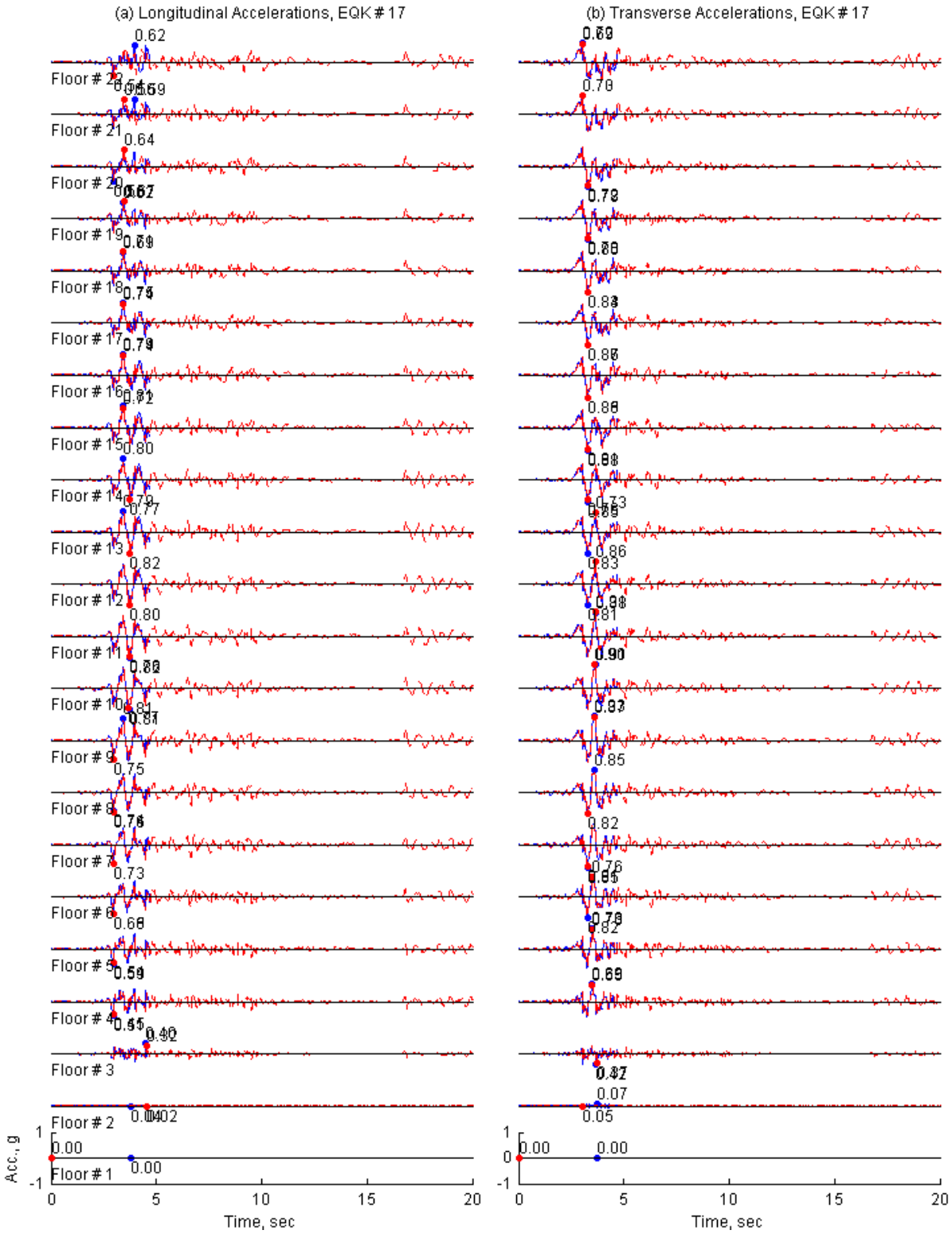

Figure II.47. Floor accelerations of 20-Story North Hollywood Hotel from *OpenSees* (solid line) and *Perform3D* (dashed lines) for ground motion 17.

Figure II.48. Floor accelerations of 20-Story North Hollywood Hotel from *OpenSees* (solid line) and *Perform3D* (dashed lines) for ground motion 18.

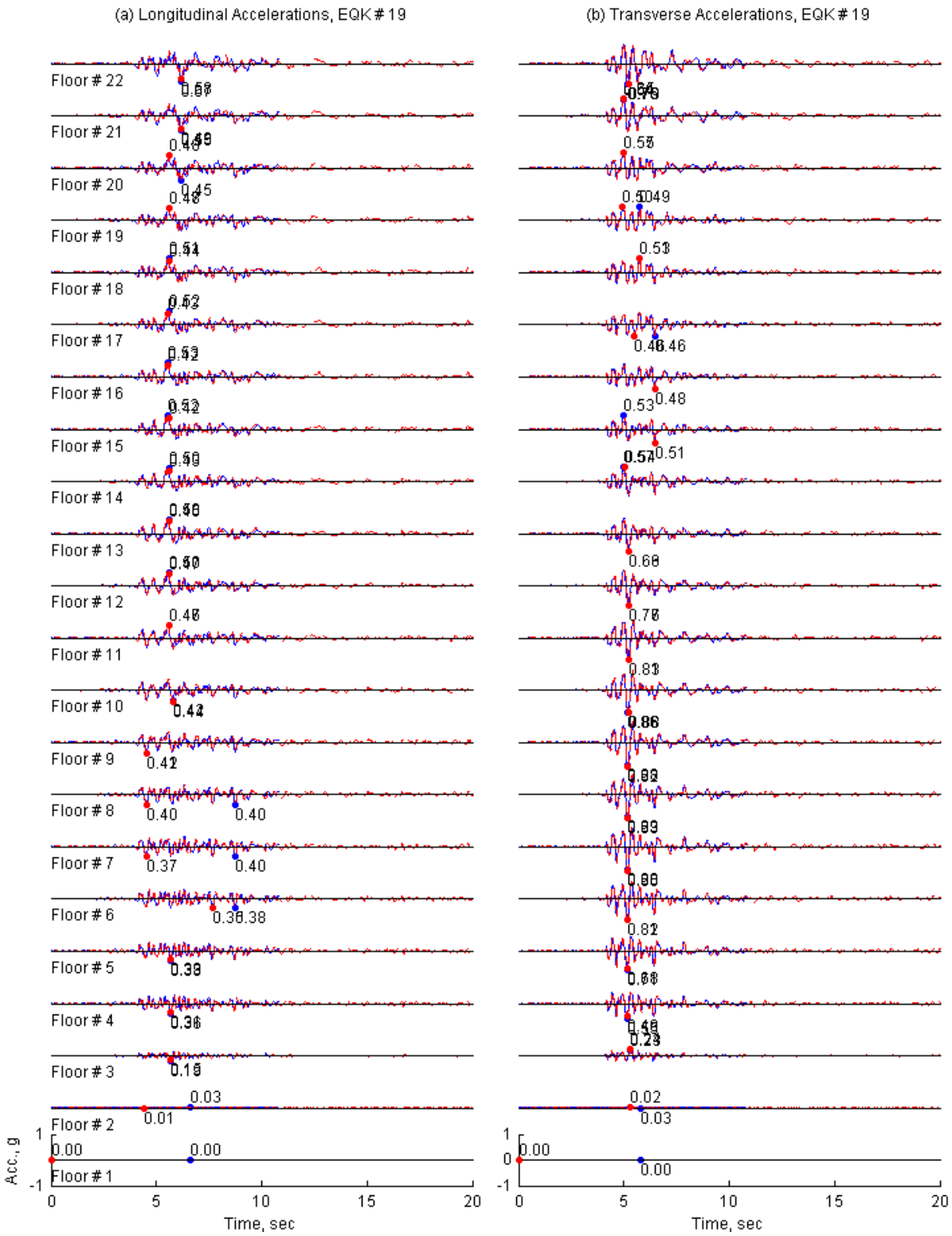

Figure II.49. Floor accelerations of 20-Story North Hollywood Hotel from *OpenSees* (solid line) and *Perform3D* (dashed lines) for ground motion 19.

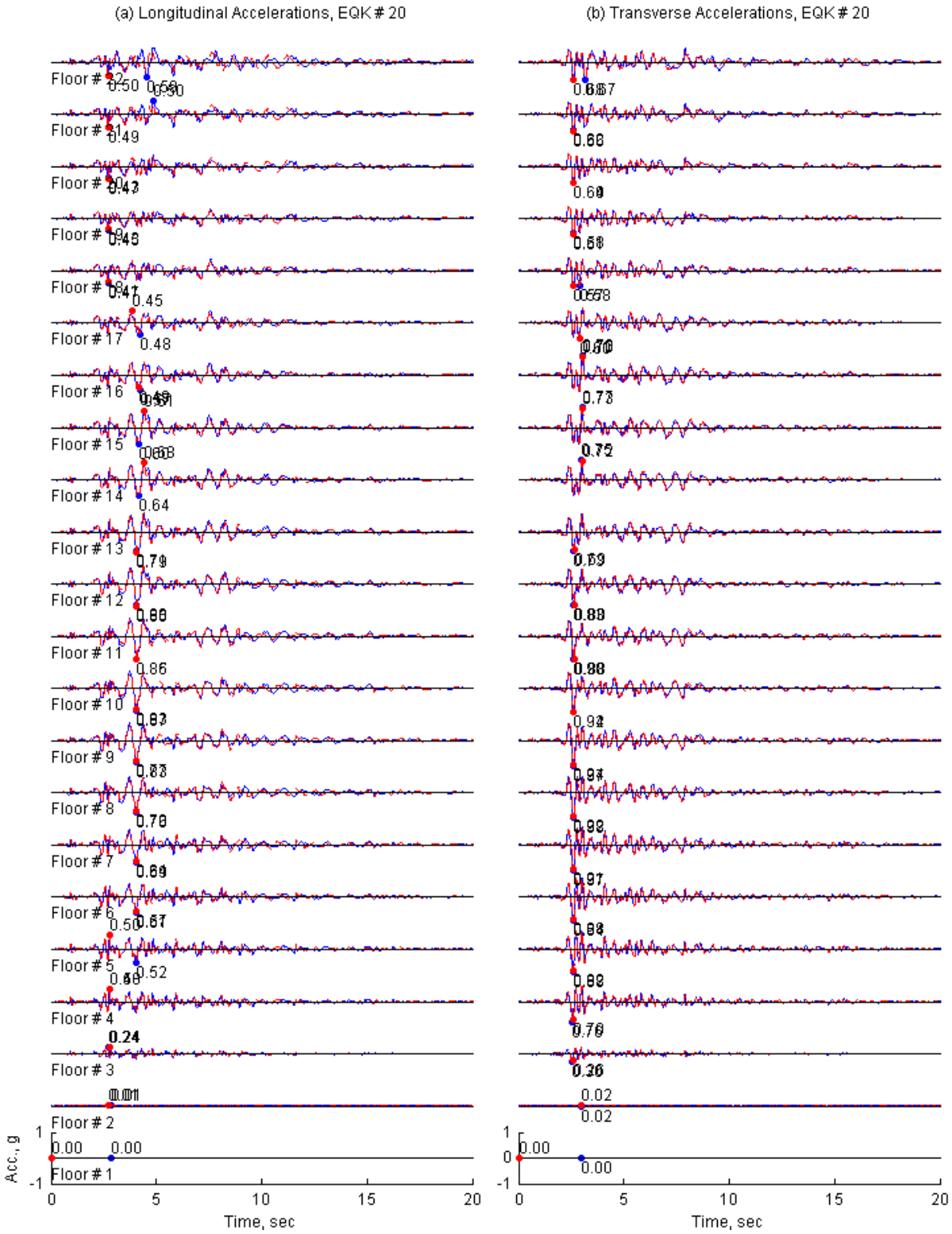

Figure II.50. Floor accelerations of 20-Story North Hollywood Hotel from *OpenSees* (solid line) and *Perform3D* (dashed lines) for ground motion 20.

Figure II.51. Floor accelerations of 20-Story North Hollywood Hotel from *OpenSees* (solid line) and *Perform3D* (dashed lines) for ground motion 21.

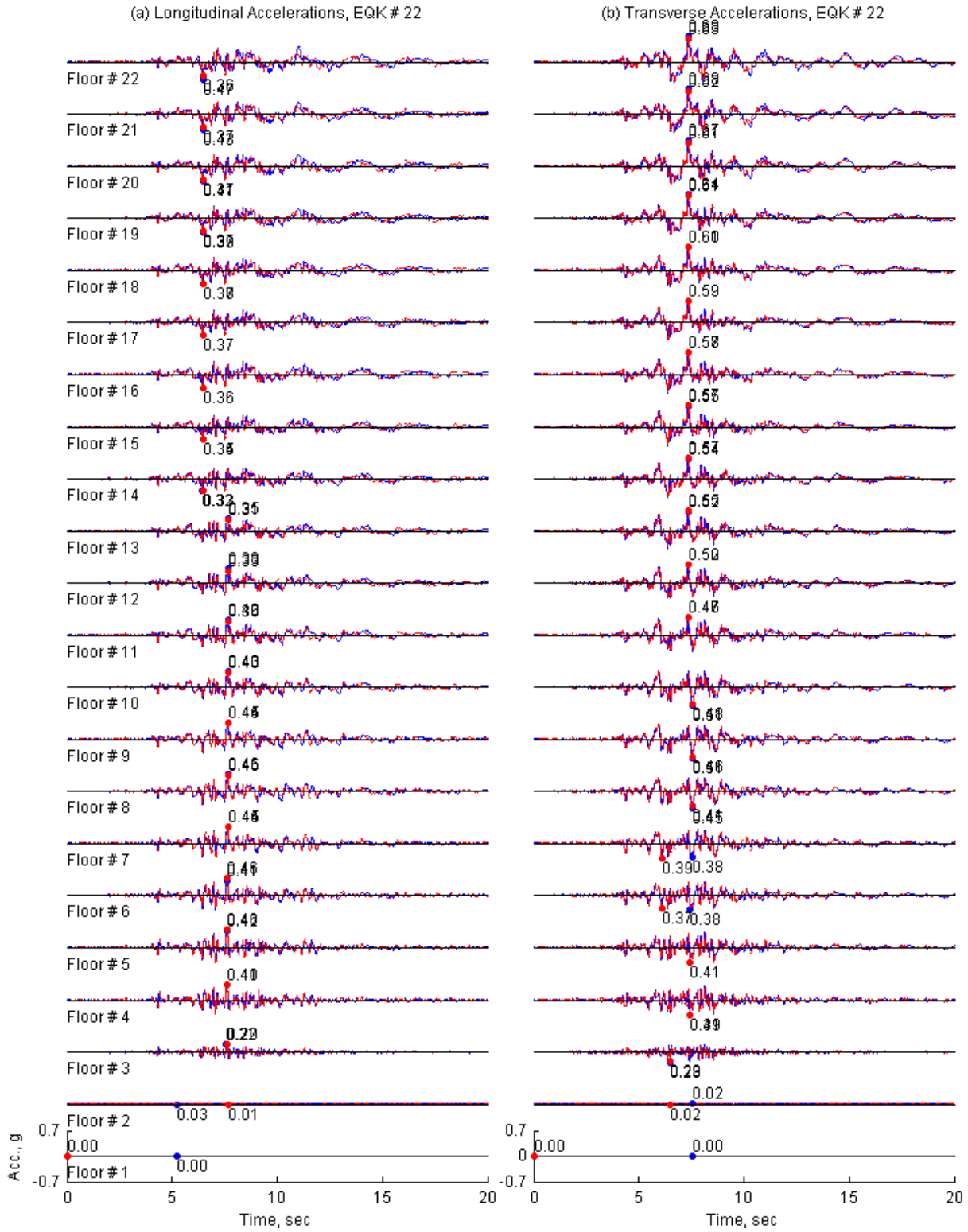

Figure II.52. Floor accelerations of 20-Story North Hollywood Hotel from *OpenSees* (solid line) and *Perform3D* (dashed lines) for ground motion 22.

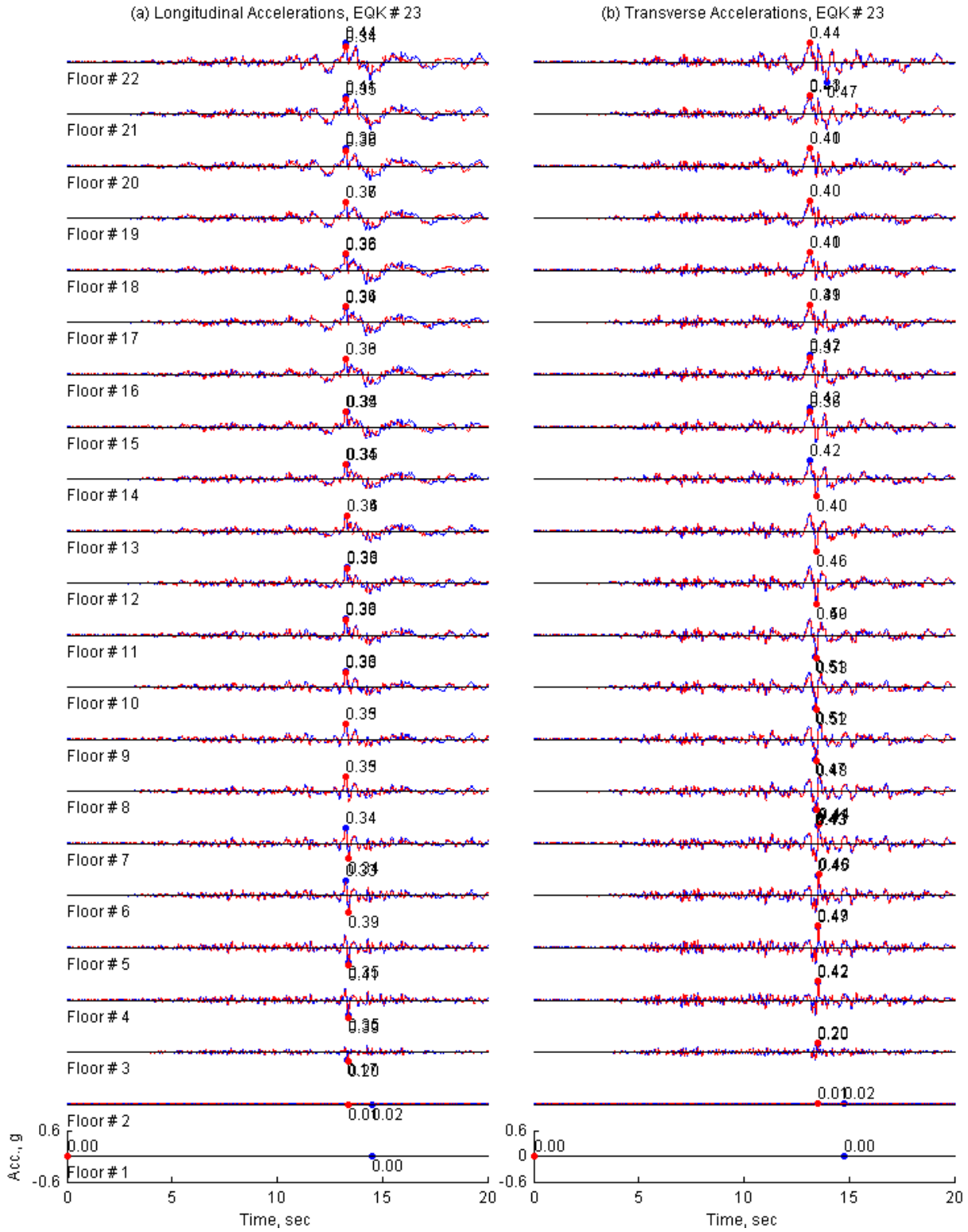

Figure II.53. Floor accelerations of 20-Story North Hollywood Hotel from *OpenSees* (solid line) and *Perform3D* (dashed lines) for ground motion 23.

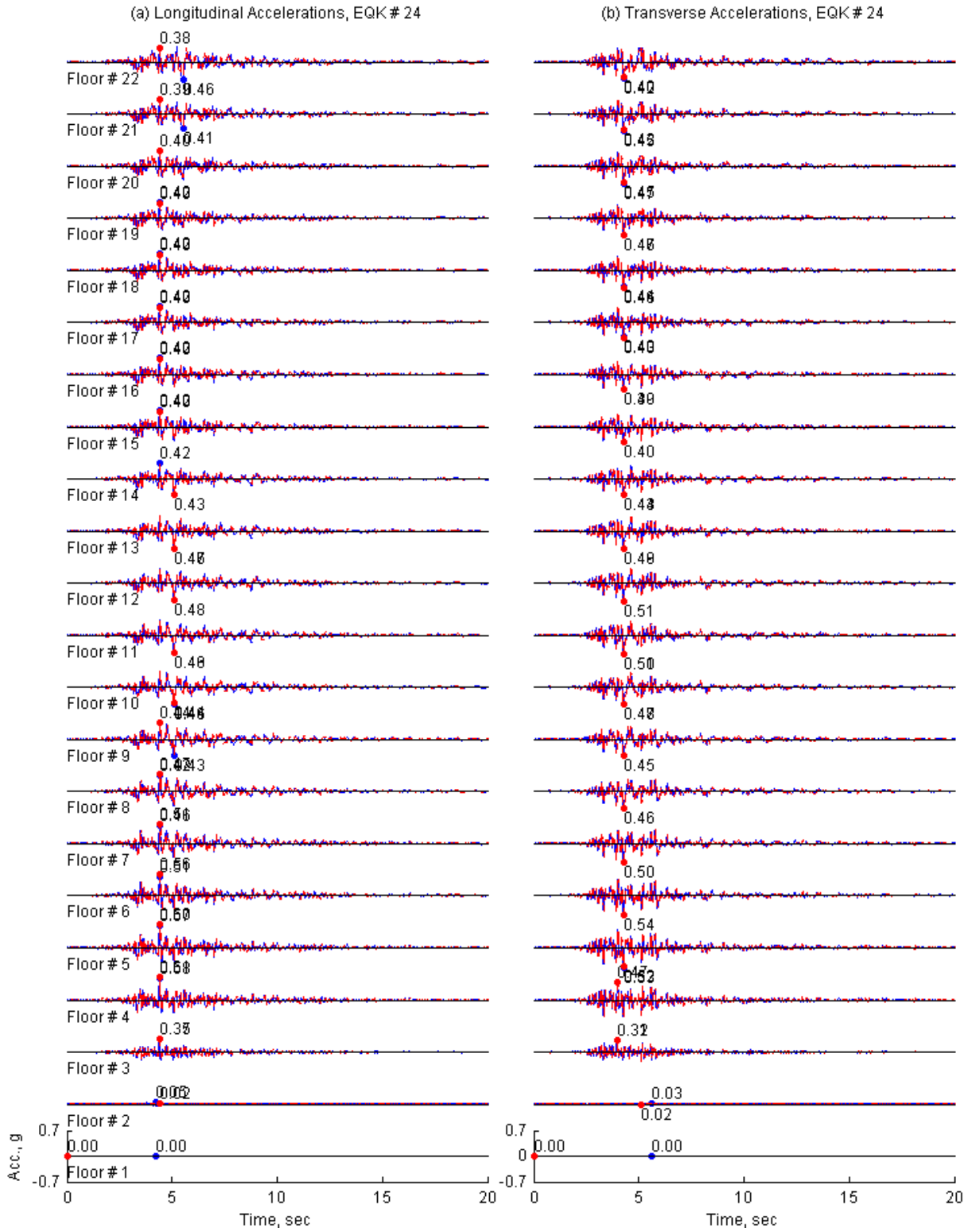

Figure II.54. Floor accelerations of 20-Story North Hollywood Hotel from *OpenSees* (solid line) and *Perform3D* (dashed lines) for ground motion 24.

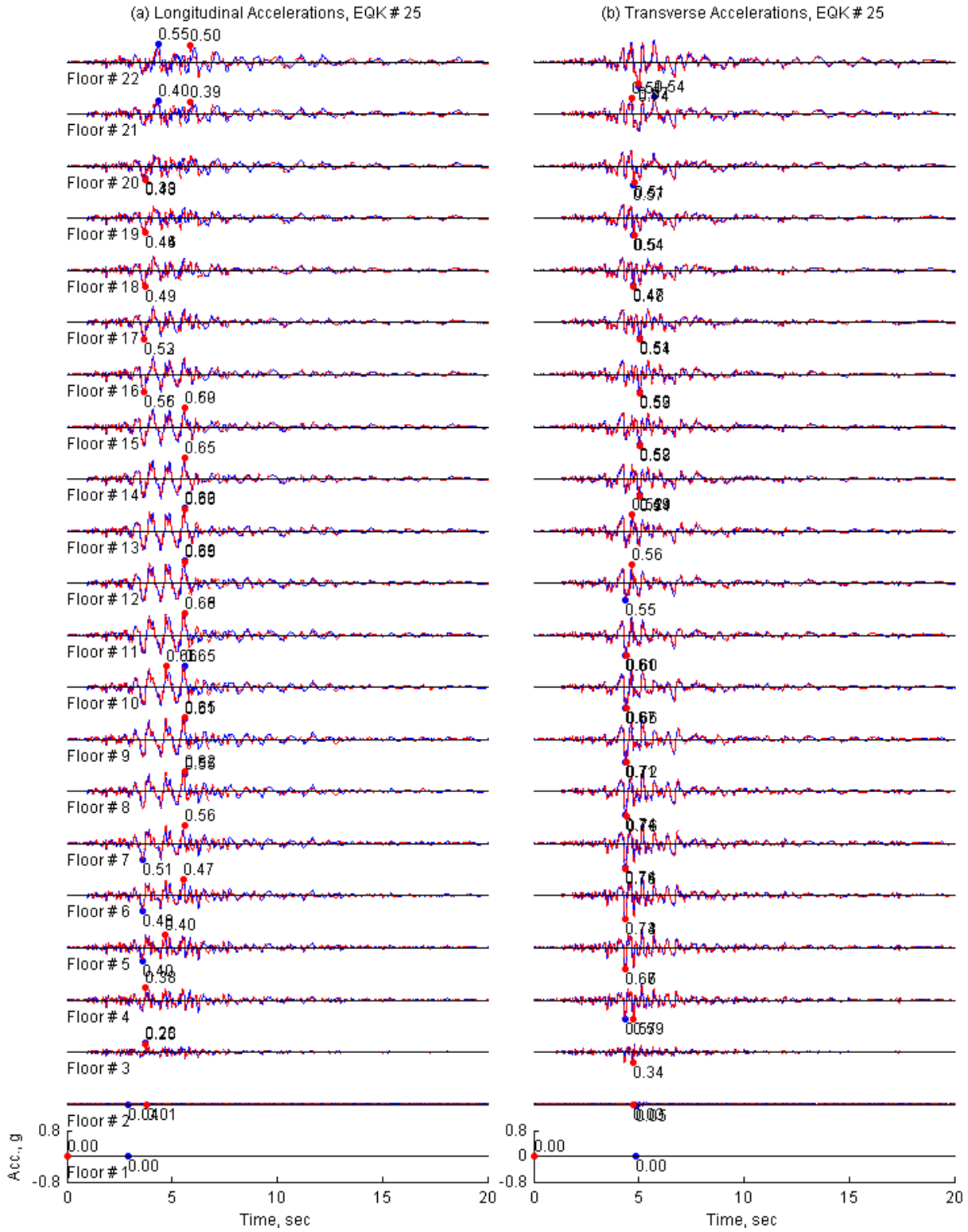

Figure II.55. Floor accelerations of 20-Story North Hollywood Hotel from *OpenSees* (solid line) and *Perform3D* (dashed lines) for ground motion 25.

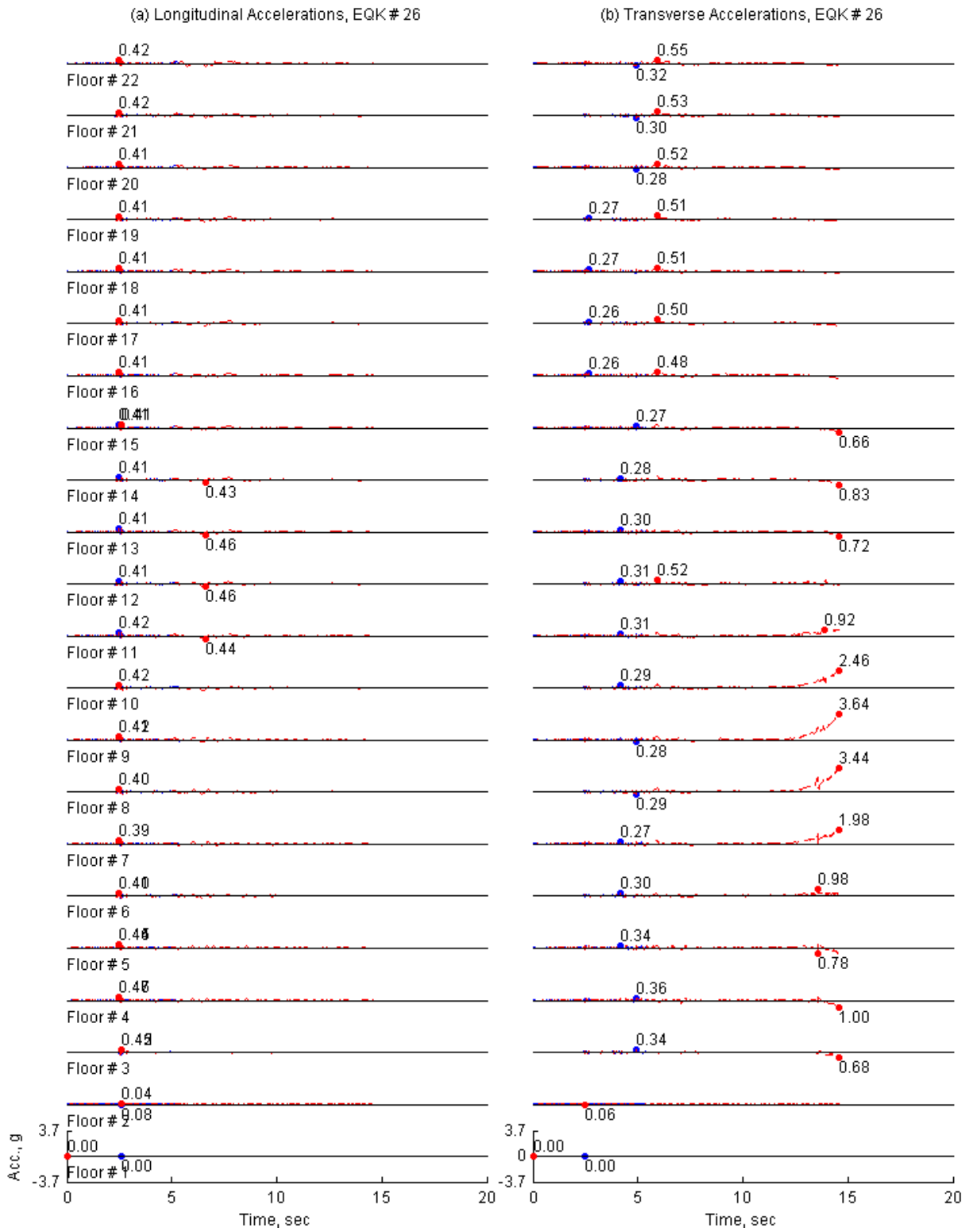

Figure II.55. Floor accelerations of 20-Story North Hollywood Hotel from *OpenSees* (solid line) and *Perform3D* (dashed lines) for ground motion 25.

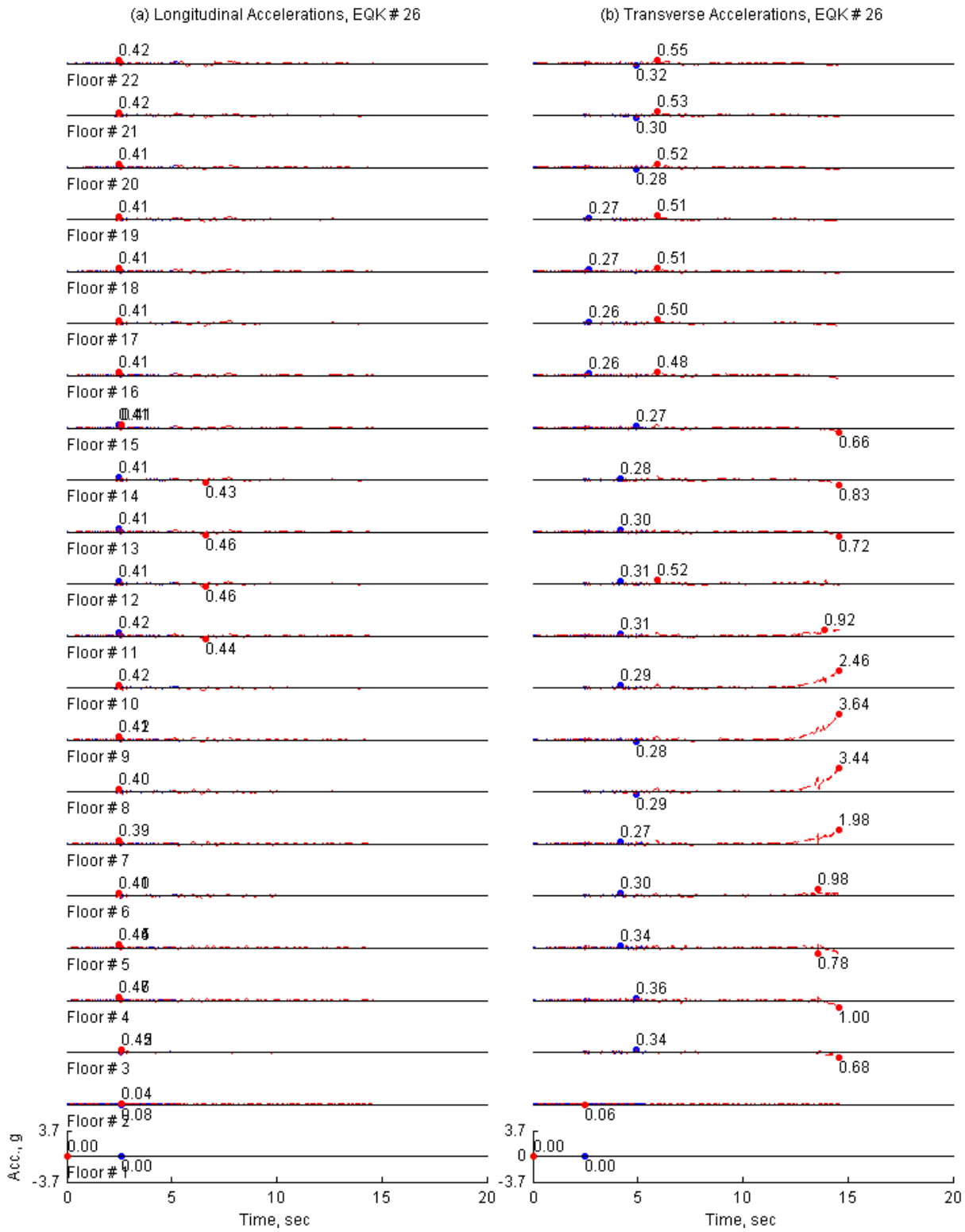

Figure II.56. Floor accelerations of 20-Story North Hollywood Hotel from *OpenSees* (solid line) and *Perform3D* (dashed lines) for ground motion 26.

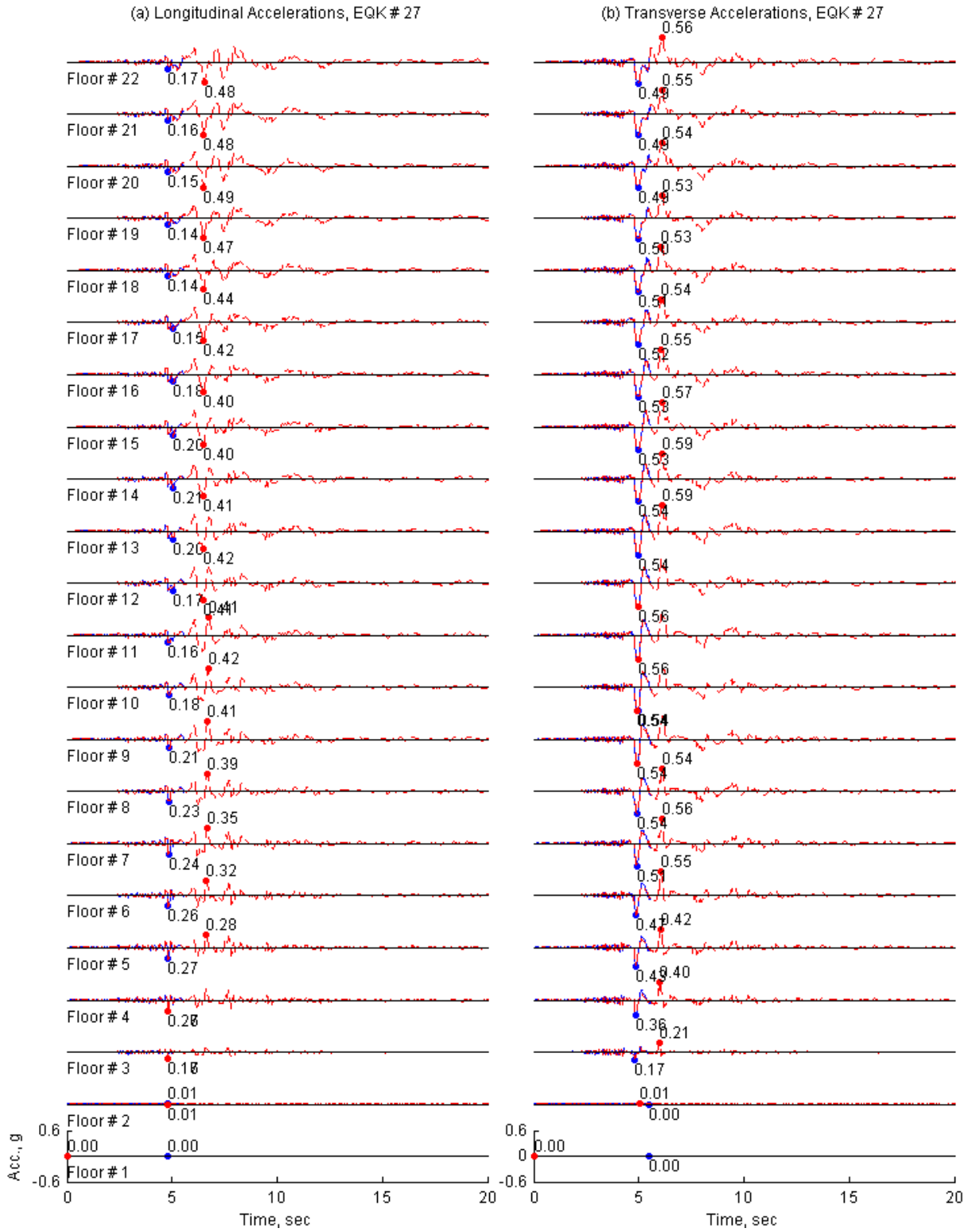

Figure II.57. Floor accelerations of 20-Story North Hollywood Hotel from *OpenSees* (solid line) and *Perform3D* (dashed lines) for ground motion 27.

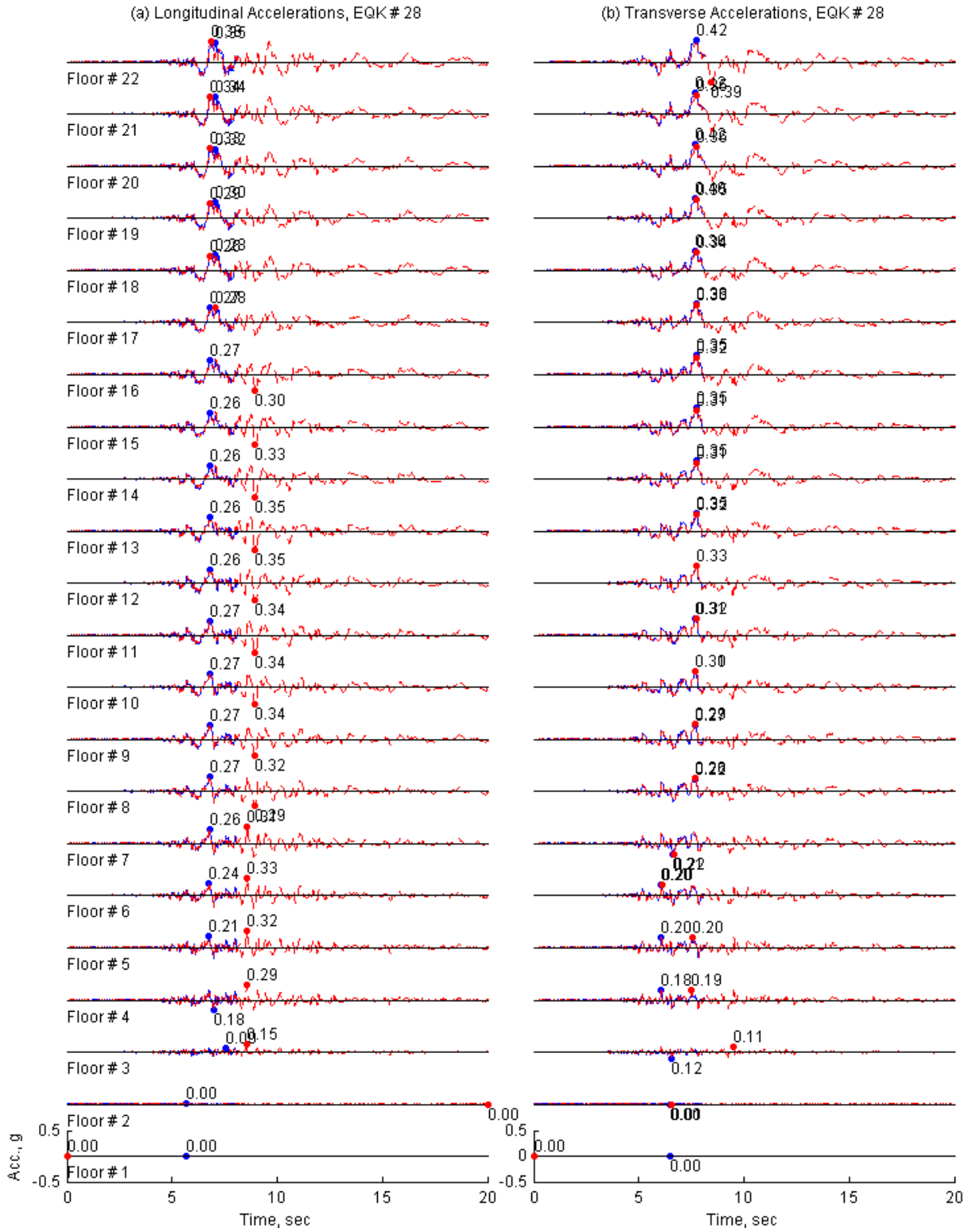

Figure II.58. Floor accelerations of 20-Story North Hollywood Hotel from *OpenSees* (solid line) and *Perform3D* (dashed lines) for ground motion 28.

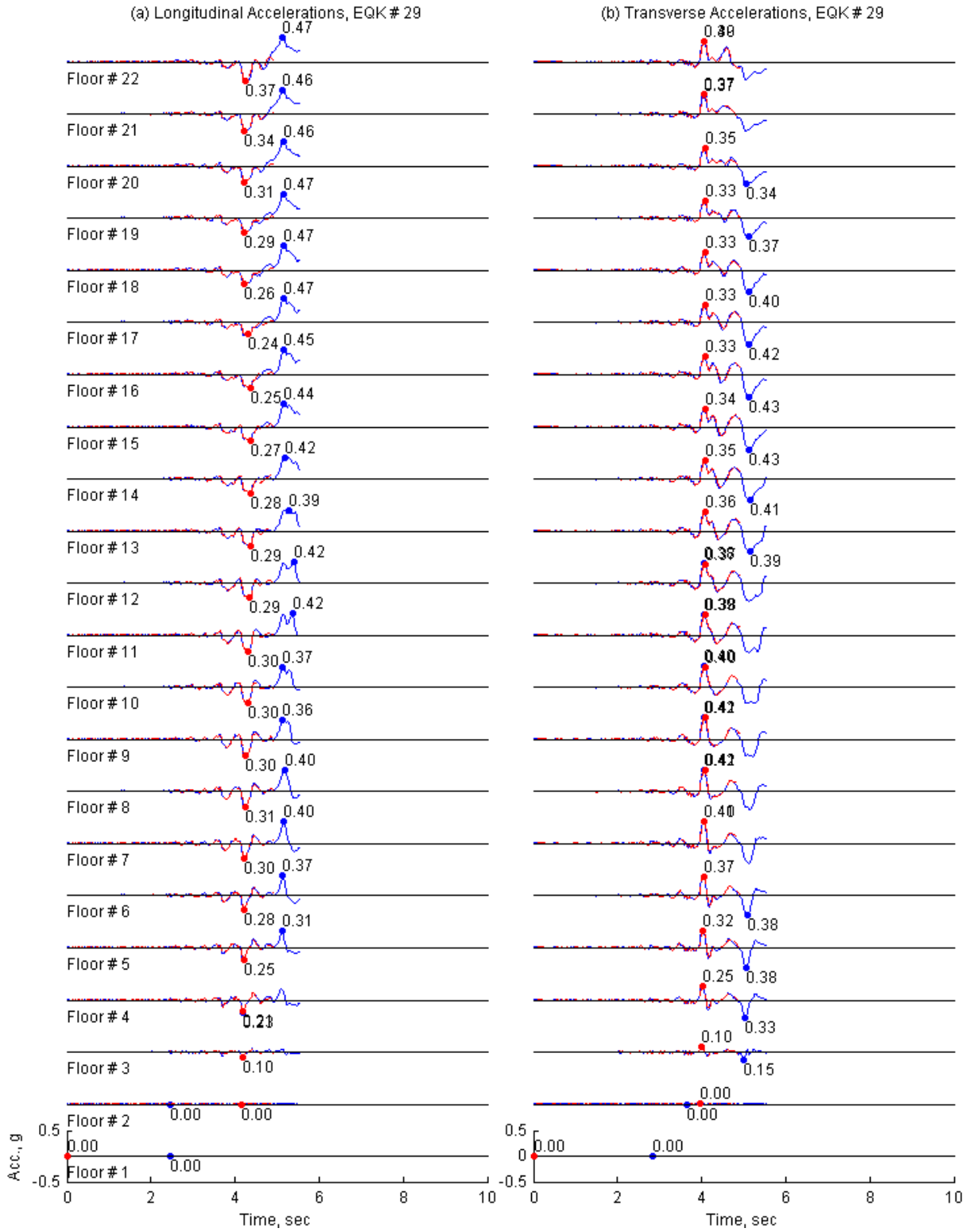

Figure II.59. Floor accelerations of 20-Story North Hollywood Hotel from *OpenSees* (solid line) and *Perform3D* (dashed lines) for ground motion 29.

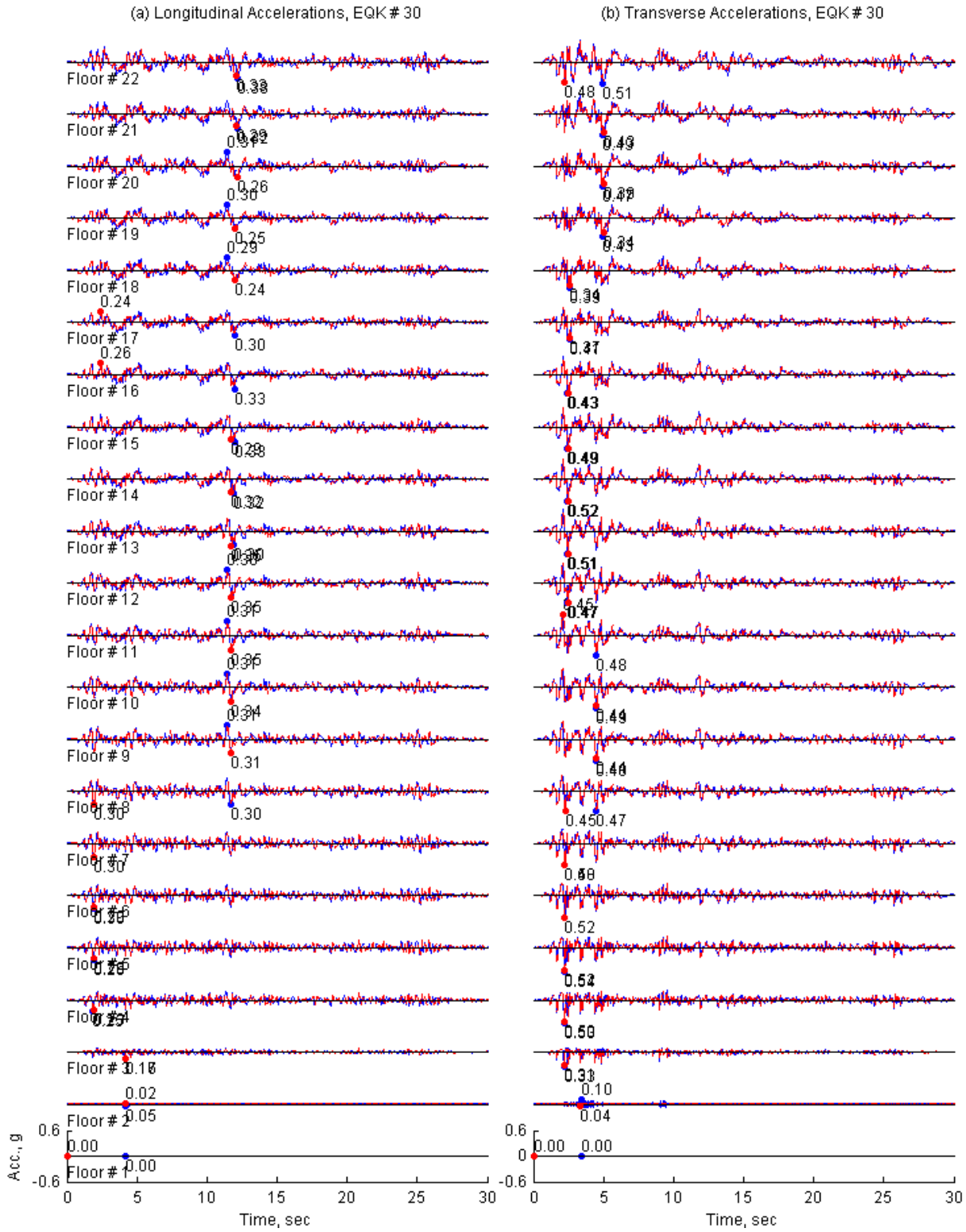

Figure II.60. Floor accelerations of 20-Story North Hollywood Hotel from *OpenSees* (solid line) and *Perform3D* (dashed lines) for ground motion 30.

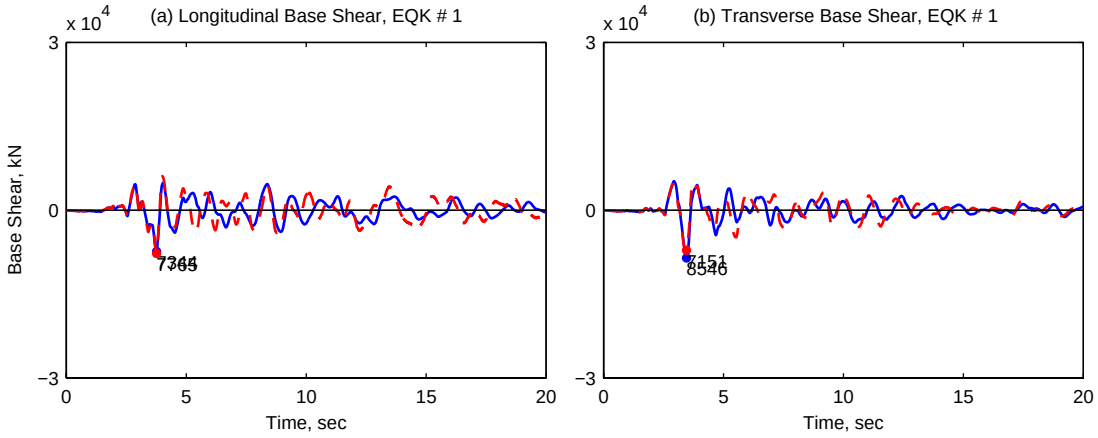

Figure II.61. Base shear of 20-Story North Hollywood Hotel from *OpenSees* (solid line) and *Perform3D* (dashed lines) for ground motion 1.

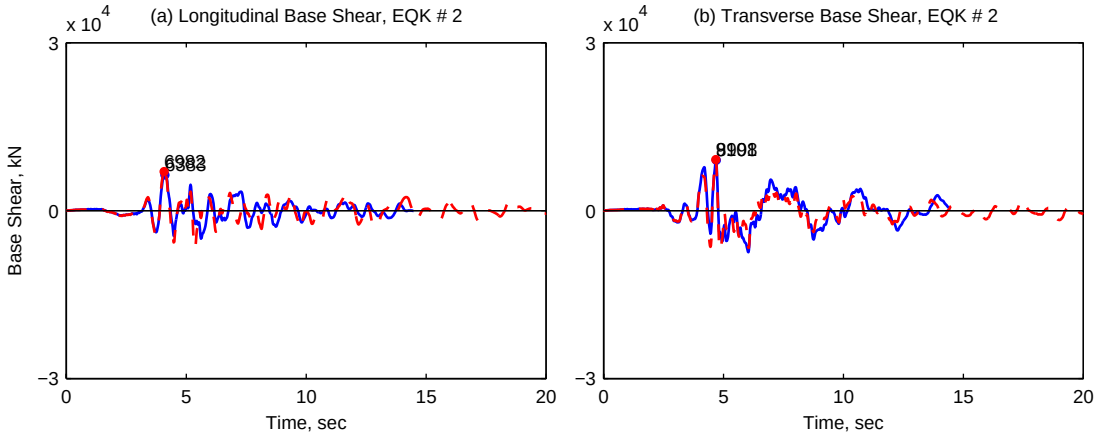

Figure II.62. Base shear of 20-Story North Hollywood Hotel from *OpenSees* (solid line) and *Perform3D* (dashed lines) for ground motion 2.

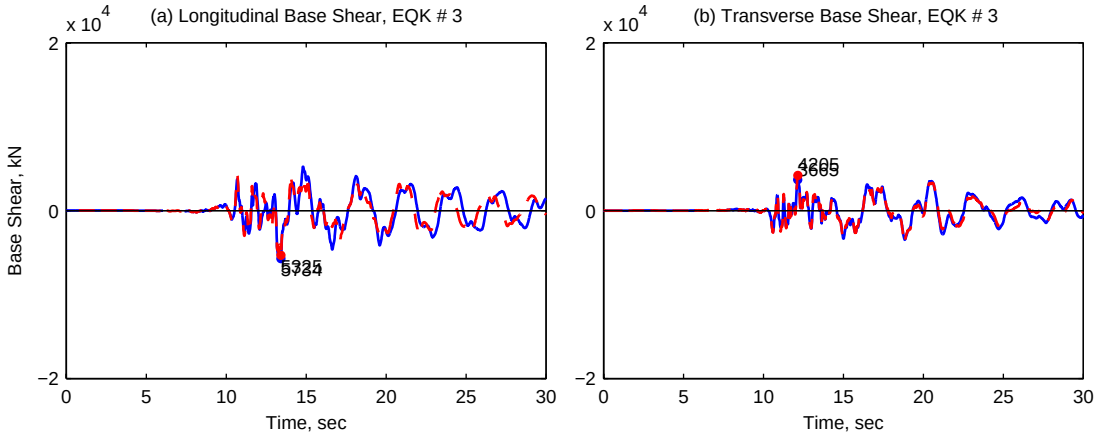

Figure II.63. Base shear of 20-Story North Hollywood Hotel from *OpenSees* (solid line) and *Perform3D* (dashed lines) for ground motion 3.

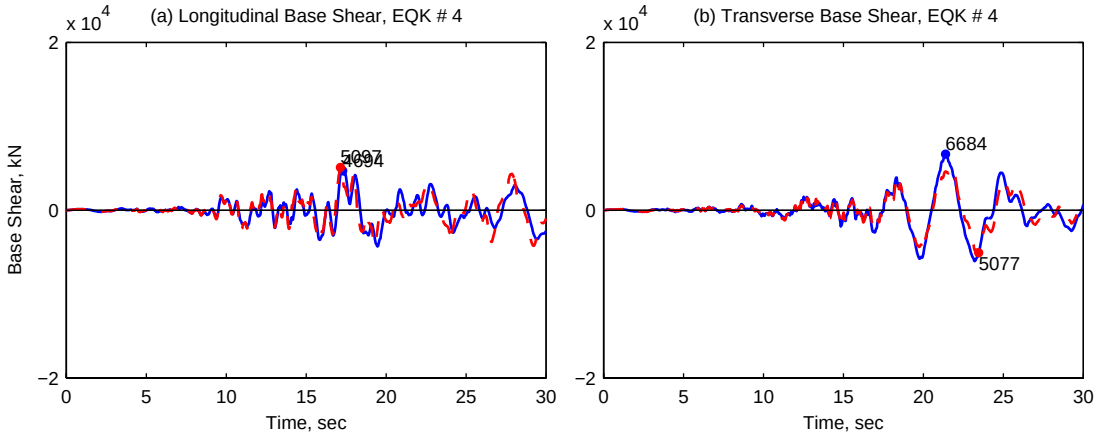

Figure II.64. Base shear of 20-Story North Hollywood Hotel from *OpenSees* (solid line) and *Perform3D* (dashed lines) for ground motion 4.

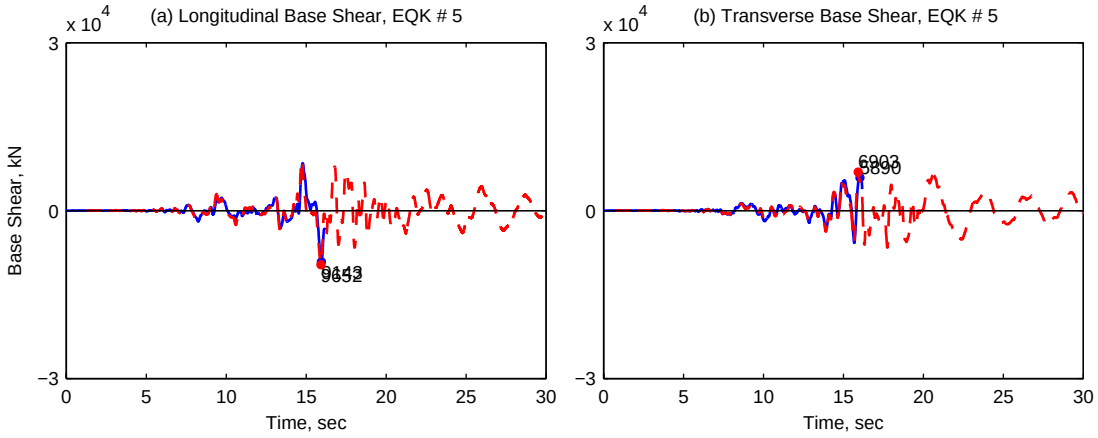

Figure II.65. Base shear of 20-Story North Hollywood Hotel from *OpenSees* (solid line) and *Perform3D* (dashed lines) for ground motion 5.

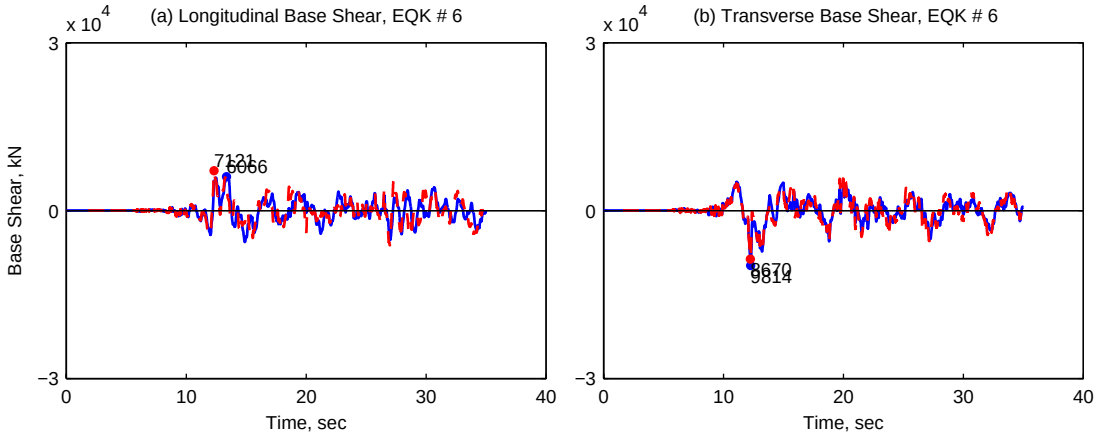

Figure II.66. Base shear of 20-Story North Hollywood Hotel from *OpenSees* (solid line) and *Perform3D* (dashed lines) for ground motion 6.

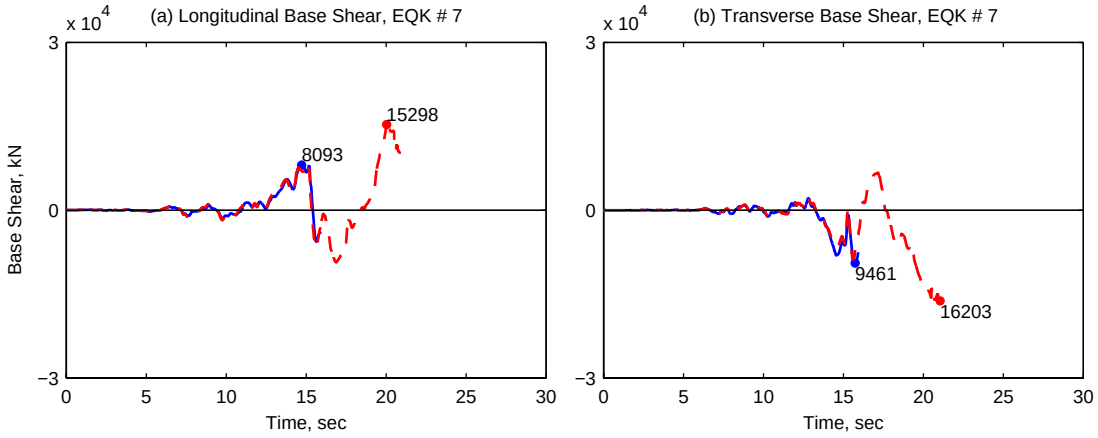

Figure II.67. Base shear of 20-Story North Hollywood Hotel from *OpenSees* (solid line) and *Perform3D* (dashed lines) for ground motion 7.

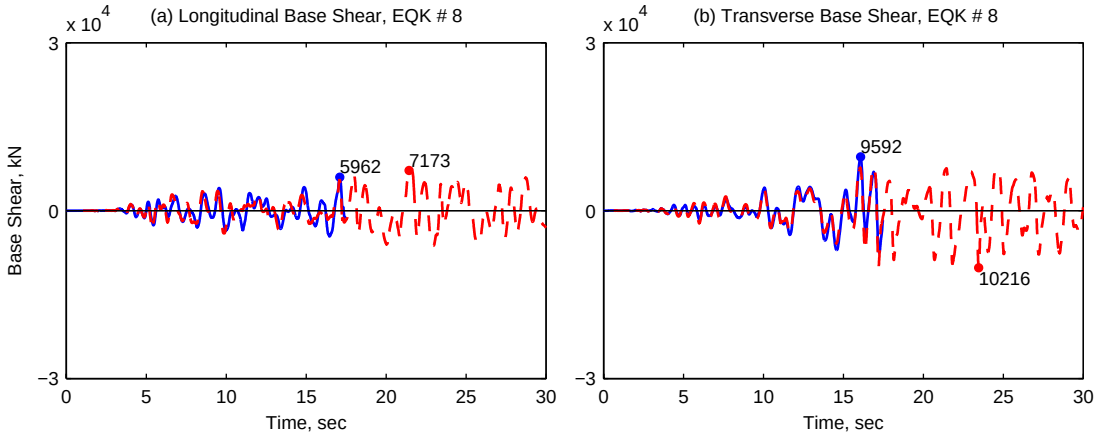

Figure II.68. Base shear of 20-Story North Hollywood Hotel from *OpenSees* (solid line) and *Perform3D* (dashed lines) for ground motion 8.

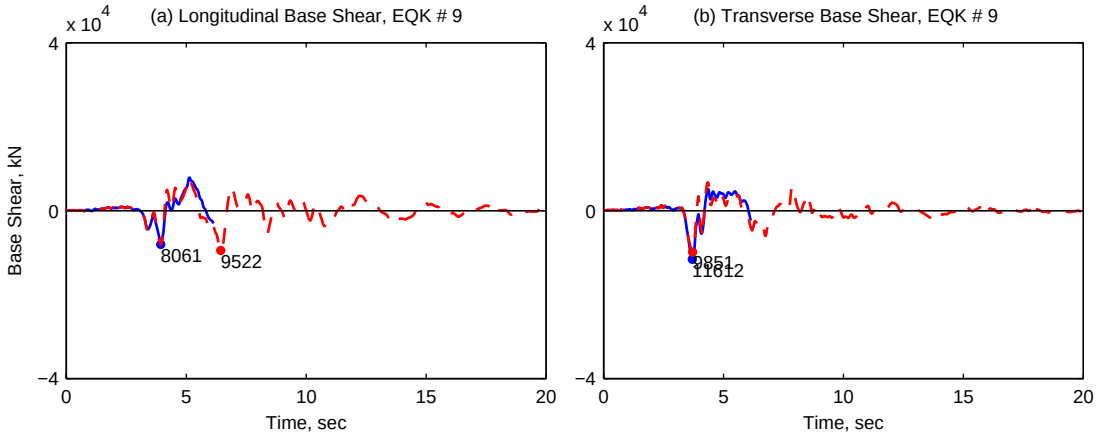

Figure II.69. Base shear of 20-Story North Hollywood Hotel from *OpenSees* (solid line) and *Perform3D* (dashed lines) for ground motion 9.

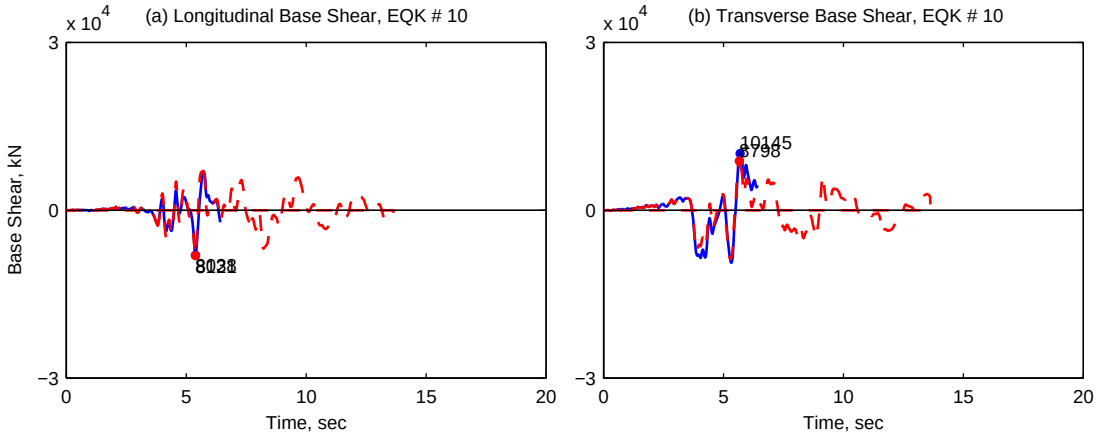

Figure II.70. Base shear of 20-Story North Hollywood Hotel from *OpenSees* (solid line) and *Perform3D* (dashed lines) for ground motion 10.

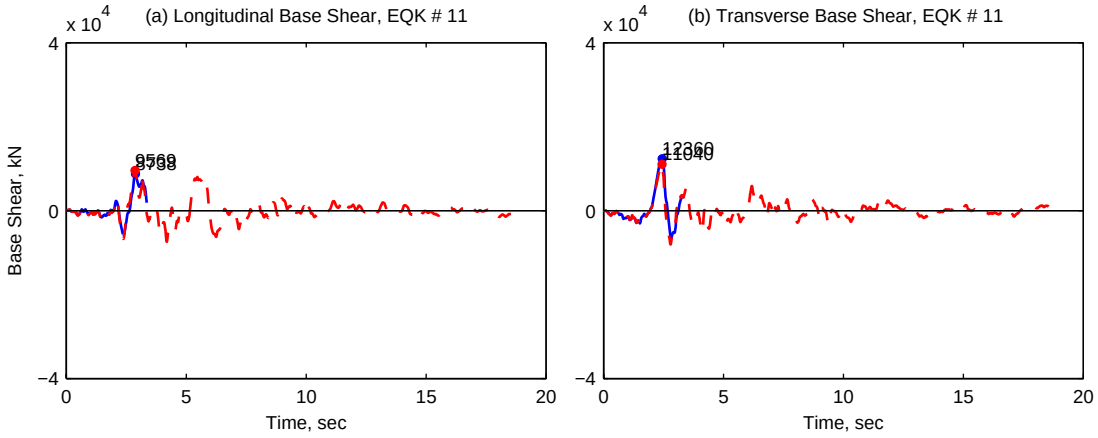

Figure II.71. Base shear of 20-Story North Hollywood Hotel from *OpenSees* (solid line) and *Perform3D* (dashed lines) for ground motion 11.

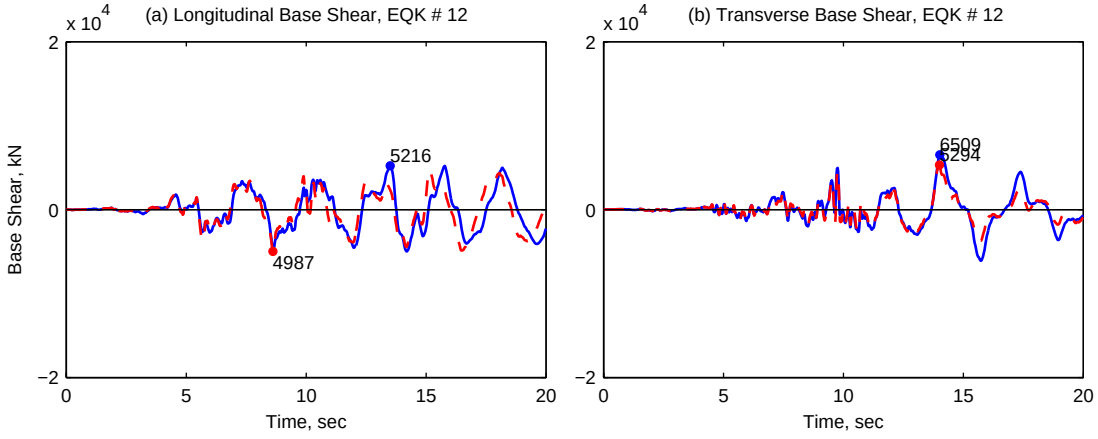

Figure II.72. Base shear of 20-Story North Hollywood Hotel from *OpenSees* (solid line) and *Perform3D* (dashed lines) for ground motion 12.

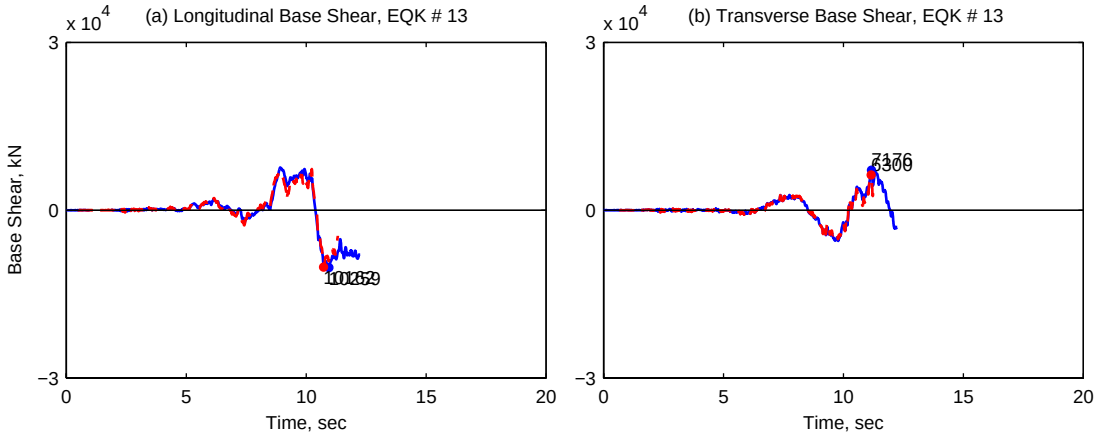

Figure II.73. Base shear of 20-Story North Hollywood Hotel from *OpenSees* (solid line) and *Perform3D* (dashed lines) for ground motion 13.

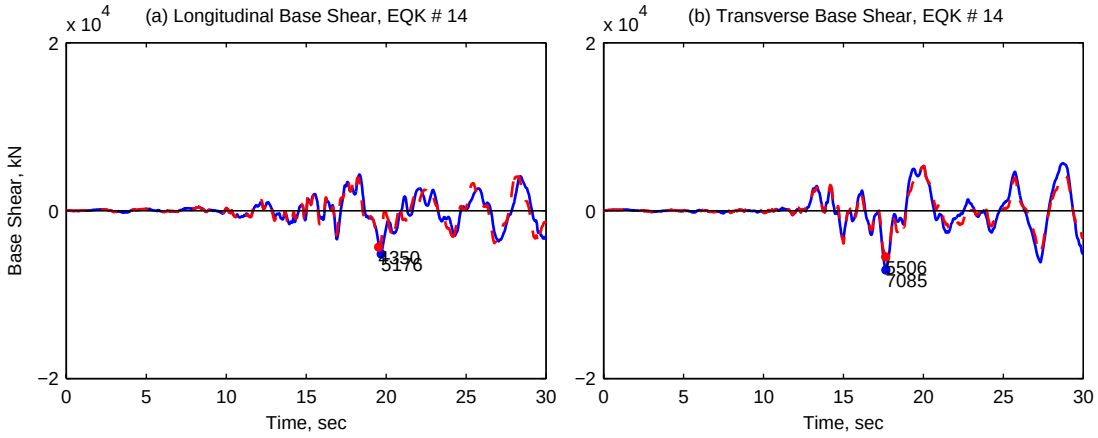

Figure II.74. Base shear of 20-Story North Hollywood Hotel from *OpenSees* (solid line) and *Perform3D* (dashed lines) for ground motion 14.

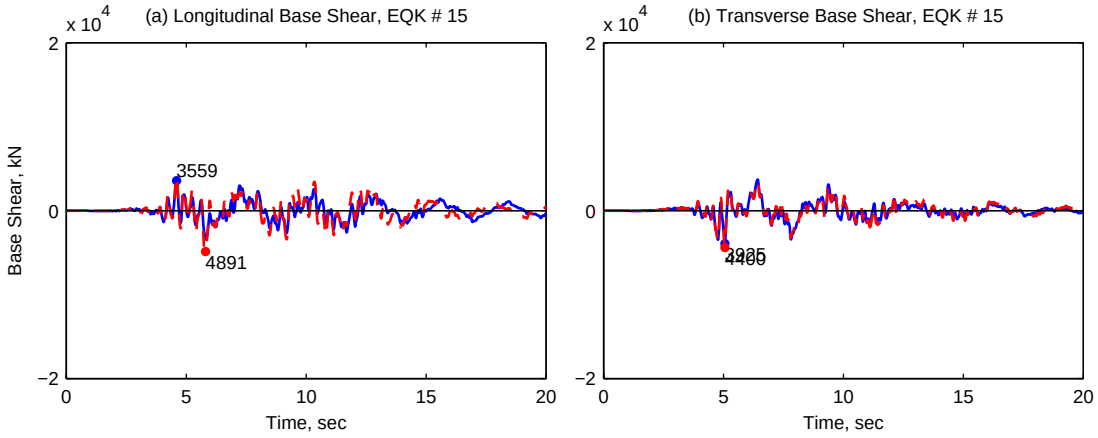

Figure II.75. Base shear of 20-Story North Hollywood Hotel from *OpenSees* (solid line) and *Perform3D* (dashed lines) for ground motion 15.

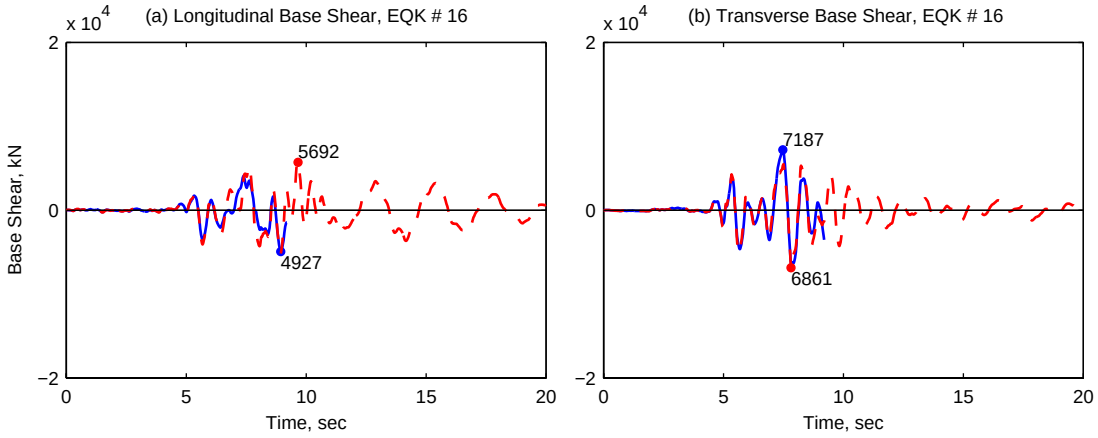

Figure II.76. Base shear of 20-Story North Hollywood Hotel from *OpenSees* (solid line) and *Perform3D* (dashed lines) for ground motion 16.

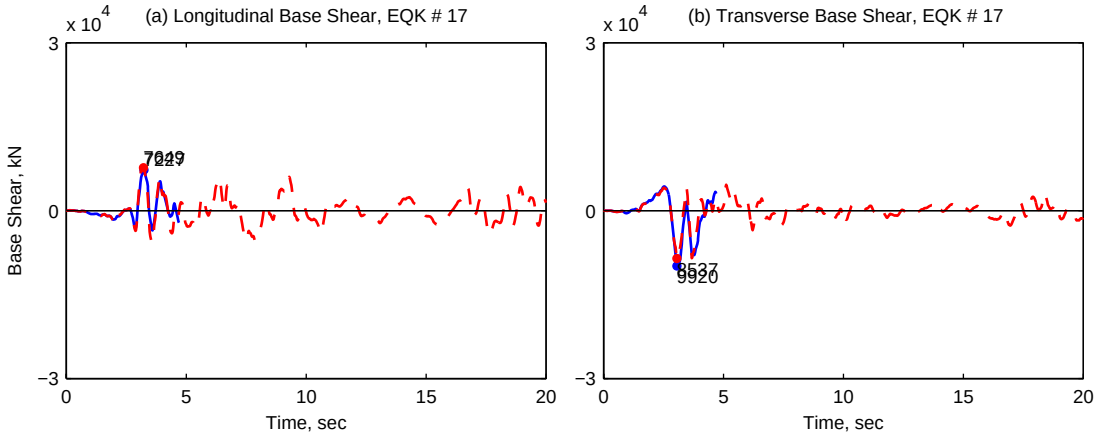

Figure II.77. Base shear of 20-Story North Hollywood Hotel from *OpenSees* (solid line) and *Perform3D* (dashed lines) for ground motion 17.

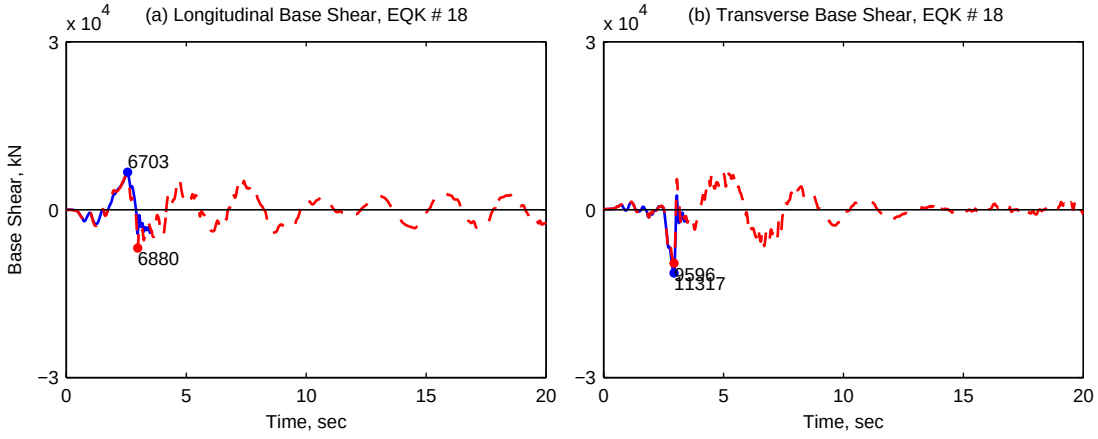

Figure II.78. Base shear of 20-Story North Hollywood Hotel from *OpenSees* (solid line) and *Perform3D* (dashed lines) for ground motion 18.

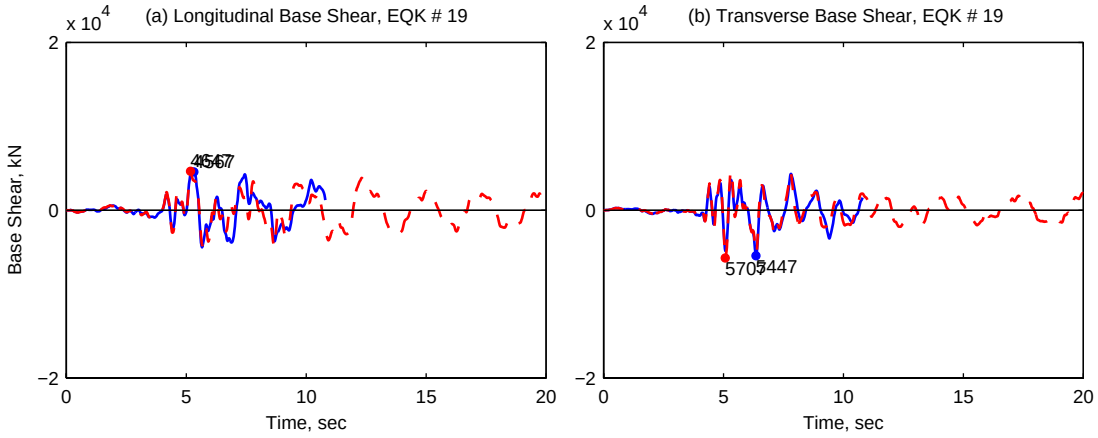

Figure II.79. Base shear of 20-Story North Hollywood Hotel from *OpenSees* (solid line) and *Perform3D* (dashed lines) for ground motion 19.

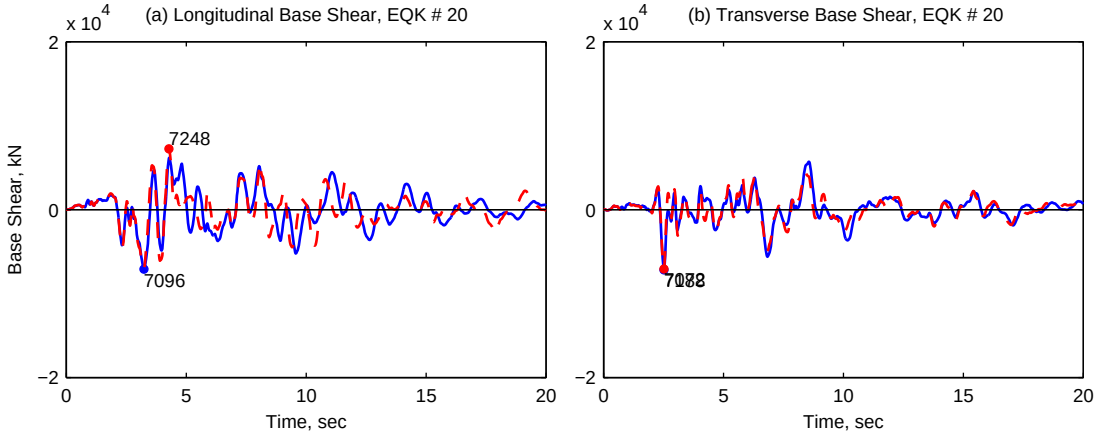

Figure II.80. Base shear of 20-Story North Hollywood Hotel from *OpenSees* (solid line) and *Perform3D* (dashed lines) for ground motion 20.

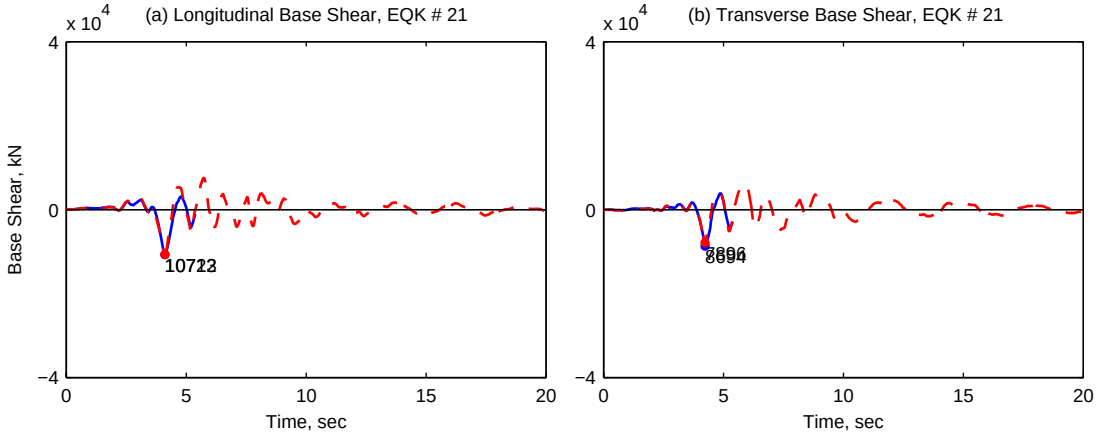

Figure II.81. Base shear of 20-Story North Hollywood Hotel from *OpenSees* (solid line) and *Perform3D* (dashed lines) for ground motion 21.

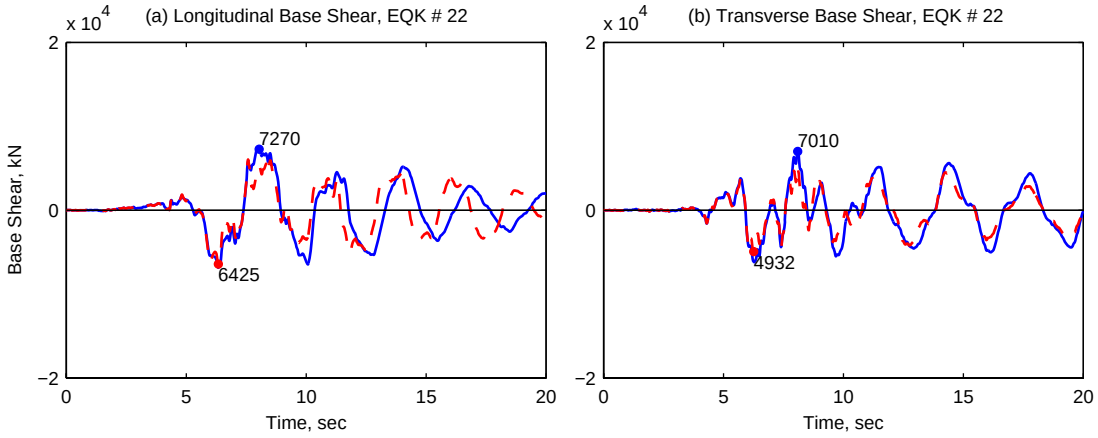

Figure II.82. Base shear of 20-Story North Hollywood Hotel from *OpenSees* (solid line) and *Perform3D* (dashed lines) for ground motion 22.

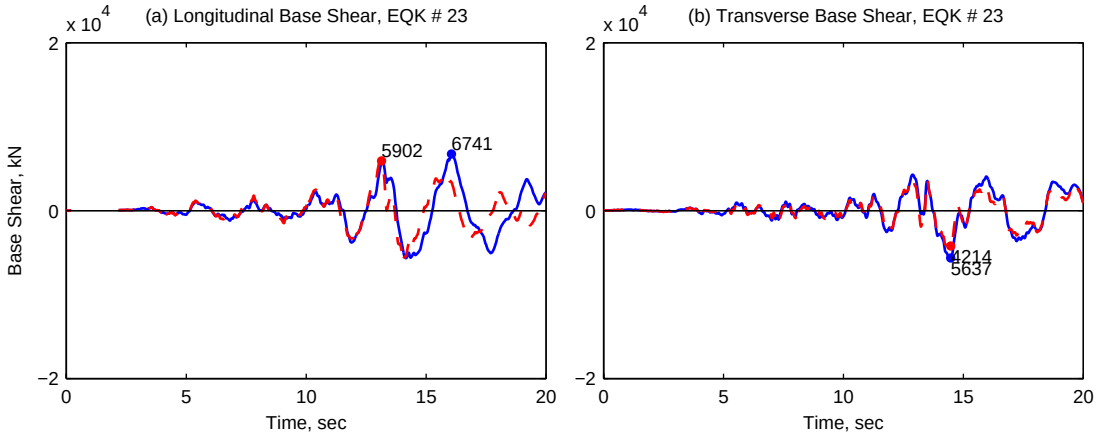

Figure II.83. Base shear of 20-Story North Hollywood Hotel from *OpenSees* (solid line) and *Perform3D* (dashed lines) for ground motion 23.

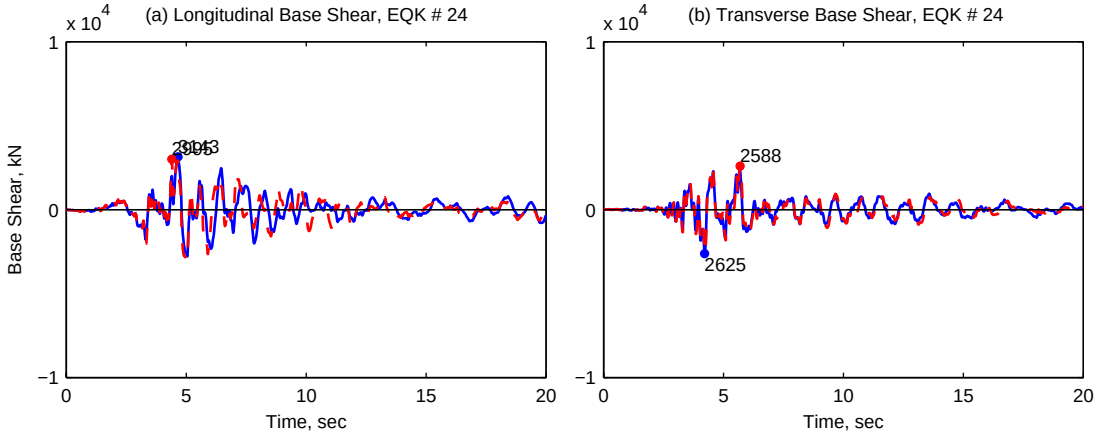

Figure II.84. Base shear of 20-Story North Hollywood Hotel from *OpenSees* (solid line) and *Perform3D* (dashed lines) for ground motion 24.

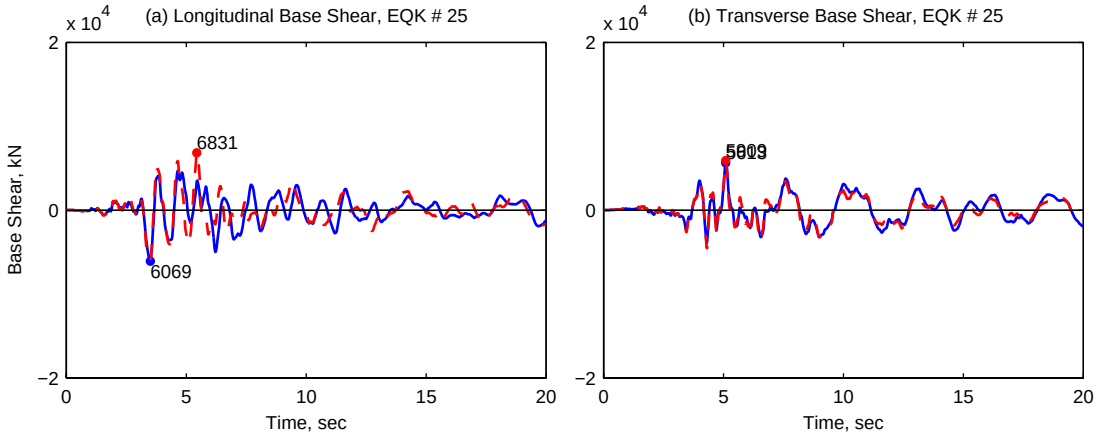

Figure II.85. Base shear of 20-Story North Hollywood Hotel from *OpenSees* (solid line) and *Perform3D* (dashed lines) for ground motion 25.

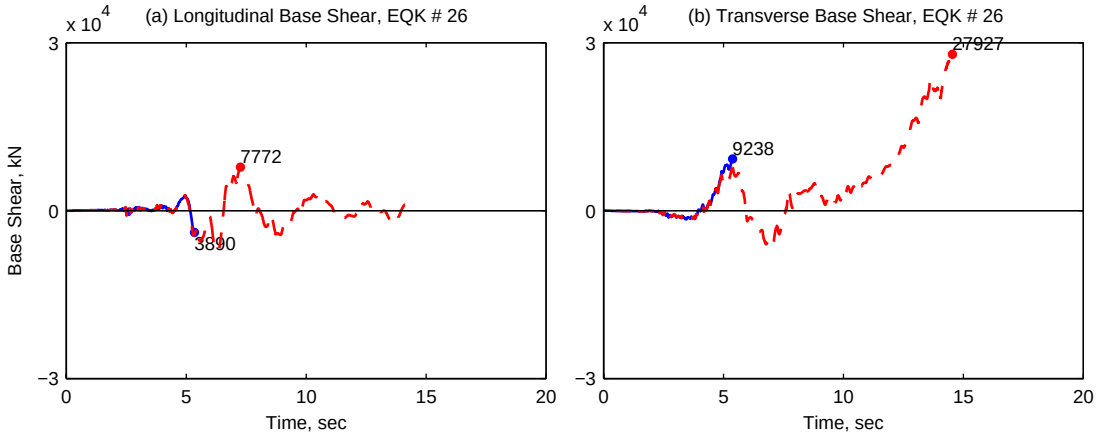

Figure II.86. Base shear of 20-Story North Hollywood Hotel from *OpenSees* (solid line) and *Perform3D* (dashed lines) for ground motion 26.

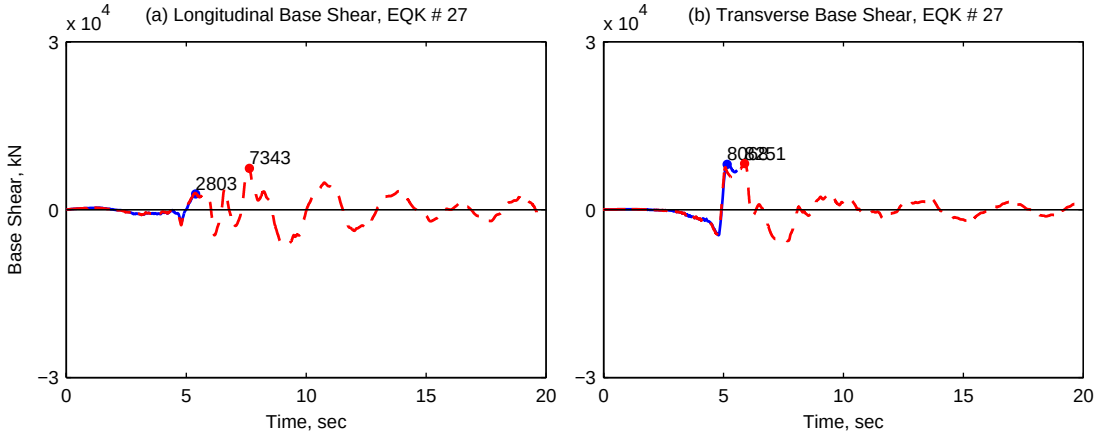

Figure II.87. Base shear of 20-Story North Hollywood Hotel from *OpenSees* (solid line) and *Perform3D* (dashed lines) for ground motion 27.

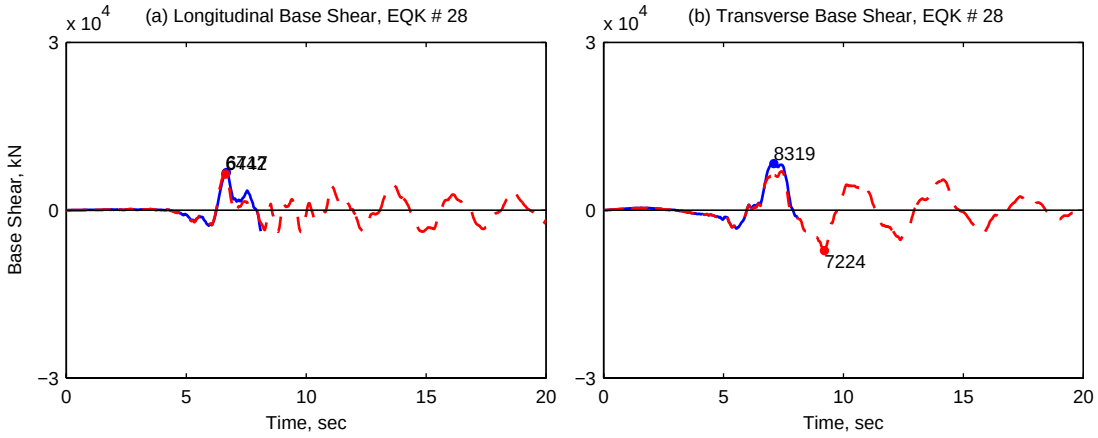

Figure II.88. Base shear of 20-Story North Hollywood Hotel from *OpenSees* (solid line) and *Perform3D* (dashed lines) for ground motion 28.

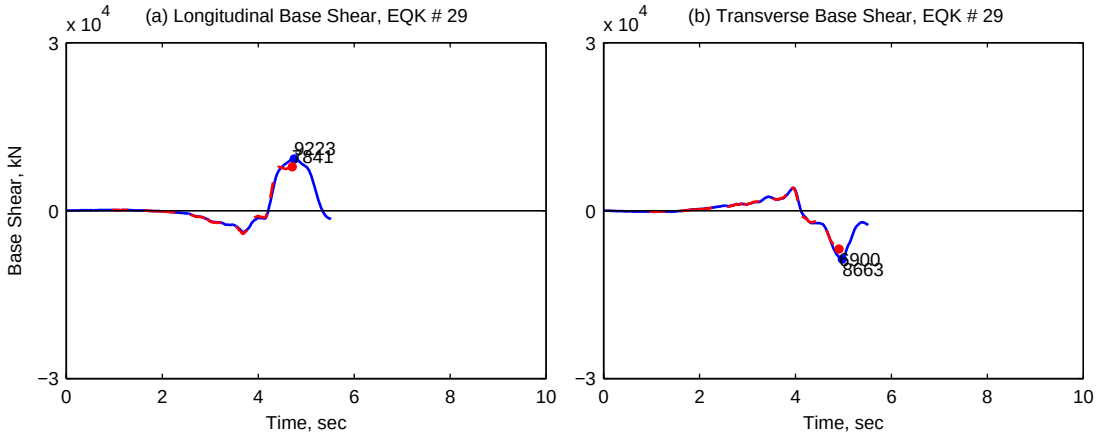

Figure II.89. Base shear of 20-Story North Hollywood Hotel from *OpenSees* (solid line) and *Perform3D* (dashed lines) for ground motion 29.

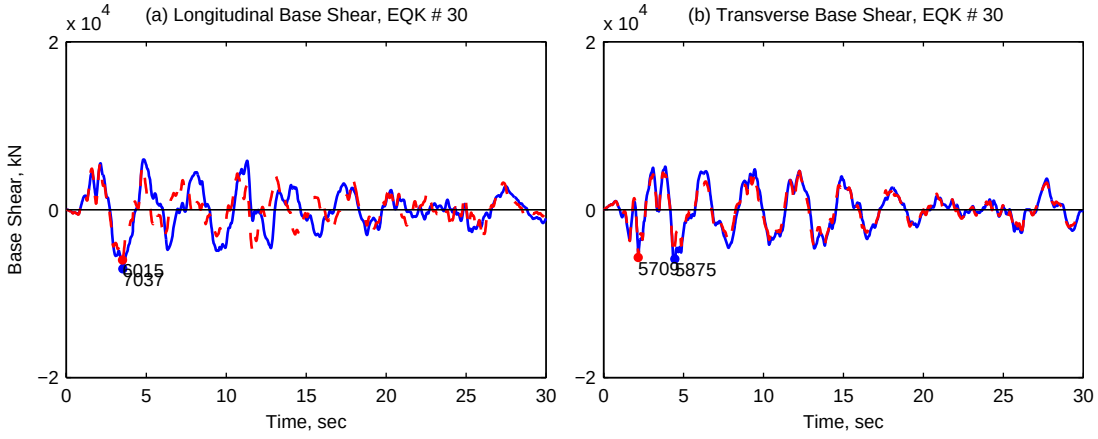

Figure II.90. Base shear of 20-Story North Hollywood Hotel from *OpenSees* (solid line) and *Perform3D* (dashed lines) for ground motion 30.

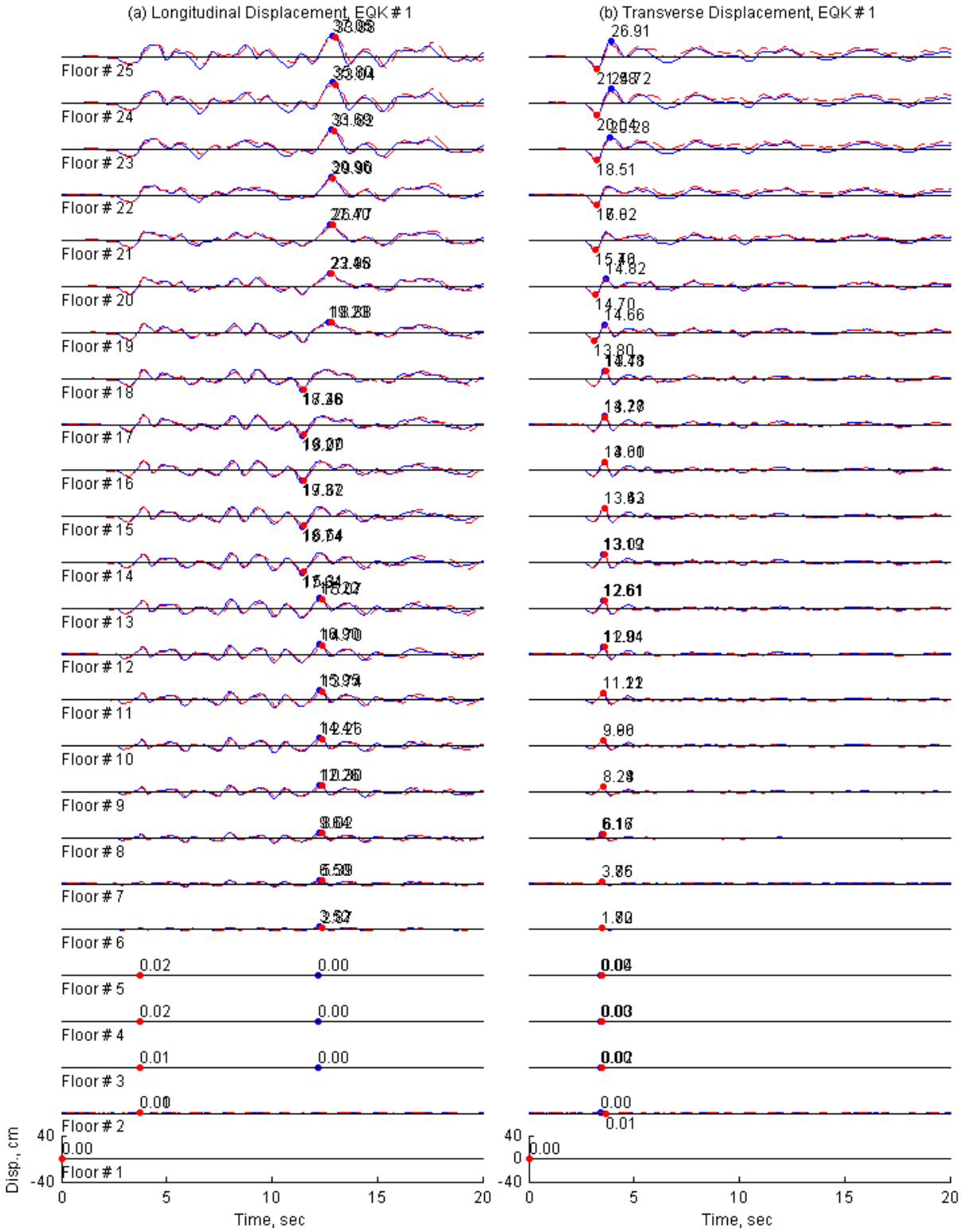

Figure II.91. Floor displacements of 19-Story Office Building in Los Angeles from *OpenSees* (solid line) and *Perform3D* (dashed lines) for ground motion 1.

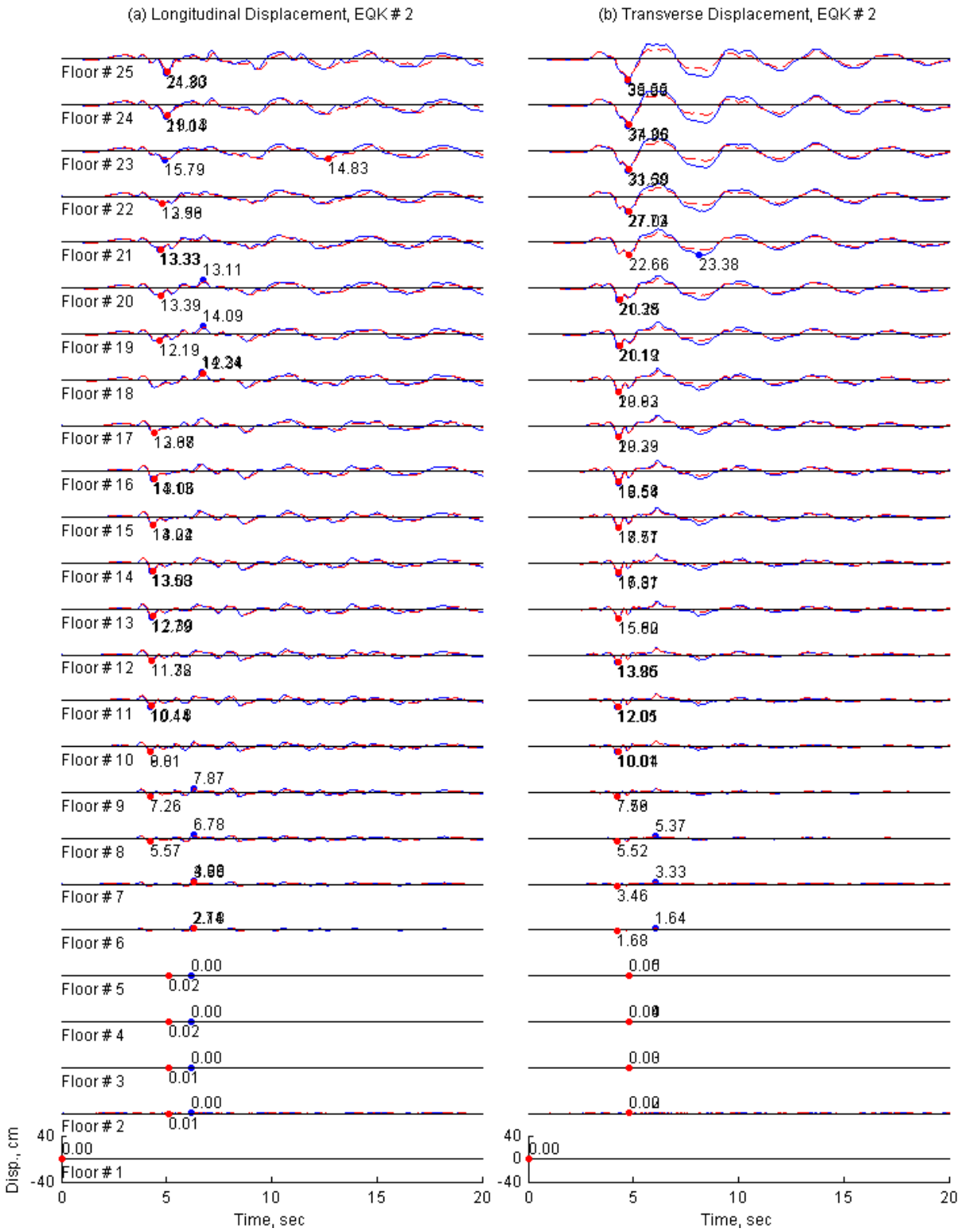

Figure II.92. Floor displacements of 19-Story Office Building in Los Angeles from *OpenSees* (solid line) and *Perform3D* (dashed lines) for ground motion 2.

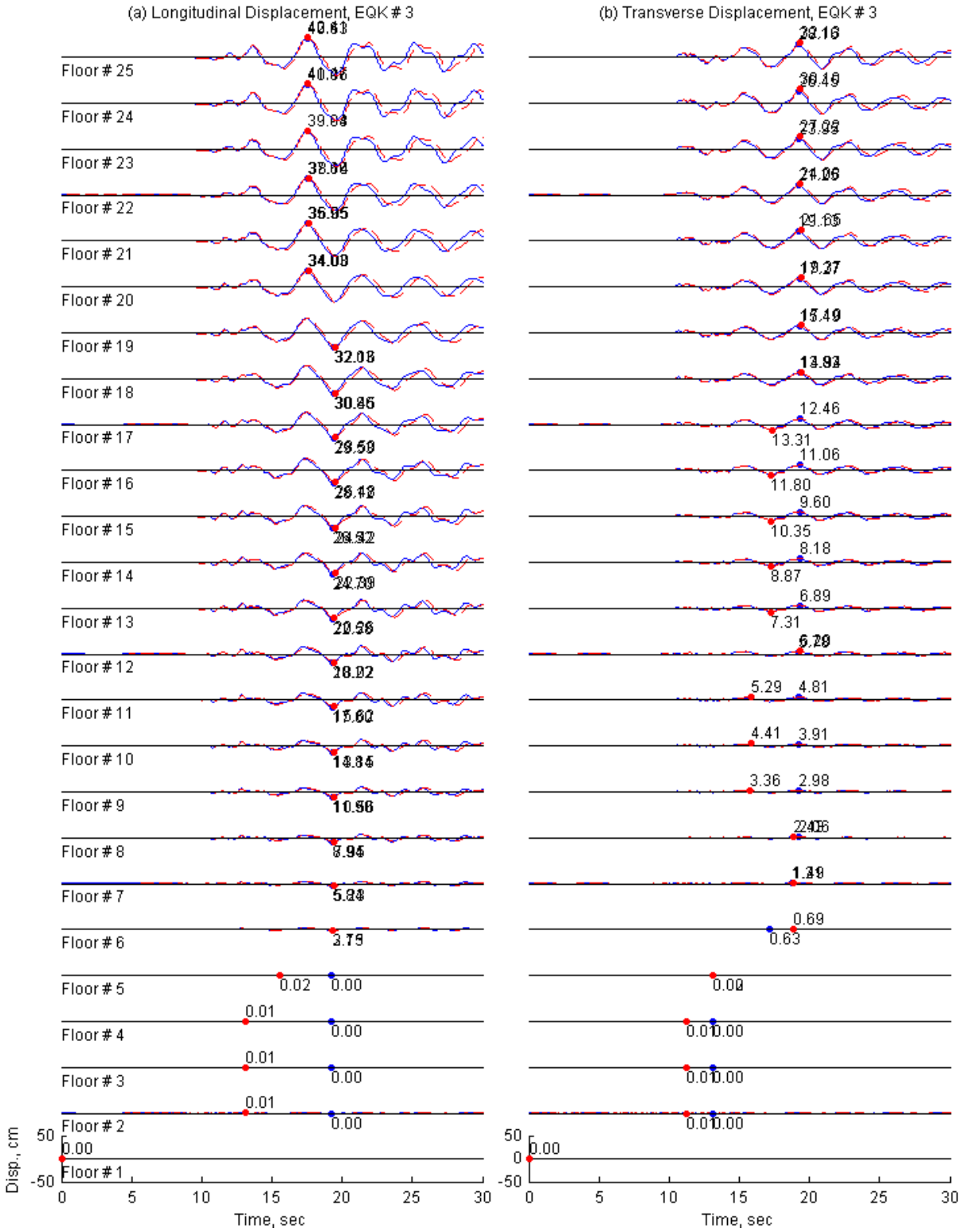

Figure II.93. Floor displacements of 19-Story Office Building in Los Angeles from *OpenSees* (solid line) and *Perform3D* (dashed lines) for ground motion 3.

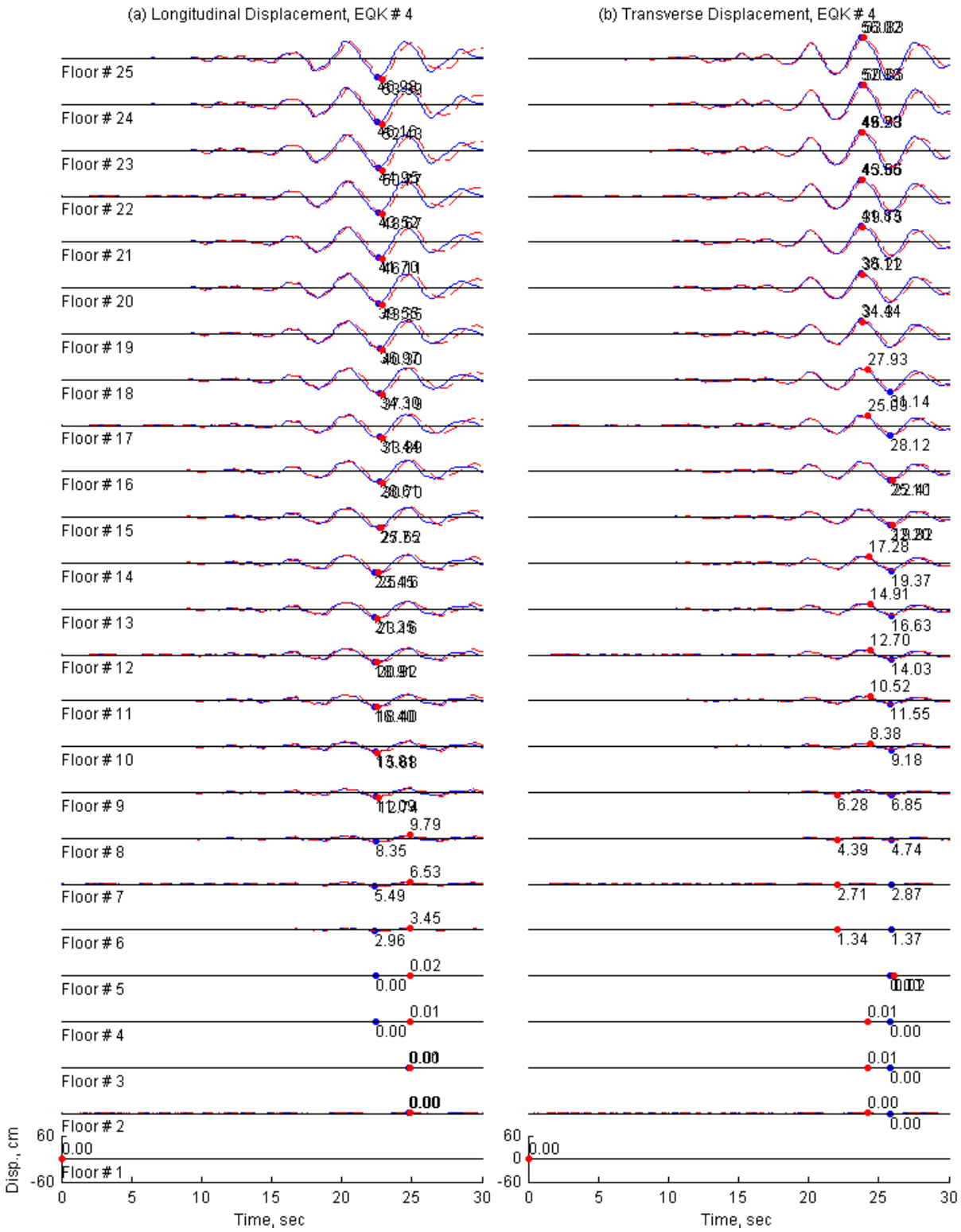

Figure II.94. Floor displacements of 19-Story Office Building in Los Angeles from *OpenSees* (solid line) and *Perform3D* (dashed lines) for ground motion 4.

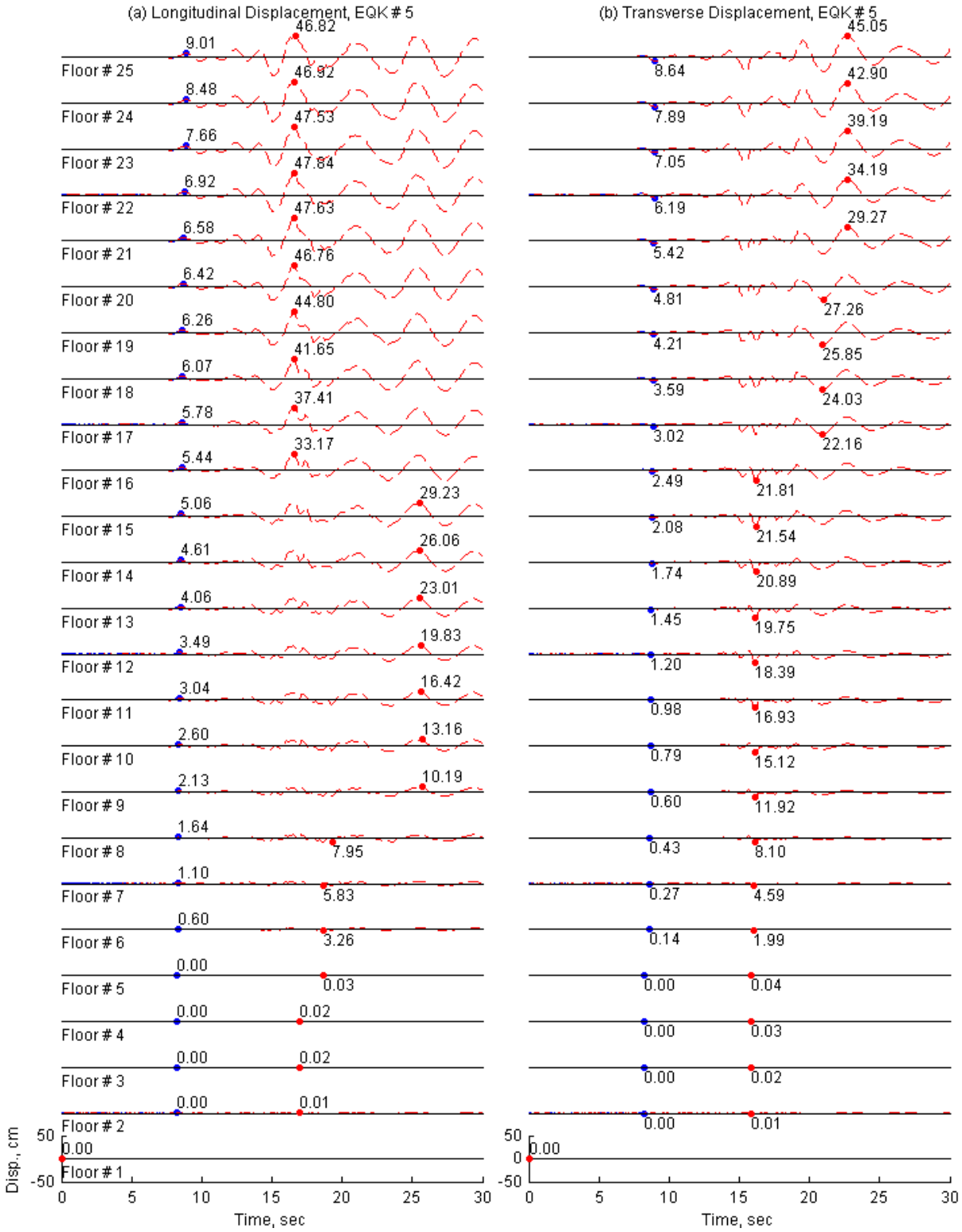

Figure II.95. Floor displacements of 19-Story Office Building in Los Angeles from *OpenSees* (solid line) and *Perform3D* (dashed lines) for ground motion 5.

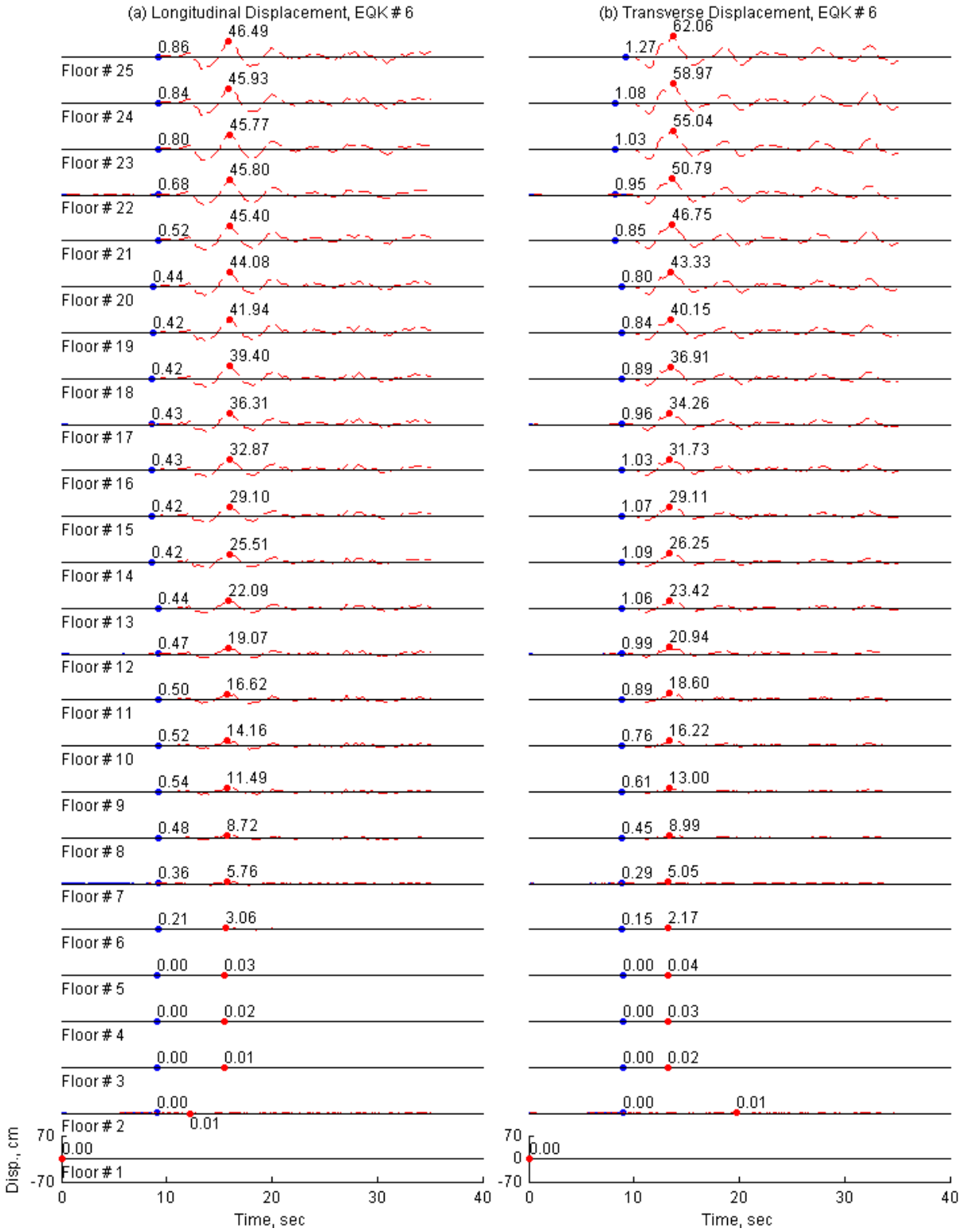

Figure II.96. Floor displacements of 19-Story Office Building in Los Angeles from *OpenSees* (solid line) and *Perform3D* (dashed lines) for ground motion 6.

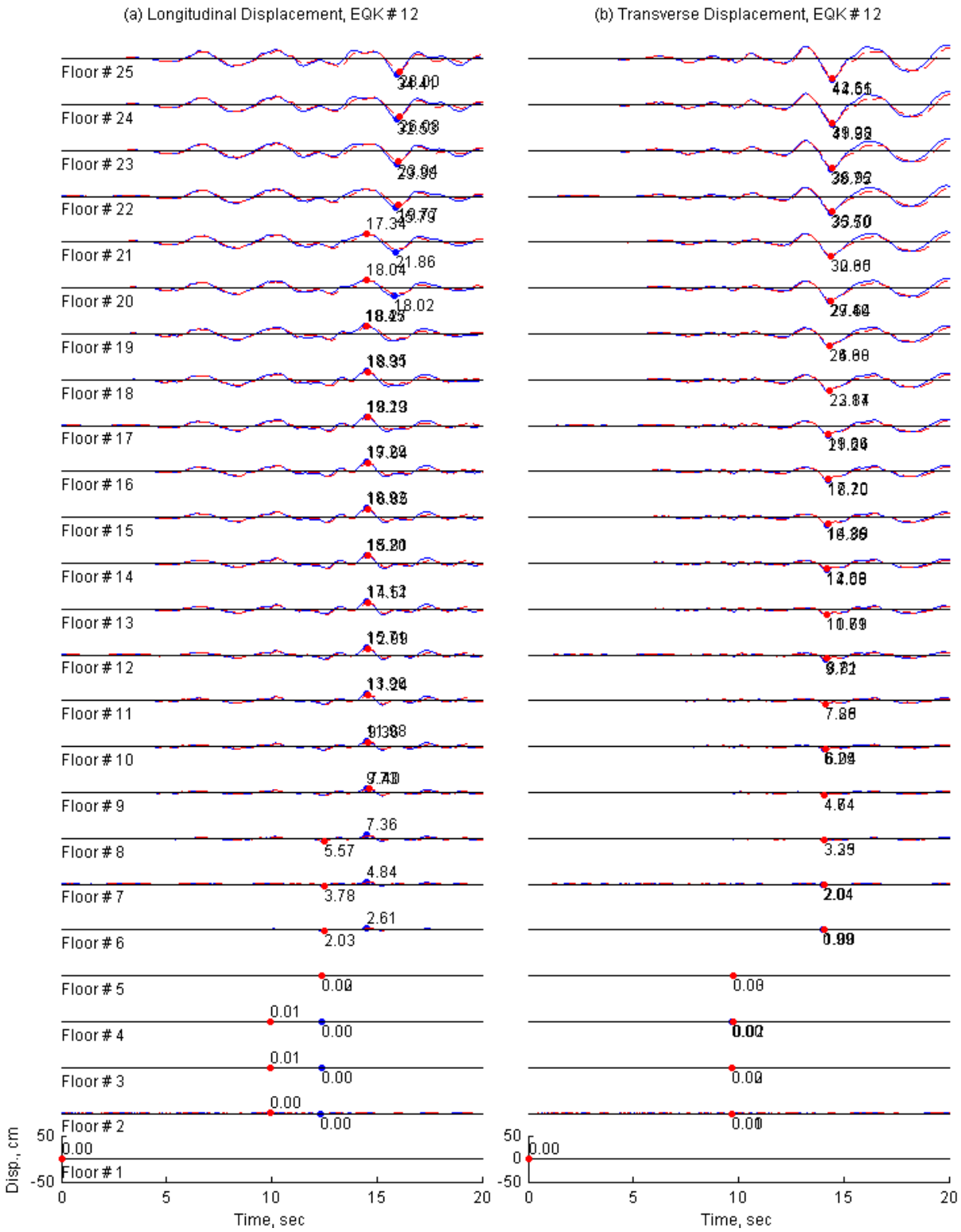

Figure II.97. Floor displacements of 19-Story Office Building in Los Angeles from *OpenSees* (solid line) and *Perform3D* (dashed lines) for ground motion 12.

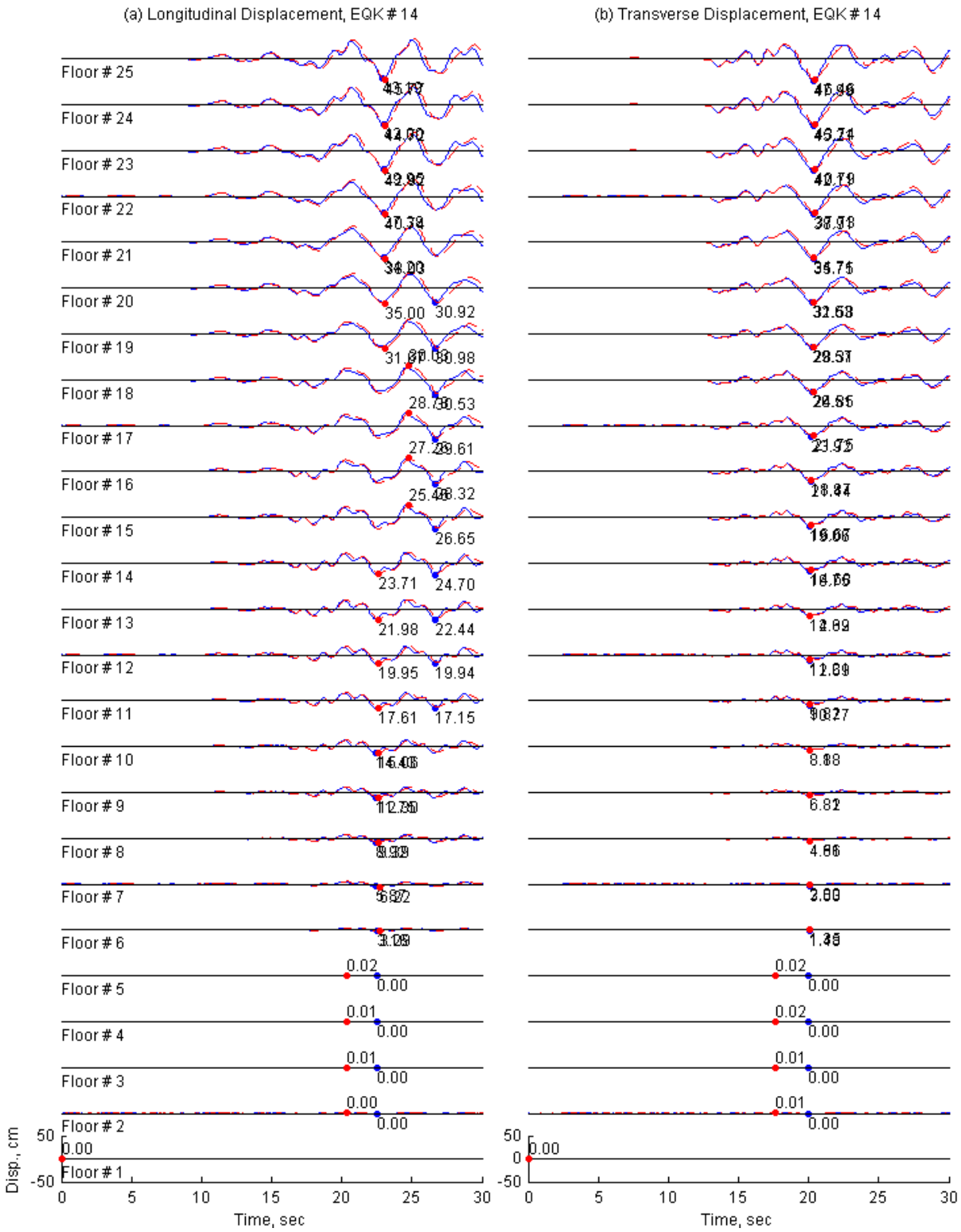

Figure II.98. Floor displacements of 19-Story Office Building in Los Angeles from *OpenSees* (solid line) and *Perform3D* (dashed lines) for ground motion 14.

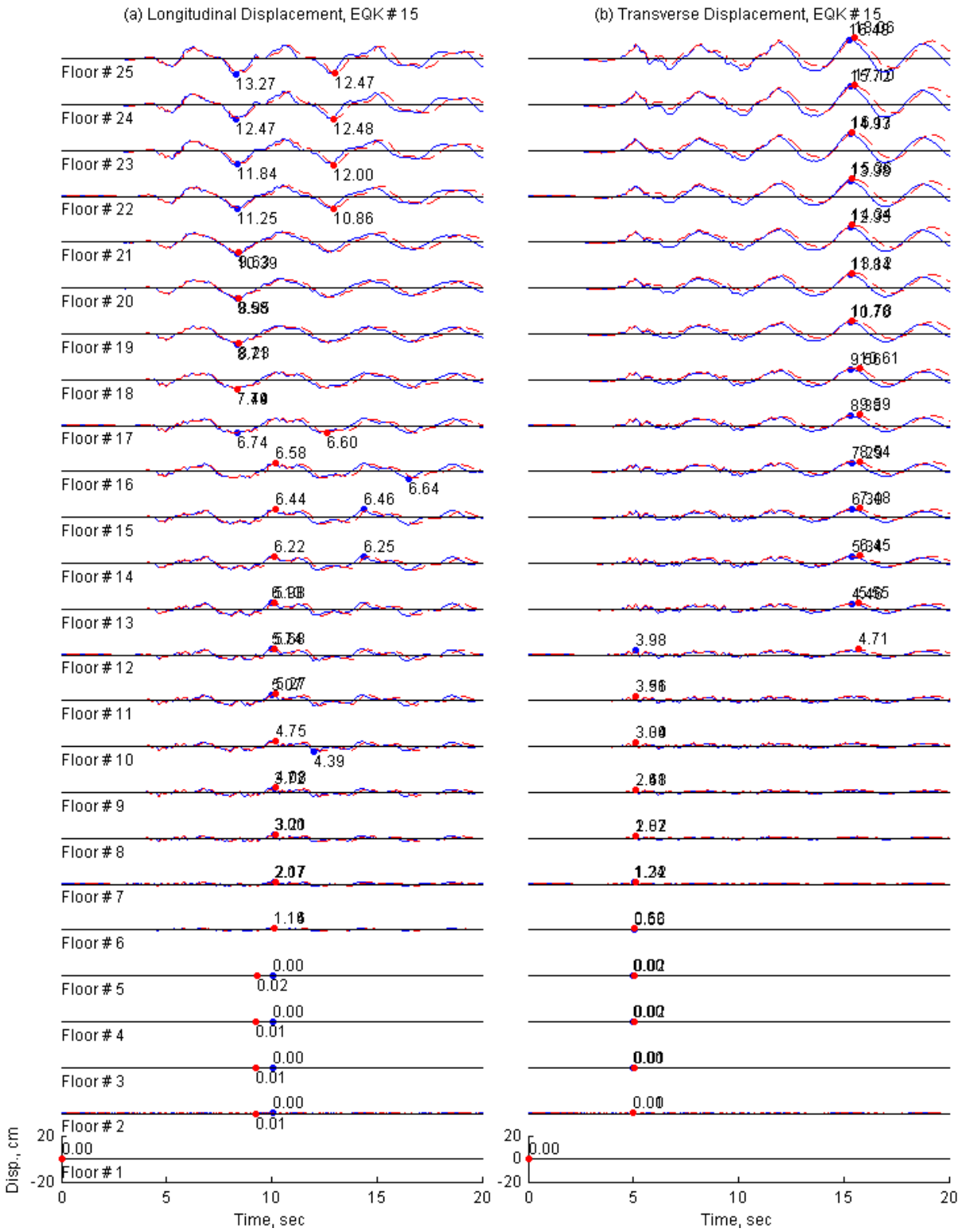

Figure II.99. Floor displacements of 19-Story Office Building in Los Angeles from *OpenSees* (solid line) and *Perform3D* (dashed lines) for ground motion 15.

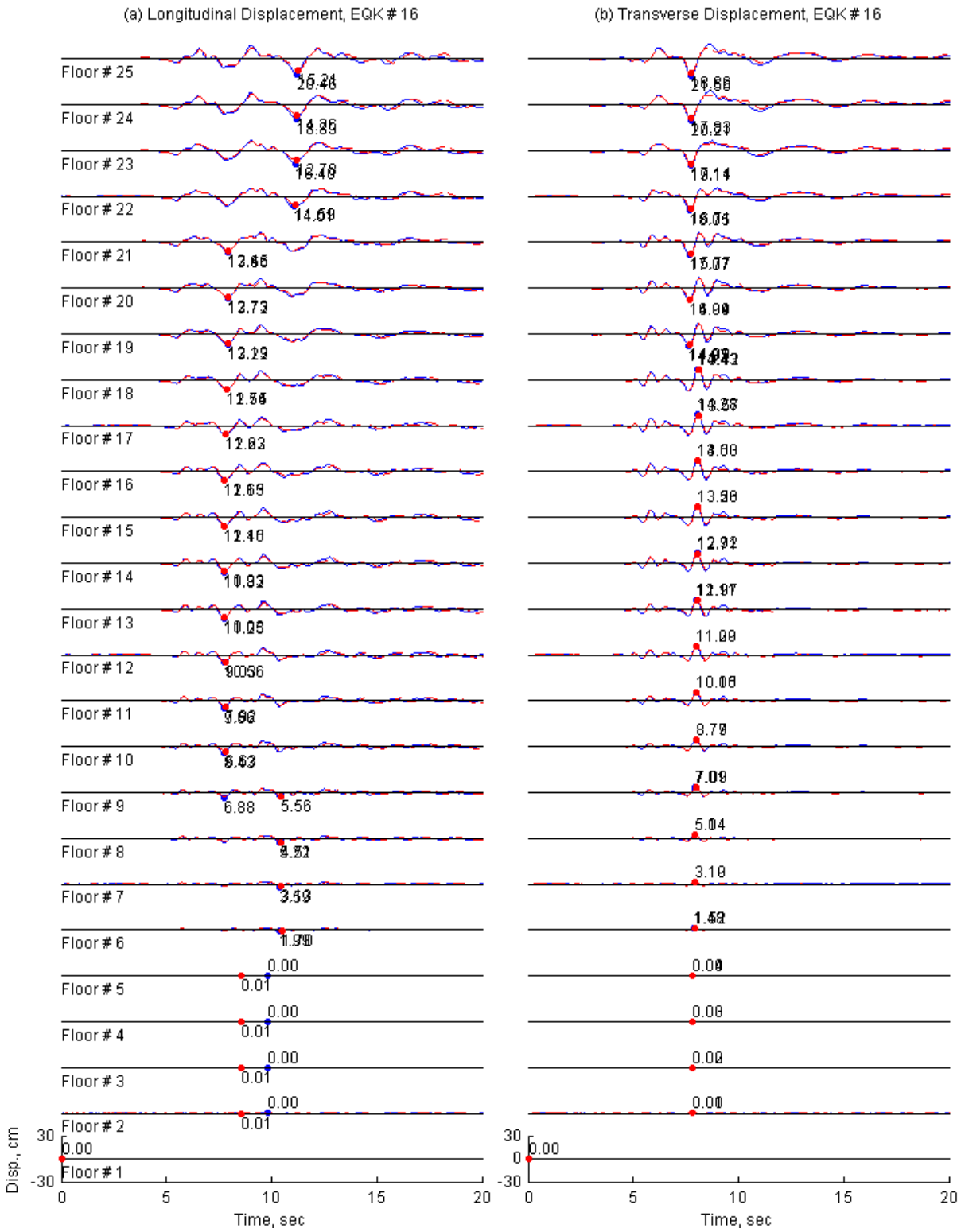

Figure II.100. Floor displacements of 19-Story Office Building in Los Angeles from *OpenSees* (solid line) and *Perform3D* (dashed lines) for ground motion 16.

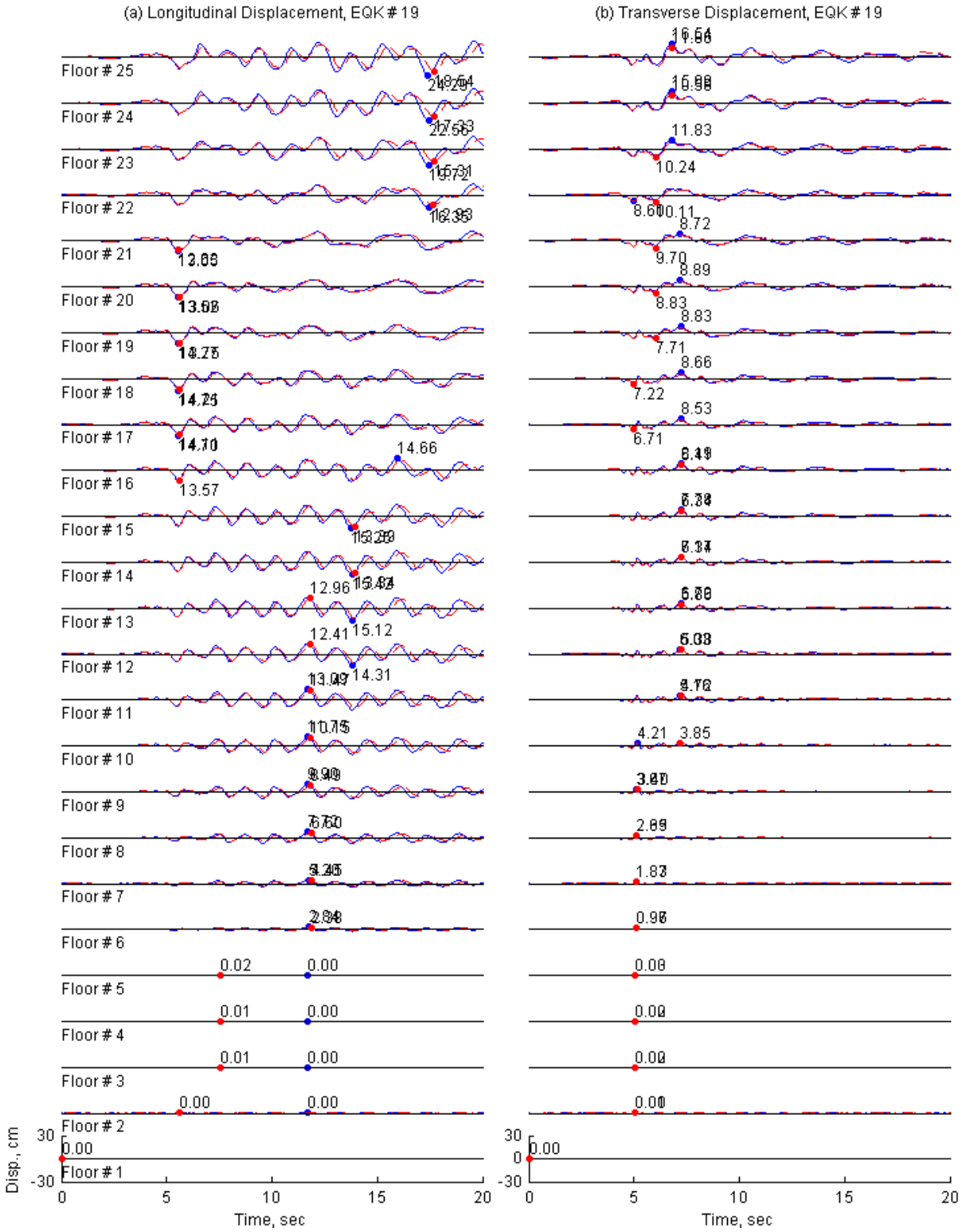

Figure II.101. Floor displacements of 19-Story Office Building in Los Angeles from *OpenSees* (solid line) and *Perform3D* (dashed lines) for ground motion 19.

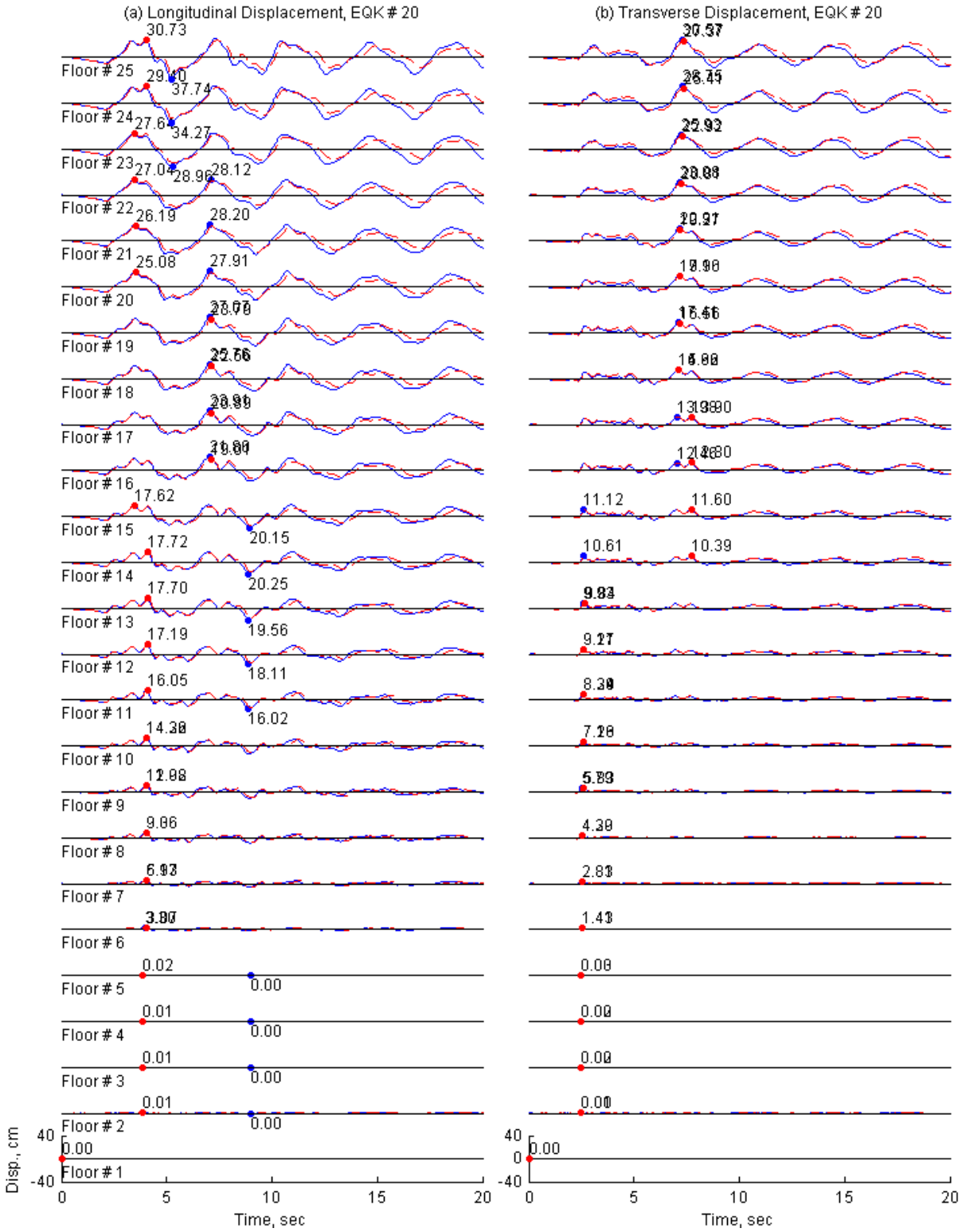

Figure II.102. Floor displacements of 19-Story Office Building in Los Angeles from *OpenSees* (solid line) and *Perform3D* (dashed lines) for ground motion 20.

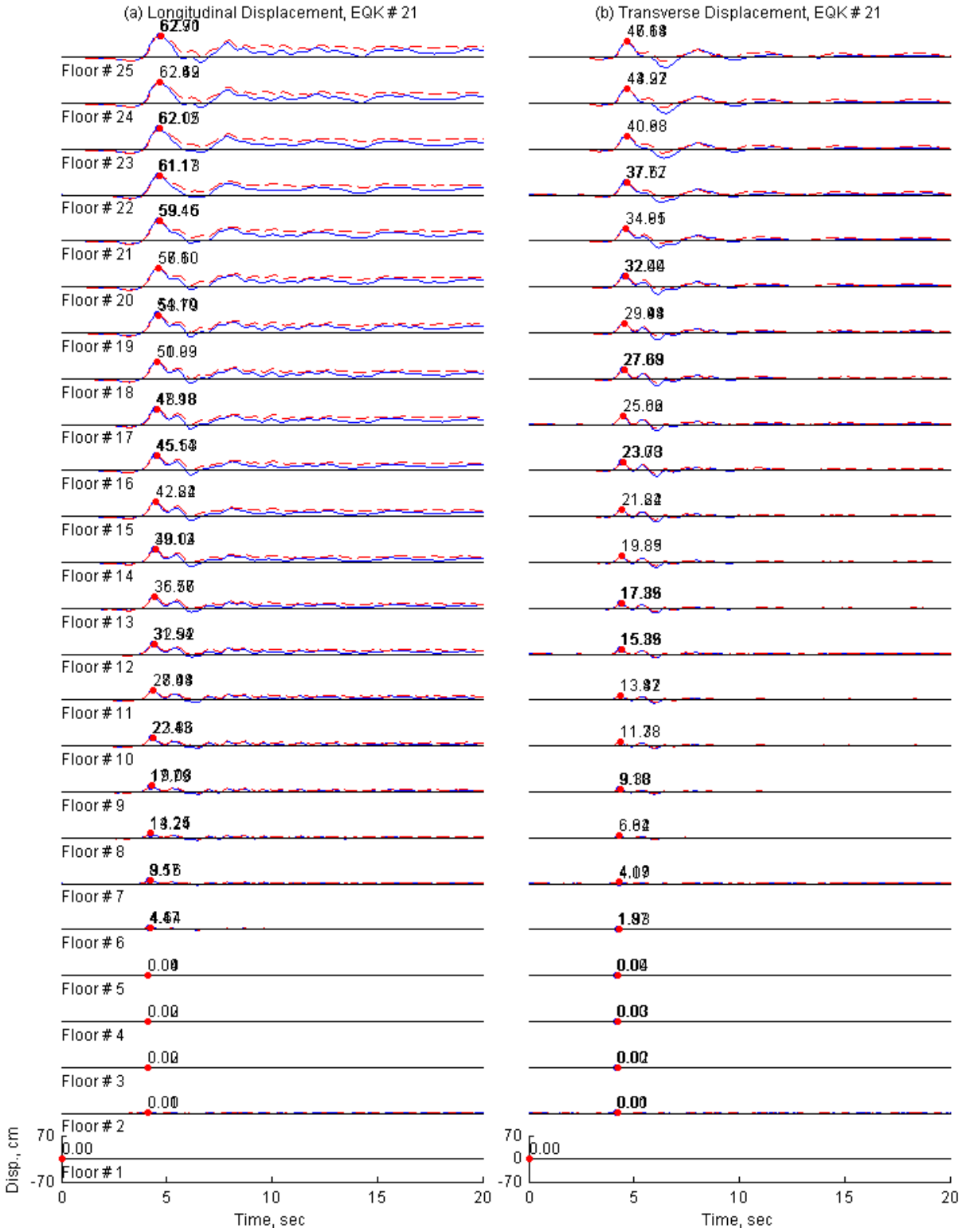

Figure II.103. Floor displacements of 19-Story Office Building in Los Angeles from *OpenSees* (solid line) and *Perform3D* (dashed lines) for ground motion 21.

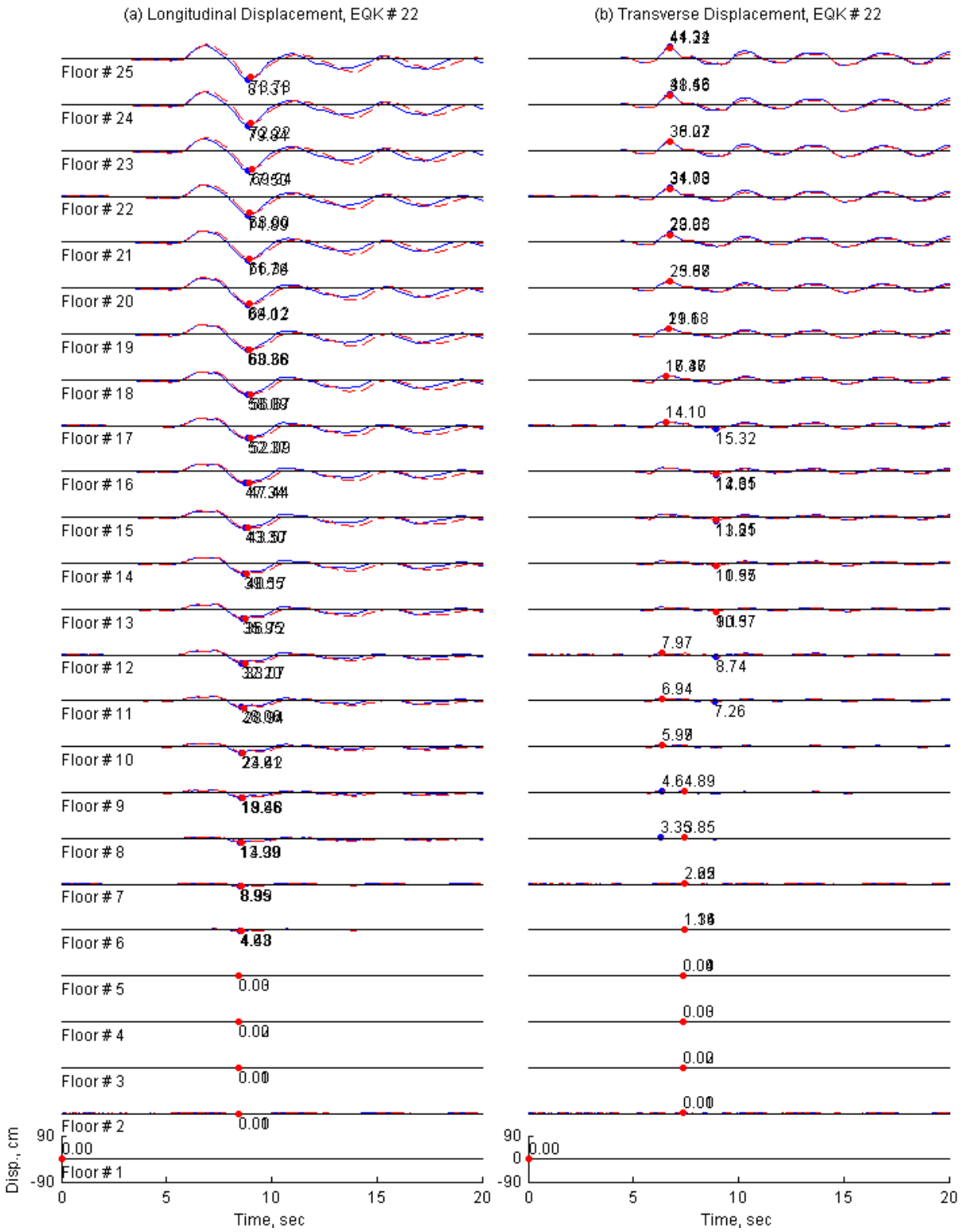

Figure II.104. Floor displacements of 19-Story Office Building in Los Angeles from *OpenSees* (solid line) and *Perform3D* (dashed lines) for ground motion 22.

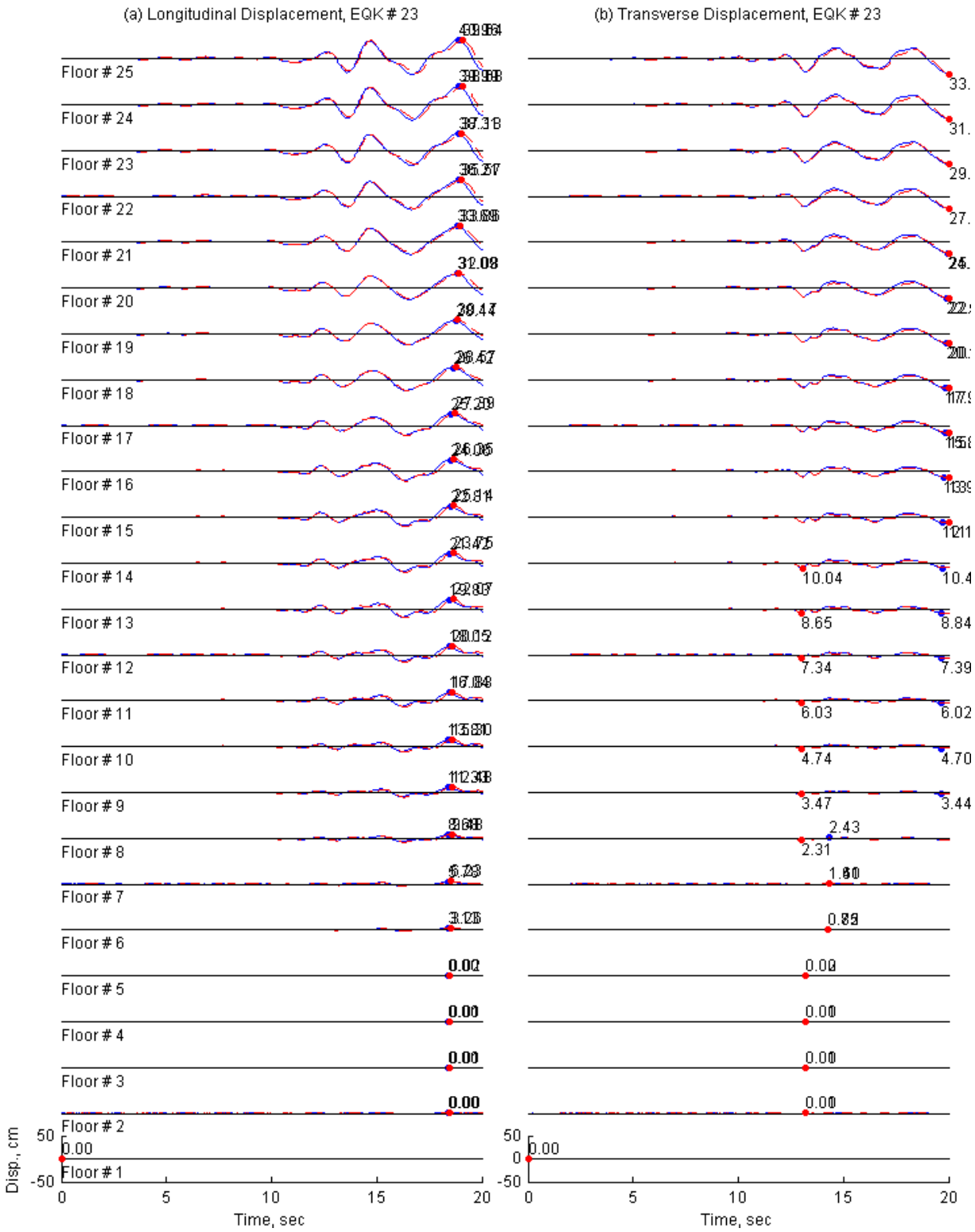

Figure II.105. Floor displacements of 19-Story Office Building in Los Angeles from *OpenSees* (solid line) and *Perform3D* (dashed lines) for ground motion 23.

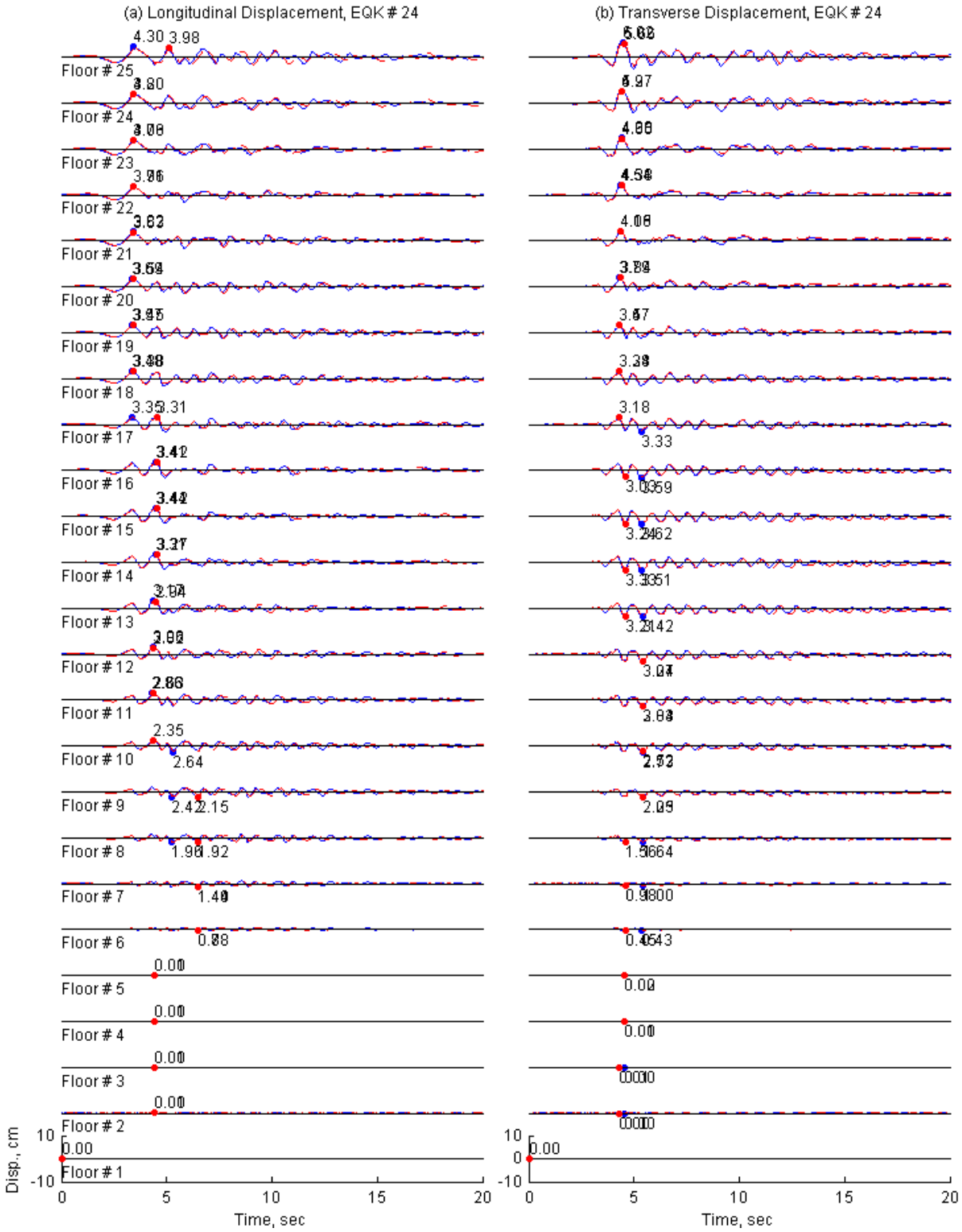

Figure II.106. Floor displacements of 19-Story Office Building in Los Angeles from *OpenSees* (solid line) and *Perform3D* (dashed lines) for ground motion 24.

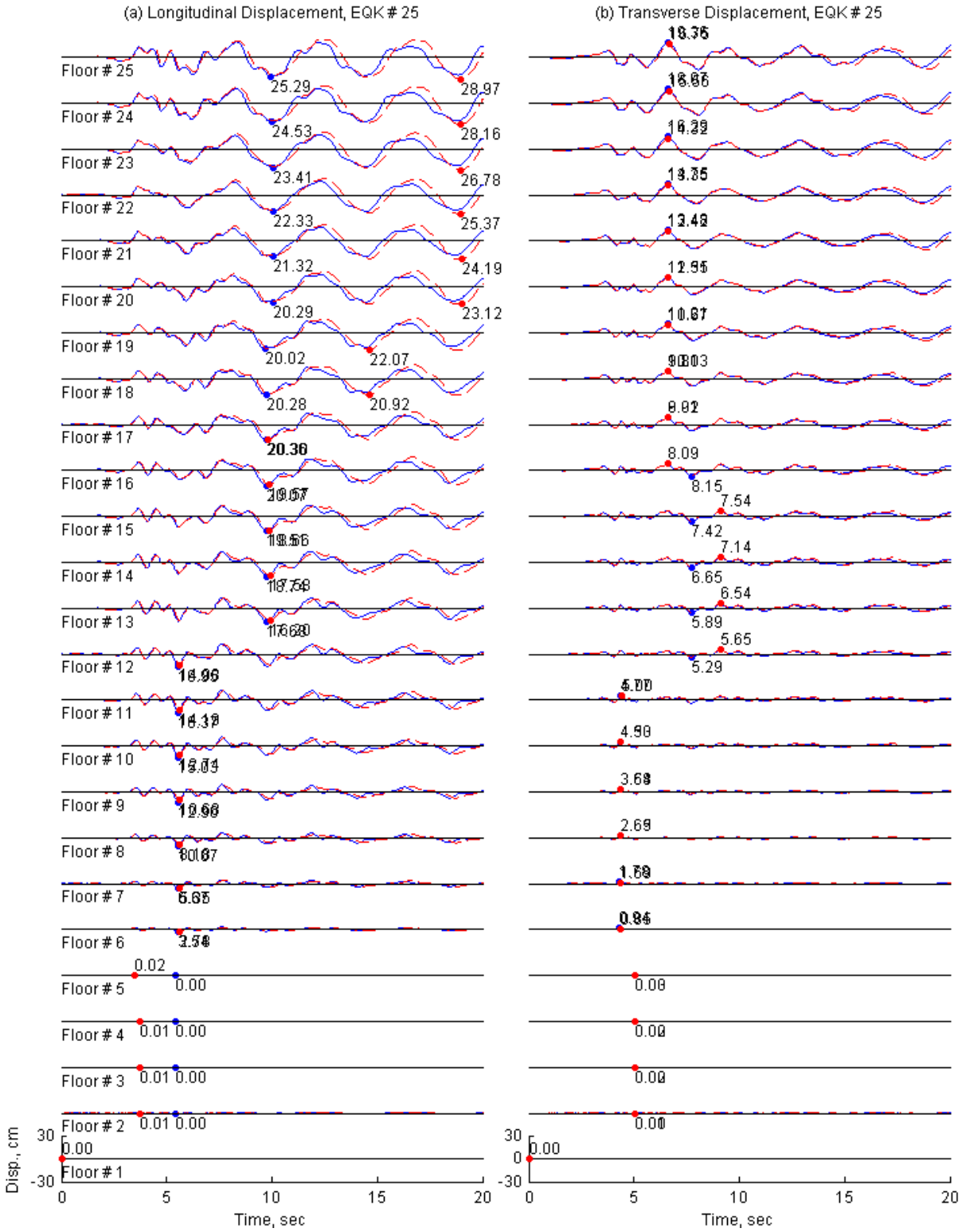

Figure II.107. Floor displacements of 19-Story Office Building in Los Angeles from *OpenSees* (solid line) and *Perform3D* (dashed lines) for ground motion 25.

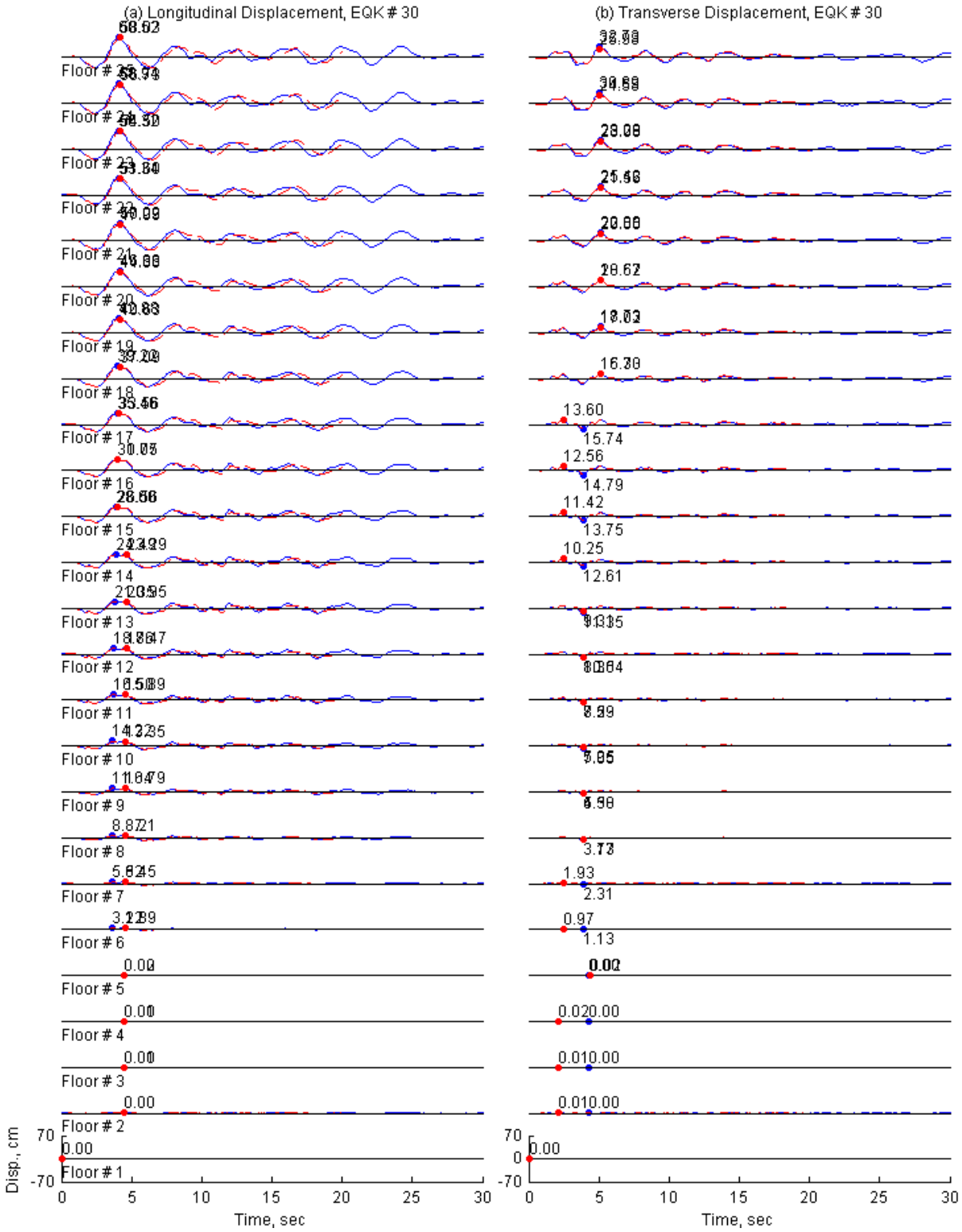

Figure II.108. Floor displacements of 19-Story Office Building in Los Angeles from *OpenSees* (solid line) and *Perform3D* (dashed lines) for ground motion 30.

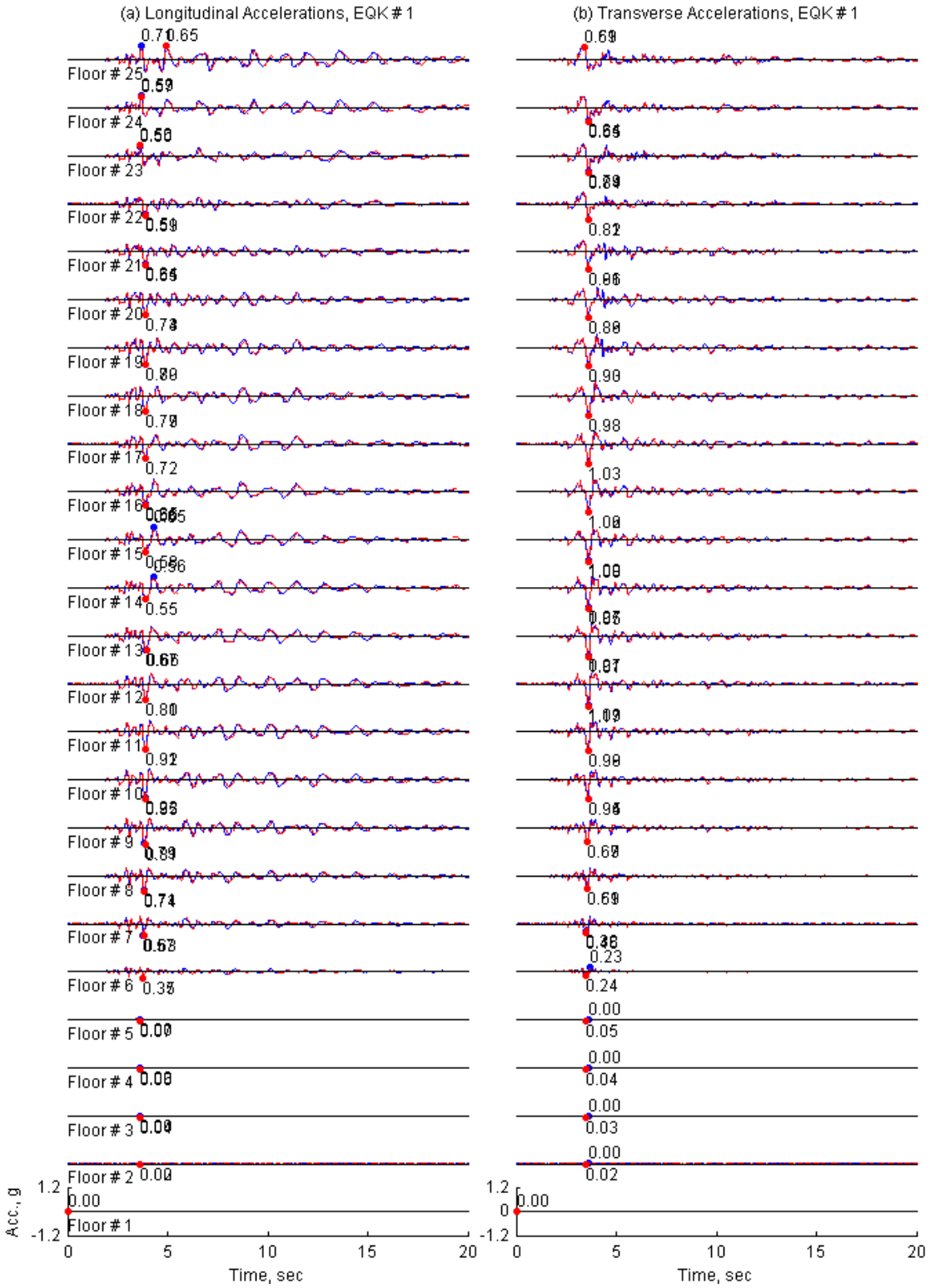

Figure II.109. Floor accelerations of 19-Story Office Building in Los Angeles from *OpenSees* (solid line) and *Perform3D* (dashed lines) for ground motion 1.

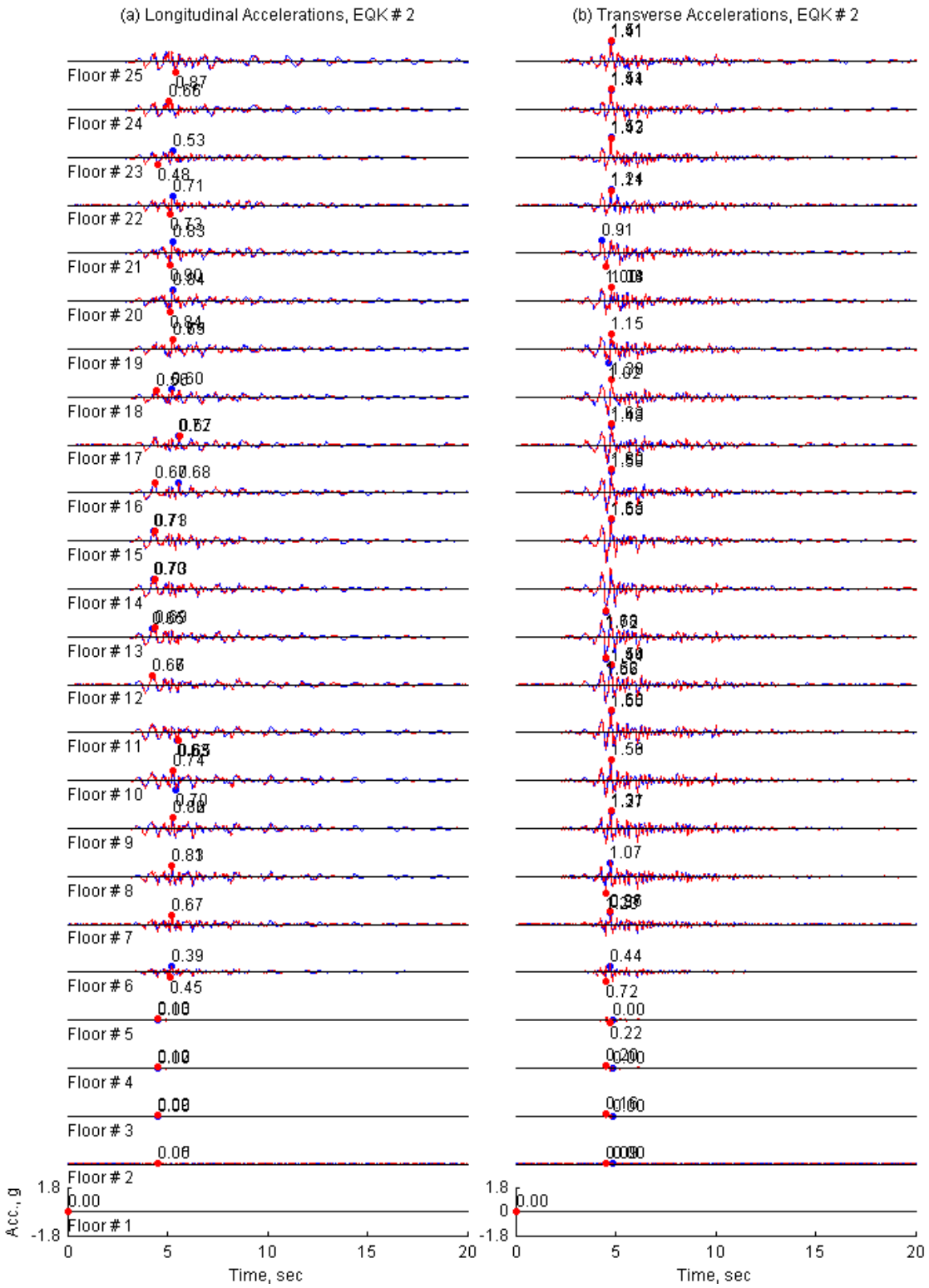

Figure II.110. Floor accelerations of 19-Story Office Building in Los Angeles from *OpenSees* (solid line) and *Perform3D* (dashed lines) for ground motion 2.

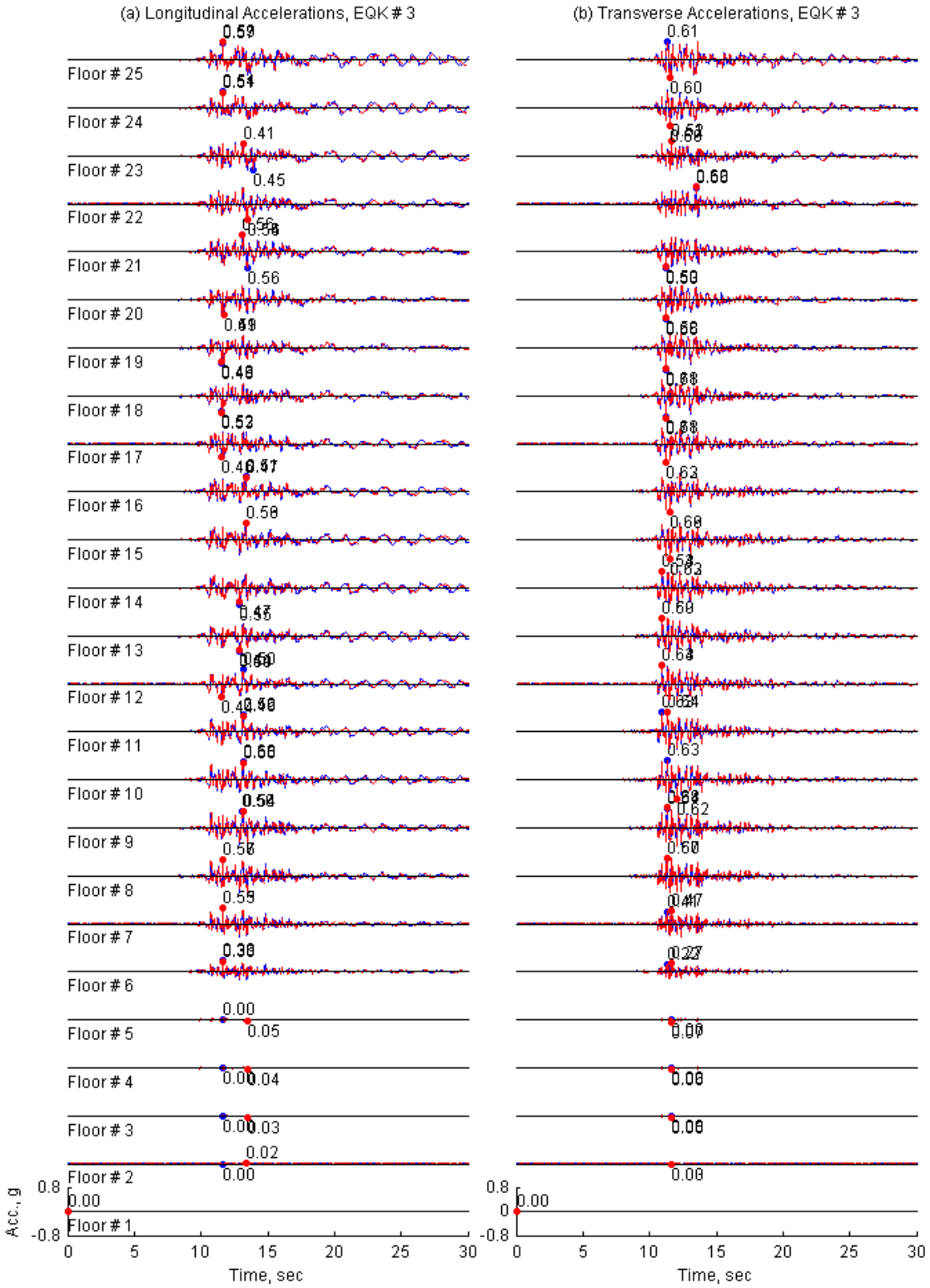

Figure II.111. Floor accelerations of 19-Story Office Building in Los Angeles from *OpenSees* (solid line) and *Perform3D* (dashed lines) for ground motion 3.

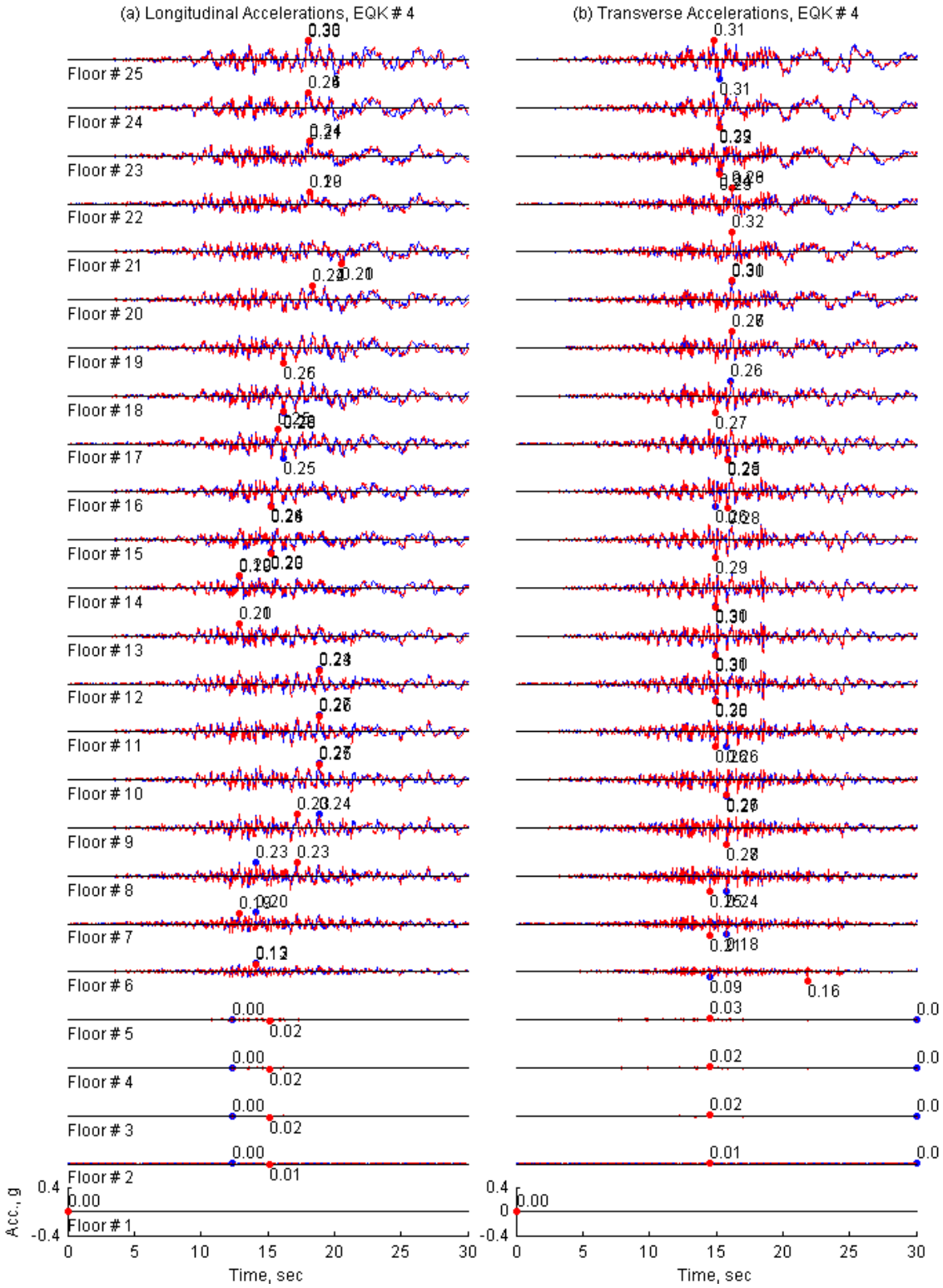

Figure II.112. Floor accelerations of 19-Story Office Building in Los Angeles from *OpenSees* (solid line) and *Perform3D* (dashed lines) for ground motion 4.

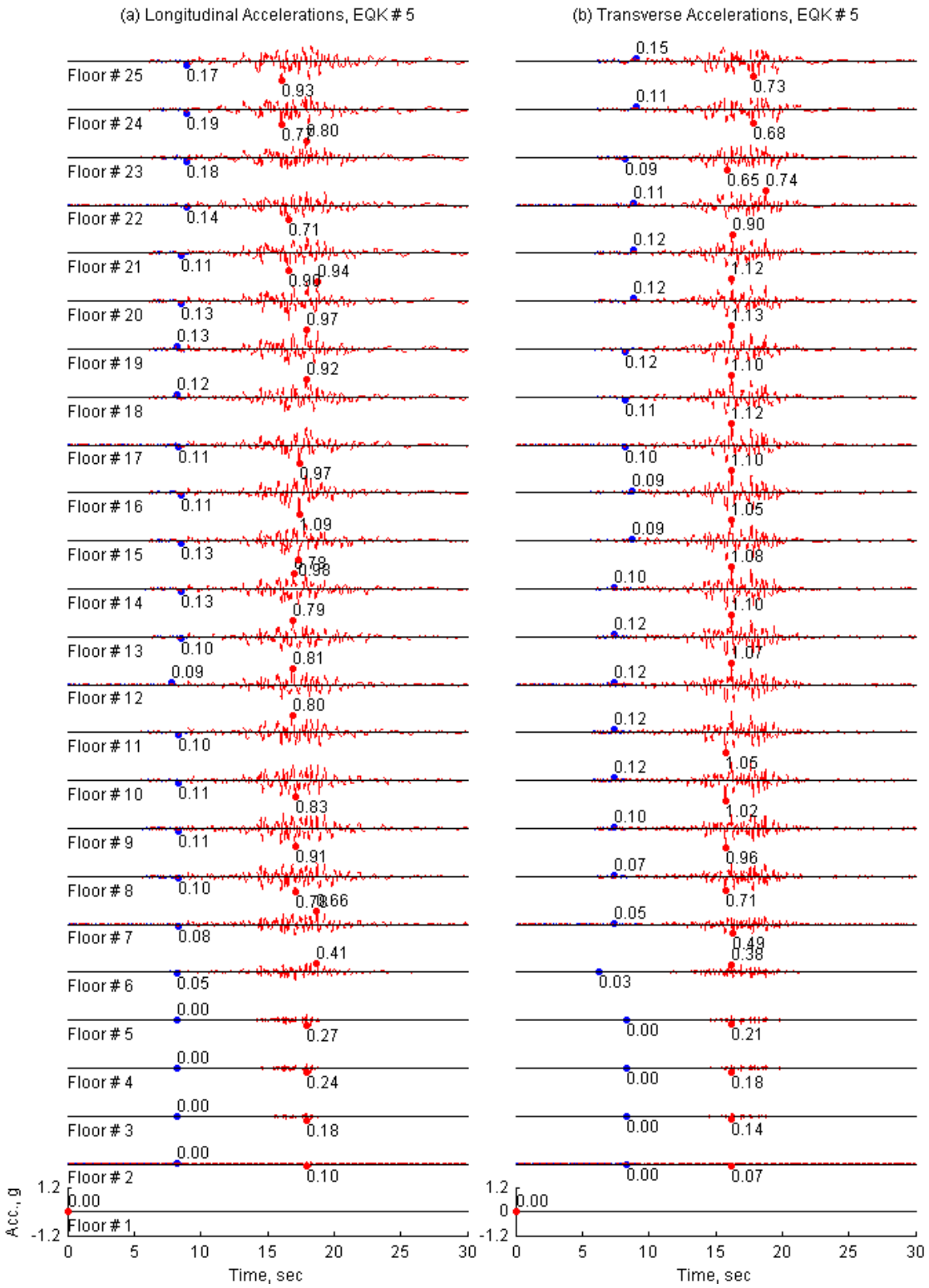

Figure II.113. Floor accelerations of 19-Story Office Building in Los Angeles from *OpenSees* (solid line) and *Perform3D* (dashed lines) for ground motion 5.

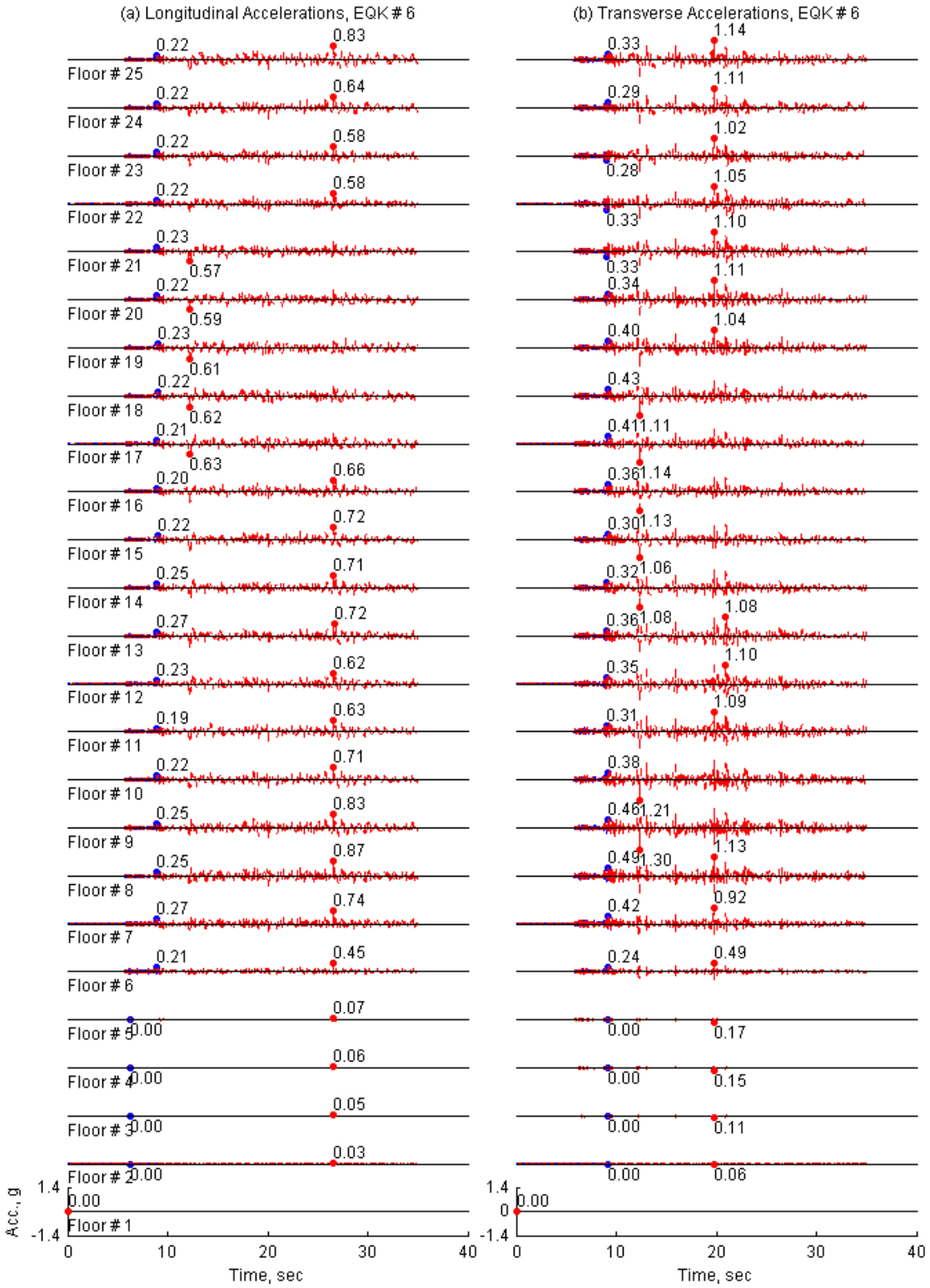

Figure II.114. Floor accelerations of 19-Story Office Building in Los Angeles from *OpenSees* (solid line) and *Perform3D* (dashed lines) for ground motion 6.

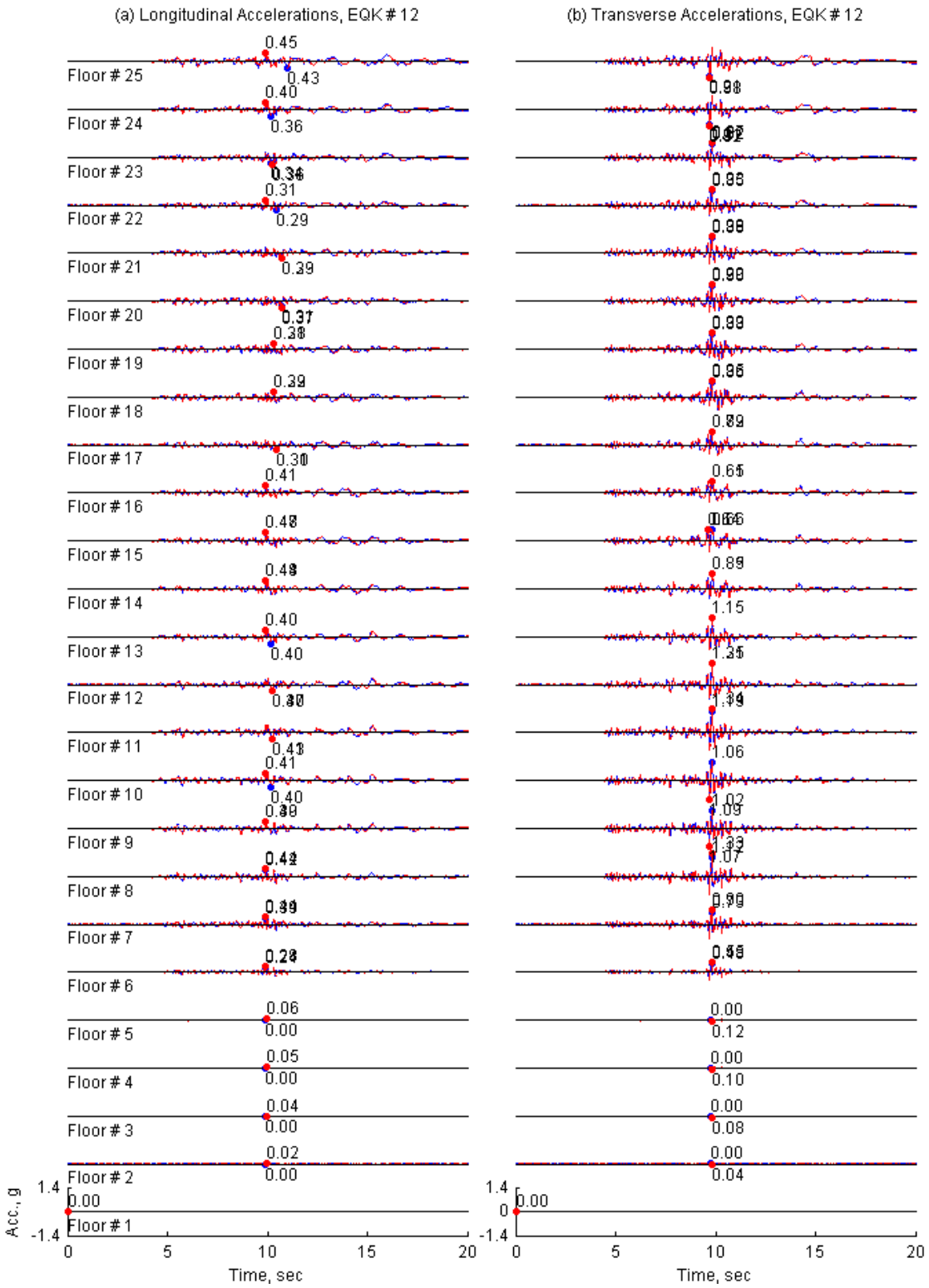

Figure II.115. Floor accelerations of 19-Story Office Building in Los Angeles from *OpenSees* (solid line) and *Perform3D* (dashed lines) for ground motion 12.

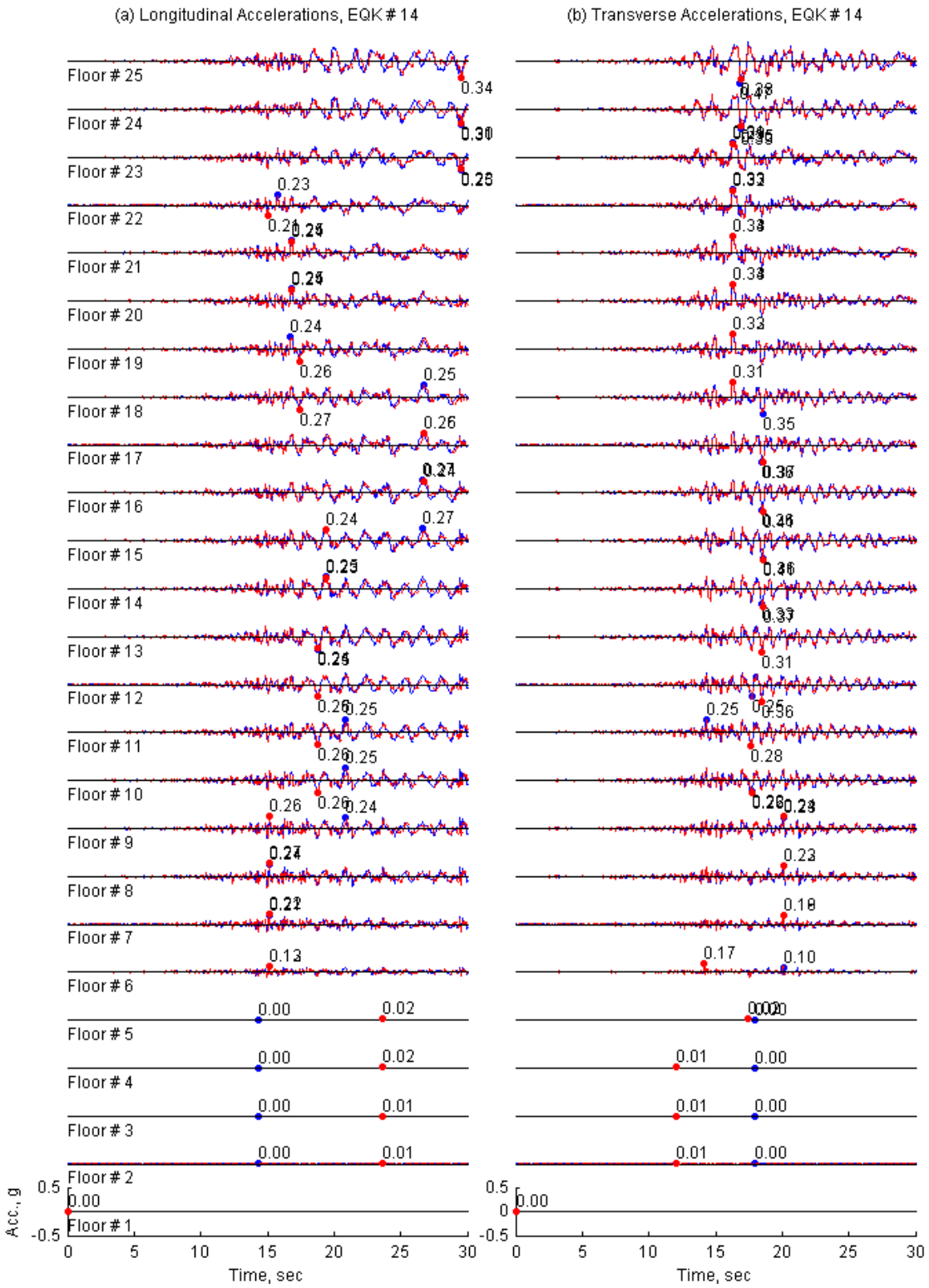

Figure II.116. Floor accelerations of 19-Story Office Building in Los Angeles from *OpenSees* (solid line) and *Perform3D* (dashed lines) for ground motion 14.

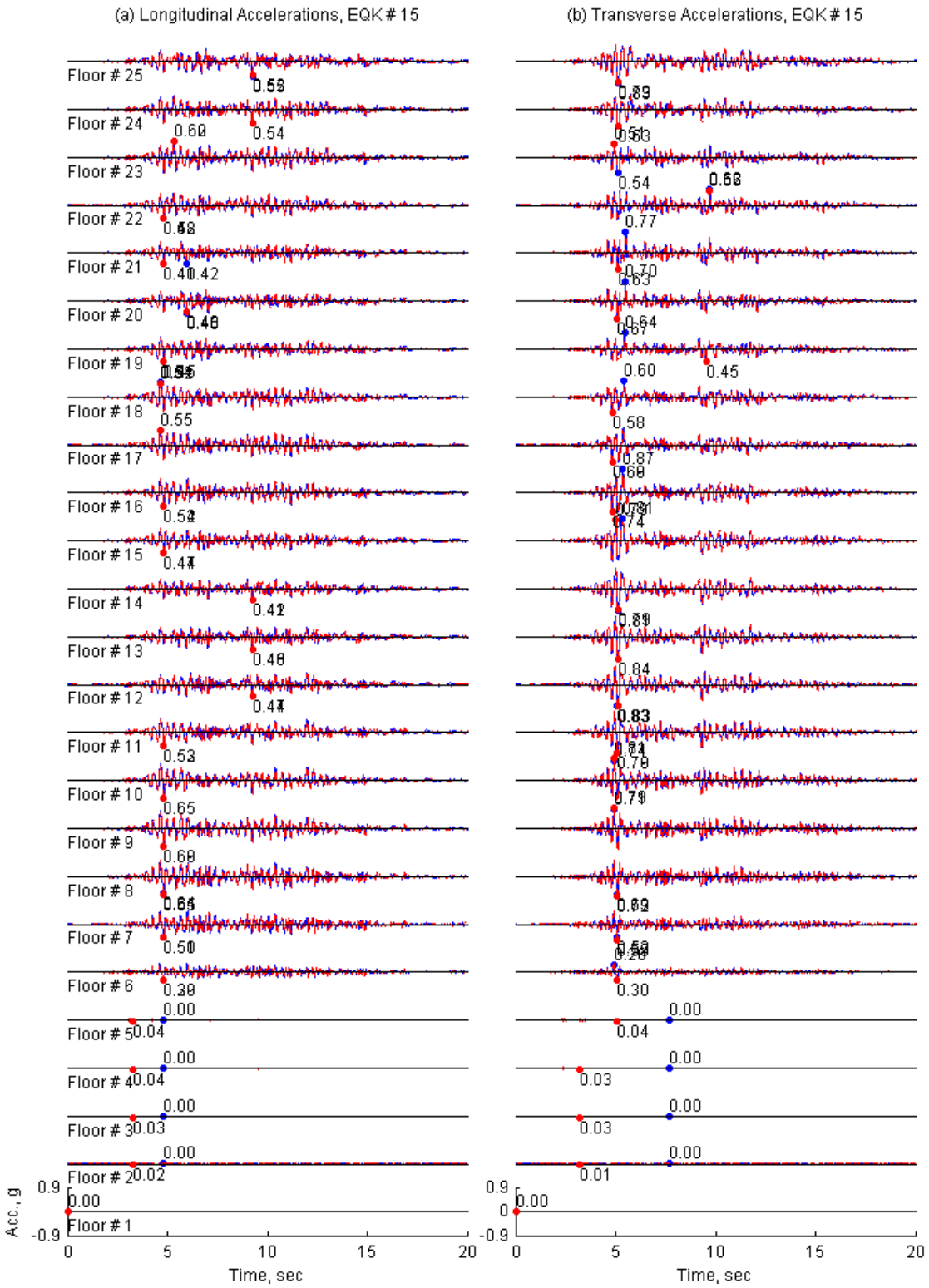

Figure II.117. Floor accelerations of 19-Story Office Building in Los Angeles from *OpenSees* (solid line) and *Perform3D* (dashed lines) for ground motion 15.

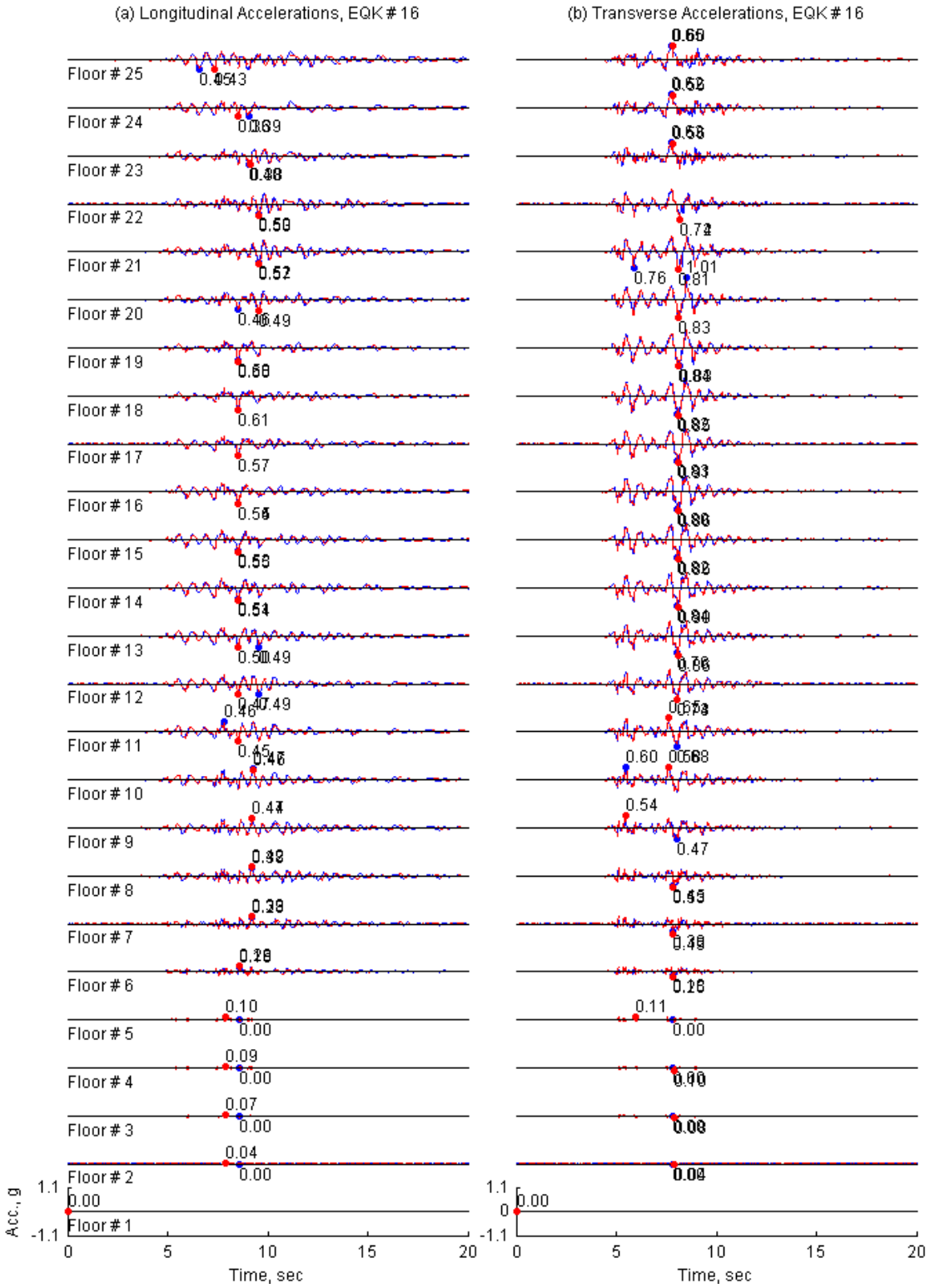

Figure II.118. Floor accelerations of 19-Story Office Building in Los Angeles from *OpenSees* (solid line) and *Perform3D* (dashed lines) for ground motion 16.

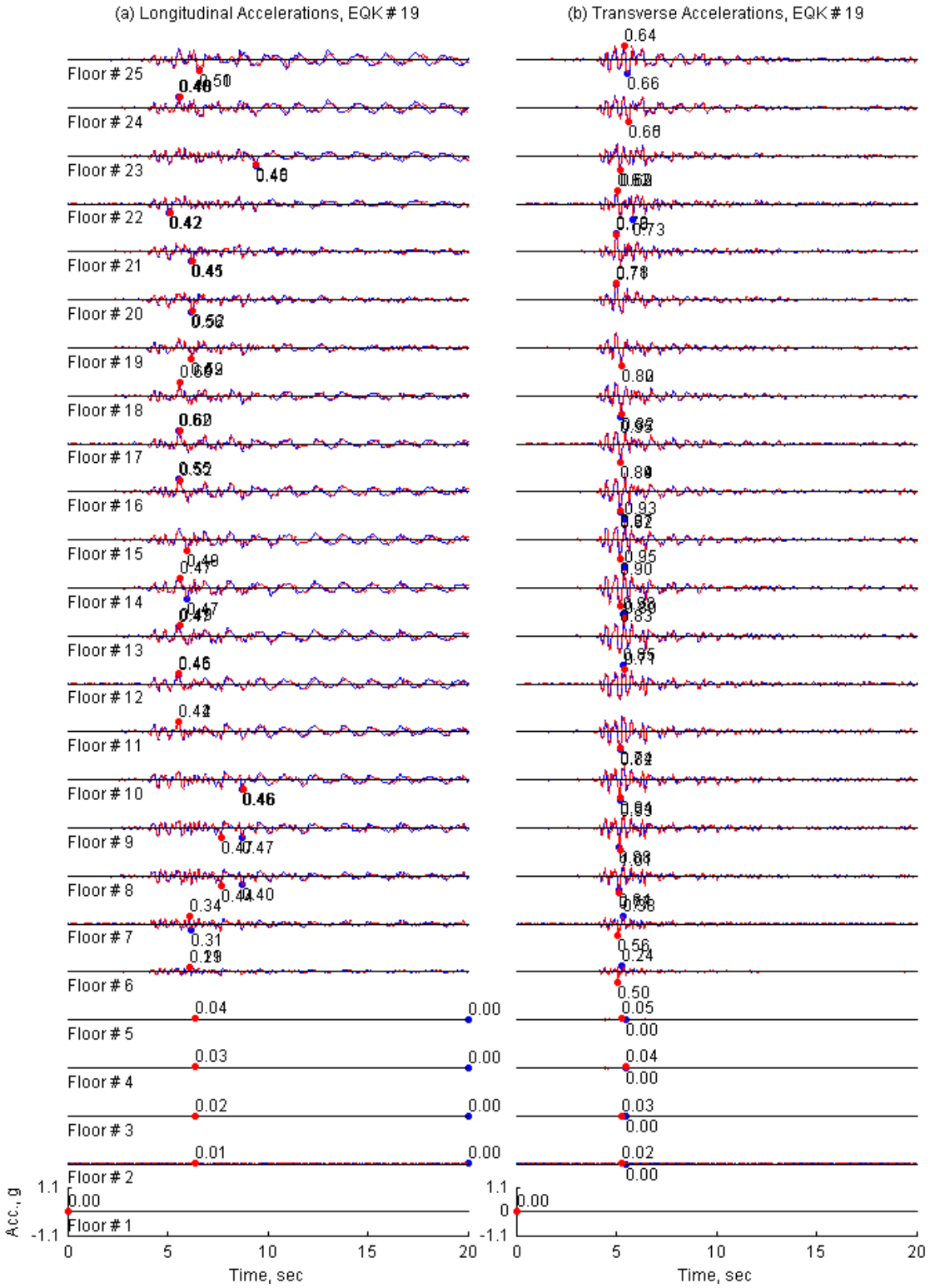

Figure II.119. Floor accelerations of 19-Story Office Building in Los Angeles from *OpenSees* (solid line) and *Perform3D* (dashed lines) for ground motion 19.

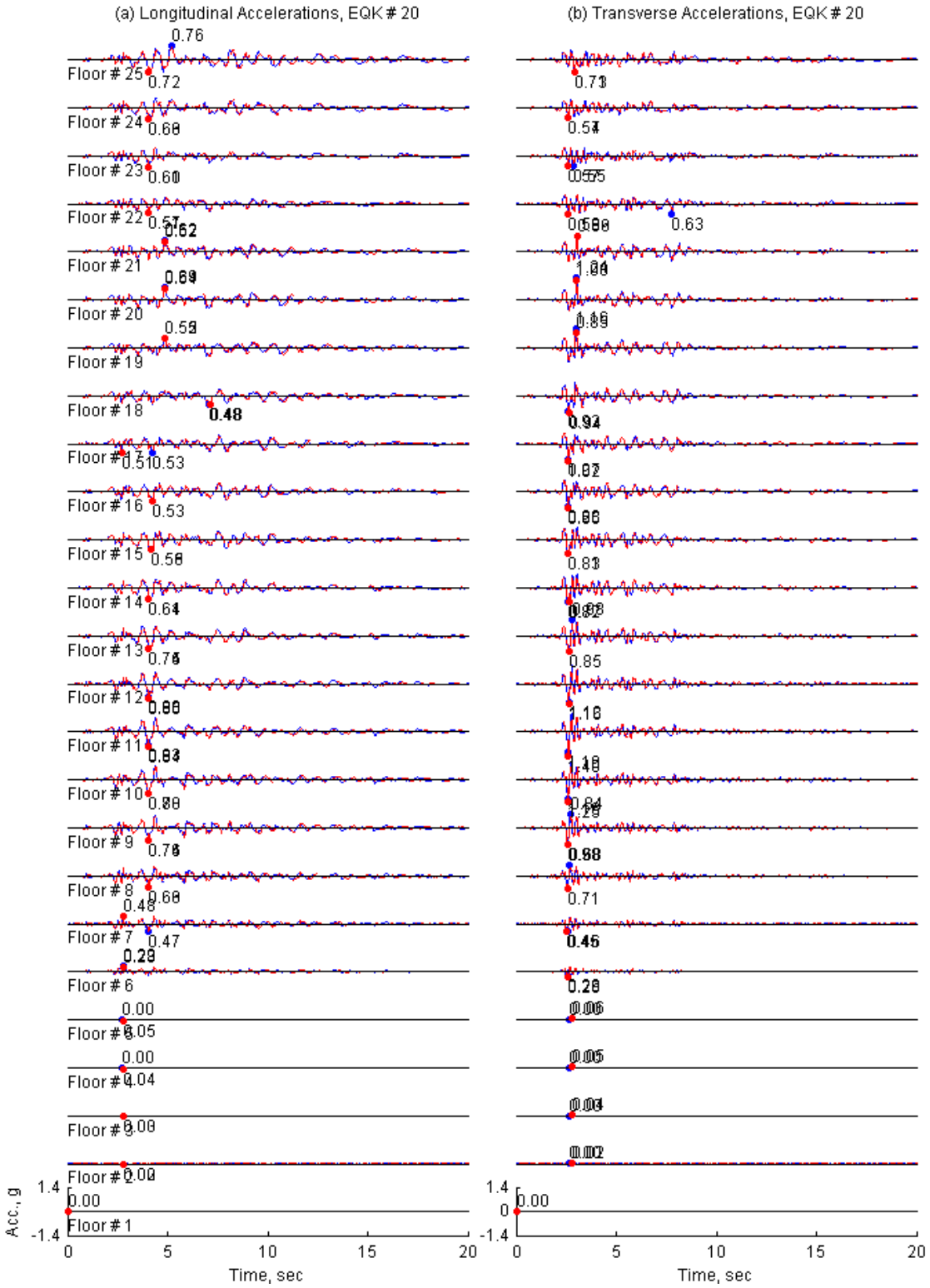

Figure II.120. Floor accelerations of 19-Story Office Building in Los Angeles from *OpenSees* (solid line) and *Perform3D* (dashed lines) for ground motion 20.

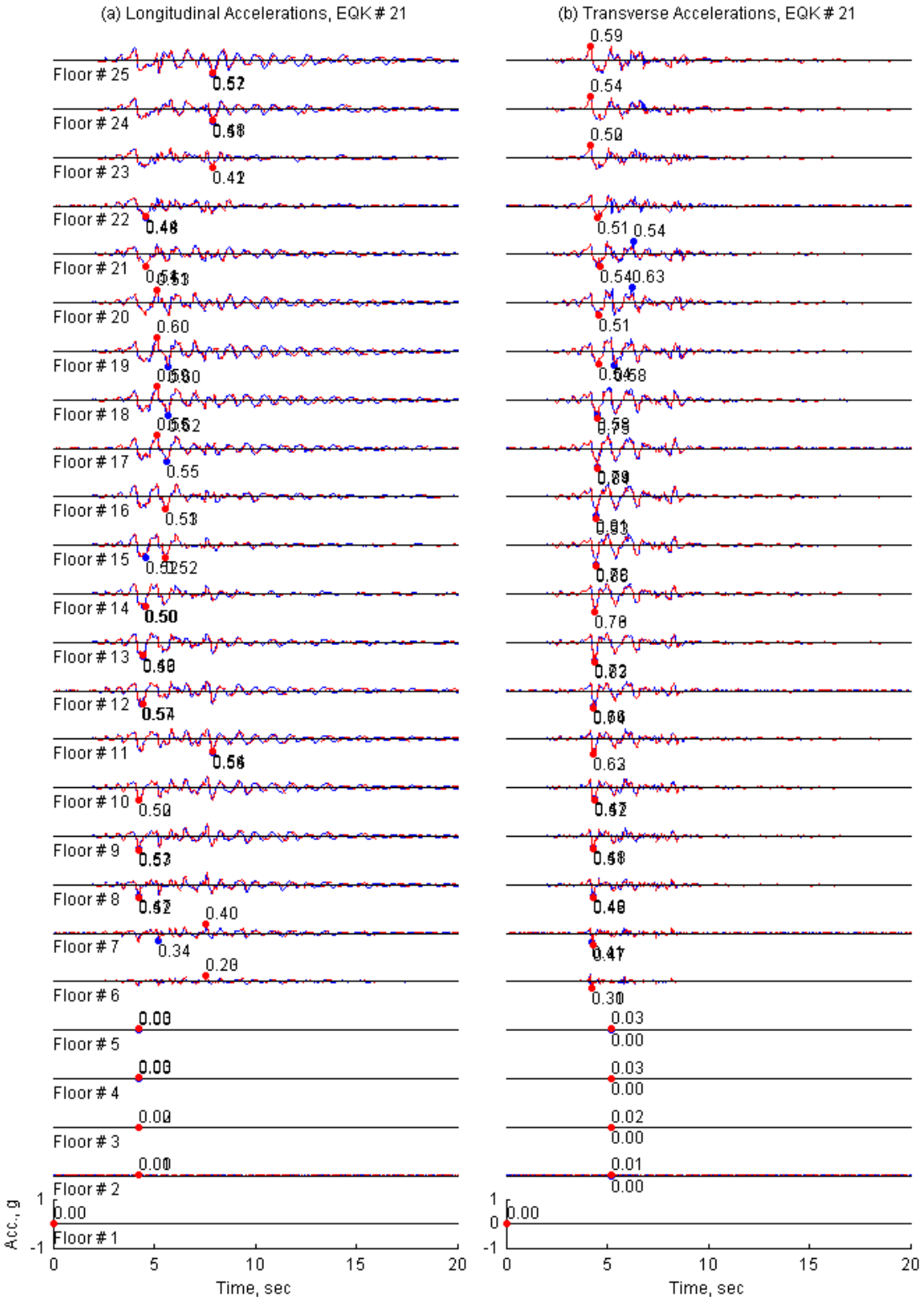

Figure II.121. Floor accelerations of 19-Story Office Building in Los Angeles from *OpenSees* (solid line) and *Perform3D* (dashed lines) for ground motion 21.

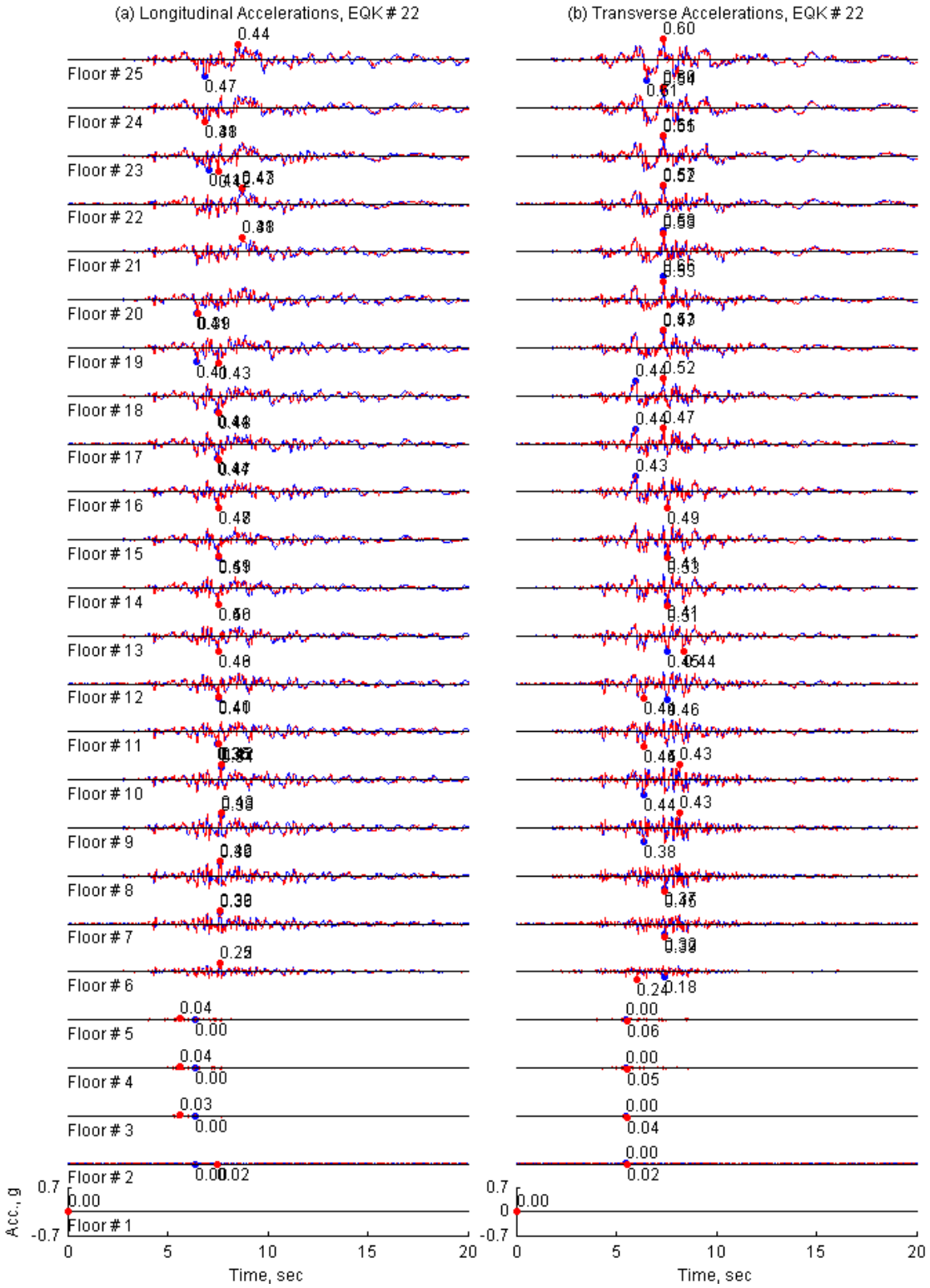

Figure II.122. Floor accelerations of 19-Story Office Building in Los Angeles from *OpenSees* (solid line) and *Perform3D* (dashed lines) for ground motion 22.

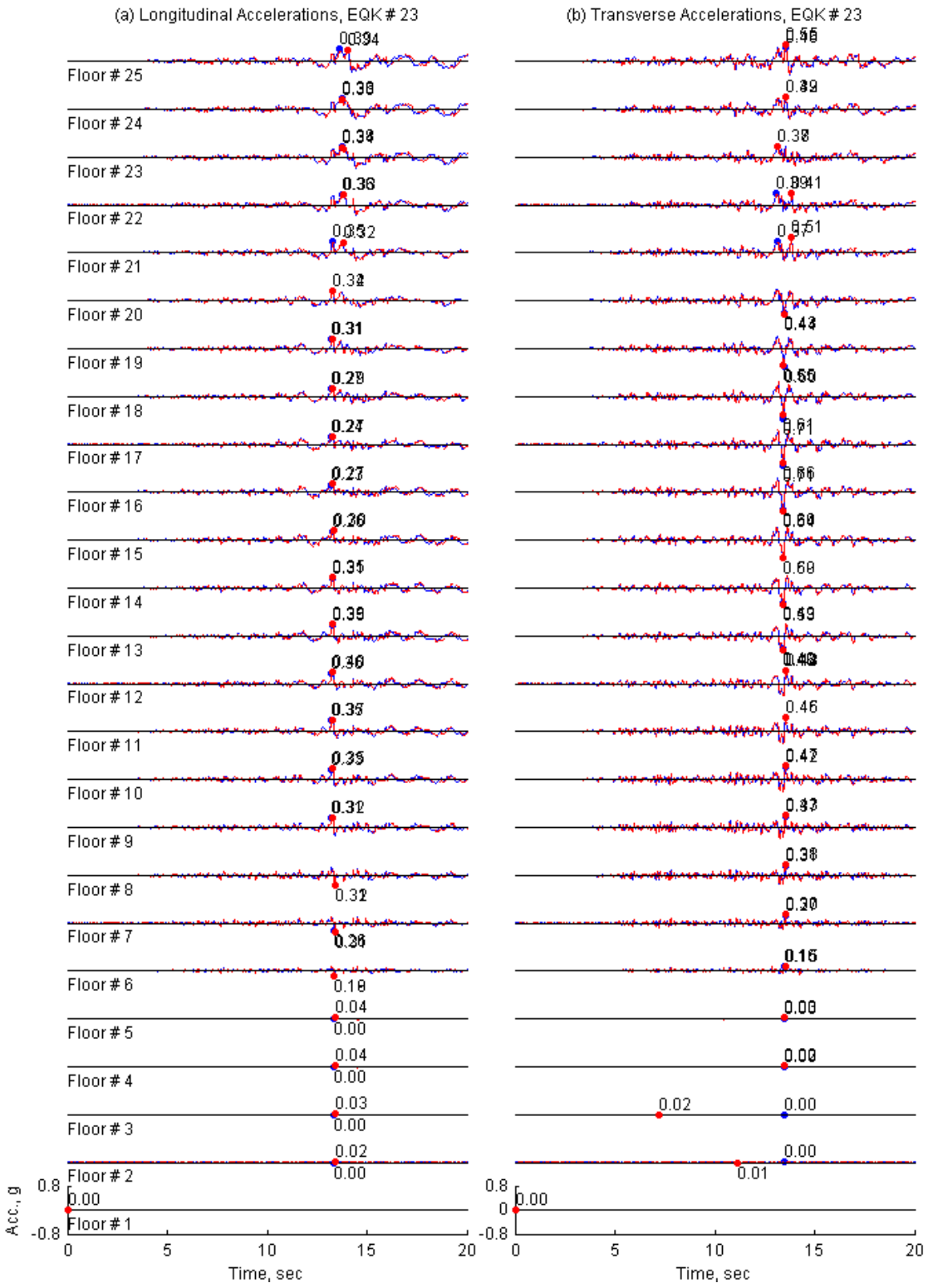

Figure II.123. Floor accelerations of 19-Story Office Building in Los Angeles from *OpenSees* (solid line) and *Perform3D* (dashed lines) for ground motion 23.

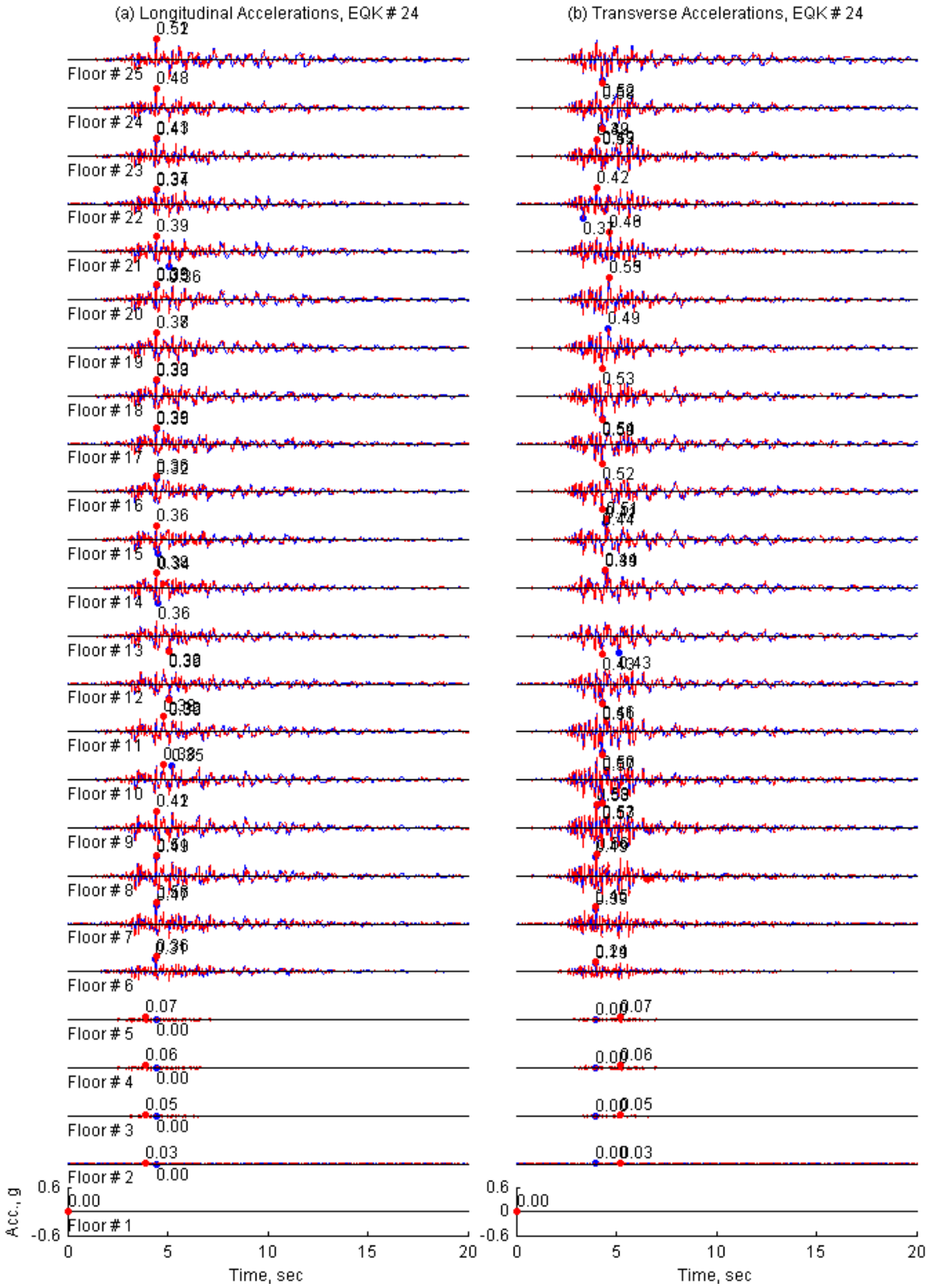

Figure II.124. Floor accelerations of 19-Story Office Building in Los Angeles from *OpenSees* (solid line) and *Perform3D* (dashed lines) for ground motion 24.

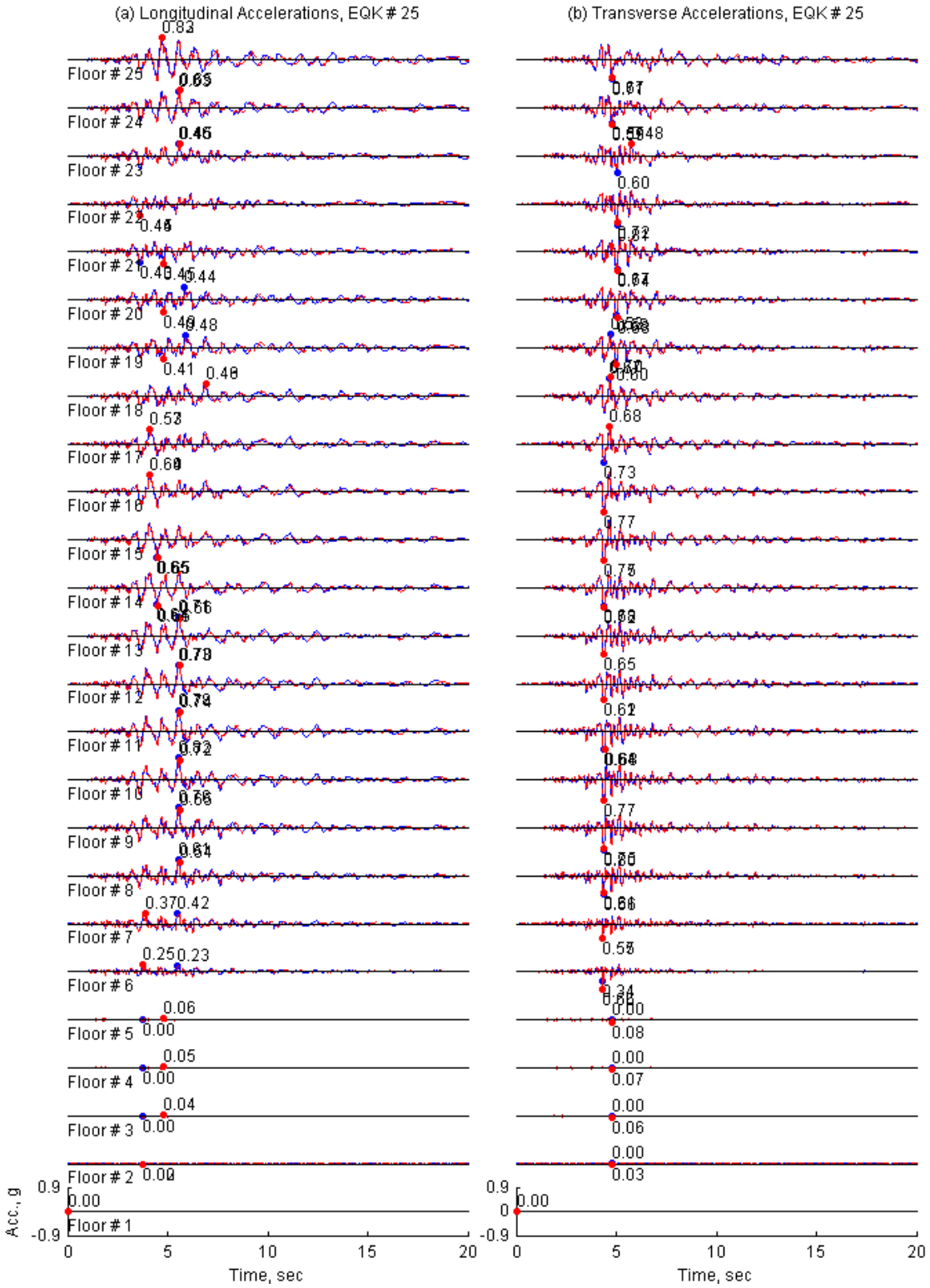

Figure II.125. Floor accelerations of 19-Story Office Building in Los Angeles from *OpenSees* (solid line) and *Perform3D* (dashed lines) for ground motion 25.

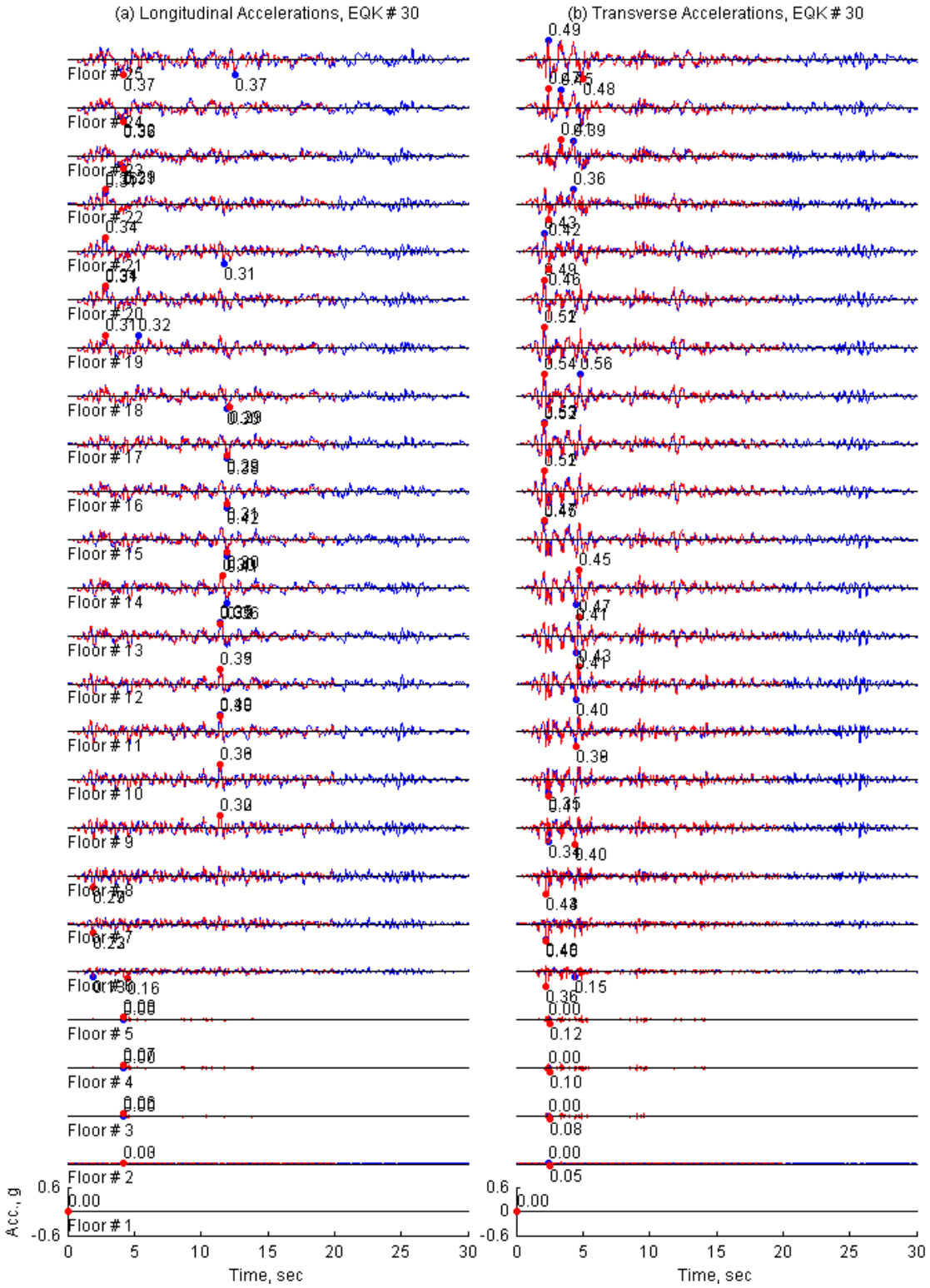

Figure II.126. Floor accelerations of 19-Story Office Building in Los Angeles from *OpenSees* (solid line) and *Perform3D* (dashed lines) for ground motion 30.

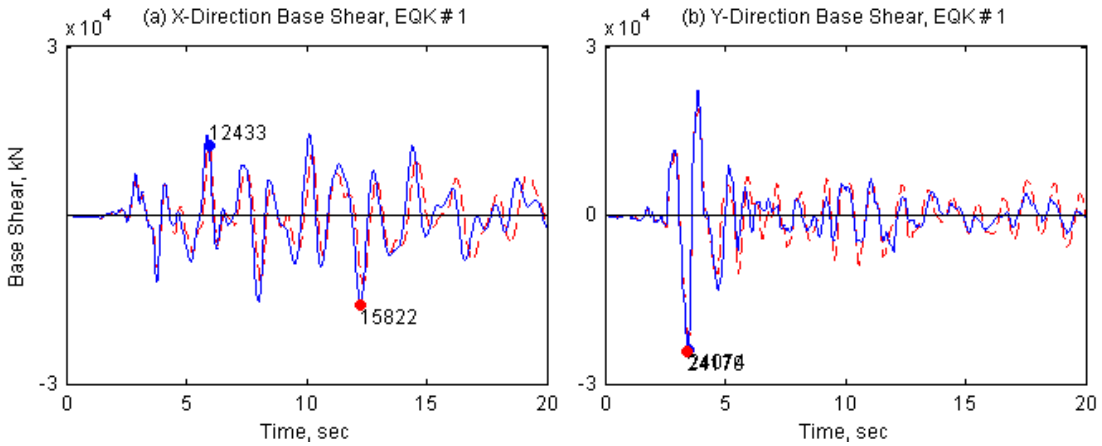

Figure II.127. Base shear of 19-Story Office Building in Los Angeles from *OpenSees* (solid line) and *Perform3D* (dashed lines) for ground motion 1.

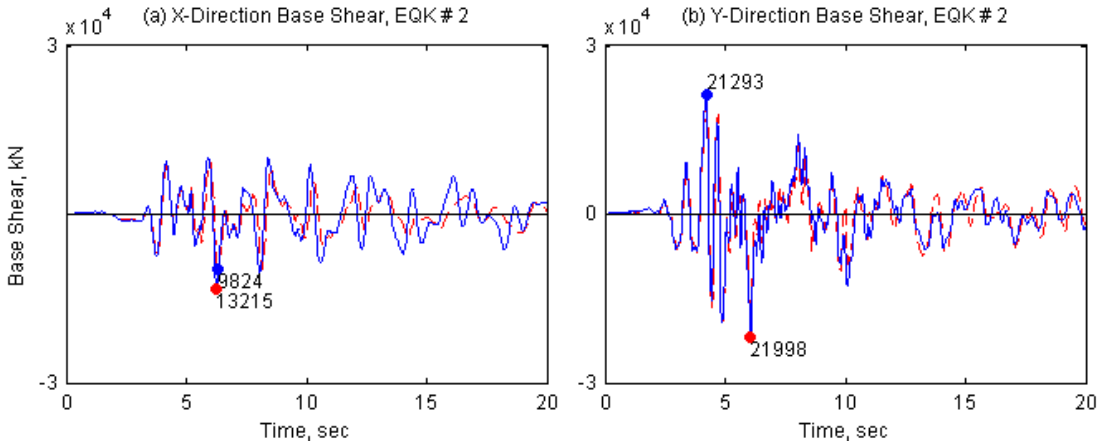

Figure II.128. Base shear of 19-Story Office Building in Los Angeles from *OpenSees* (solid line) and *Perform3D* (dashed lines) for ground motion 2.

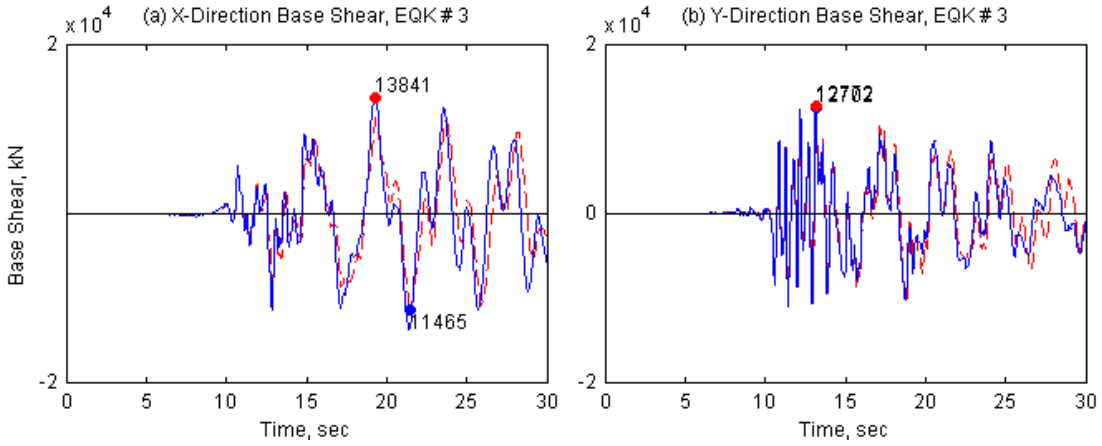

Figure II.129. Base shear of 19-Story Office Building in Los Angeles from *OpenSees* (solid line) and *Perform3D* (dashed lines) for ground motion 3.

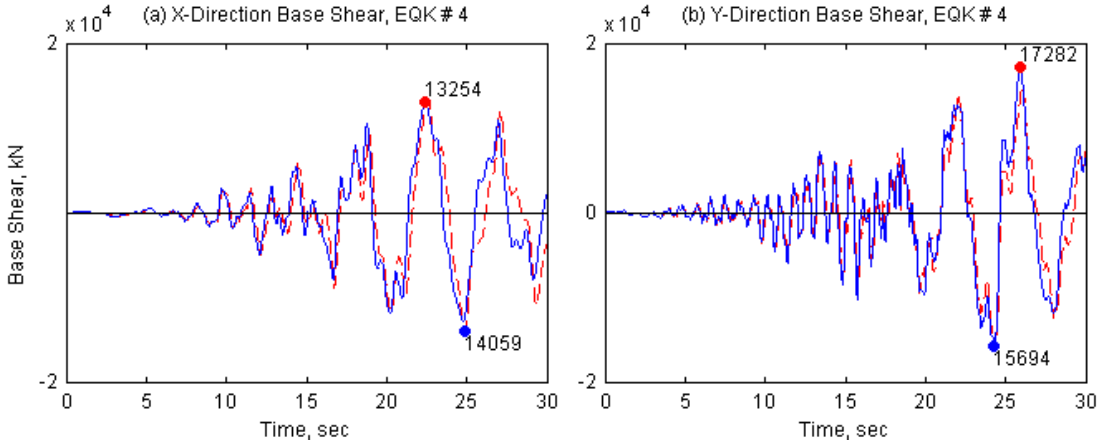

Figure II.130. Base shear of 19-Story Office Building in Los Angeles from *OpenSees* (solid line) and *Perform3D* (dashed lines) for ground motion 4.

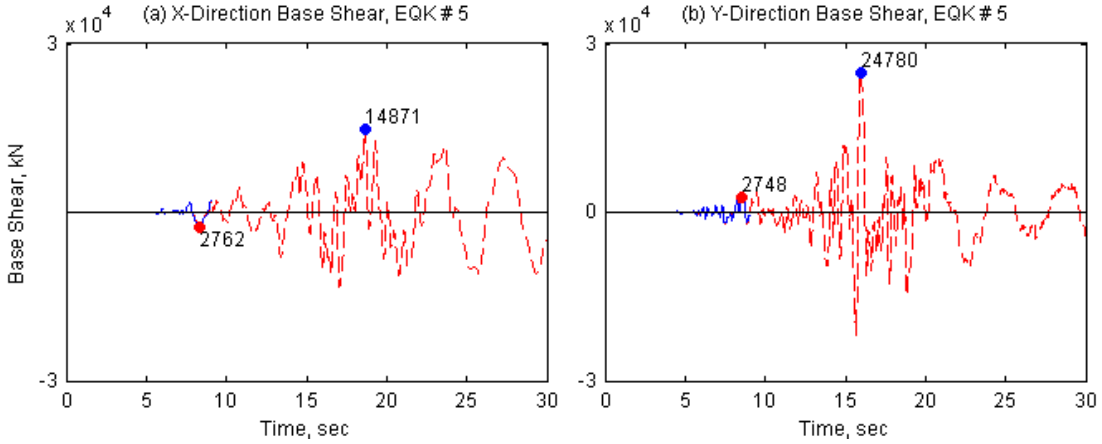

Figure II.131. Base shear of 19-Story Office Building in Los Angeles from *OpenSees* (solid line) and *Perform3D* (dashed lines) for ground motion 5.

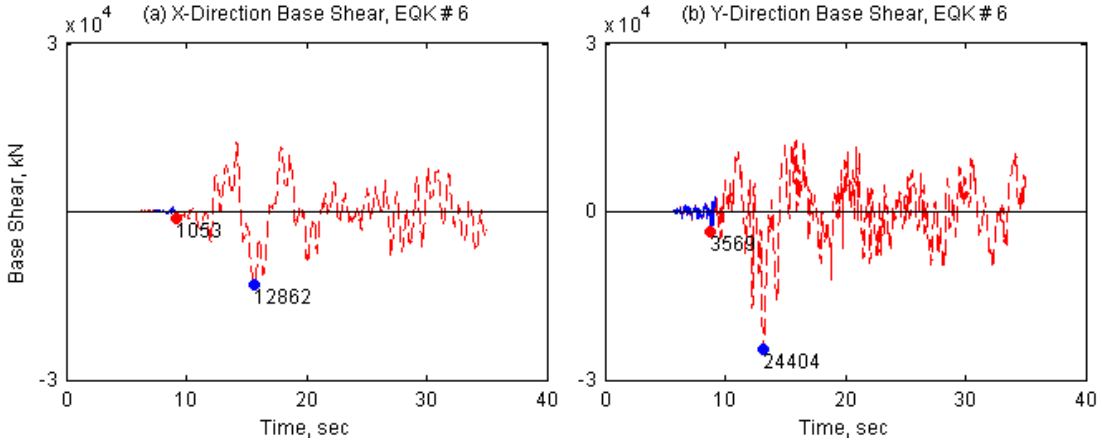

Figure II.132. Base shear of 19-Story Office Building in Los Angeles from *OpenSees* (solid line) and *Perform3D* (dashed lines) for ground motion 6.

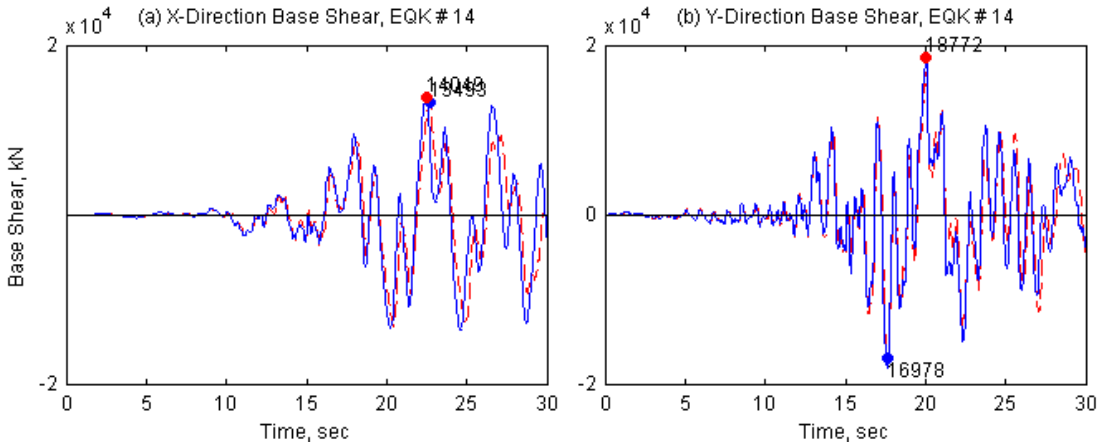

Figure II.134. Base shear of 19-Story Office Building in Los Angeles from *OpenSees* (solid line) and *Perform3D* (dashed lines) for ground motion 14.

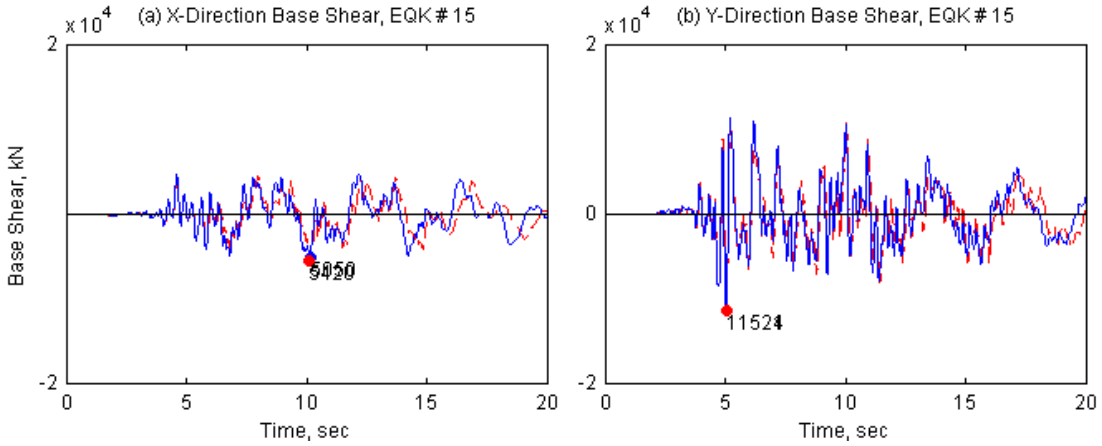

Figure II.135. Base shear of 19-Story Office Building in Los Angeles from *OpenSees* (solid line) and *Perform3D* (dashed lines) for ground motion 15.

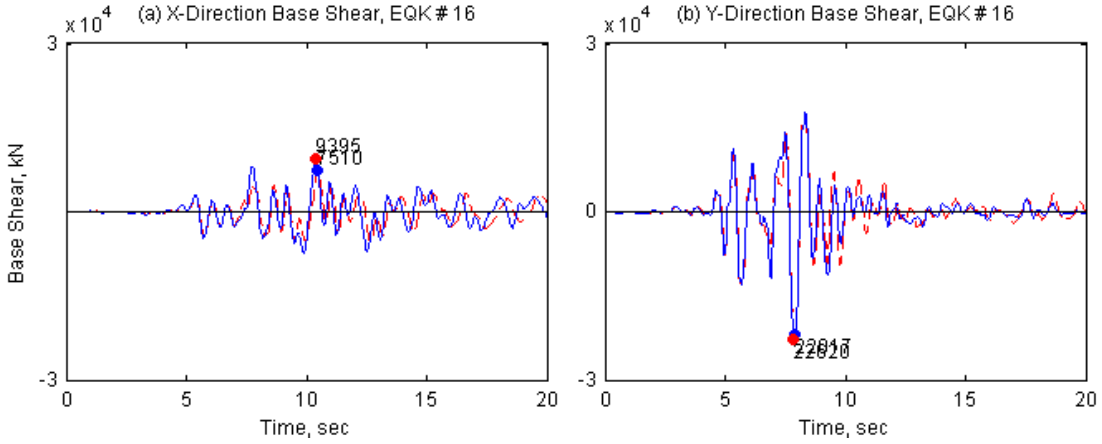

Figure II.136. Base shear of 19-Story Office Building in Los Angeles from *OpenSees* (solid line) and *Perform3D* (dashed lines) for ground motion16.

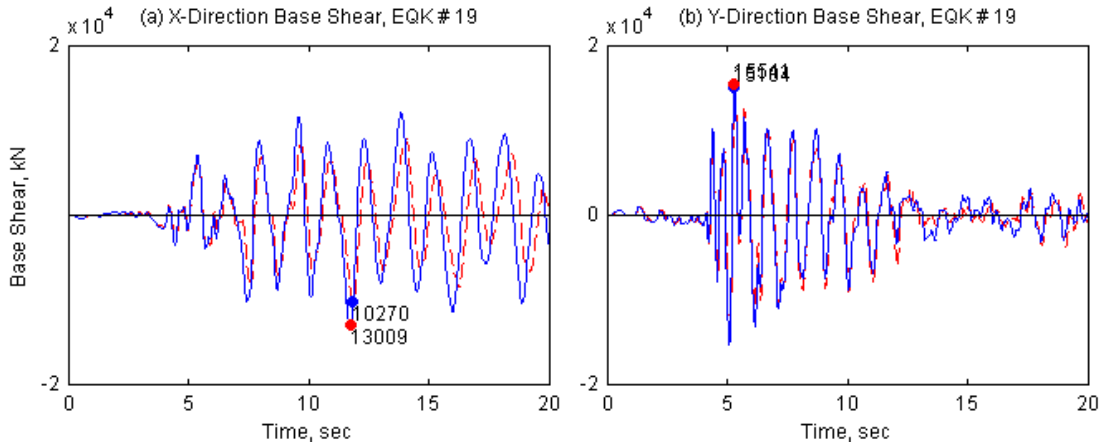

Figure II.137. Base shear of 19-Story Office Building in Los Angeles from *OpenSees* (solid line) and *Perform3D* (dashed lines) for ground motion 19.

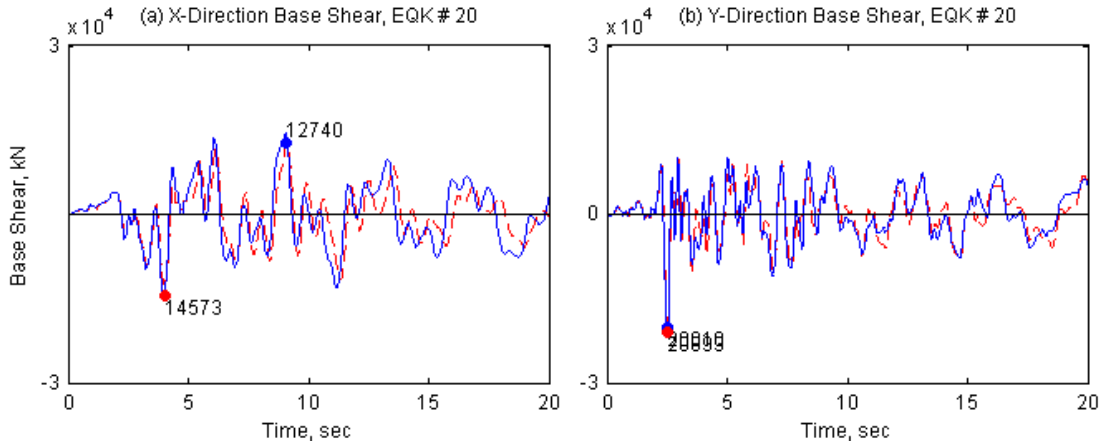

Figure II.138. Base shear of 19-Story Office Building in Los Angeles from *OpenSees* (solid line) and *Perform3D* (dashed lines) for ground motion20.

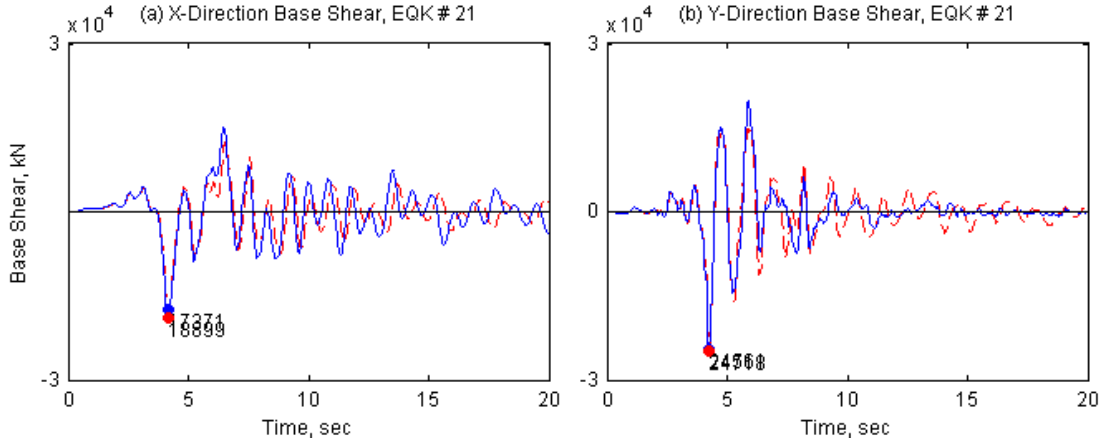

Figure II.139. Base shear of 19-Story Office Building in Los Angeles from *OpenSees* (solid line) and *Perform3D* (dashed lines) for ground motion21.

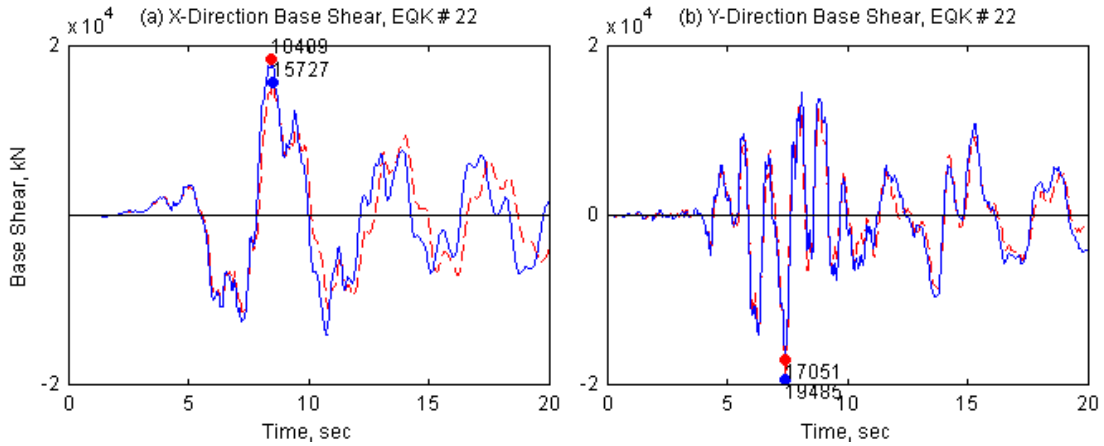

Figure II.140. Base shear of 19-Story Office Building in Los Angeles from *OpenSees* (solid line) and *Perform3D* (dashed lines) for ground motion 22.

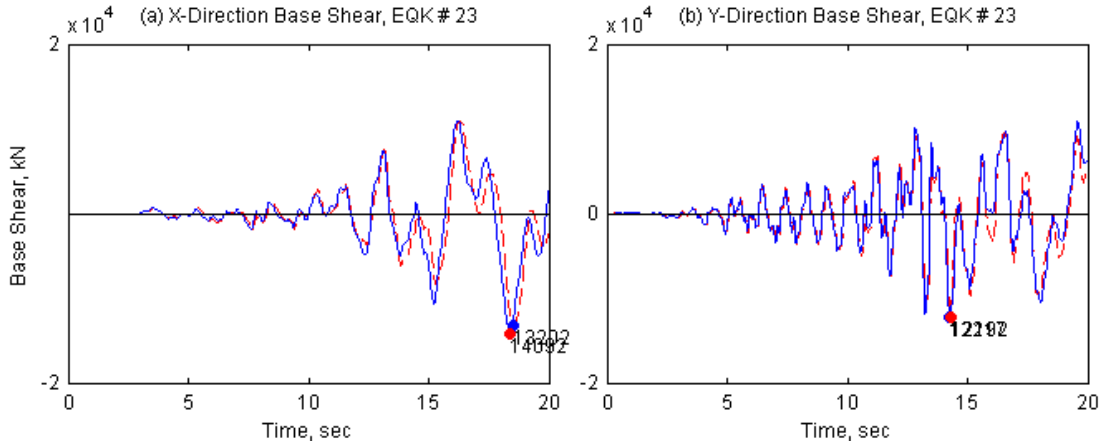

Figure II.141. Base shear of 19-Story Office Building in Los Angeles from *OpenSees* (solid line) and *Perform3D* (dashed lines) for ground motion 23.

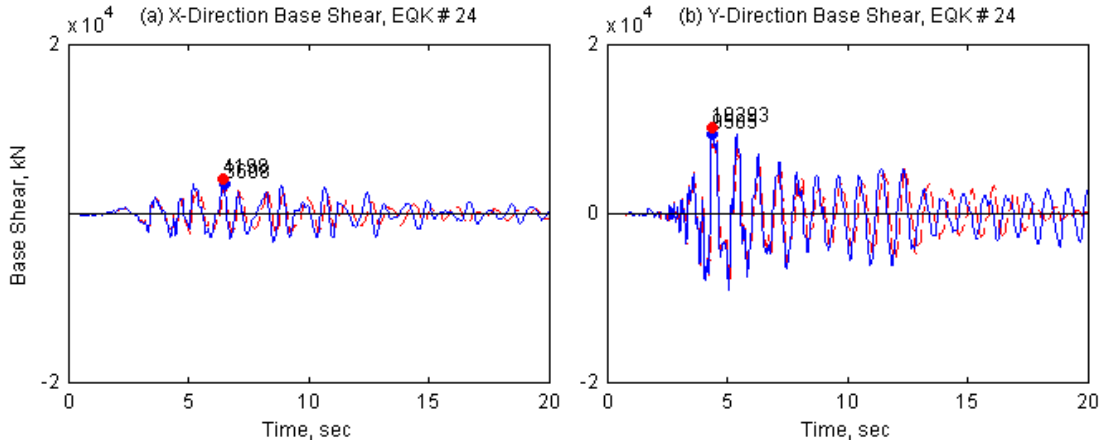

Figure II.142. Base shear of 19-Story Office Building in Los Angeles from *OpenSees* (solid line) and *Perform3D* (dashed lines) for ground motion 24.

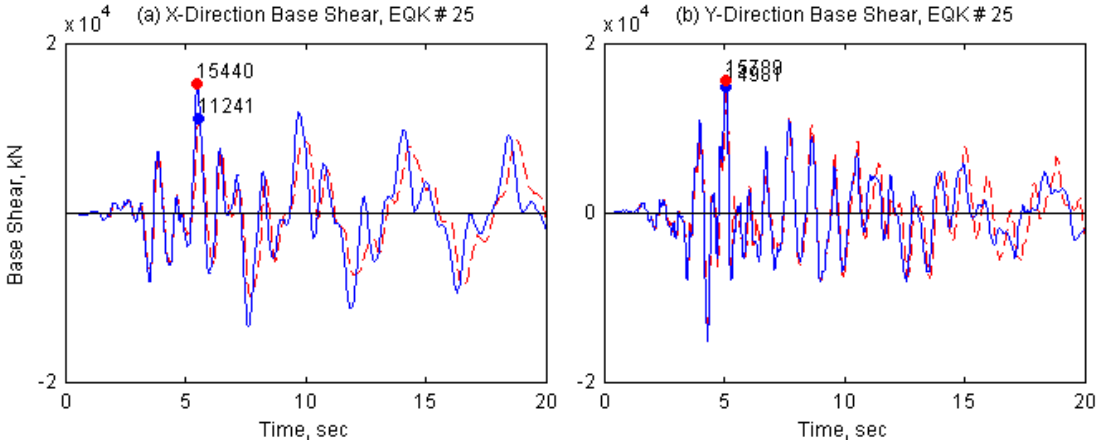

Figure II.143. Base shear of 19-Story Office Building in Los Angeles from *OpenSees* (solid line) and *Perform3D* (dashed lines) for ground motion 25.

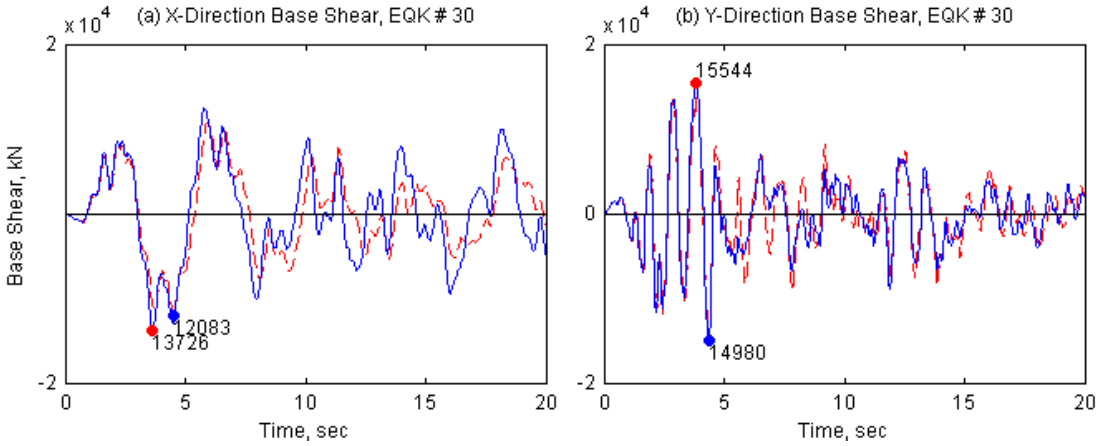

Figure II.144. Base shear of 19-Story Office Building in Los Angeles from *OpenSees* (solid line) and *Perform3D* (dashed lines) for ground motion 30.

APPENDIX III. HISTORIES OF TRUE AND ESTIMATED BASE SHEARS

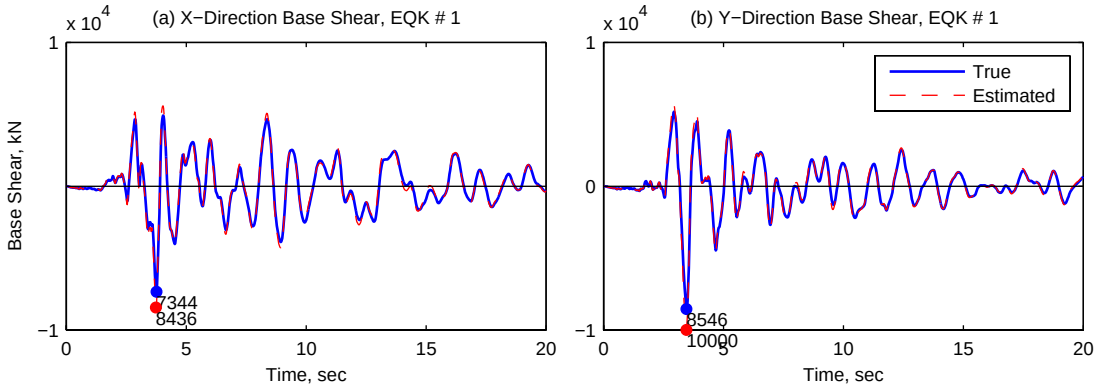

Figure III.1. True and estimated base shears of 20-Story North Hollywood Hotel from *OpenSees* for ground motion 1.

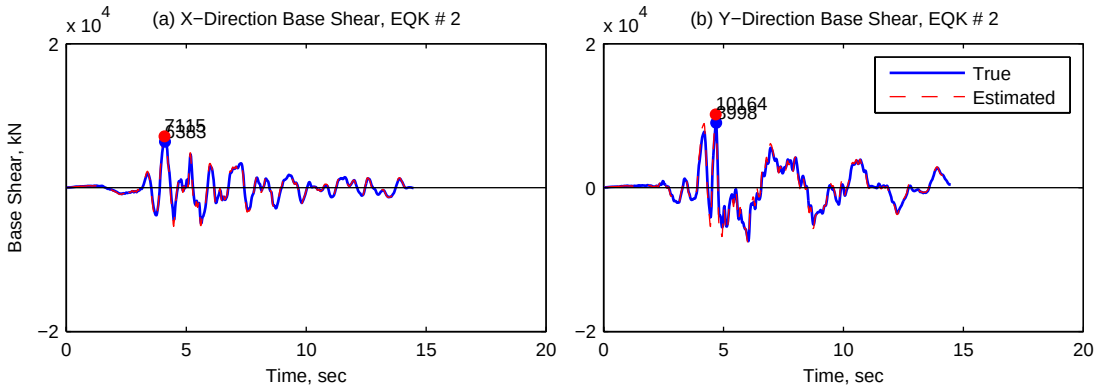

Figure III.2. True and estimated base shears of 20-Story North Hollywood Hotel from *OpenSees* for ground motion 2.

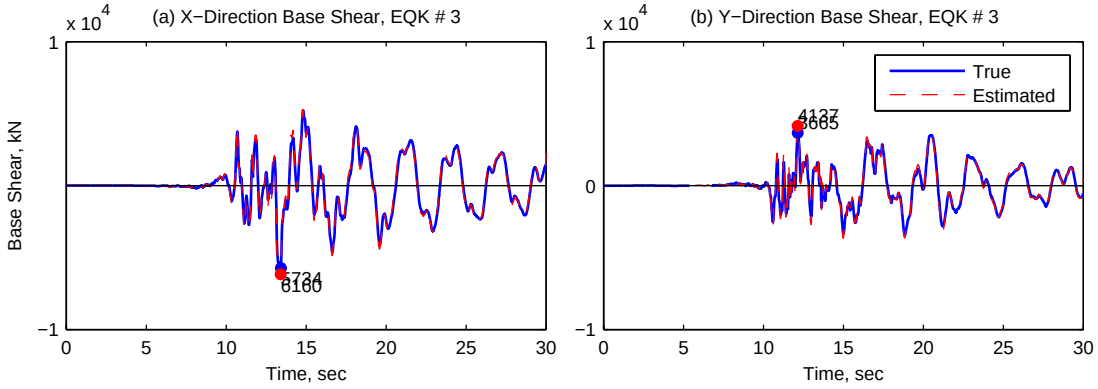

Figure III.3. True and estimated base shears of 20-Story North Hollywood Hotel from *OpenSees* for ground motion 3.

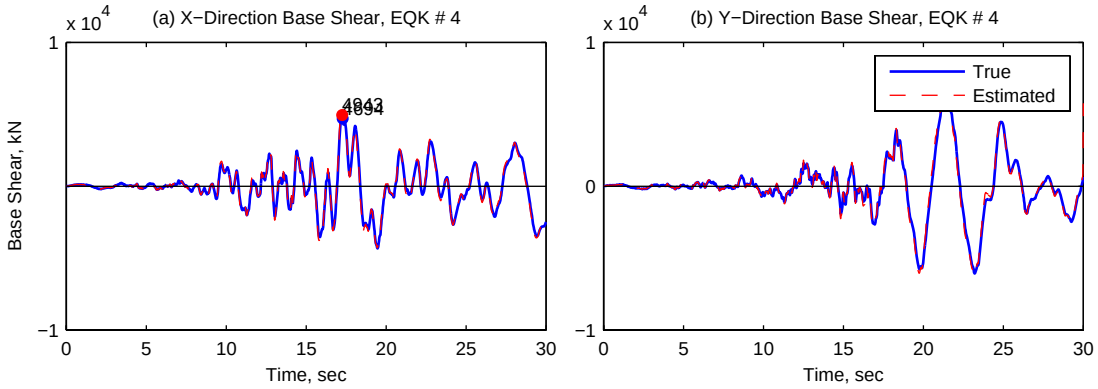

Figure III.4. True and estimated base shears of 20-Story North Hollywood Hotel from *OpenSees* for ground motion 4.

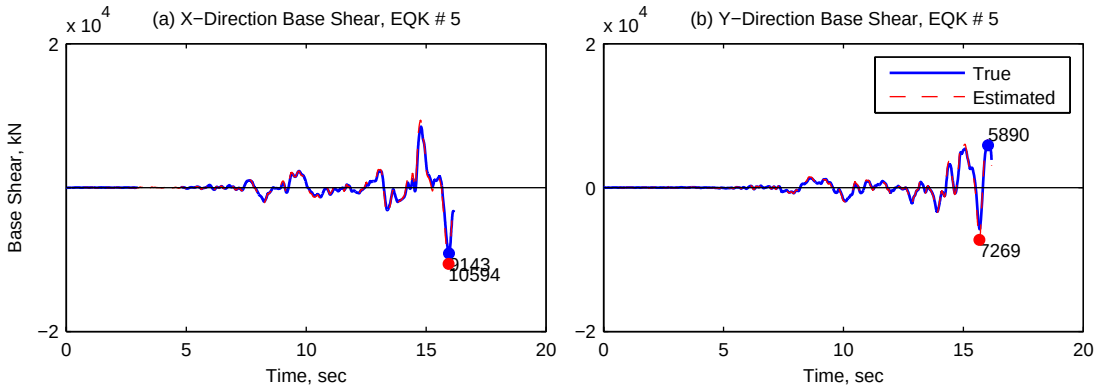

Figure III.5. True and estimated base shears of 20-Story North Hollywood Hotel from *OpenSees* for ground motion 5.

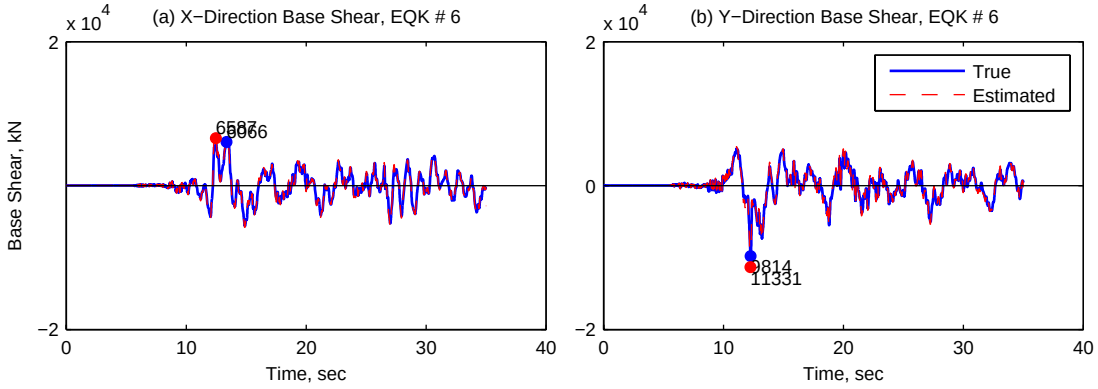

Figure III.6. True and estimated base shears of 20-Story North Hollywood Hotel from *OpenSees* for ground motion 6.

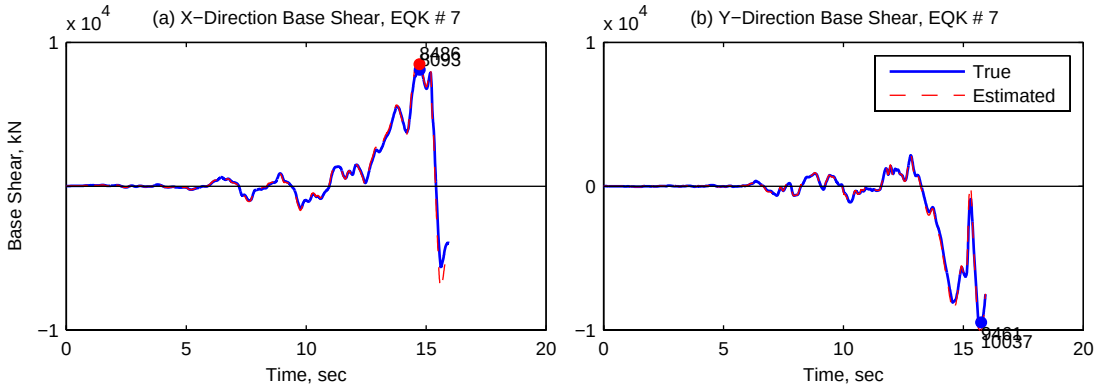

Figure III.7. True and estimated base shears of 20-Story North Hollywood Hotel from *OpenSees* for ground motion 7.

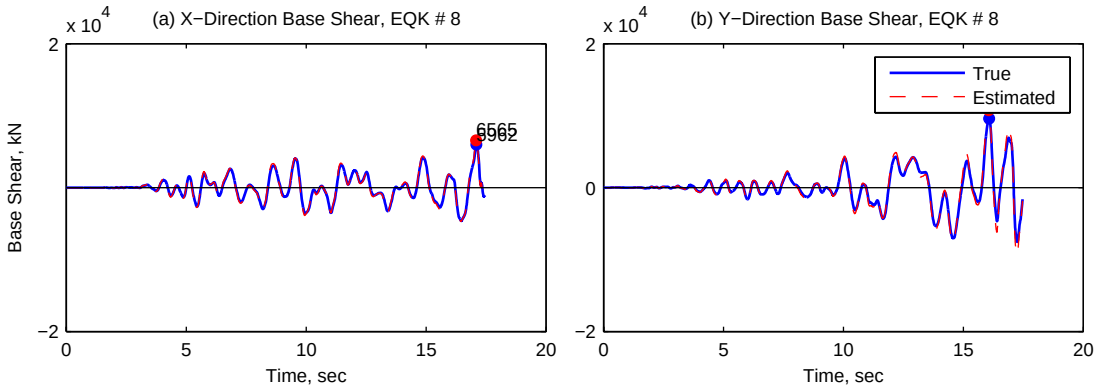

Figure III.8. True and estimated base shears of 20-Story North Hollywood Hotel from *OpenSees* for ground motion 8.

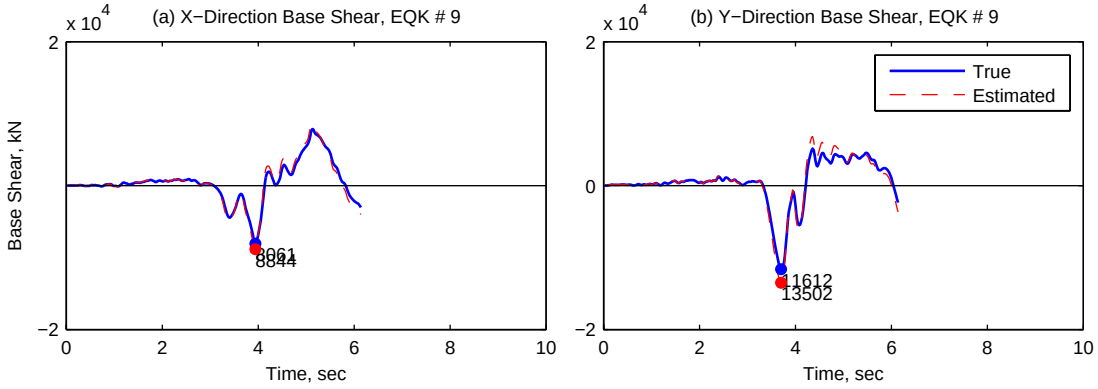

Figure III.9. True and estimated base shears of 20-Story North Hollywood Hotel from *OpenSees* for ground motion 9.

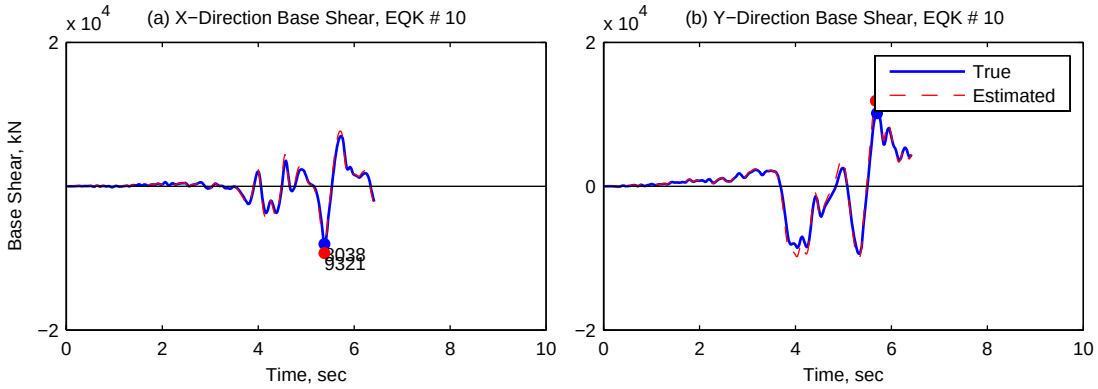

Figure III.10. True and estimated base shears of 20-Story North Hollywood Hotel from *OpenSees* for ground motion 10.

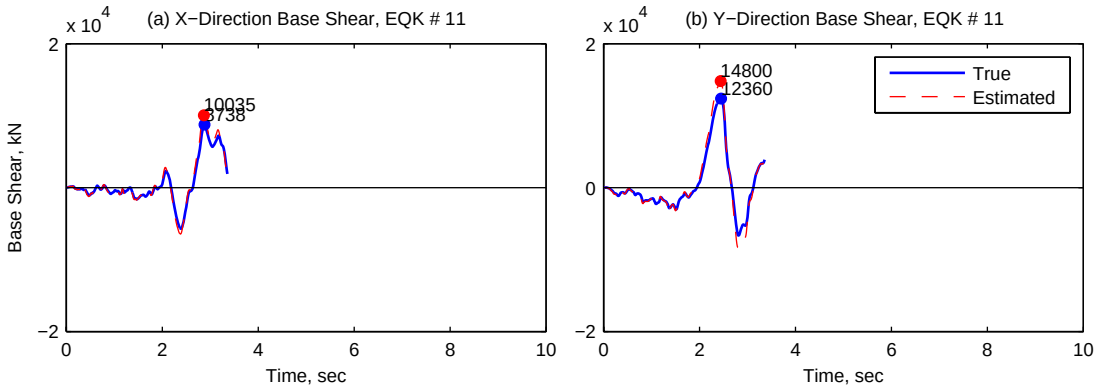

Figure III.11. True and estimated base shears of 20-Story North Hollywood Hotel from *OpenSees* for ground motion 11.

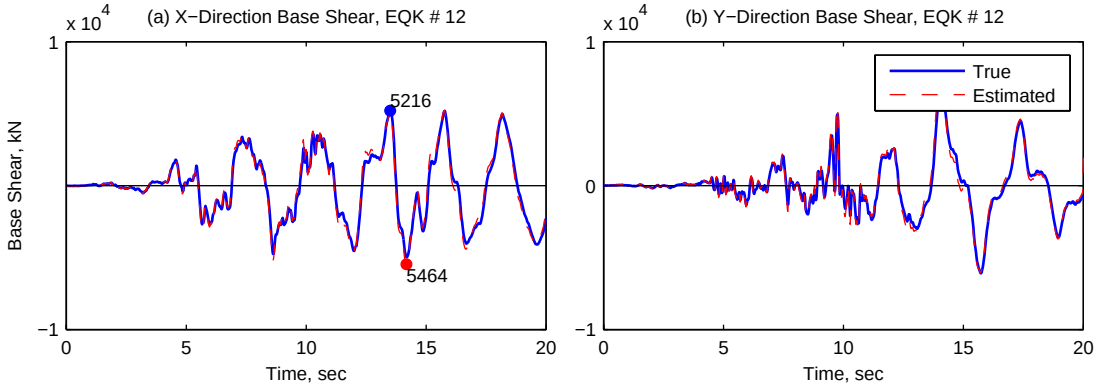

Figure III.12. True and estimated base shears of 20-Story North Hollywood Hotel from *OpenSees* for ground motion 12.

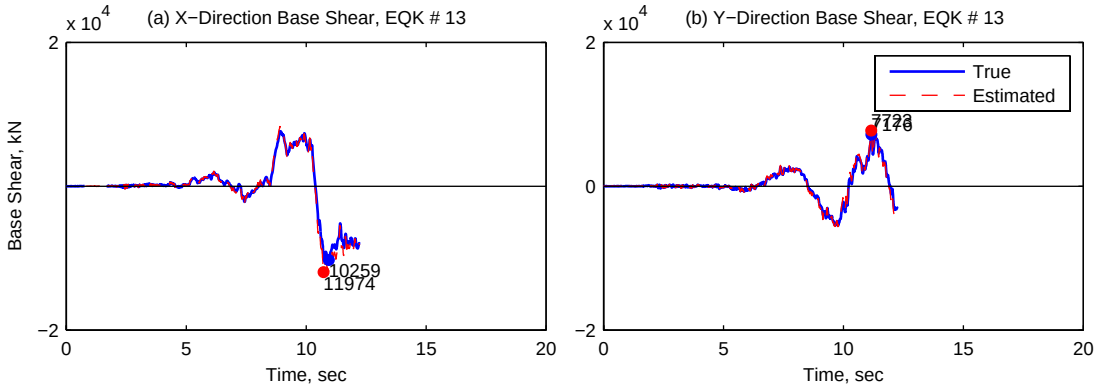

Figure III.13. True and estimated base shears of 20-Story North Hollywood Hotel from *OpenSees* for ground motion 13.

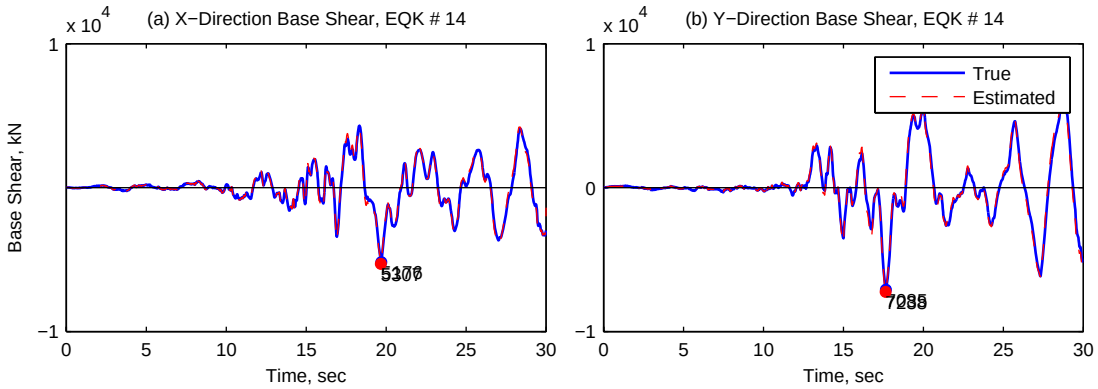

Figure III.14. True and estimated base shears of 20-Story North Hollywood Hotel from *OpenSees* for ground motion 14.

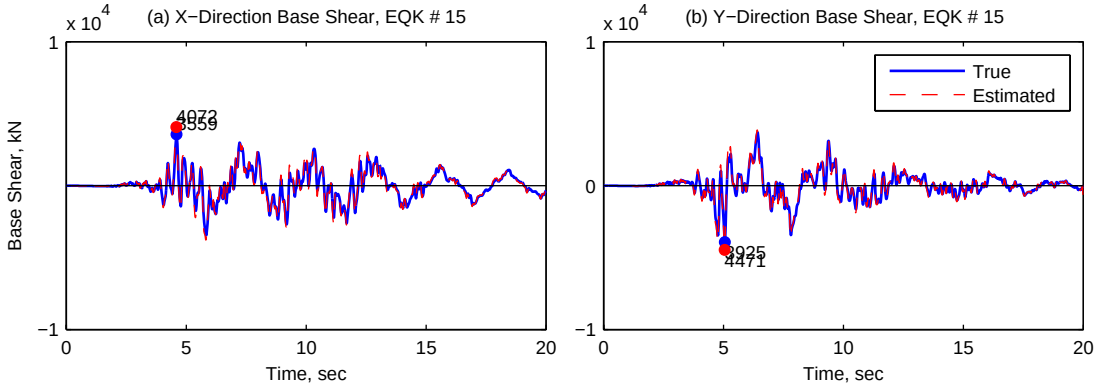

Figure III.15. True and estimated base shears of 20-Story North Hollywood Hotel from *OpenSees* for ground motion 15.

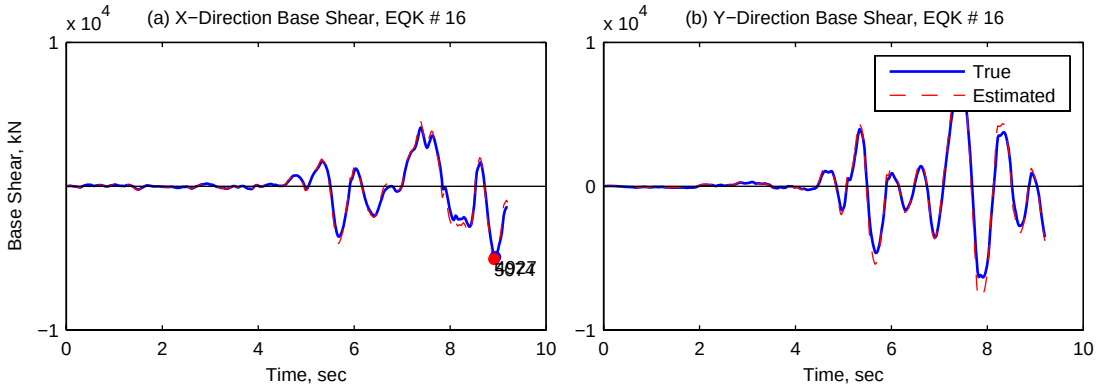

Figure III.16. True and estimated base shears of 20-Story North Hollywood Hotel from *OpenSees* for ground motion 16.

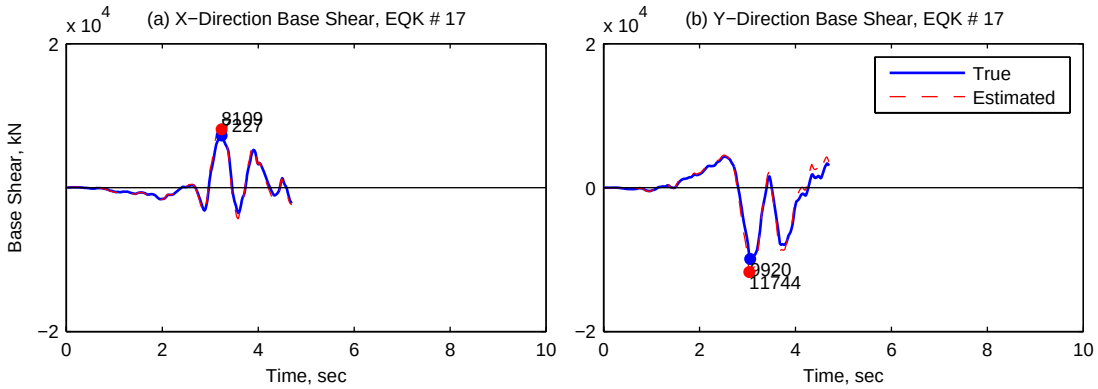

Figure III.17. True and estimated base shears of 20-Story North Hollywood Hotel from *OpenSees* for ground motion 17.

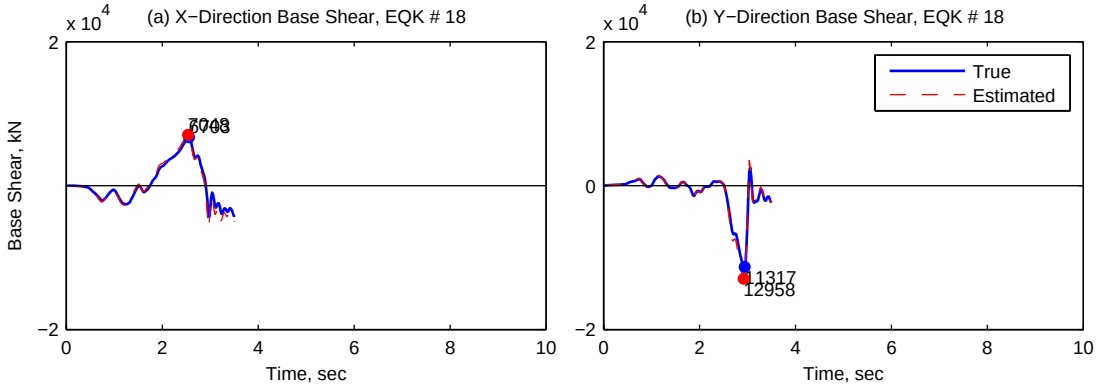

Figure III.18. True and estimated base shears of 20-Story North Hollywood Hotel from *OpenSees* for ground motion 18.

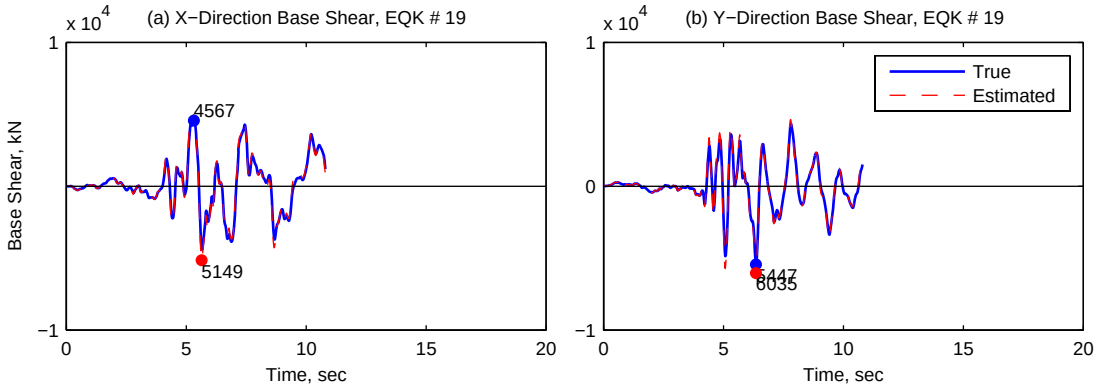

Figure III.19. True and estimated base shears of 20-Story North Hollywood Hotel from *OpenSees* for ground motion 19.

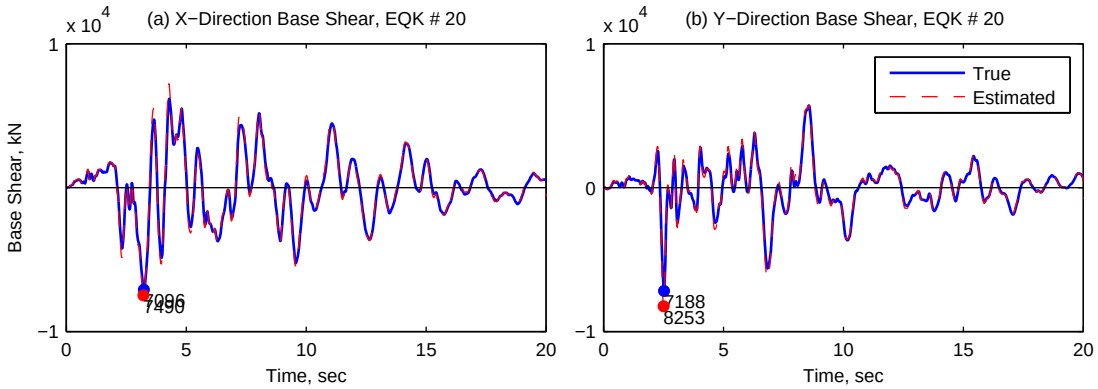

Figure III.20. True and estimated base shears of 20-Story North Hollywood Hotel from *OpenSees* for ground motion 20.

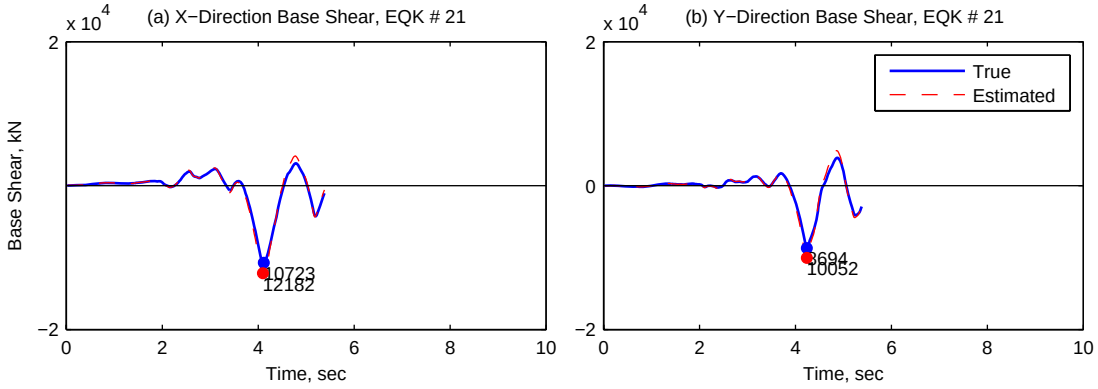

Figure III.21. True and estimated base shears of 20-Story North Hollywood Hotel from *OpenSees* for ground motion 21.

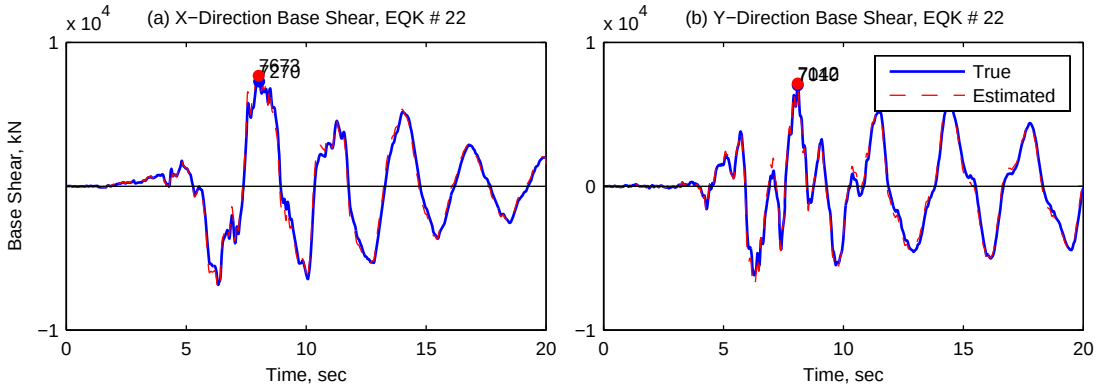

Figure III.22. True and estimated base shears of 20-Story North Hollywood Hotel from *OpenSees* for ground motion 22.

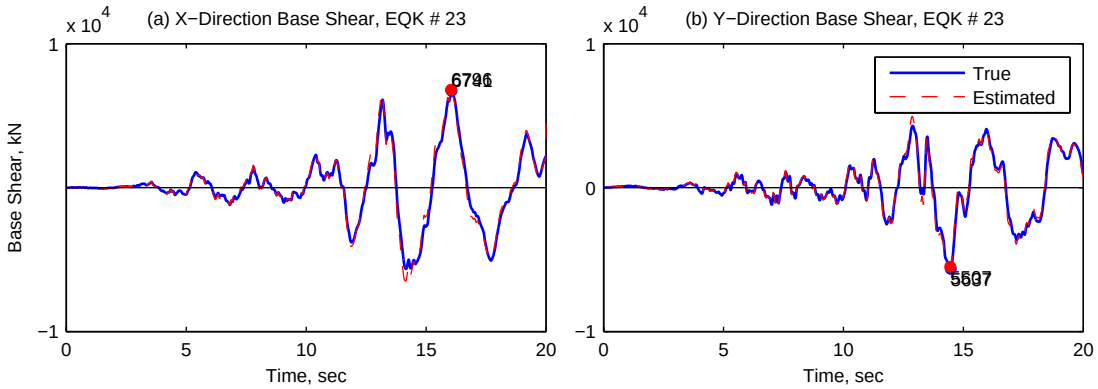

Figure III.23. True and estimated base shears of 20-Story North Hollywood Hotel from *OpenSees* for ground motion 23.

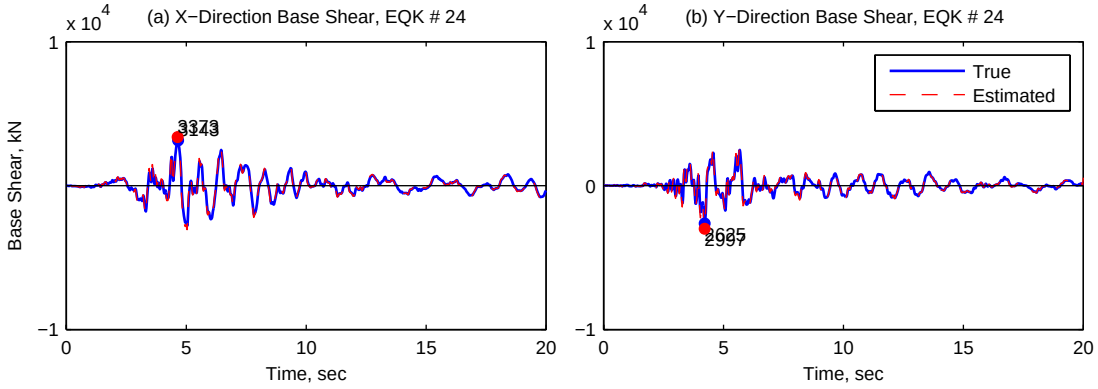

Figure III.24. True and estimated base shears of 20-Story North Hollywood Hotel from *OpenSees* for ground motion 24.

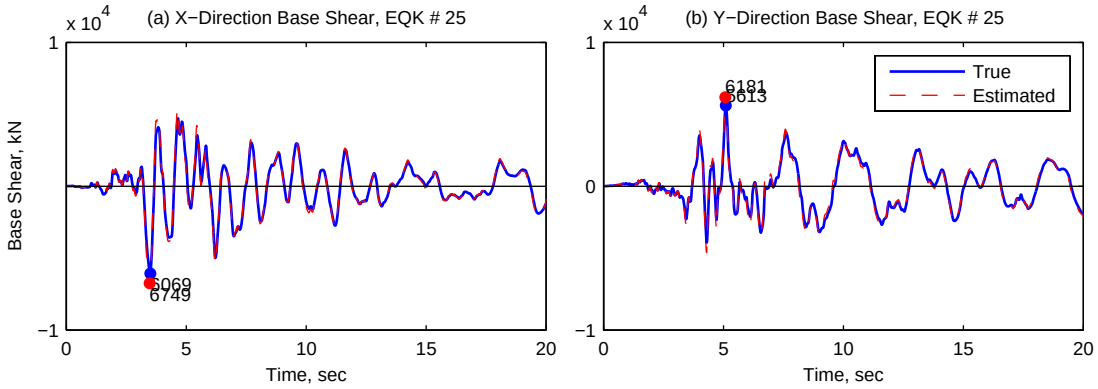

Figure III.25. True and estimated base shears of 20-Story North Hollywood Hotel from *OpenSees* for ground motion 25.

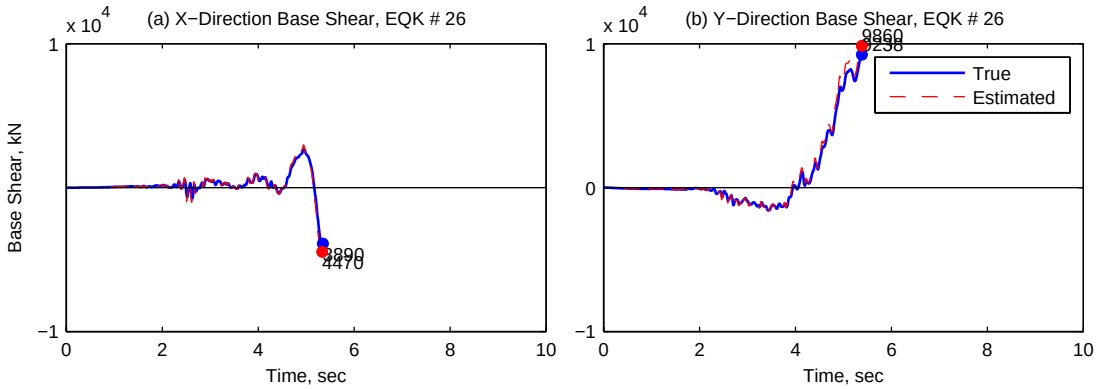

Figure III.26. True and estimated base shears of 20-Story North Hollywood Hotel from *OpenSees* for ground motion 26.

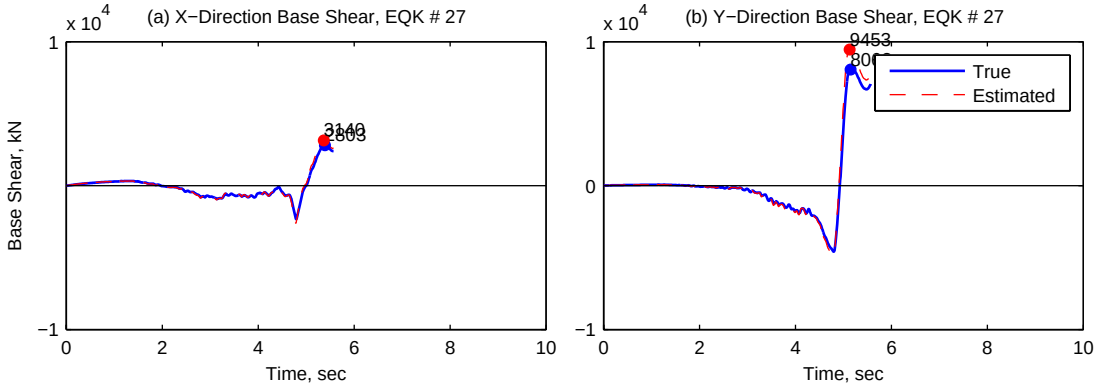

Figure III.27. True and estimated base shears of 20-Story North Hollywood Hotel from *OpenSees* for ground motion 27.

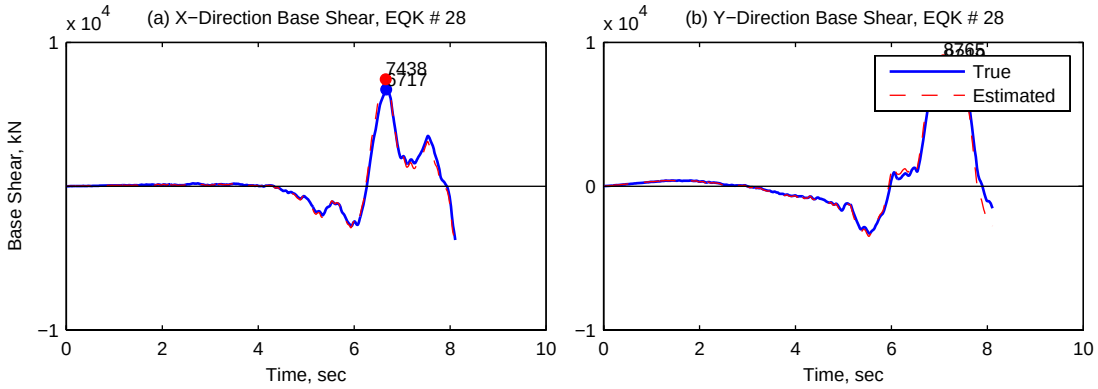

Figure III.28. True and estimated base shears of 20-Story North Hollywood Hotel from *OpenSees* for ground motion 28.

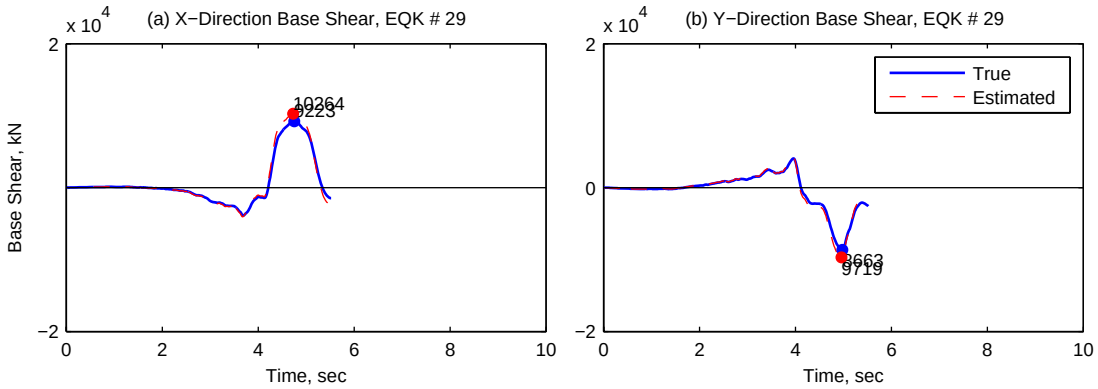

Figure III.29. True and estimated base shears of 20-Story North Hollywood Hotel from *OpenSees* for ground motion 29.

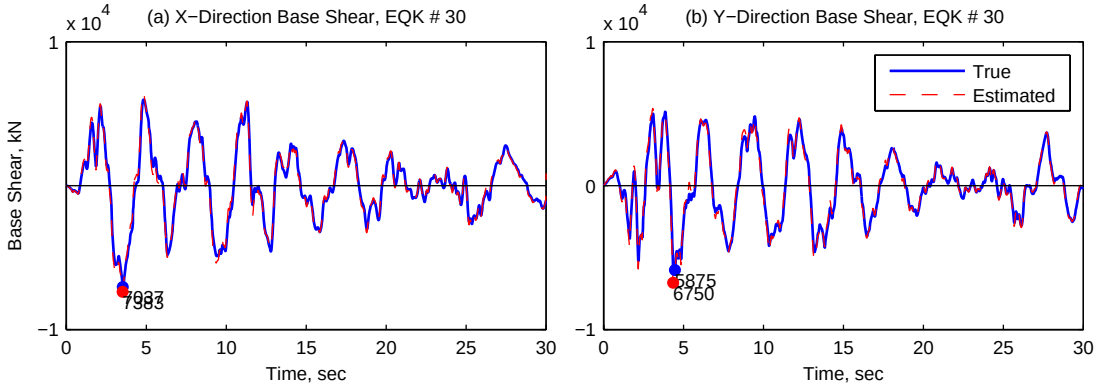

Figure III.30. True and estimated base shears of 20-Story North Hollywood Hotel from *OpenSees* for ground motion 30.

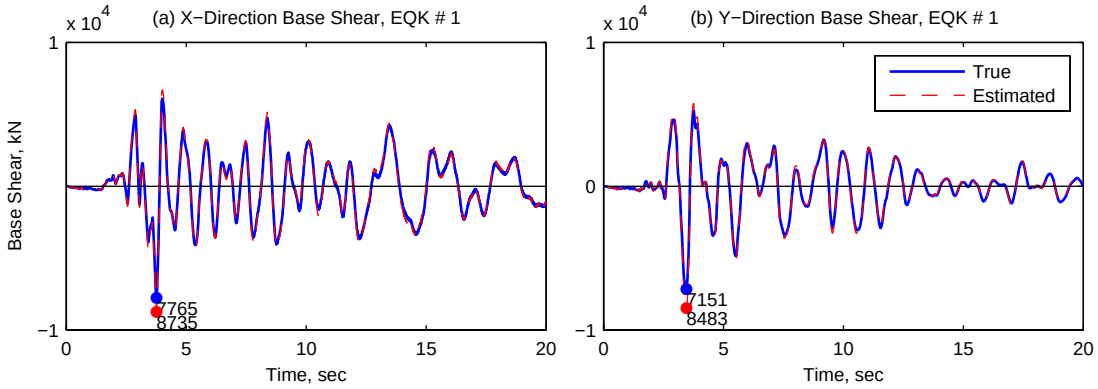

Figure III.31. True and estimated base shears of 20-Story North Hollywood Hotel from *Perform3D* for ground motion 1.

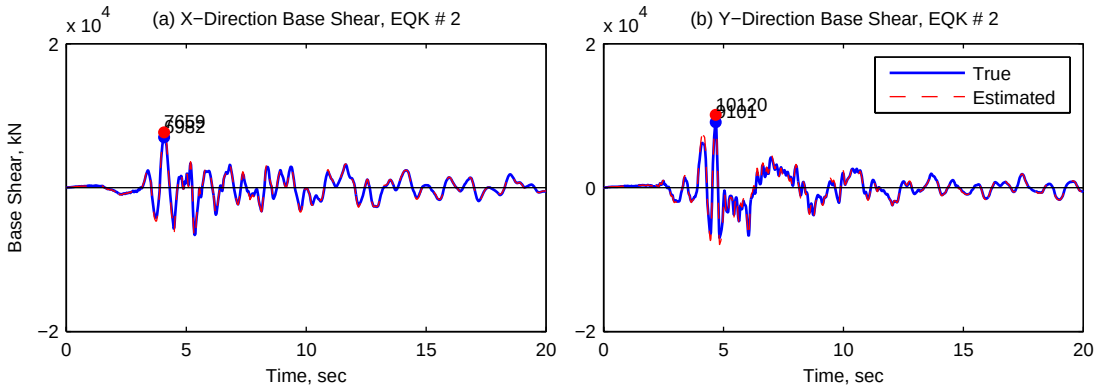

Figure III.32. True and estimated base shears of 20-Story North Hollywood Hotel from *Perform3D* for ground motion 2.

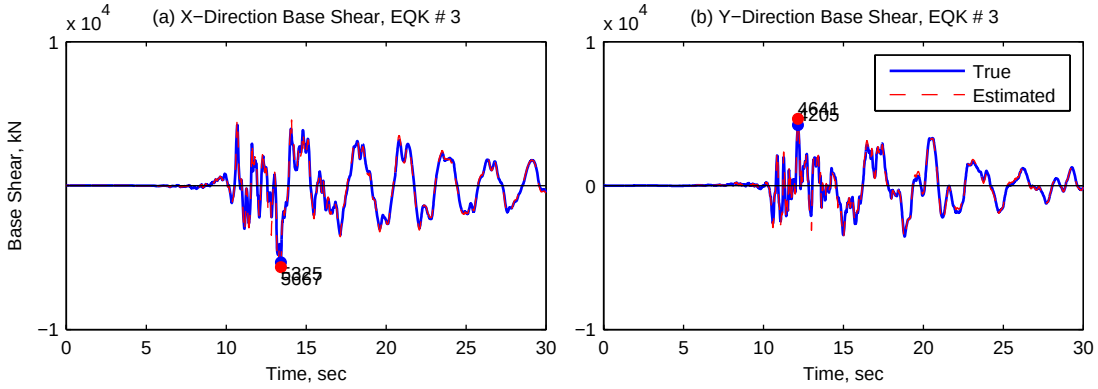

Figure III.33. True and estimated base shears of 20-Story North Hollywood Hotel from *Perform3D* for ground motion 3.

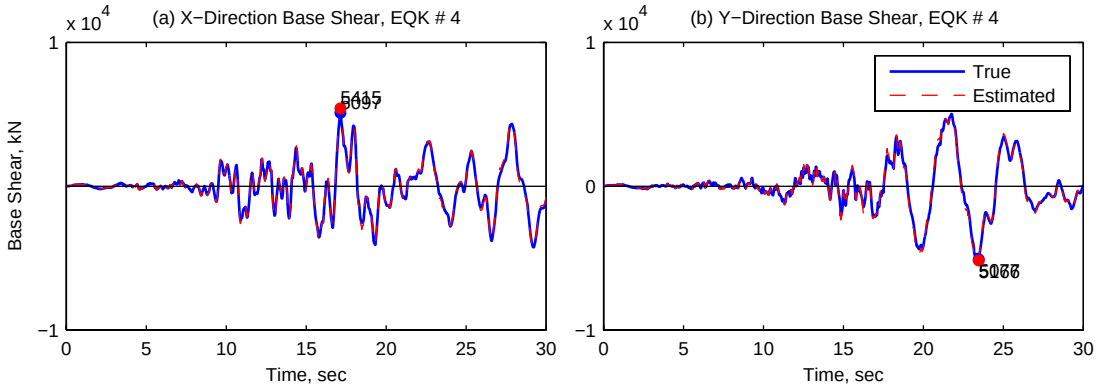

Figure III.34. True and estimated base shears of 20-Story North Hollywood Hotel from *Perform3D* for ground motion 4.

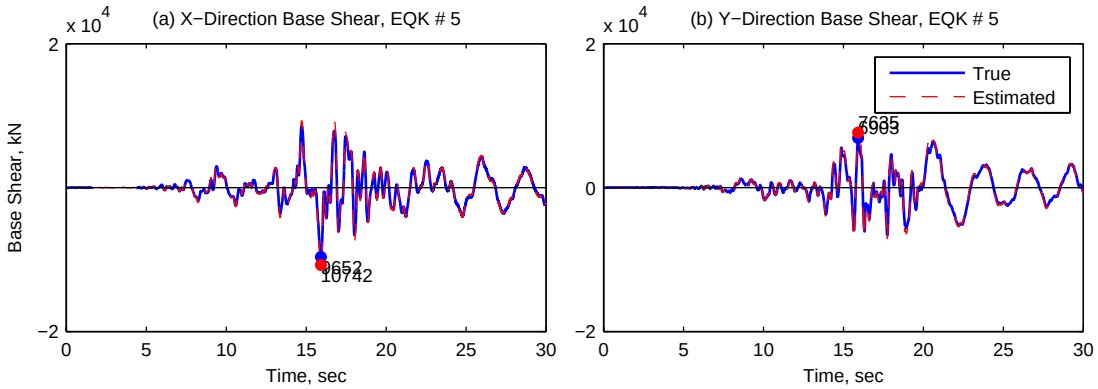

Figure III.35. True and estimated base shears of 20-Story North Hollywood Hotel from *Perform3D* for ground motion 5.

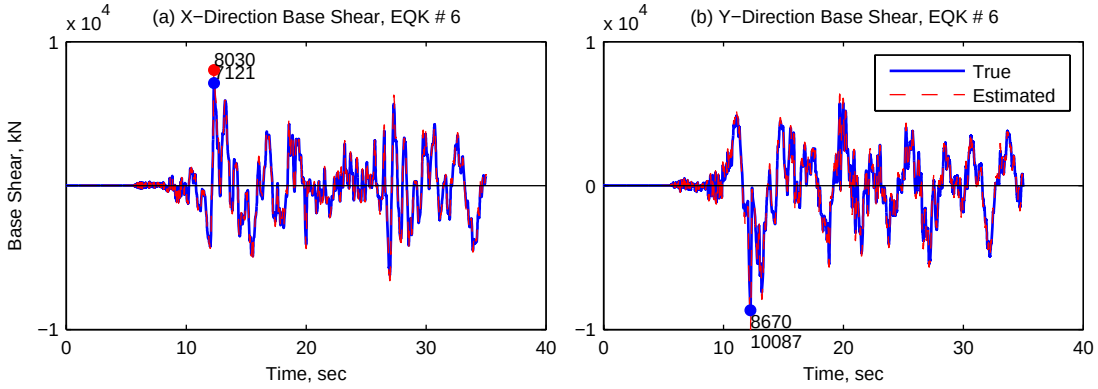

Figure III.36. True and estimated base shears of 20-Story North Hollywood Hotel from *Perform3D* for ground motion 6.

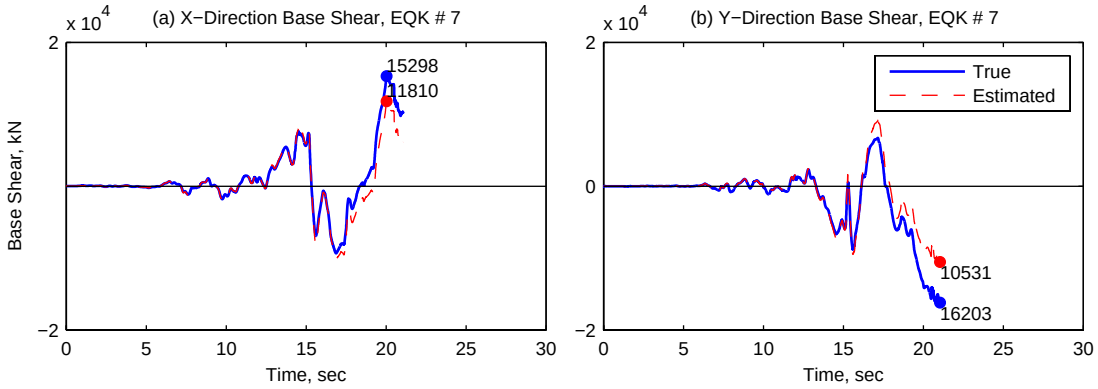

Figure III.37. True and estimated base shears of 20-Story North Hollywood Hotel from *Perform3D* for ground motion 7.

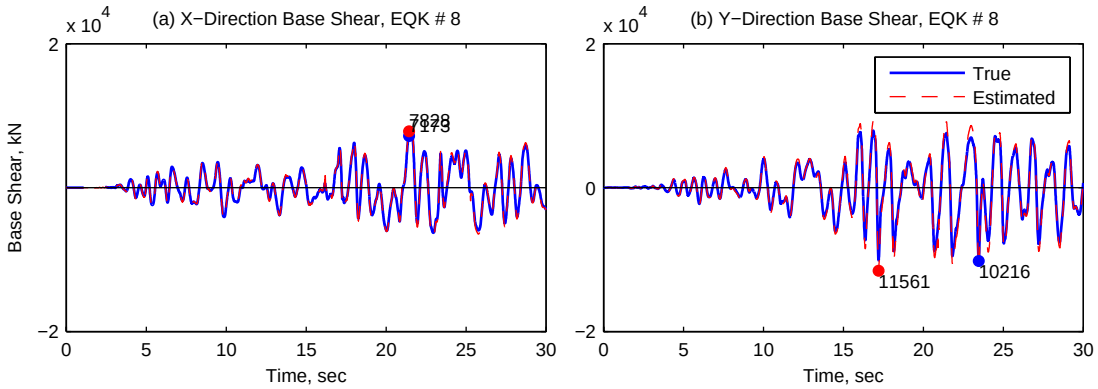

Figure III.38. True and estimated base shears of 20-Story North Hollywood Hotel from *Perform3D* for ground motion 8.

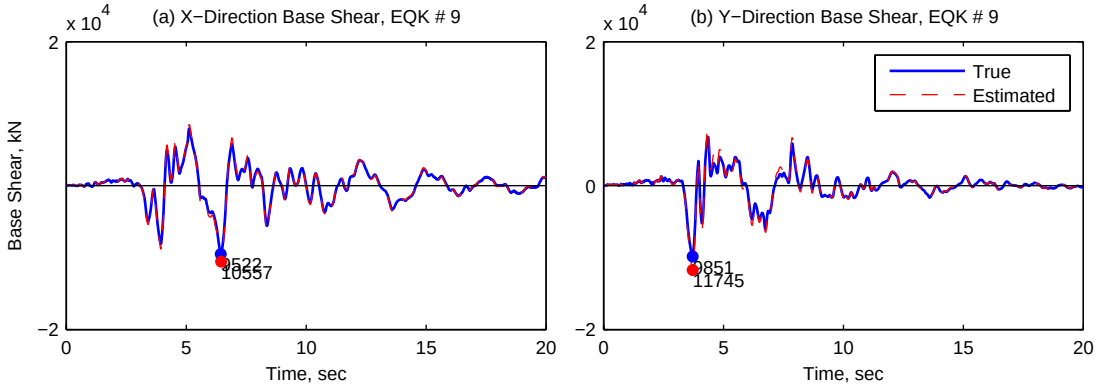

Figure III.39. True and estimated base shears of 20-Story North Hollywood Hotel from *Perform3D* for ground motion 9.

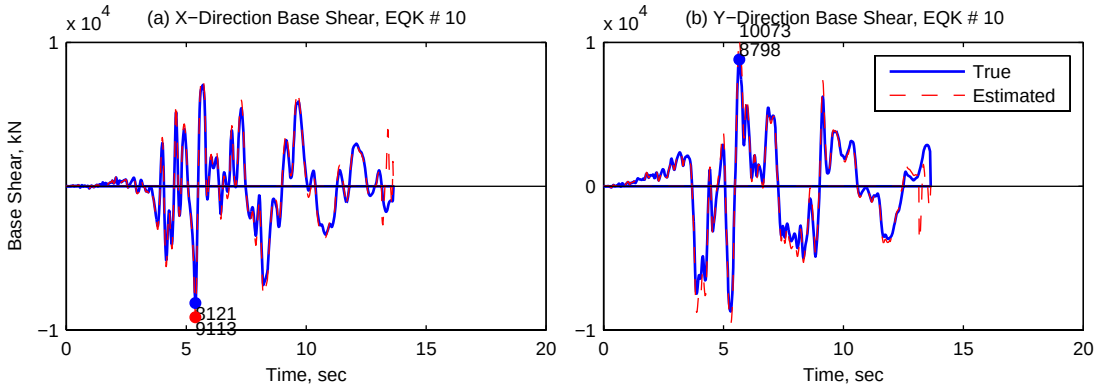

Figure III.40. True and estimated base shears of 20-Story North Hollywood Hotel from *Perform3D* for ground motion 10.

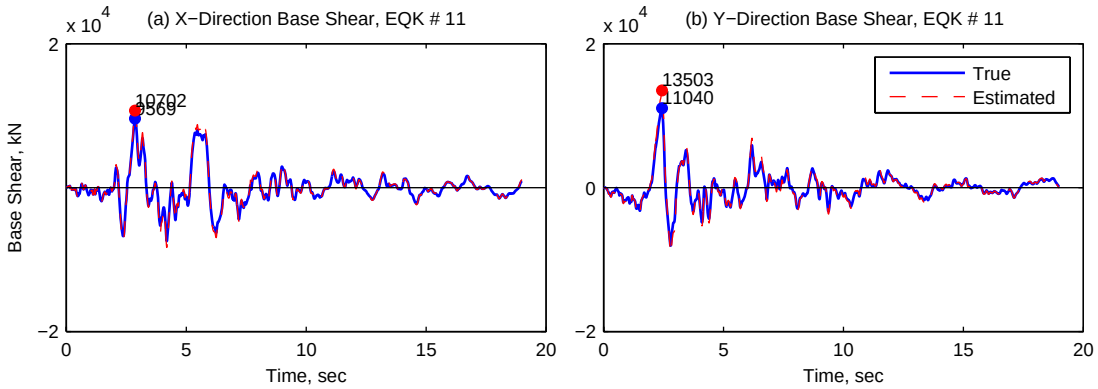

Figure III.41. True and estimated base shears of 20-Story North Hollywood Hotel from *Perform3D* for ground motion 11.

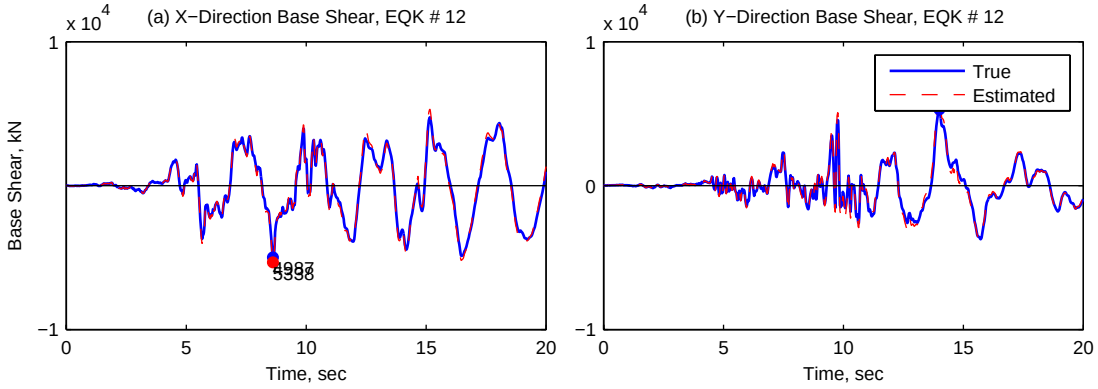

Figure III.42. True and estimated base shears of 20-Story North Hollywood Hotel from *Perform3D* for ground motion 12.

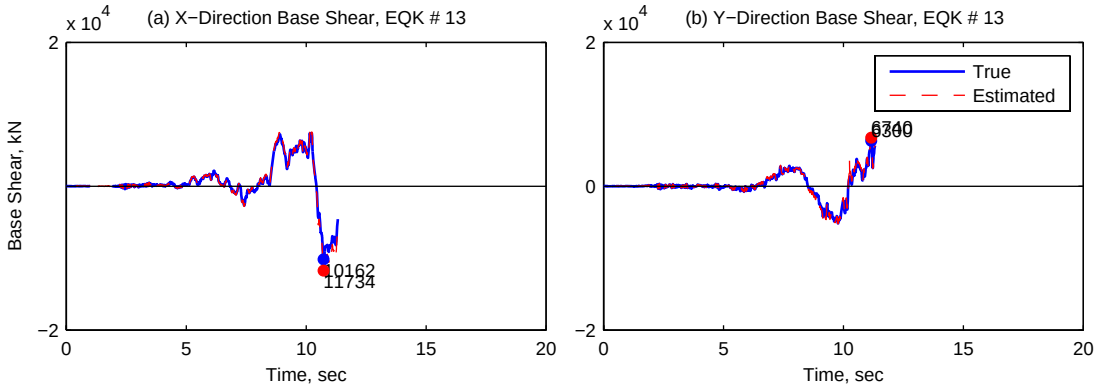

Figure III.43. True and estimated base shears of 20-Story North Hollywood Hotel from *Perform3D* for ground motion 13.

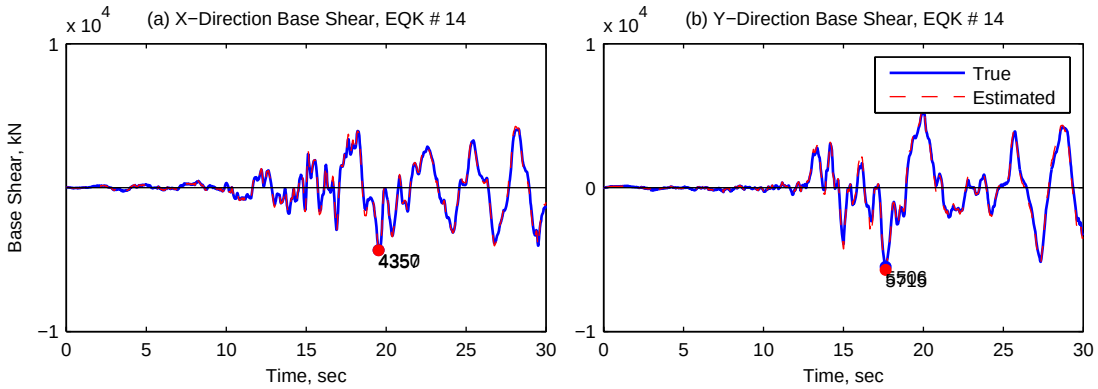

Figure III.44. True and estimated base shears of 20-Story North Hollywood Hotel from *Perform3D* for ground motion 14.

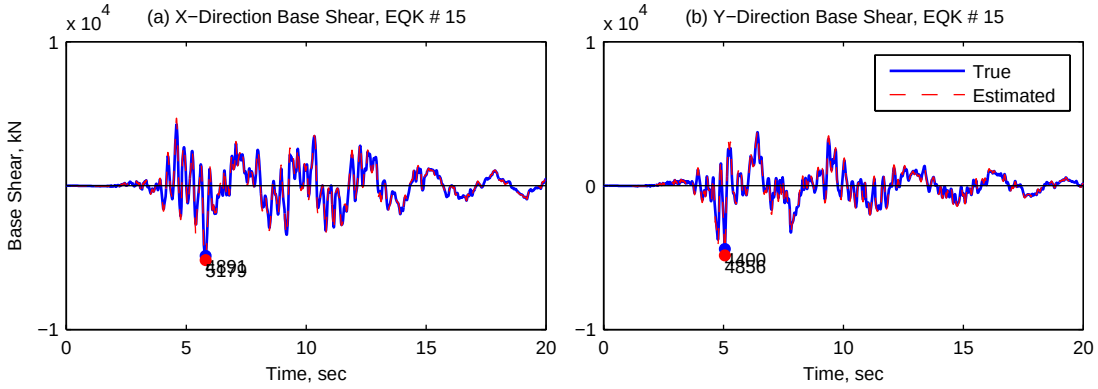

Figure III.45. True and estimated base shears of 20-Story North Hollywood Hotel from *Perform3D* for ground motion 15.

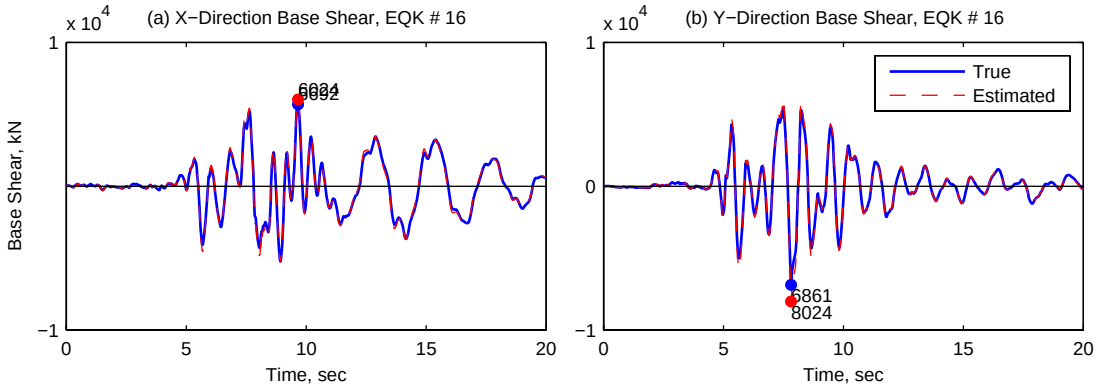

Figure III.46. True and estimated base shears of 20-Story North Hollywood Hotel from *Perform3D* for ground motion 16.

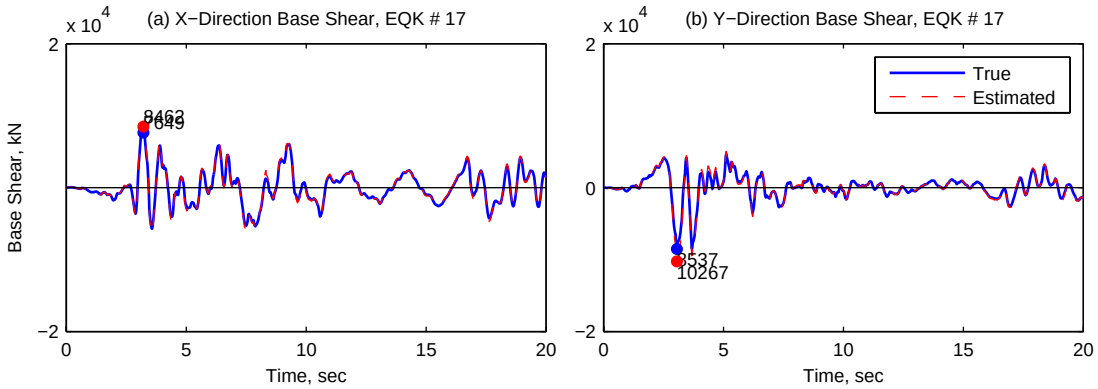

Figure III.47. True and estimated base shears of 20-Story North Hollywood Hotel from *Perform3D* for ground motion 17.

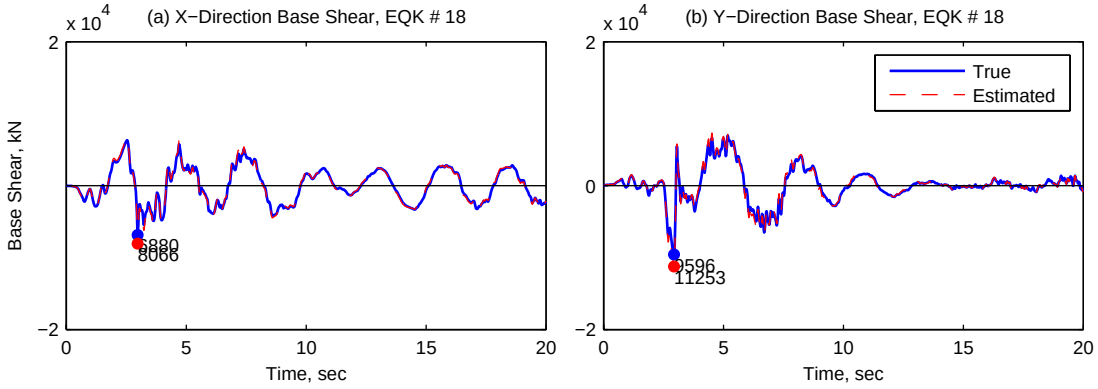

Figure III.48. True and estimated base shears of 20-Story North Hollywood Hotel from *Perform3D* for ground motion 18.

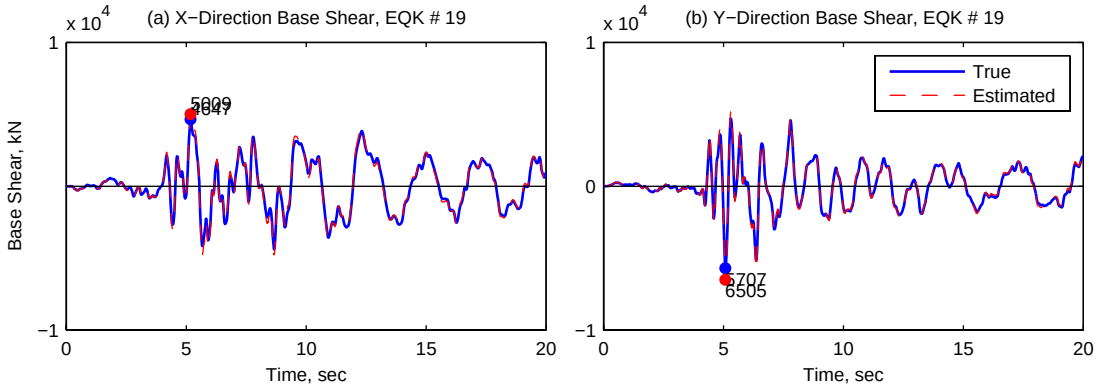

Figure III.49. True and estimated base shears of 20-Story North Hollywood Hotel from *Perform3D* for ground motion 19.

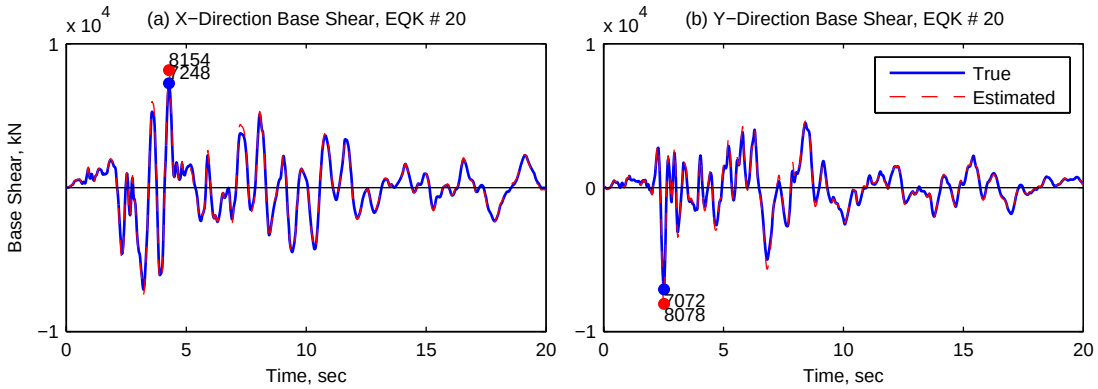

Figure III.50. True and estimated base shears of 20-Story North Hollywood Hotel from *Perform3D* for ground motion 20.

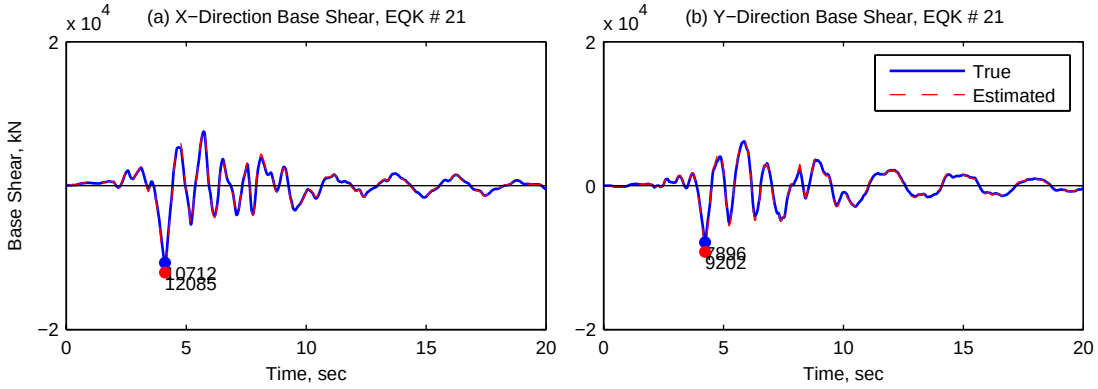

Figure III.51. True and estimated base shears of 20-Story North Hollywood Hotel from *Perform3D* for ground motion 21.

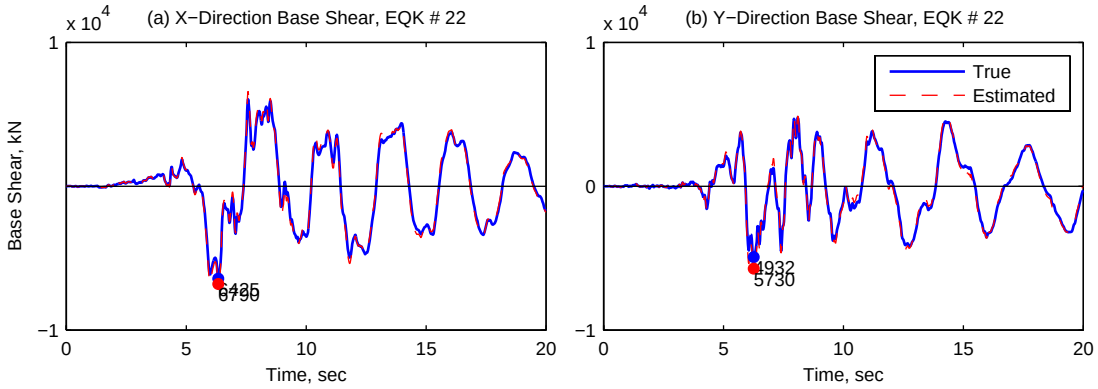

Figure III.52. True and estimated base shears of 20-Story North Hollywood Hotel from *Perform3D* for ground motion 22.

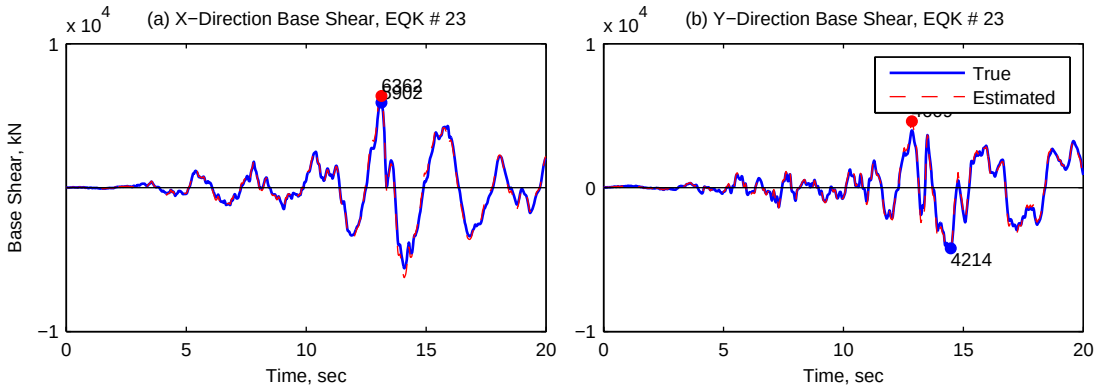

Figure III.53. True and estimated base shears of 20-Story North Hollywood Hotel from *Perform3D* for ground motion 23.

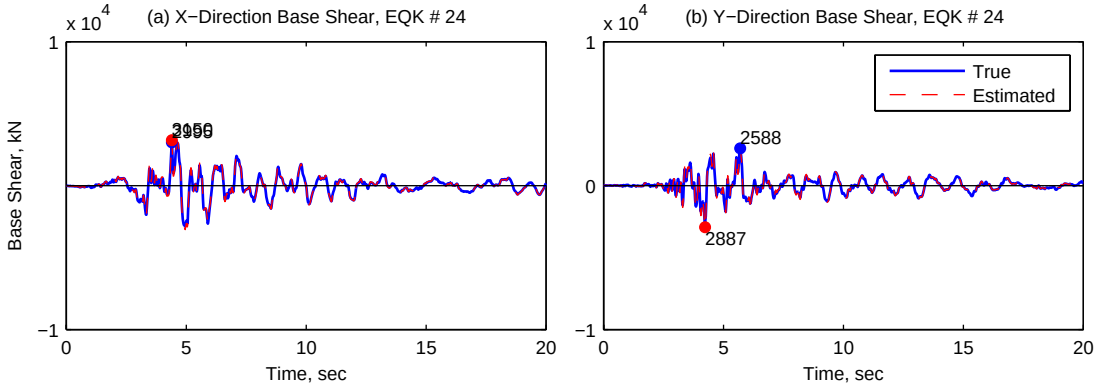

Figure III.54. True and estimated base shears of 20-Story North Hollywood Hotel from *Perform3D* for ground motion 24.

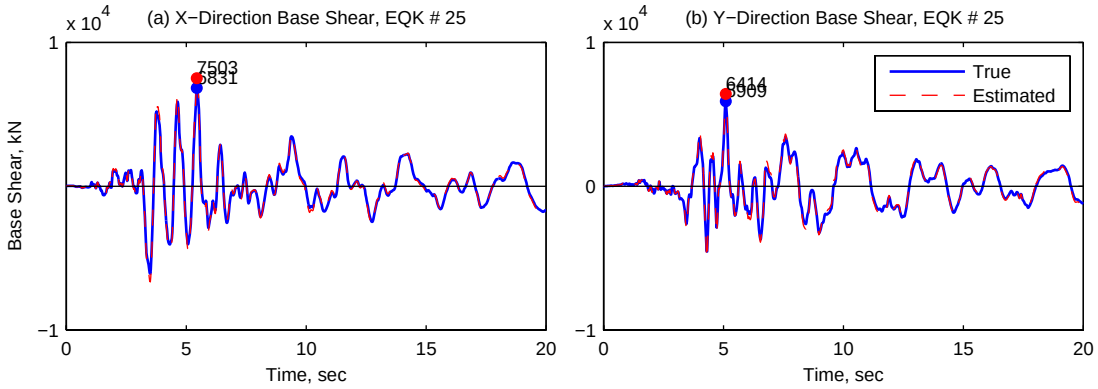

Figure III.55. True and estimated base shears of 20-Story North Hollywood Hotel from *Perform3D* for ground motion 25.

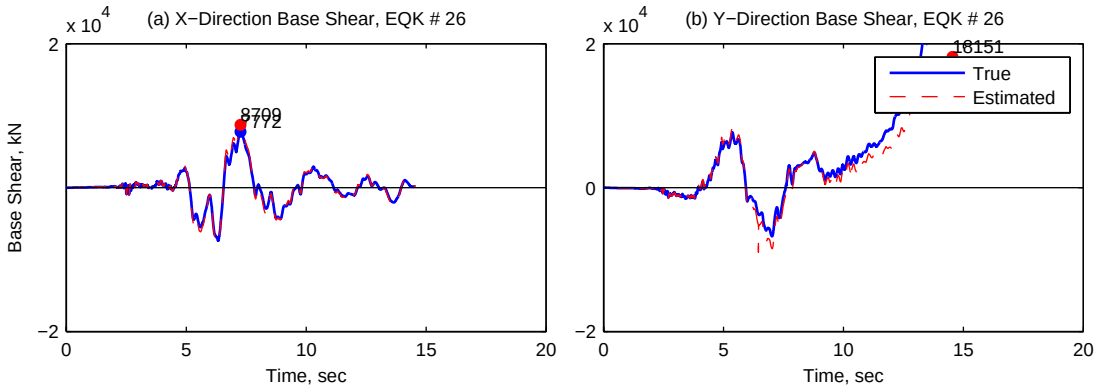

Figure III.56. True and estimated base shears of 20-Story North Hollywood Hotel from *Perform3D* for ground motion 26.

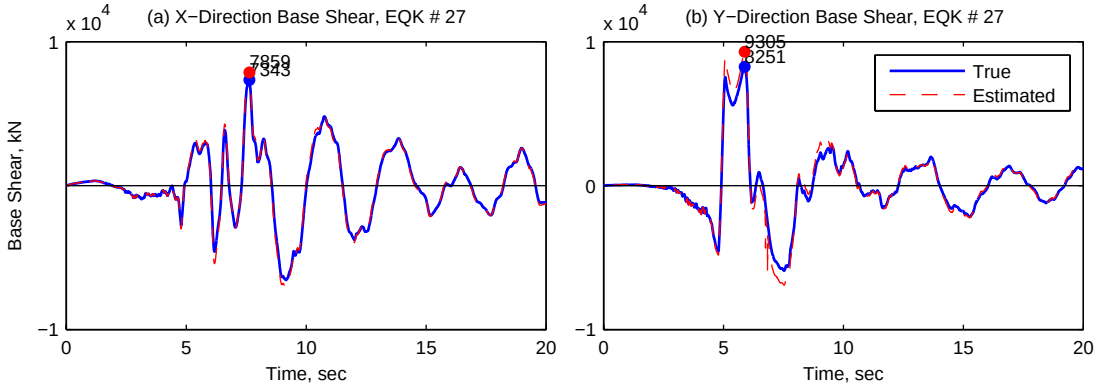

Figure III.57. True and estimated base shears of 20-Story North Hollywood Hotel from *Perform3D* for ground motion 27.

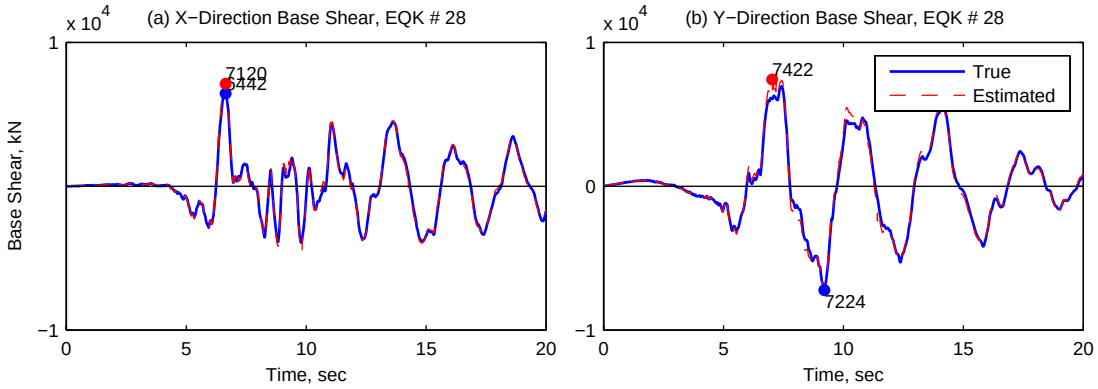

Figure III.58. True and estimated base shears of 20-Story North Hollywood Hotel from *Perform3D* for ground motion 28.

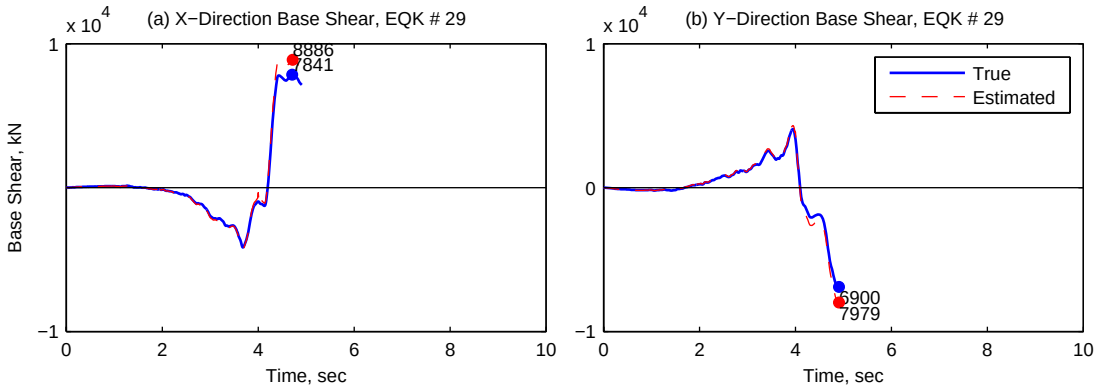

Figure III.59. True and estimated base shears of 20-Story North Hollywood Hotel from *Perform3D* for ground motion 29.

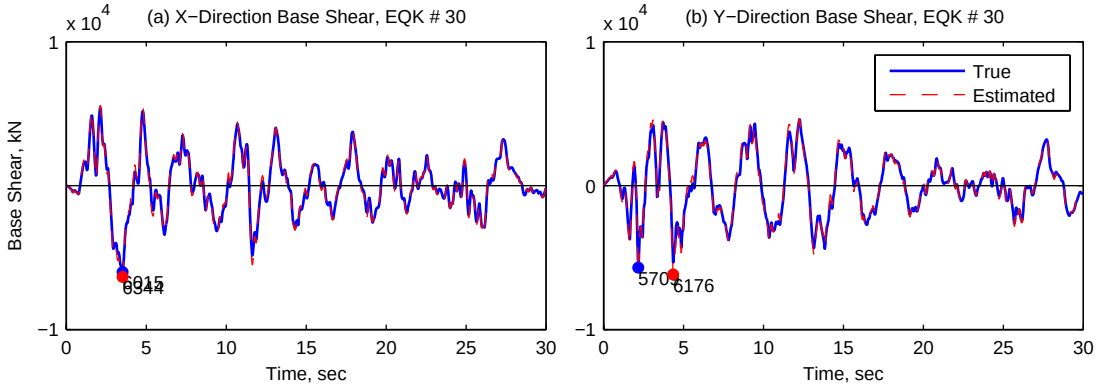

Figure III.60. True and estimated base shears of 20-Story North Hollywood Hotel from *Perform3D* for ground motion 30.

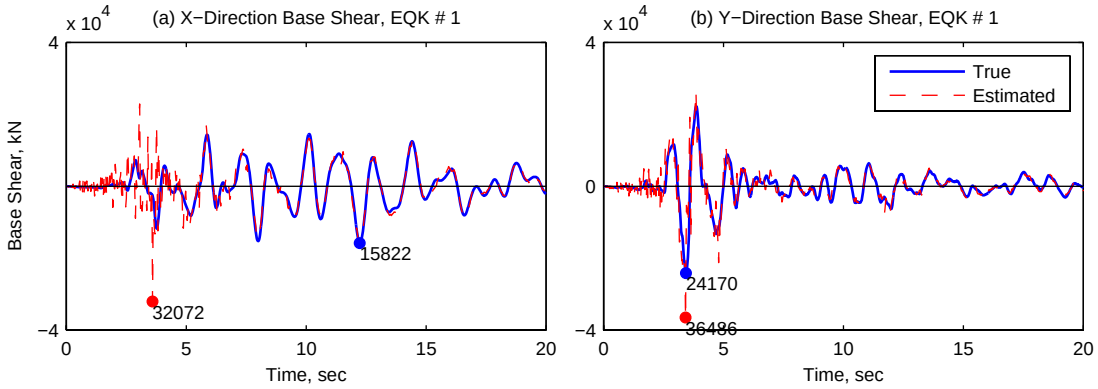

Figure III.61. True and estimated base shears of 19-Story Office Building in Los Angeles from *OpenSees* for ground motion 1.

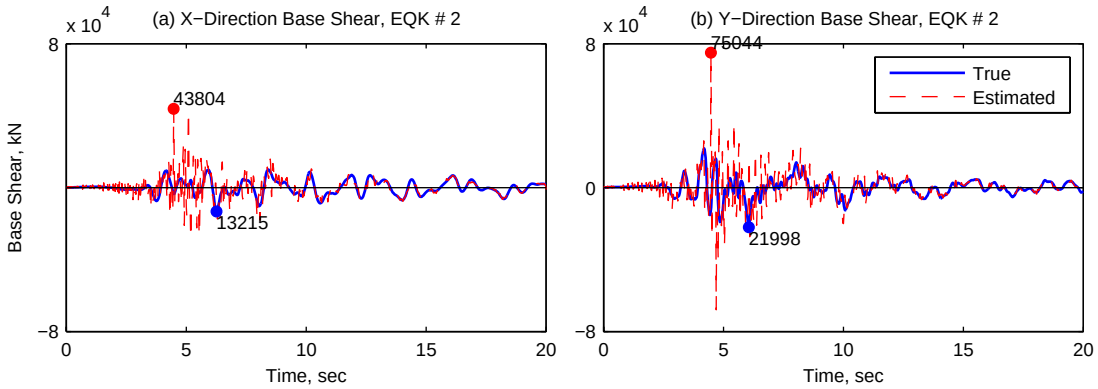

Figure III.62. True and estimated base shears of 19-Story Office Building in Los Angeles from *OpenSees* for ground motion 2.

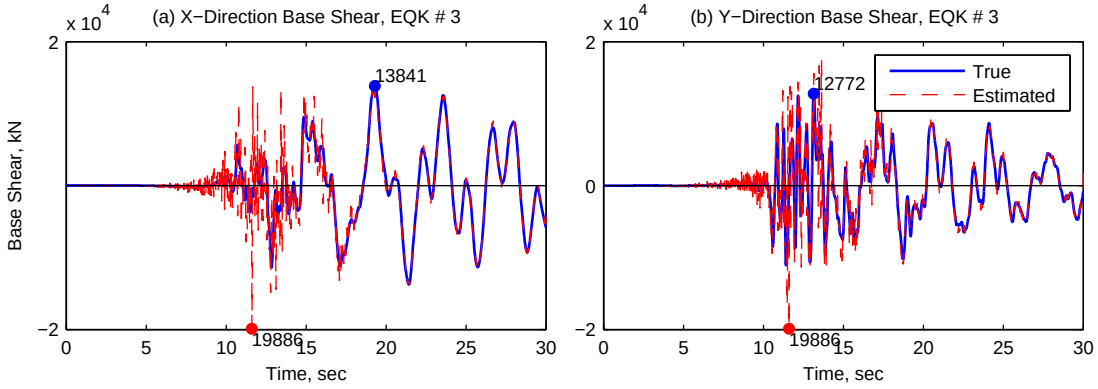

Figure III.63. True and estimated base shears of 19-Story Office Building in Los Angeles from *OpenSees* for ground motion 3.

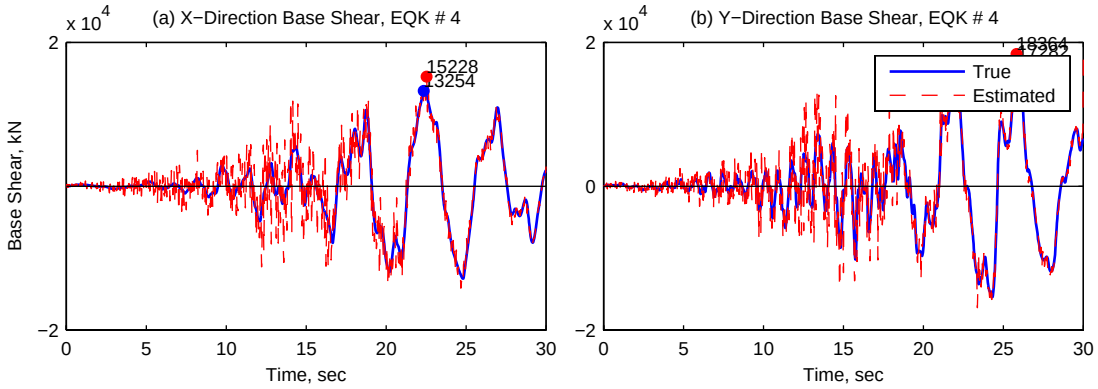

Figure III.64. True and estimated base shears of 19-Story Office Building in Los Angeles from *OpenSees* for ground motion 4.

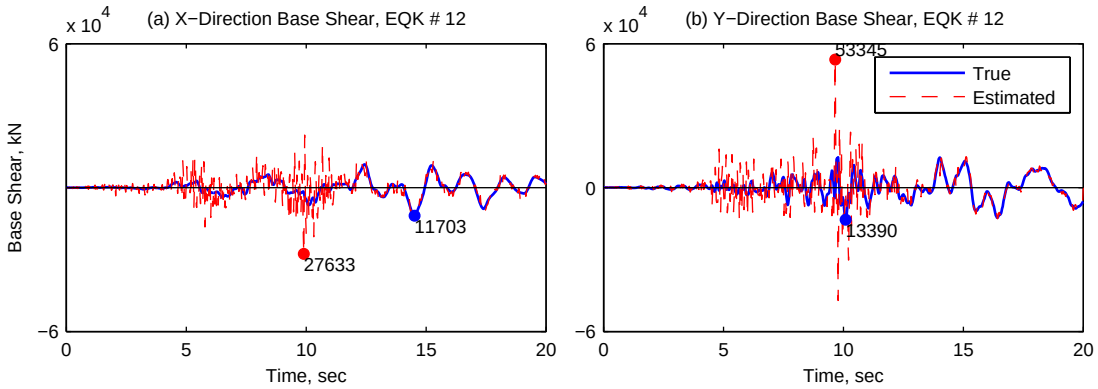

Figure III.65. True and estimated base shears of 19-Story Office Building in Los Angeles from *OpenSees* for ground motion 12.

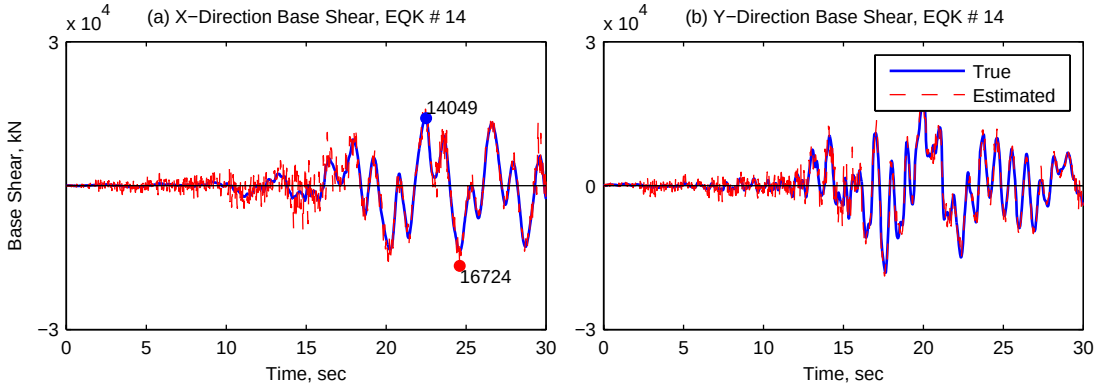

Figure III.66. True and estimated base shears of 19-Story Office Building in Los Angeles from *OpenSees* for ground motion 14.

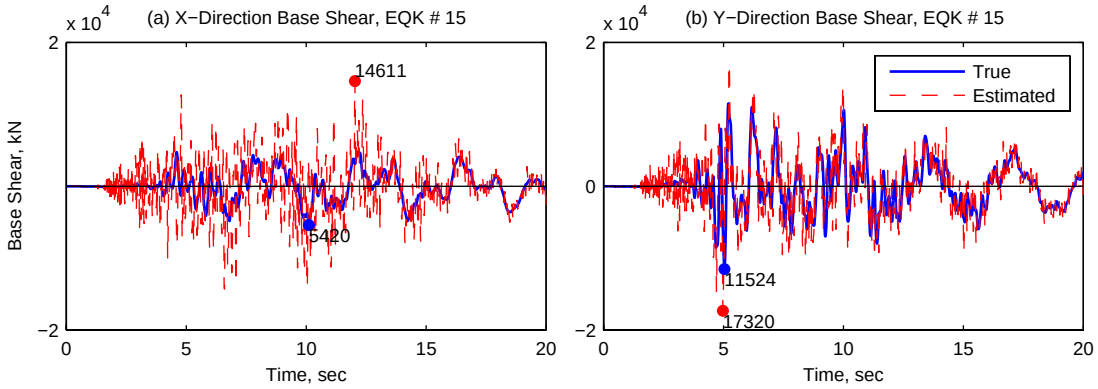

Figure III.67. True and estimated base shears of 19-Story Office Building in Los Angeles from *OpenSees* for ground motion 15.

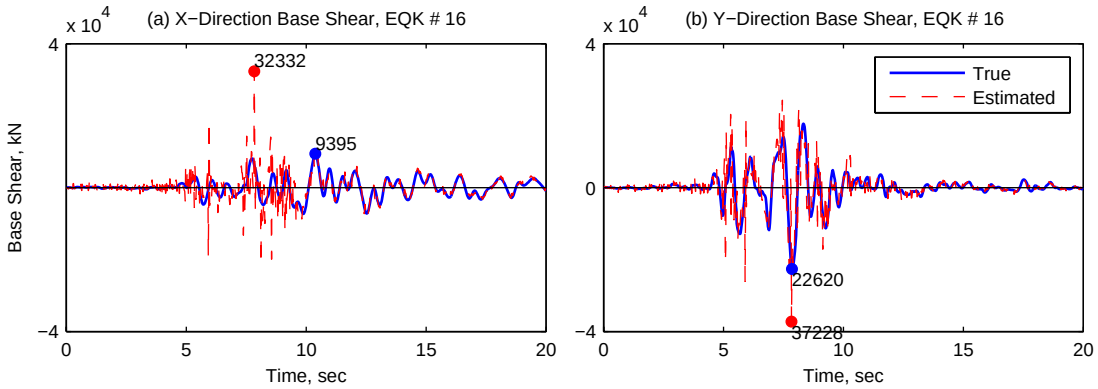

Figure III.68. True and estimated base shears of 19-Story Office Building in Los Angeles from *OpenSees* for ground motion 16.

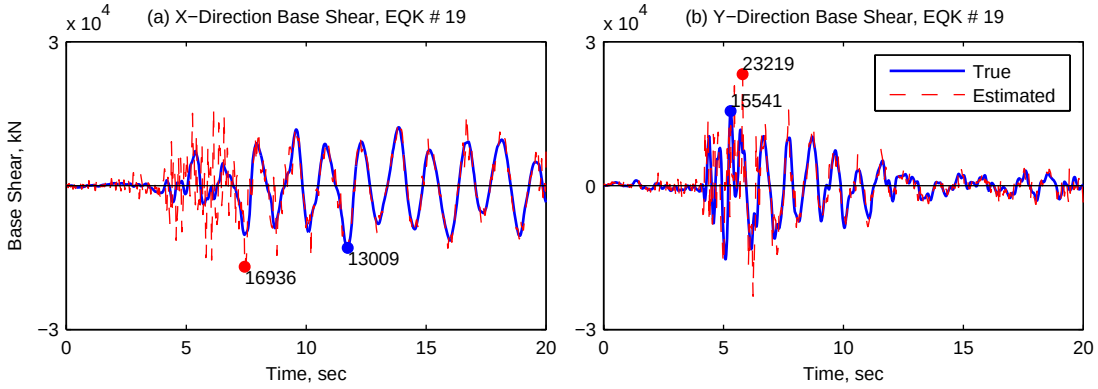

Figure III.69. True and estimated base shears of 19-Story Office Building in Los Angeles from *OpenSees* for ground motion 19.

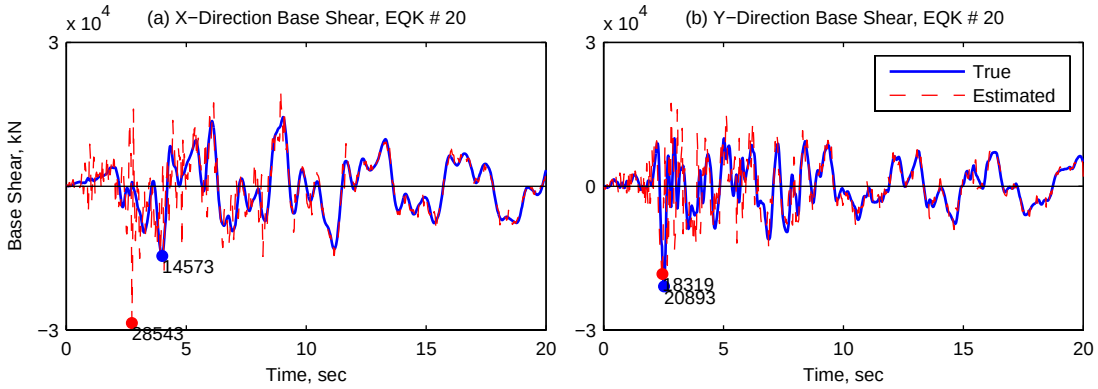

Figure III.70. True and estimated base shears of 19-Story Office Building in Los Angeles from *OpenSees* for ground motion 20.

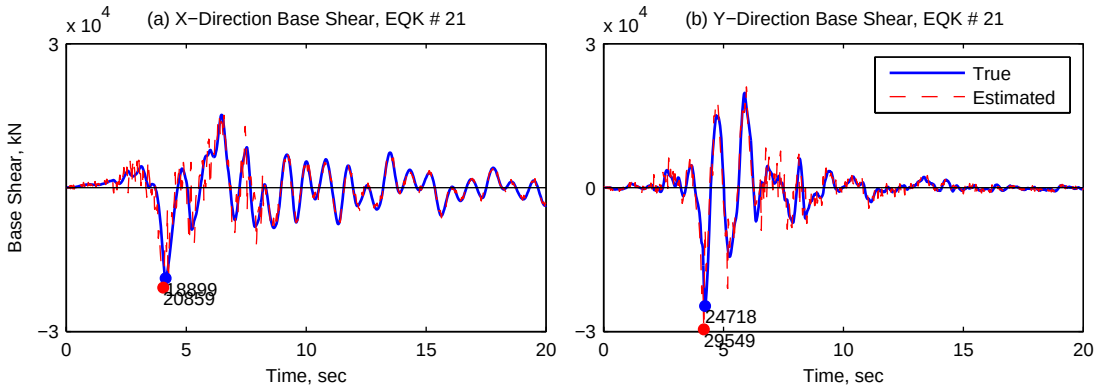

Figure III.71. True and estimated base shears of 19-Story Office Building in Los Angeles from *OpenSees* for ground motion 21.

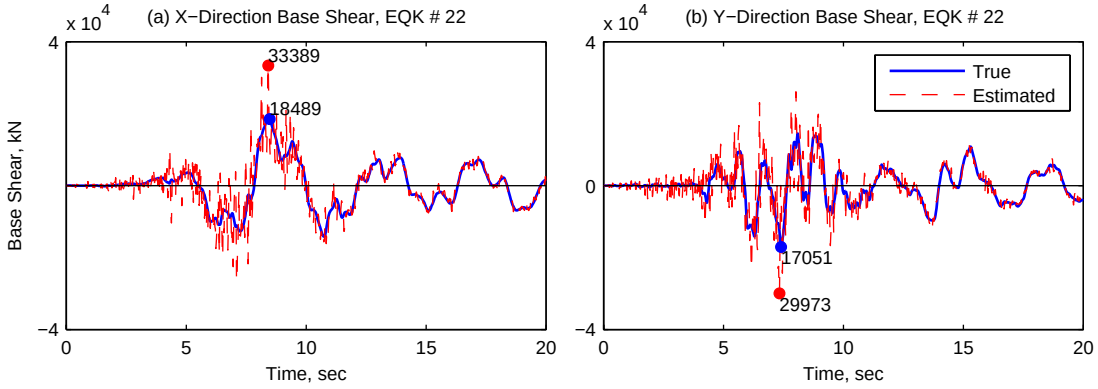

Figure III.72. True and estimated base shears of 19-Story Office Building in Los Angeles from *OpenSees* for ground motion 22.

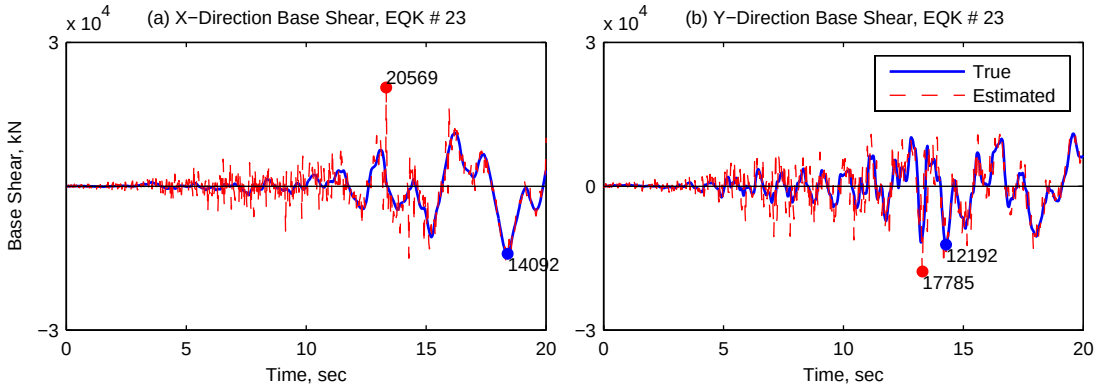

Figure III.73. True and estimated base shears of 19-Story Office Building in Los Angeles from *OpenSees* for ground motion 23.

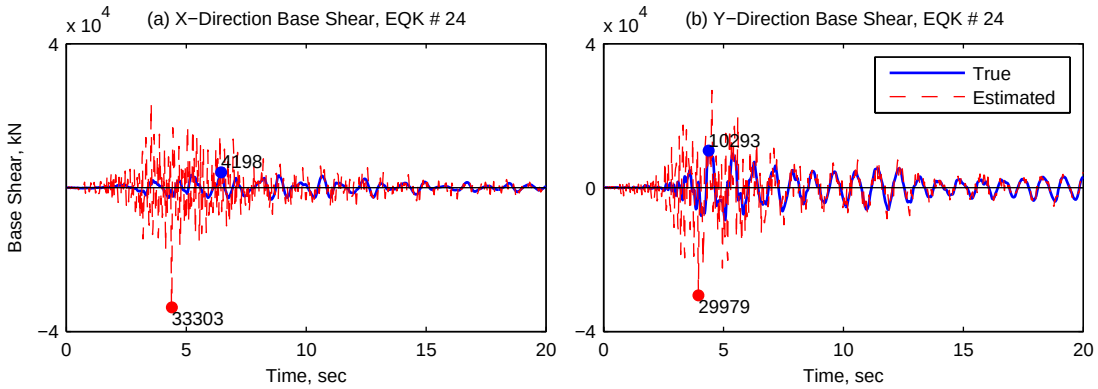

Figure III.74. True and estimated base shears of 19-Story Office Building in Los Angeles from *OpenSees* for ground motion 24.

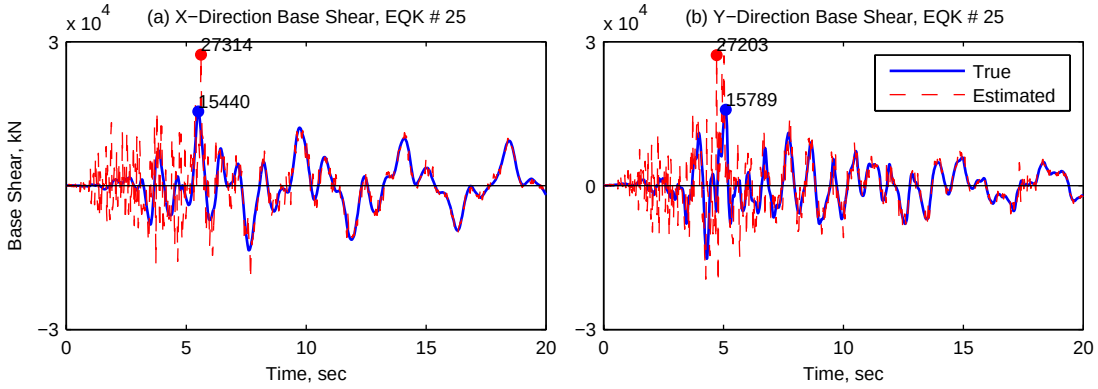

Figure III.75. True and estimated base shears of 19-Story Office Building in Los Angeles from *OpenSees* for ground motion 25.

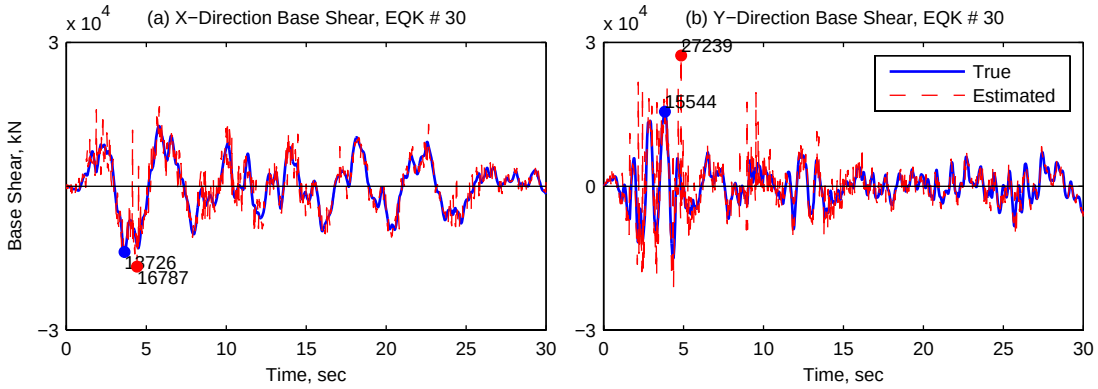

Figure III.76. True and estimated base shears of 19-Story Office Building in Los Angeles from *OpenSees* for ground motion 30.

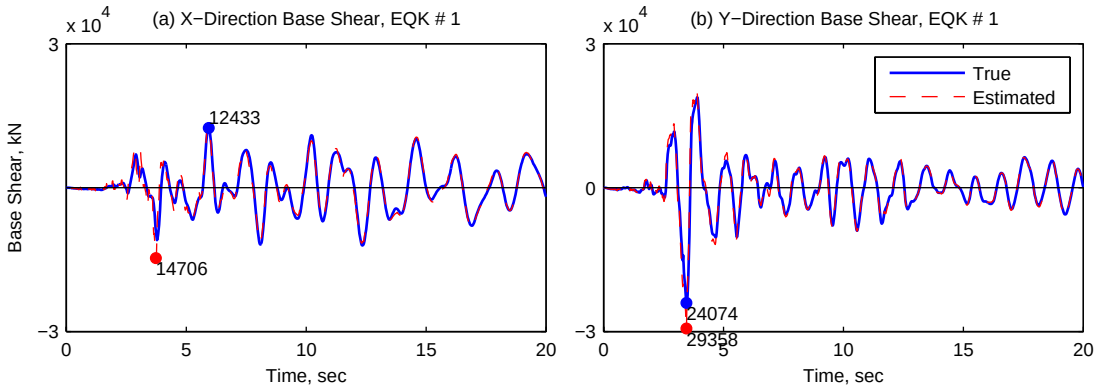

Figure III.77. True and estimated base shears of 19-Story Office Building in Los Angeles from *Perform3D* for ground motion 1.

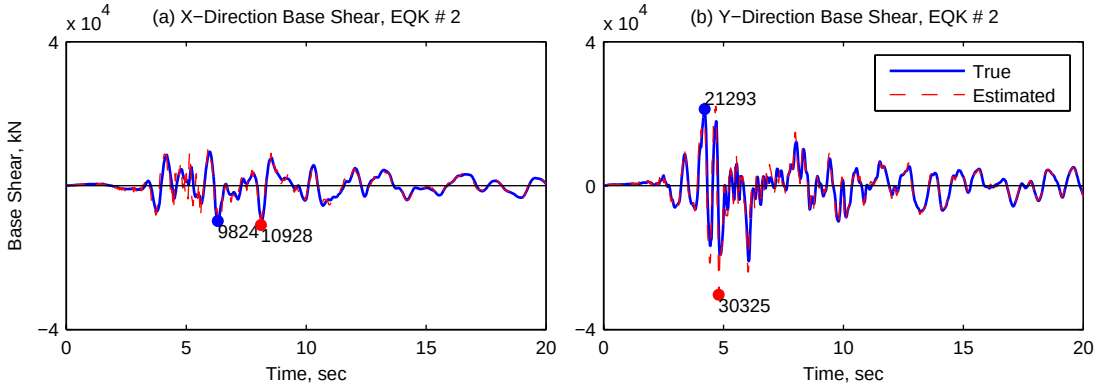

Figure III.78. True and estimated base shears of 19-Story Office Building in Los Angeles from *Perform3D* for ground motion 2.

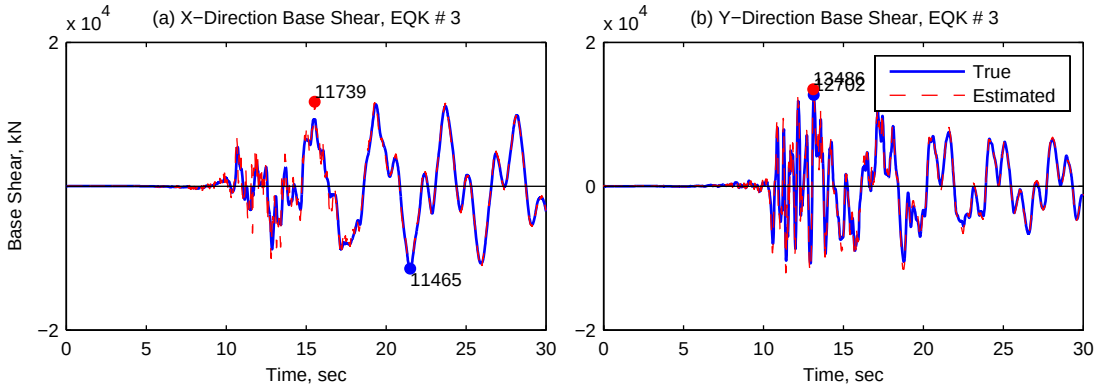

Figure III.79. True and estimated base shears of 19-Story Office Building in Los Angeles from *Perform3D* for ground motion 3.

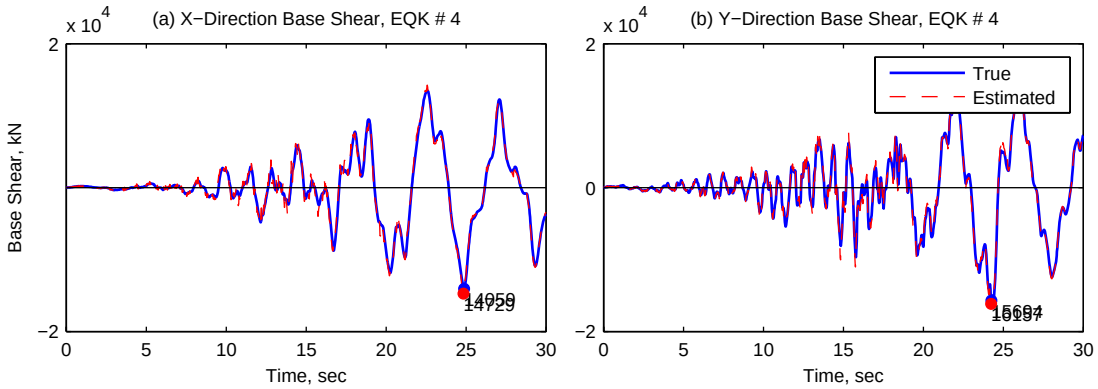

Figure III.80. True and estimated base shears of 19-Story Office Building in Los Angeles from *Perform3D* for ground motion 4.

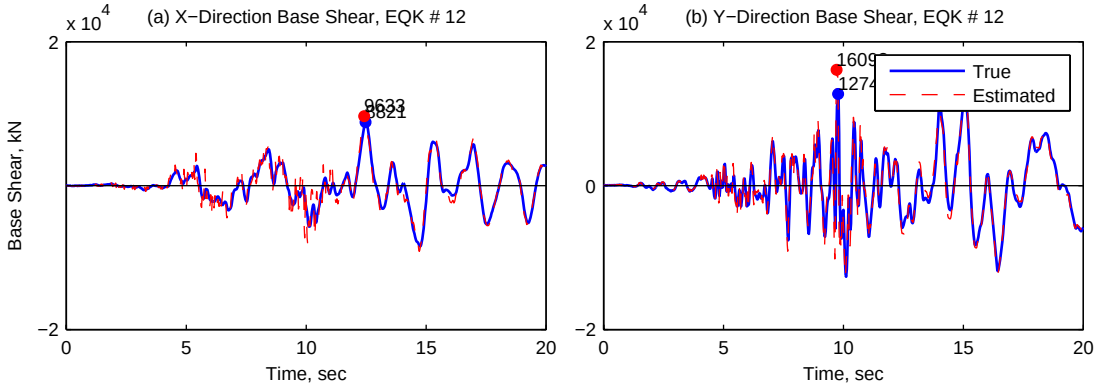

Figure III.81. True and estimated base shears of 19-Story Office Building in Los Angeles from *Perform3D* for ground motion 12.

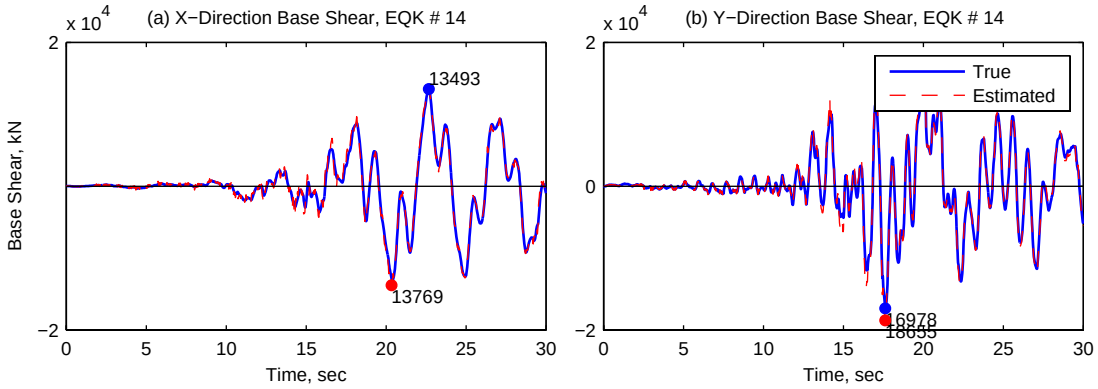

Figure III.82. True and estimated base shears of 19-Story Office Building in Los Angeles from *Perform3D* for ground motion 14.

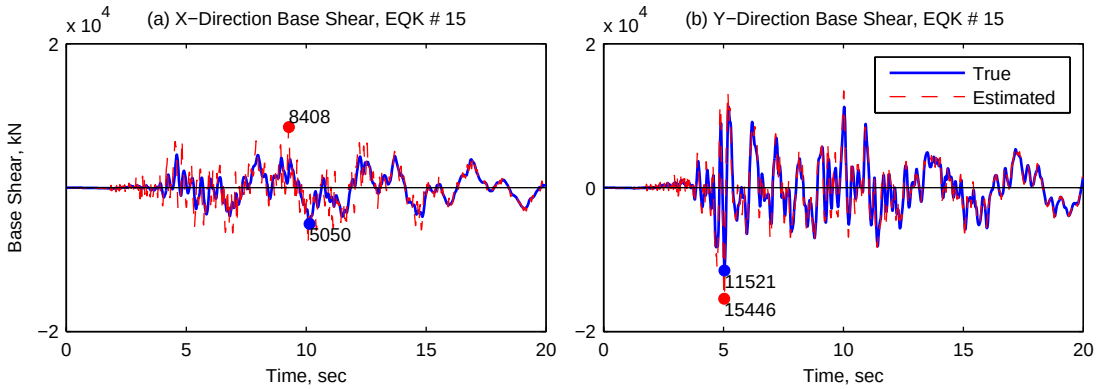

Figure III.83. True and estimated base shears of 19-Story Office Building in Los Angeles from *Perform3D* for ground motion 15.

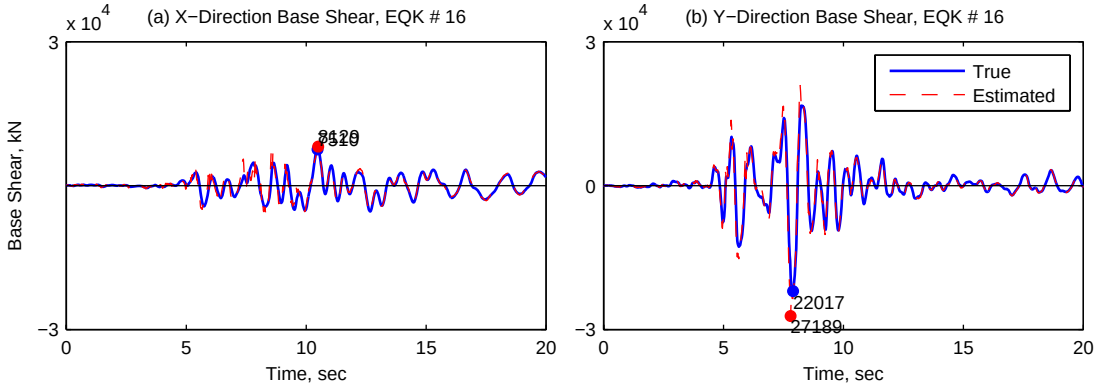

Figure III.85. True and estimated base shears of 19-Story Office Building in Los Angeles from *Perform3D* for ground motion 16.

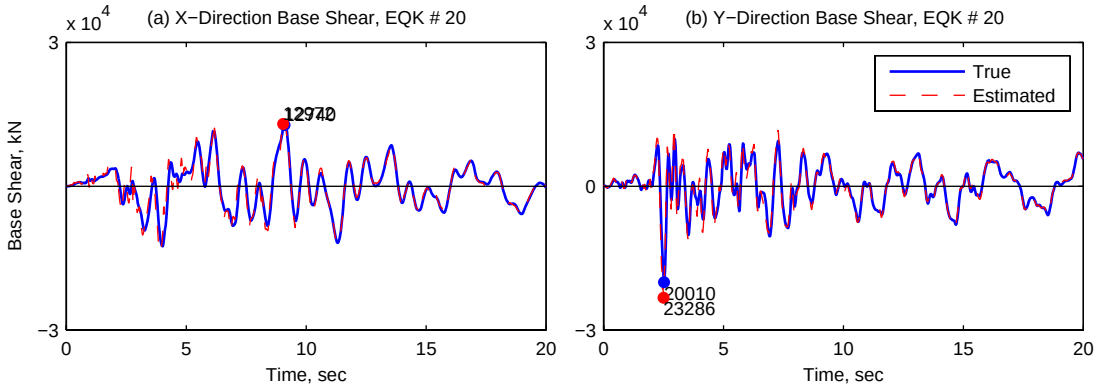

Figure III.86. True and estimated base shears of 19-Story Office Building in Los Angeles from *Perform3D* for ground motion 20.

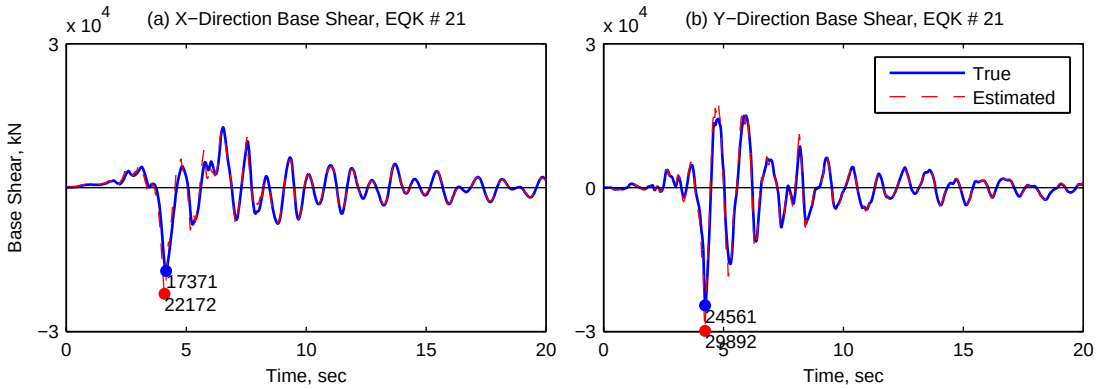

Figure III.87. True and estimated base shears of 19-Story Office Building in Los Angeles from *Perform3D* for ground motion 21.

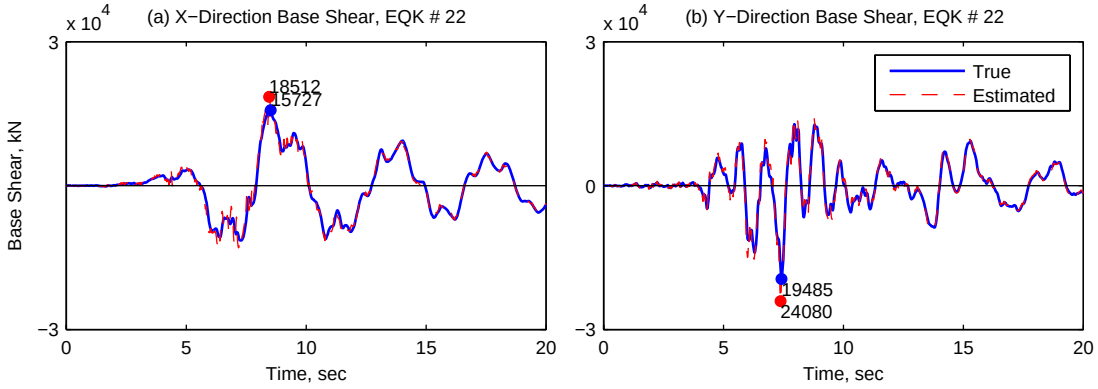

Figure III.88. True and estimated base shears of 19-Story Office Building in Los Angeles from *Perform3D* for ground motion 22.

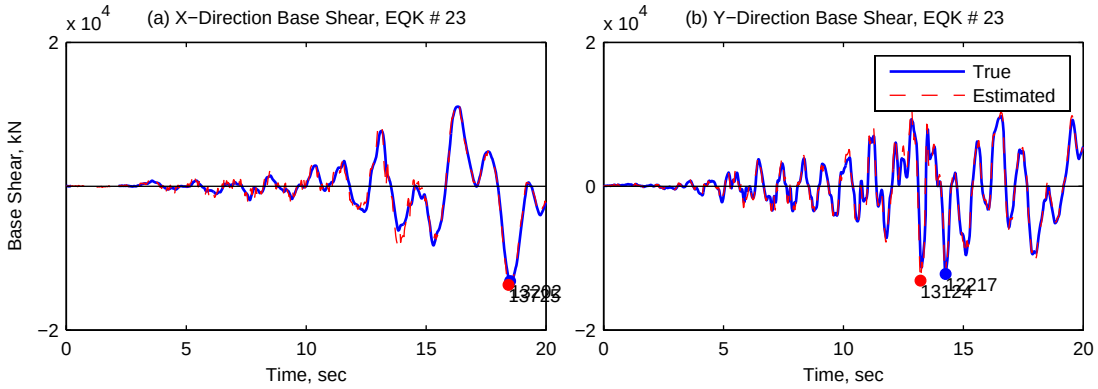

Figure III.89. True and estimated base shears of 19-Story Office Building in Los Angeles from *Perform3D* for ground motion 23.

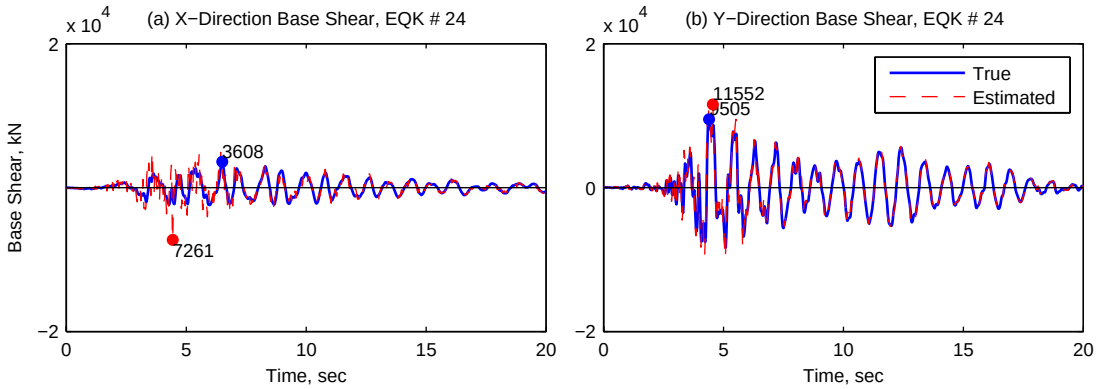

Figure III.90. True and estimated base shears of 19-Story Office Building in Los Angeles from *Perform3D* for ground motion 24.

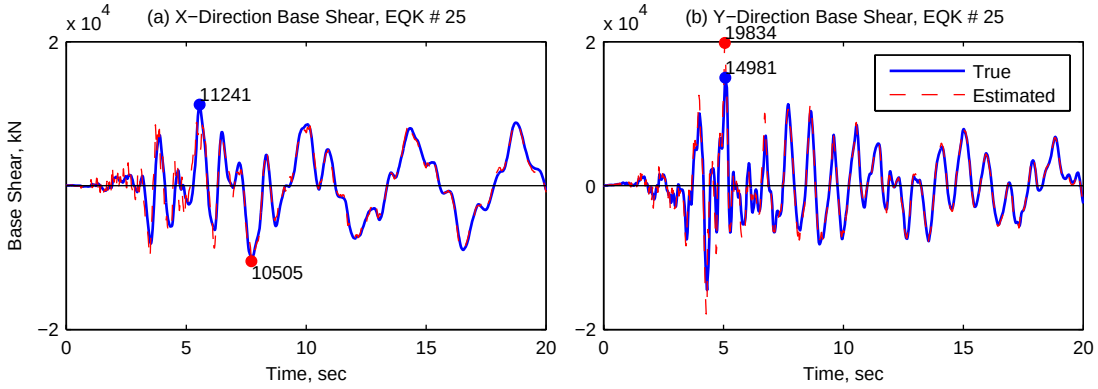

Figure III.91. True and estimated base shears of 19-Story Office Building in Los Angeles from *Perform3D* for ground motion 25.

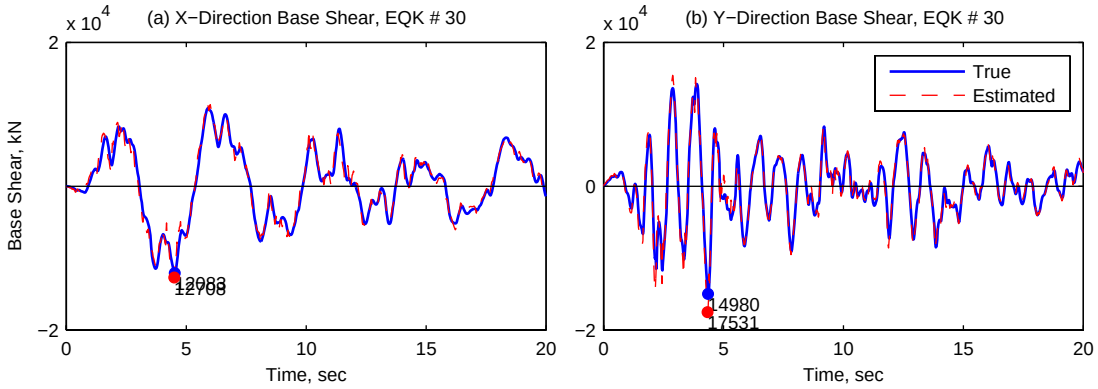

Figure III.92. True and estimated base shears of 19-Story Office Building in Los Angeles from *Perform3D* for ground motion 30.